Nanoparticles in aqueous environments: A physicochemical and ecotoxicological study of cerium dioxide

By

Paula Cole

A thesis submitted to
The University of Birmingham
for the degree of
Doctor of philosophy

School of Geography, Earth and Environmental Sciences
College of Life and Environmental Sciences
The University of Birmingham, UK

July 2011

Abstract

The unique properties which make cerium dioxide (ceria) nanoparticles (NPs) so useful in e.g. catalytic applications, pose a real risk to environmental systems and species alike. Increasing our knowledge of ceria NP characteristics in a range of aquatic systems was a contributing theme of this thesis. Nano-ceria particle sizes (d_H) were found to significantly change due to adjustments in media composition. The addition of Suwannee River fulvic acid to an aquatic media decreased d_H up to 88%, significantly increased the negative charge measured from zeta potential (ζ) and increased Ce dissolution by 2%. The presence of test biota significantly increased d_H up to 80%, further increased the ζ negative charge and increased Ce dissolution up to 63%, predicted as being due to the presence of exudates. Nanotoxicological investigations using *P. subcapitata* showed a convincing size-dependent toxicity to well-defined synthesized nano-ceria particles. EC_{50} values of 5 nm to 35 nm ceria particles (0.013 mgL to 0.8 mgL respectively) showed between 600 and 10 fold increases in toxic response compared to commercial nano-ceria particles (EC_{50} 8 mgL). EC_{50} of 5 nm and 35 nm ceria particles showed significant metabolic differences compared to controls indicating a cellular response of *P. subcapitata* as a function of nano-ceria size and dose. Although metabolomic extraction methods are sensitive to cell density and temperature changes, metabolomic analysis has huge potential in future environmental nanoecotoxicological applications using *P. subcapitata*. It was evident from this study that further work is still required to help develop methods of NP characterisations under environmental conditions with a necessity for a future NP modelling protocol.

For

Mum and Dad

xx

Acknowledgements

I would like to open my personal acknowledgments to NERC for the financial support which made this research possible. I would like to express my gratitude to my supervisor, Professor Jamie Lead for giving me the opportunity to perform my PhD and for all the encouragement, advice and blind-eyes you've given me throughout the past four years. You have the patients of a saint! Thanks also must be given to my secondary supervisor Dr. Lesley Batty for her support on matters of the heart-here's to our new found friendship and to the only place we know such matters can be conducted with professionalism and comfort...Bratby. Particular thanks go to my external and internal examiners Professor Jim Readman and Dr Josh Rappoport for taking the time to read my thesis.

Thank you to my husband Ian, who without fail made me laugh every single day throughout the good, the bad and the downright stupid. I love you very much and without your support, I would never have got through this.

Many people made the analysis of this work possible through their expertise and technical support. I would like to thank Dr. Steve Baker for the ICP-MS element analyses and Dr. Louise Male for her support during XRD analysis. I must thank Yon and Ruth for the high quality AFM and TEM images and analysis you helped me with. I would also like to express my gratitude to Mohammed for his excellent TEM support and for the work we performed together. Further gratitude must be given to Ruth Merrifield, who made my entire third year much easier. You make the AFM look so easy and make days on the TEM go so much quicker. To my little tea-fiend, Geo-bar eating double-Dan mate.

I must also take this opportunity to thank all the people involved in the collaborative studies. Thank you Professor Vicky Stone, Dr. Birgit Gaiser and Phillip Rosenkranz at Napier University and also a big thank you must go to Professor Charles Tyler and your team at Exeter University including Dr. Blair Johnson and Rhys Goodhead. Particular thanks must go to Dr Simon Apte, Dr.

Nicola Rogers and Dr. Brad Angel at the CSIRO laboratories in Sydney for accommodating me during my training and for your invaluable contribution to the results you helped me to interpret. Dr. Mark Viant and Dr. Ulf Sommer need particlular thanks for the support and advice during the metabolmic study conducted. Here's to no more long e-mails!

Special thanks must go out to the procrastination team. Without the crazy lunch time stories of Kate's continual Perker-tube breakage, the wrong shoes and of course the wrong gas along with Jessie's tales of stupid students and newly caught diseases; Adams constant look of despair, lack of lab work, increased library days and early morning's home and of course, the weekly supply of Salim's rubbish excuses and Sue's innocence, the world would have been a bleaker place. In fact, without the tea breaks, pub lunches, Friday cakes and 'team' support, my thesis may have been completed months earlier, although the struggle of writing was made all the easier. A big thank you goes to Michaela for your great advice and support – now its mine! So I thank all team members, for taking me with you on your quest through the thesis barricades.

Impeding regards must go to the technical world, specifically the inventors and makers of the iPod and all musical practitioners, with special thanks to Travis, The Scissor Sisters and Gloria Gaynor for help through writers block. You've paved the way for my thesis to be a reality.

To close my genuine thanks, there has to be a personal thank you to my Mum and Dad. How you coped with me over the years I do not know, but I would like to dedicate this thesis to your continual words of encourage, belief in me and obvious devotion over the years. Without your advice and guidance I would never have reached my dream of researching new science. Thank you mama and papa Cole ☺

I. Contents

II. List of figures

Chapter 1

Chapter 2

Chapter 3

Chapter 4

Chapter 5

Chapter 6

Chapter 7

III. List of Tables

Chapter 1

Chapter 2

Chapter 3

Chapter 4

Chapter 5

Chapter 6

Chapter 7

IV. List of Equations

Chapter 2

Chapter 3

Chapter 4

V. Common Abbreviations

2D	2-dimensions
3D	3-dimentisonal
Å	Angstrom
AFM	Atomic force microscopy
BET	Brunauer Emmet and Teller
^{o}C	Degrees Celsius
ca	from the Latin circa (around, about)
$Ca(NO_3)_2$	Calcium nitrate
Ceria	Cerium oxide/CeO_2
CSIRO	Commonwealth Science and Industrial Research Organisation
d_H	Hydrodynamic diameter
dH_2O	Deionised water
d_{XRD}	mean crystallite diameter of the particle
DLS	Dynamic light scattering
DLVO	Derjaguin-Landau-Verwey-Overbeek theory
EC (50)	Effective concentration (at 50% to the control)
Ecotoxicity	Environmental toxicity assessments
EDTA	Ethylenediaminetetraacetic acid
EDL	Electric double layer
EDX	Qualitative element analysis
EELS	Electron energy loss spectroscopy
EEM	Excitation-emission matrix
Em λ	Emission wavelength
ENPs	Engineered nanoparticles
Ex λ	Excitation wavelength
FWHM	Full-width half-maximum
h	Hour
HRTEM	High resolution TEM
ICP-MS	Inductively coupled plasma mass spectrometry

In vitro	A test performed in glass or plastic
In vivo	An experiment using a whole living organism
ISO	International Standards organization
JCPDS	The Joint Committee on Powder Diffraction Standards
KD	Kilo Dalton
kV	Kilo volts
L	Litre
LM	Light microscope
LOEC	Lowest observable effective concentration
m	meters
M	Molar
mbar	Millibar
mg/L	milligram per litre – parts per million
min	minutes
ml	millilitres
mM	Milli-molar
MNP	Manufactured nanoparticles
MS	Mass spectrometry
mV	Milli-volts
Nanoecotoxicity	Environmental toxicity assessments using NPs
Nano-ceria	Ceria nanoparticles
nm	Nanometer being 10^{-9} m.
NOEC	No observable effect concentration
NOM	natural organic material
NP	Nanoparticle
OECD	Organization for Economic Co-operation and Development
OM	Organic matter
OS	Oxidative stress
PdI	Polydispersity index
PEC	Predicted environmental concentration
PIPES	Piperazine-1,4-bis(2-ethanesulfonic acid) $C_8H_{18}N_2O_6S_2$)

PNEC	Predicted no effect concentration
ppb	Parts-per-billion
ppm/mg/L	Parts-per-million/milligrams per litre
Pzc	Point of zero charge
PP	Polypropylene (PP)
PVP	poly(N-vinylpyrrolidin-2-one (PVP)
QD	Quantum dots
REE	Rare earth elements
ROS	Reactive oxygen species
rcf	relative centrifugal force
rpm	Revolutions per minute
S	Aspect ratio
s	Seconds
SA	Surface Area
SPR	Surface Plasmon resonance
SRFA	Suwannee River Fulvic Acid
SSA	Specific surface area
TEM	Transmission electron microscope
TiO_2	Titanium dioxide
TOC	Total organic carbon
UFP	Ultra fine particles
UF	Ultra filtration
UV-vis	Ultra-Violet visible spectrometry
USEPA	United States Environment Protection Agency
%v/v	Volume concentration (volume/volume)
XRD	X-ray diffraction
μm	Micrometer being 10^{-6} m.
μg	Microgram
μg/L	Microgram per litre
ζ	Zeta potential
Z-Ave	Z-average intensity weighted translational diffusion coefficient.

1 Introduction

1.1 Chapter Summary

Nanoparticle research has increased dramatically over the past two decades, due to the ever increasing commercial use of nano-enabled products. The increasing use of nanomaterials induces the potential hazards and associated risks from their manufacture, transportation, waste disposal and management processes. As with any new chemical entering the consumer workplace, nanoparticle (NP) toxicity assessments must be conducted to determine potential risks. Previously conducted environmental toxicity assessments (ecotoxicity) using NPs (nanoecotoxicity) have seldom considered the physical and chemical (physicochemical) characteristics of test NPs in the media they are dispersed in. The findings from such studies can therefore be limiting, due to a lack of information regarding whether, how, or why the physicochemical characteristics of NPs change from pre- to post-organism exposure. Identifying any changes in NP characteristics under such conditions may help to determine if an organism or the media NPs are dispersed in, helps prevent or accentuate the associated nanoecotoxicity observed during these studies. The intention of this thesis was to investigate the environmental behaviour and potential toxicological effects associated with cerium dioxide (ceria) NPs in a range of aquatic systems by measure of their physicochemical characterisations. Nanotoxicological effects of ceria as a function of size and dose was also conducted, using freshwater algae as the test specie and the novel approach of metabolomic analysis as a tool for assessing observed toxicity.

1.2 Chapter organisation

This chapter opens with a general introduction to NPs and nanoscience along with the reasons for this research to be conducted. This chapter closes with the aims and objectives of the work conducted and the general thesis outline.

1.3 What are nanoparticles?

Natural aquatic colloids are complex mixtures of different physical, chemical, organic or inorganic (Buffle *et al*., 1998) and biological phases (Gibson *et al*., 2007) in suspension (Jullien and Botet, 1987), which play an important role in aquatic processes. Naturally occurring colloids can be considered as the nanostructures of environmental systems (Buffle, 2006) and NPs can be classed as the smallest fractions of colloids, (Baalousha and Lead, 2007). As a perspective, a nanometer (nm) is the dimension of 10^{-9} m where the diameter of an atom can be between 0.1-0.2 nm (Haken and Wolf, 2004). The behaviour NPs exhibit when dispersed in aquatic systems has been described using the Derjaguin and Landau, and Verwey and Overbeek (DLVO) theory for colloidal material, based on the attractive and repulsive forces acting upon a particle (Derjaguin and Landau, 1941; Verwey, 1947). NPs however have variable properties compared to the same chemical form at the micrometer scale, such as increased surface area and reactivity, where the DLVO theory can not always be applied. Due to the novel properties NPs display, NPs have found their way into a number of commercial and manufactured products, summarised in Table 1-1.

Table 1-1 Applications of common nanoparticles

Nanoparticle	Application	Property	Reference
Cerium dioxide	Fuel additives, catalysts, glass polishing	Improves combustion efficiency	Mullholland and Bauer, 2000
Silver	Clothing	Antibacterial properties	Silver, 2003
Zero valent iron	Ground/surface water cleaning	Breaks down chlorinated organic compounds	Phenrat *et al*., 2007; Kuzma, 2007
Titanium dioxide	Paints Sun creams Self-cleaning windows	Pigmentation/ transparency Better UV protection/ Breaks down dirt	Aitken *et al*., 2006; Kashiwada, 2006 Borm *et al*., 2006
Zinc oxide	Sunscreens and cosmetics	Scatters and absorbs ultraviolet rays	Aitken *et al*., 2006
Gold	Medical applications as vectors in tumour therapy Nano-electrics	Particles of radioactive gold isotope serve as a radiation source. Gold is a highly efficient conductor and remains free of corrosion	Klaine *et al*., 2008 Sun *et al*., 2001
Nano-encapsulated vitamins and minerals	Changing food texture and even nutritional value	Changes the way food tastes; turn red wine into white; Sieve out lactose from milk	Quintanilla-Carvajal *et al.*, 2010; Palmer, 2007
Carbon nanotubes	Sporting equipment, clothing; Space elevators	Strong and lightweight	Zhu *et al*., 2006 Lubick, 2007
Gallium selenide	Solar cells	Light absorption	Zhu *et al*., 2006
Iron	Improve MRI images of cancer tumors	Magnetic properties	Lodhia *et al*., 2010

Such NP products and technological developments include the fight and prevention of disease (Morones *et al*., 2005) improvements in pharmaceuticals (Chapman, 2006) and medicines through drug delivery systems (Garnet and Kallinteri, 2006). ICT, energy production and land remediation (Linkov *et al*., 2007) by enhanced filtration applications (Savage and Diallo, 2005) has also benefited from nanotechnology. In the biological sciences many uses of metal NPs are being explored for biosensors (Nam *et al*., 2003; Tkachenko *et al*., 2003). With the increasing use of NPs there is an increased threat to

environmental systems and organisms from potential exposure to these novel particles.

1.4 Historical relevance of nanoparticles

Particles in the nano-sized range have been present on the Earth for millions of years (Nowack and Bucheli, 2007) exposing humans and the environment throughout evolutionary history (Haasch *et al*., 2005). Although NPs have been used unknowingly for over 17,000 years in e.g. pottery and stained glass (Colomban, 2009) it was not until the appearance of the internal combustion engine, power plants and extensive burning of fossil fuels (Navarro *et al*., 2008) that NP use and associated exposure increased significantly, increasing NP risk to the environment (Biswas and Wu, 2005). Humans may therefore be directly affected by NPs through exposure to air, soil and water or indirectly by consuming plants or animals which have accumulated NPs (Figure 1-1).

Most NPs that are currently in use today have been made from transition metals, metal oxides, silicon and carbon (Dreher, 2004). More recently, NPs have attracted a lot of attention because of our increasing ability to synthesize and manipulate them (Nowack and Bucheli, 2007), giving them further unique properties for manufacture and commercial use. However they are formed, NPs appear central to many natural processes (Colvin, 2003) and must be used with some caution.

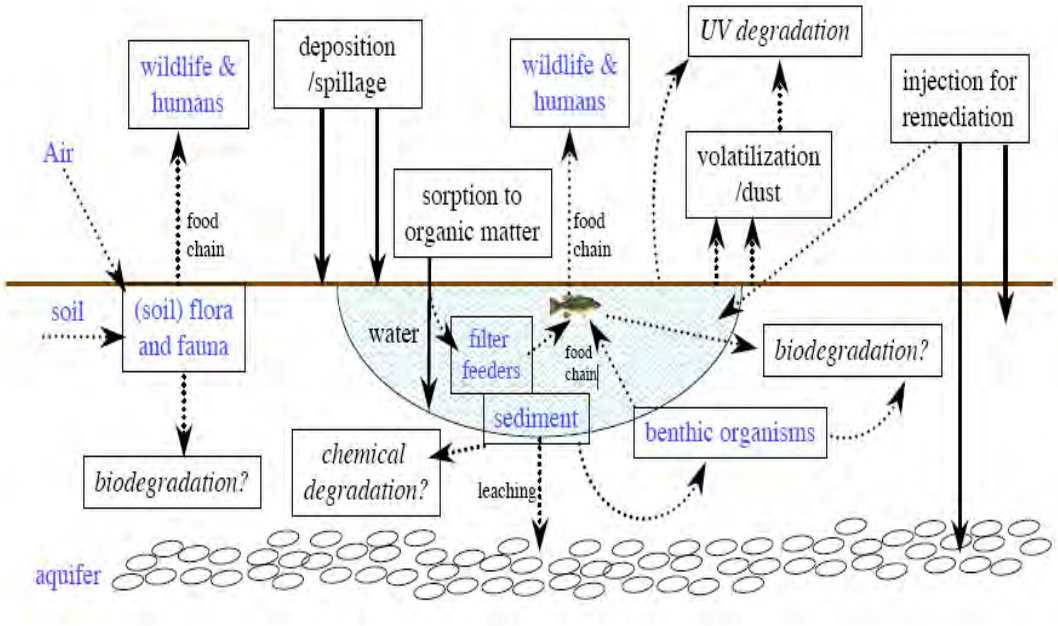

Figure 1-1 Routes of exposure, uptake and distribution of NPs in the environment
Solid lines indicate routes which have been demonstrated in the laboratory or field or which are currently in use (remediation). Italics indicate possible degradation routes, which the blue lettering indicates possible sinks and sources of NPs taken from Oberdörster *et al*., (2000).

1.5 What is nanoscience and nanotechnology?

Richard Feynman is credited as being the first person to see the potential for manipulating matter at the nano-scale (Fadeel *et al*., 2007) as first described in a famous lecture to the American Physical Society in 1959 (Park, 2007). The term 'nanotechnology' however, was first used in 1974 by a Japanese engineer, Norio Taniguchi (Fadeel *et al*., 2007) to describe precision engineering with tolerances of a micron or less (Park, 2007). Over the past decade (RSRAE, 2004) the ability to engineer, manufacture and produce materials at the nano-scale has triggered rapid product development. With increasing technological advances in e.g. electron, confocal and atomic force microscopes, the ability to observe NPs at the angstrom (Å) level and physically manipulate materials at the atomic scale

has become common place. Nanotechnology has recently been classed as the industrial revolution of the 21st Century (Bankinter, 2006). Nanoscience is the science of precisely designed engineered nanoscale materials, integrating engineering with biology, chemistry and physics (Borm *et al*., 2006). Nanotechnology provides a significant technology platform to solve problems in diverse areas as energy, water purification, food storage and therapeutics (Tinkle, 2008). Nanoscience is the ability to work at the molecular level, atom by atom, to create larger structures with fundamentally new molecular organisation, novel properties and functions (Alvarez, 2006). There is therefore an increasing commercial demand for NPs because of their wide applicability in a growing number of fields like electronics and medicine (Bali *et al*., 2006).

1.6 The need for this research

Due to their unique physical and chemical properties, NPs have raised interest in commercialisation for a variety of products. As these materials make their way into industrial and consumer products, there is the potential for their unintended introduction into the environment (Lecoanet *et al*., 2004; Brant *et al*., 2005). These discharges are likely to increase as the industry grows, yet the unknown toxicity of NPs reiterates the immense gaps in our knowledge which is leading to difficulties in risk assessment and management (Handy *et al*., 2008b) of NPs. Aquatic environments may be particularly vulnerable to NP exposure by anthropogenic and natural particle releases e.g. as effluent from industry, wastewater or rainwater runoff (Lovern *et al*., 2007).

Because of the unique characteristics exhibited by NPs, the interaction of the particle with its environment also changes which may in turn lead to an increase in observed ecotoxicological effects (Park *et al*., 2007). Characteristic variations associated with NPs may produce adverse responses in organisms (Robichaud *et al*., 2005) specifically aquatic species. The properties and behaviour therefore of individual NPs must be understood to enable a better idea of fate and behaviour of individual NPs and effects on ecotoxicity within natural environments. Understanding the environmental health and safety implications associated with exposures of NPs will help to facilitate the appropriate measures required in addressing the design, manufacture, use and disposal of NP products. This will help prevent or minimise the risk to biota and human health and prevent associated damage to the environment, (Nel *et al*., 2006).

Effective risk management prior to NP production will also offer positive opportunities for future NP use. While classical chemical compounds are routinely subjected to well-established toxicity tests prior to release to the public, no such procedures currently exist for nanomaterials (Brunner *et al*., 2006) and therefore remains to be determined (Chapman, 2006). The characterisation of commercial cerium dioxide (ceria) particles, in a range of aquatic media in the presence and absence of test species, undertaken during this thesis, underpins the required areas of work highlighted above. A further investigation into the toxicological effects of synthesized ceria NPs (nano-ceria) to environmentally

relevant freshwater algae specie, using a novel metabolomic approach of analysis, further compliments this work.

1.7 Aims and objectives

It was the rationale of this work to investigate a number of particle parameters, together with potential ecotoxicological hazards under conditions most favourable for a range of aquatic ecotoxicity test species. These organisms included the crustacean *Daphnia Magna*; the freshwater fish *Cyprinus carpio*, the tropical fish *Danio rerio* and freshwater algal specie *Pseudokirchneriella subcapitata*. Much work was conducted in collaboration with Napier University, Scotland; Exeter University, England and the Commonwealth Scientific Industrial Research Organisation (CSIRO), Australia, where indicated. Three main aims and associated objectives of this research are outlined in Table 1-2.

Table 1-2 Aims and objectives for thesis chapters
a) Chapter 5; b) Chapter 6; c) Chapter 7 aims and objectives

AIMS **A**
To determine the physicochemical characteristics of commercial ceria nanoparticles in a range of synthetic aquatic test media in the presence and absence of organisms.
Objectives
Conduct a range of analyses to adequately characterise a number of physicochemical properties of nano-ceria when dispersed in a range of ecotoxicity test media.
Compare the physicochemical characteristics of ceria NPs during exposure and none exposure assessments.

AIMS **B**
Ascertain the toxic effects associated with nano-ceria as a function of size to *Pseudokirchneriella subcapitata.*
Objectives
Determine the physicochemical characteristics of synthesized nano-ceria particles as made and in media appropriate for *P. subcapitata* tests.
Determine, where possible, the toxic effects of synthesized nano-ceria as a function of size and dose to *P. subcapitata*.

AIMS **C**
Investigate the mechanisms of toxicity from nano-ceria particles to *Pseudokirchneriella subcapitata* using metabolomic analysis.
Objectives
To develop a method for optimal metabolite extraction from *P. subcapitata*.
Determine where possible, the mechanism of synthesised nano-ceria toxicity to *P. subcapitata* as a function of size and dose.
Critically assess metabolomic use for future nano-ecotoxicity research.

1.8 Thesis structure

This thesis opens with an introduction to NP research with the associated aims and objectives of this work. Chapter 2 provides a basis for the theory relating to NP research including risks, hazards and associated properties of NPs with an emphasis on ceria particle research. The third chapter is an account of the range of analytical techniques conducted addressing the basic theory, methodologies and analytical preparation used. The fourth chapter explains the variety of laboratory methods used including the fundamental concepts of safety, waste

disposal and media preparation. Chapter 5 presents results which quantify the various characterisations of commercial ceria particles in a range of aquatic media in the presence and absence of biota undertaken collaboratively. Chapter 6 investigates the ecotoxicity associated with synthesized nano-ceria as a function of size and dose to *Pseudokirchneriella subcapitata*. Chapter 7 continues from Chapter 6 by investigating the use of a novel and potential future nanoecotoxicological tool of metabolomic analysis. The thesis closes with conclusions, evaluation and recommendations for future research using ceria NPs in Chapter 8.

2 Background

2.1 Chapter summary

This chapter begins with a summary of NP sources, properties, types and applications. This leads into the environmental considerations of NP exposure, hazard and behaviour. Detail into the chemistry, uses and associated risks of ceria particles is followed by a brief synopsis covering the broad and specifically the environmentally relevant research previously conducted on nano-ceria particles.

2.2 Nanoparticle definitions, classifications and nomenclature

2.2.1 Nomenclature

Much debate still exists regarding the nomenclature associated with nanoscience, nanotechnology and NPs, resulting in many documents being published. Such documents include the Royal Commission on Environmental Pollution (RCEP, 2008); United States Environmental Protection Agency (USEPA, 2007) and the American Society for Testing and Materials, (ASTM, 2007). NP definitions from such documents include;

"…a solid entity with size from approximately 1 nm to 100 nm in at least two dimensions that has been produced by a manufacturing process".

The British Standards Institution, (BSI, 2007; pp4);

"*…nanomaterials as those which have structured components with at least one dimension less than 100nm*".

The Royal Society and Royal Academy of Engineering Nanotechnology (RSRAEN, 2004; pp7), and

"…*when describing a nanomaterial it is important to describe not only the mean particle size but also the size of the primary particles…information on the presence of agglomerates/aggregates should be presented*."

Scientific Committee on Emerging and Newly Identified Health Risks, (SCENIHR, 2009; pp7).

Although a variety of terms are used for NPs, the shear nature of a given particle (e.g. size, shape and associated toxicity) may aid in determining their terminology (Section 2.2.3). The sources of NPs are also varied from natural, anthropogenic and manufactured processes with their associated impacts being quite diverse. Such diversity observed with NP effects further complicates the terminology and therefore the definitions currently used for NPs. A particles dimension must therefore be determined by the individual, prior to NP studies, for future reference.

2.2.2 Natural, anthropogenic and manufactured nanoparticles

Table 2-1 offers an overview of the known anthropogenic and natural sources of NPs. NPs in air are traditionally referred to as ultrafine particles (UFPs) while in soil and water they are termed colloids, (Klaine *et al*., 2008), all with a size distribution between 1 nm to 1 µm.

Table 2-1 Sources of natural and anthropogenic nanoparticles

Classification		Source	Reference
None-Anthropogenic	Natural	Forest fires and Volcanoes; Atmospheric, Sea salt; Pollen; Viruses; Hydrothermal systems; Soil erosion.	Oberdörster *et al*., 2005; Park 2007; Navarro *et al*., 2008 Haasch *et al*., 2005 Luther and Rickard 2003, Handy *et al*., 2008a.
Anthropogenic	Incidental	Internal combustion engines, Power plants, Incinerators, Frying	Oberdörster *et al*., 2005
Anthropogenic	Engineered/ manufactured (Intentional)	Controlled particle shape and size to deliver metal, metal oxides, semi-conductors, carbon and polymers for commercial applications. Drug delivery systems and water treatment technologies.	Oberdörster *et al*., 2005 Handy, 2007

2.2.2.1 Natural nanoparticles

Natural NPs can be found in waters, soils and sediments. Natural NPs can act as precursors for the formation of larger particles in the atmosphere, influencing global climate, atmospheric chemistry and transport of pollutants (Nowack and Bucheli, 2007). Natural biogeochemical processes and weathering of minerals such as iron oxides and silicates produce nanoscale colloids, (Masciangioli and Zhang, 2003) which may also have special properties. Nano-scale colloids can be important in the fate, transport, transformation and bioavailability of other environmentally harmful substances such as chemical fertilisers and nutrients.

2.2.2.2 Incidental nanoparticles

Incidental NPs (INPs) are generated in an uncontrolled manner and are usually physically and chemically heterogeneous, (Schulte and Salamanca-Buentello, 2007). INPs are largely derived from anthropogenic sources, created as a result of action by man e.g. from grinding of primary or secondary minerals and through combustion processes.

2.2.2.3 Intentional nanoparticles

Manufactured NPs (MNPs) are often termed engineered NPs (ENPs), which are particles that are produced by man due to the particles specific nano-technological properties. MNPs, such as those commercially purchased and used during this study, are defined as material with one dimension between 1 nm and 100 nm in size. MNPs have been synthesized or artificially manipulated for a specific purpose and may be found in various shapes (Park, 2007), sizes and with a variety of surface chemistries. MNPs can be made of single elements like carbon or silver or a mixture of elements or molecules (Joner *et al*., 2008). MNPs can be classified according to their chemical composition and properties and are designed with very specific physicochemical properties for use as electrical, thermal, mechanical and imaging industries (Dreher, 2004). MNPs can be produced by a huge range of procedures including top-down and bottom-up strategies (Ju-Nam and Lead, 2008). A “top down” approach is where macroscopic material is broken down to the nanoscale. The “bottom up” approach is where individual atoms or molecules are coaxed or self-assembled

into NPs (Kuzma, 2007). MNPs are used to produce materials such as nano-wires for nano-scale circuits, hi-tech waterproof clothing, medical imaging and instrument coatings (Handy, 2007). MNPs are also being used in personal-care products such as cosmetics and sunscreens and may therefore enter the environment on a continual basis from the discharge of such consumer products.

2.2.3 Definitions

It is well-known that NPs in aquatic systems do not retain their individual sizes, resulting in agglomerates of NPs. These can be larger than 100 nm in diameter resulting in the 100 nm classification being quite arbitrary (Borm *et al*., 2006). The term 'nano' should perhaps also infer a material within a dimension that offers unique properties compared with bulk material of the same chemical compound. Engineered inorganic metal and metal oxide NPs have therefore been re-classified as particles below 20–30 nm due to their novel size-dependent properties, rather than their actual particle size, by Auffan *et al*., (2009). For the purpose of this thesis the term 'nanoparticle' is defined as an individual particle between 1-100 nm or an aggregated form of the same material from which was originally derived from a diameter between 1-100 nm. These dimensions are initially identified from the manufacturers of the commercially produced powdered particles used during this study or defined from characterisations conducted following particle synthesis.

2.3 Types and uses of nanoparticles

Although this thesis focuses on the metal oxide particle of ceria, it was considered important to briefly review the variety of NPs in use as research materials today.

2.3.1 Carbon

One of the first documented classes of nanomaterials originated with the 1985 discovery of the 60-carbon atom hollow fullerene sphere, by Kroto *et al*., (1985), referred to as the Buckminsterfullerene and later as the Buckyball. Fullerenes can be spherical, ellipsoid or cylindrical [Ajie *et al*., (1990); Mowrey *et al*., (1991)] in shape and are stronger than steel but very flexible and lightweight (Borm *et al*., 2006).

2.3.1.1 Graphene

Research using nano-carbon compounds lead to the recent development of graphene. The Nobel Prize in Physics 2010 (Nobel Prize, 2010) was awarded jointly to Andre Geim and Konstantin Novoselov for their;

"…*groundbreaking experiments regarding the two-dimensional (2D) material, graphene*".

The perfect structure of graphene, being a million times thinner than paper, stronger than diamond and more conductive than copper (Chodos, 2009) have many potential future applications.

2.3.2 Inorganic NPs

2.3.2.1 Quantum dots

NPs of metals, metal oxides and transition-metal oxides have generated vast interest in recent years. Inorganic NPs include quantum dots (QDs), or artificial atoms, which are small (2-10 nm) assemblies of metal, metal oxide or semiconductor materials with novel electronic, optical, magnetic and catalytic properties (Aitken *et al*., 2006). QDs may have a reactive core made out of metal or semiconductor such as cadmium selenide, cadmium telluride, indium phosphide or zinc selenide, which controls its optical properties (Klaine *et al*., 2008).

2.3.2.2 Metal nanoparticles

Metal NPs have long been used in a number of applications (Table 2-2) most commonly silver, gold and iron. Metal sulphide NPs also exist in the environment through natural processes including abiotic and biologically-mediated mineral precipitation.

2.3.2.3 Metal oxide nanoparticles

Metal oxides, such as titanium dioxide (TiO_2) and ceria form a class of special interest among manufactured inorganic NPs. This is due to the unique properties such as being photo- and catalytic-reactive (Yuan *et al*., 2008). Metal oxides are also important components of natural aqueous systems.

2.3.3 Uses of nanoparticles

Table 2-2 Uses of commonly manufactured nanoparticles

Particle	Uses	Reference
Fullerenes and Buckyballs	Cosmetics and photoconductors	Loutfy *et al*., 2002
	Optics, electronic materials and superconductors.	Alargova *et al*., 2001
Buckminsterfullerene C_{60}	Led to the advance of nanotechnology and in the associated nanotoxicity investigations observed today.	Tong *et al*., 2007
Graphene	Sensitive sensors that could register pollution at the molecular level. Transparent touch screens, light panels and solar cells. Maybe used to convert plastics into electronic conductors for future applications.	Novoselov *et al*., 2004
QDs	Medical imaging and sensors.	Aitken *et al*., 2006
Silver	Microbial at low concentrations and used to treat burns, wound and ulcers and are used to coat catheters.	Silver, 2003
	Clothing and semiconductor industries.	Tillman, 2004
	Photosensitive components and catalysts.	Liu *et al*., 2007
	Dental resin composites.	Herrera *et al*., 2001
	Cosmetics.	Jeon *et al*., 2003
Zero-valent iron	Treatment of contaminated groundwater.	Phenrat *et al*., 2007
Gold	Drug delivery systems, catalysts and more recently in electrons in flexible conducting inks and films.	Klaine *et al*., 2008

2.4 Nanoparticle properties and environmental effects

A range of properties makes MNPs quite different from the bulk material of the same chemical composition. Such properties include high tensile strength, rapid diffusion, high elastic limit and heat tolerances, (Thill *et al*., 2006). MNPs can exhibit high chemical stability, hydrophobic or hydrophilic properties, (Thill *et al*., 2006), ultra-violet light blocking capability and antimicrobial activity (Kashiwada,

2006) compared to the same chemical in the bulk form. A range of NP characteristics including particle size; shape; surface charge and associated changes in bond lengths, bond angles and vacancies (Wigginton *et al*., 2007), surface coatings; crystal structure; dissolution and aggregation behaviour for example, can all affect the fate, transport, bioaccumulation and particle behaviour in aquatic systems and thus to comparative (nano)ecotoxicity studies. The following is a short account of some of the more commonly applied NP properties used to determine NP behaviour and associated risk during nanoecotoxicity studies.

2.4.1 Specific surface area

NPs have a much greater specific surface area (SSA) than the same mass of materials at the micro-scale (Aitken *et al*., 2006) which increases the proportion of atoms or molecules which are distributed on the surface, rather than in the interior of the material (Park *et al*., 2007; Ju-Nam and Lead, 2008). As Figure 2-1 indicates, as the size of the particle decreases, the SSA exposed to the environment increases. Increasing the SSA increases the surface free energy (Zhang *et al*., 2003) and abundant reactive sites on the surface of NPs (Navarro *et al*., 2008). Increased SSA may (Hansen *et al*., 2006) or may not (Hsiao and Huang, 2011) increase the cytotoxic mechanisms compared against particle size alone. A higher surface energy can also make NPs interact (Borm *et al*., 2006) and agglomerate, potentially reducing the NPs bioavailability.

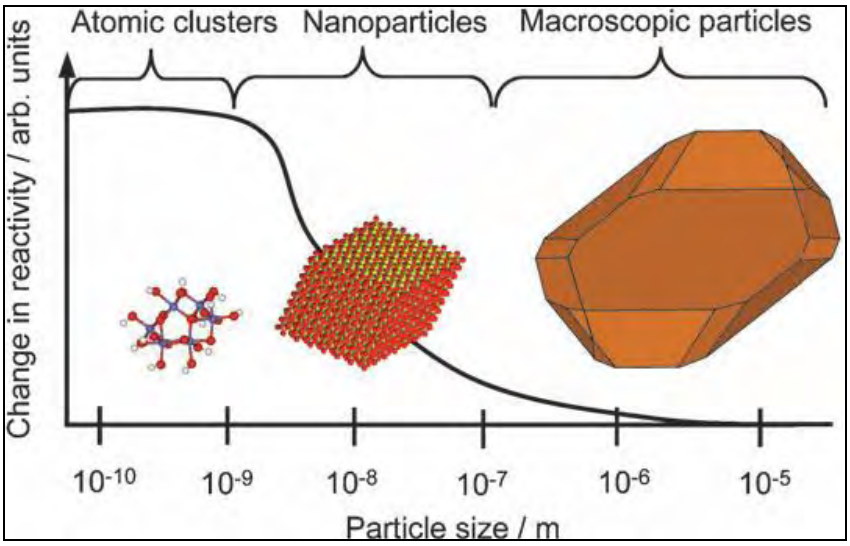

Figure 2-1 Generalised size-dependent reactivity of a material.
As the particle transitions from macroscopic (bulk-like) to atomic, (nano-like) reactivity can increase or decrease depending on the material and the chemical reaction involved (Wigginton *et al.*, 2007).

2.4.2 Size

The property of particles can alter depending upon the particle size (Hoet *et al*., 2004). When the dimensions of a solid material become very small, the physical (melting point, electrical conductivity), and chemical reactivity due to the change in SSA can become very different from those of the same material in a bulk form, (Borm *et al*., 2006; Madden and Hochella, 2005). These changes in physicochemical characteristics due to NP size can cause increased toxicological effects to exposed aquatic biota and cells compared against the bulk particles of the same chemical form.

2.4.3 Shape

Shape changes can also change colloid stability, due to quantum confinement effects (Qu *et al*., 2004) and must be taken into account when particles are

produced. Structural deviations in NPs relative to bulk materials are not well understood (Gilbert *et al*., 2004) and theoretical models of NPs generally assume they have bulk-like interior structures. Variation in shape of a particular NP may also have effects associated with toxicity (Tarantola *et al*., 2010). Different NP shapes may increase interactions to organisms (Ispas *et al*., 2009) and organic materials (Bar-llan *et al*., 2009) allowing particles to potentially become more bioavailable.

2.4.4 Aggregation behaviour and DLVO theory

Particles in aquatic dispersions may, under some circumstances, collide with each other as the kinetic energy, provided mainly from Brownian motion, (O'Melia, 1980) is sufficient enough to overcome repulsive forces acting on them (Stumm and Morgan, 1996). This collision allows particles to attach to each other leading to agglomeration of some particles, or aggregation of particles, which is a more permanent attached state. The collision of NPs can be described theoretically following the two mathematical models presented by the DLVO theory.

2.4.4.1 DLVO Theory

The DLVO theory attempts to calculate the total interaction energy (V_T) by identifying the interactions between particles in close proximity (Stumm and Morgan, 1996) using the electrostatic attractive van der Waals forces (Balnois *et al*., 2007) (V_A), and the repulsive (V_R) interactions of particles (Equation 2-1).

The attractive van der Waals forces are weak forces which only dominate at short distance as expressed in Equation 2-2, (Wamkam *et al*., 2011), where A is the Hamaker constant (J) and D is the particle separation (m).

Equation 2-1 Total interaction energy
Taken from Wamkam *et al.*, (2011)

$$V_T = V_A + V_R$$

Equation 2-2 Attractive van der Waals forces

$$V_A = \frac{-A}{(12\pi D^2)}.$$

The repulsive forces come from the electric surface charge, which is influenced by the paticles double layer, expressed as Equation 2-3 where *a* is the particle radius (m), ε is the solvent solubility, ζ is the zeta potential (mV) and κ is a function of the ionic composition (κ^{-1} is the length of the electric double layer).

Equation 2-3 Repulsive forces
Taken from Wamkam *et al.*, (2011)

$$V_R = 2\pi\varepsilon a\zeta^2 \exp(-\kappa D)$$

2.4.4.2 Stability of colloidal dispersions

It is predicted by the DLVO theory (Figure 2-2a) that for low ionic strength solutions the distance at which the effects of the charged particle surfaces are felt is large enough that there remains a sufficient energy barrier to maintain stability.

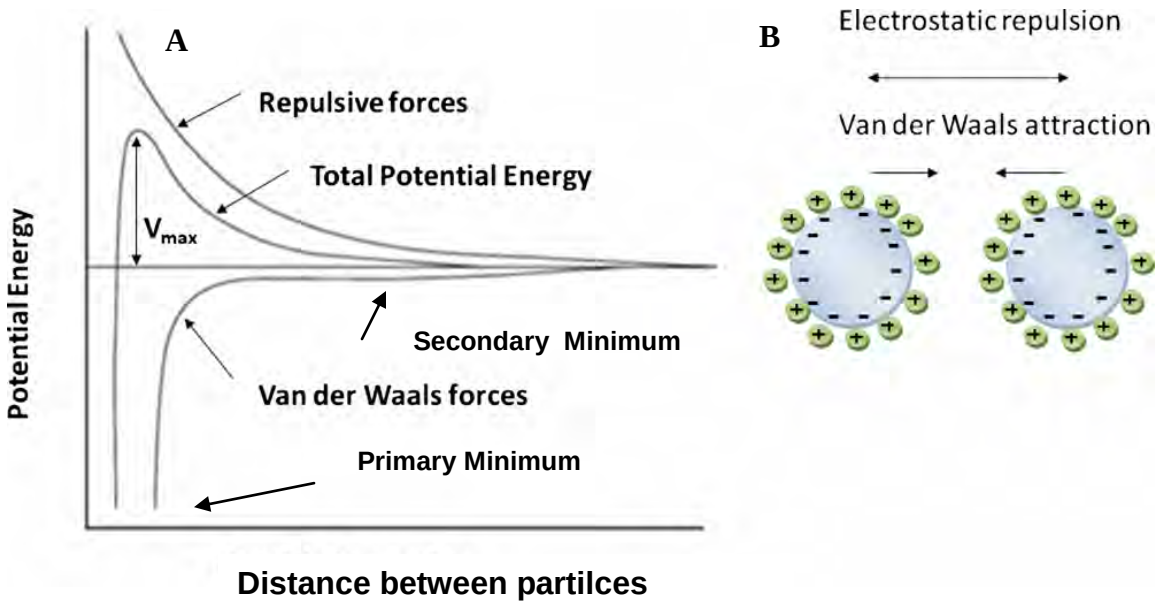

Figure 2-2 The DLVO theory
a) DLVO theory in graphical form. b) Repulsive and attractive forces acting on a particle. Taken from Wamkam *et al.*, (2011).

As the ionic strength increases the energy barrier becomes smaller and the suspension is predicted as being very unstable. The attachment within the primary energy minimum is effectively irreversible. In some cases a secondary energy minimum develops when particle attachment is reversible by mechanical action or by changing the ionic strength (or pH) of the solution. In situations involving high salt concentrations, there is a possibility of a secondary minimum where a much weaker and potentially reversible adhesion between particles exists (Wamkam *et al*., 2011). These weak flocs (agglomerated solid matter) are sufficiently stable not to be broken up by Brownian motion, but may dissociate under an externally applied force such as sonication. Attractive forces are primarily obtained from a particles surface charge, which defines the electrical field around each particle (Buffle *et al*., 1998).

The repulsive forces are primarily from the double layers (Jiang *et al*., 2009) surrounding a particle (Figure 2-2b). If the particles collide with sufficient energy to overcome the repulsive barrier, the attractive force will pull them into contact where they adhere strongly and irreversibly together. Therefore if the particles have a sufficiently high repulsion, the dispersion will resist flocculation and the colloidal system will be stable. However if a repulsion mechanism does not exist then flocculation or coagulation will eventually take place. With NPs, if static charges are not strong enough, the van der Waals forces will be greater allowing aggregation to occur, resulting in sedimentation of the particle suspension. Particle aggregation can be prevented through electrostatic or steric manipulations.

2.4.4.3 Controlling particle stability

Electrostatic changes on the particles surface can be conducted by increasing the particle surface charge through pH manipulation or changing the ionic strength of a solution. The point at which the particles calculated charge is zero (Pzc) is the state at which particle aggregation will be at its greatest, due to reduced particle repulsion. Steric manipulation of a particles coating may be engineered using a ligand e.g. polymers. Particle coatings form a double electric layer leading to functionalised particle surface changes which increase the repulsion forces acting between particles of the same chemical form. The thickness of the electric double layer (EDL) is a function of solution ionic strength, with an increase in ionic strength leading to a decrease in double layer thickness

(Jiang *et al*., 2009). As the EDL repulsion is lowered by pH or ionic strength changes, particles can approach and adhere to each other, leading to flocculation (Eggleston and Jordan, 1998).

2.4.4.4 Limitations of the DLVO theory

The DLVO can be used to quantitatively estimate the energy of a colloidal system. The DLVO theory however has some limitations with NP dispersion estimations as NP dispersions are somewhat variable in characteristics compared to bulk particle dispersions. For example, the DLVO theory is only applicable if there is no interference with diffusive or attractive forces (Kallay and Žalac, 2002). Also NPs generally do not show electrostatic stabilisation (Kallay and Žalac, 2002) and coagulate with lower repulsive forces much faster than larger particles, (Leppard, 1995). In the course of aggregation, NPs may exhibit a complete overlap of the diffuse layers, further reducing the ability to apply the common DLVO theory. The DLVO theory also does not include the effects of particle shape, charge, heterogeneity and surface roughness which may also influence the collision efficiency of NPs (Elimelech *et al*., 1995; Bhattacharjee *et al*., 2000). The DLVO theory is also not effective in describing effects associated with dilute dispersions with low salt concentrations (Ise and Sogami, 2005) often used in some characterisation and nano toxicity studies.

2.5 Nanoparticles in the environment

With an estimated production of MNPs at 2000 tons in 2004, expected to increase to 58,000 tons in 2011 to 2020 (Maynard, 2006 pp.10), MNPs are likely to enter the environment by accidental manufacturing effluent or from spillage during shipping and handling (Oberdörster *et al*., 2005). MNPs may leak out of a material or be worn off over the period of its use and may therefore reach the environment through landfills and other methods of disposal. With all this in mind, it is alarming to know that there is currently a limited knowledge of toxic effects on wildlife (Handy, 2007), drinking water and food chain disruption of these materials. Previous research has shown NPs of the same chemical form of relatively benign bulk materials, produce severe toxic effects at relatively low exposure concentrations, to a range of biota. For example, Aruoja *et al*., (2009) found bulk TiO_2 were less toxic (EC_{50} 35.9 mg Ti/l) than the equivalent nano formulation (EC_{50} 5.83 mg Ti/l) to *Pseudokirchneriella subcapitata*. Understanding the environmental impact of NPs to a range of taxonomical groups is therefore vital to ensure any environmental impact will be avoided. Environmental risk of NPs can be categorised as Equation 2-4.

Equation 2-4 Risk calculation

Risk = exposure X hazard

The following is a short account describing an environmental risk model of NPs entering the natural aqueous environment focussing on exposure, hazard, toxicity and risk.

2.5.1 Exposures of nanoparticles

Exposure can be defined as the concentration of a substance in a (aquatic) media multiplied by the duration of contact (Lauwerys, 1998). Although there is an increased production of MNPs in commercial products, causing an increase in the potential release of MNPs to environmental systems, the concentrations of this release maybe relativity low. With variable pathways and transportation routes within environmental systems, (Figure 1-1) particle aggregation and changes in particle chemistry may reduce the actual exposure experienced by biota.

The uptake and bioaccumulation of particles from environmental systems may also vary specie to specie. NPs may directly or indirectly affect ecosystem functions like primary and secondary production although the actual environmental concentrations present in aquatic systems are still unclear (Griffitt *et al*., 2008). The emerging ecotoxicological literature reviewed [Klaine, (2009); Scown *et al*., (2010); Bhatt and Tripathi, (2010)] however, shows that toxic effects on fish and invertebrates can often occur at relatively low concentrations of NPs. This poses a real threat to NP manufacturing and waste disposal issues in the future.

2.5.2 Cellular pathways of nanoparticles

There are three conceptualised entry routes to describe the potential pathways of NPs into cells, as shown in Figure 2-3. These pathways include the direct

diffusion of NPs across the cell wall/membrane, the process of endocytosis and movement through the cell via ion channels.

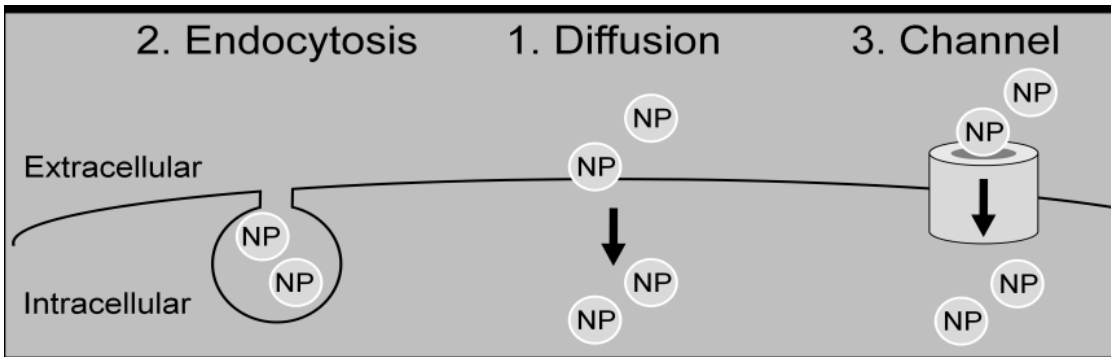

Figure 2-3. Potential mechanisms of nanoparticle entry into cells. 1, Direct diffusion across a cell, 2, endocytosis mechanism of the cell and 3, ion channelling routes for transporting NPs. Taken from Rapopport *et al.*, (2011).

Diffusion is the movement of molecules (e.g. CO_2, H_2O) from a region of high concentration to a region in which they are less concentrated. Diffusion depends on the motion of the molecules and continues until the system in which the molecules are found reaches a state of equilibrium. A cell may also engulf useful molecules such as proteins which are too large to pass through the plasma or cell membrane in a process is called endocytosis. NPs may get coated by proteins which are identified by the cell as desirable and may subsequently be taken into the cell through this mechanism of endocytosis. The third possible route of NP entry into a cell is through ion channels. Ion channels are the cell's membrane proteins that give rise to selective permeability (Purves *et al.,* 2001). Ion channels have pores that permit particular ions to cross the neuronal membrane and mediate the flow of ions across the plasma membrane of cells. There are different types of ion channels operate like a gate, opened or closing

by a chemical signal, (Purves *et al.,* 2001). Ions may dissolve from the surface of a NP due to the high reactivity of the NPs surface compared to the bulk material. Such ions may therefore enter the cell through this ion transportation mechanism.

The physicochemical characteristics of a NP can affect the ability of the NP to enter the cell by these identified pathways. Factors affecting how fast a particle will diffuse including temperature, size and variety of particle type in the system and associated surface charges on the NP along with the nature of the material that the molecules are moving through, will affect the rate and ability of the particle to diffuse. The NPs physical parameters of size, dissolution rates and binding capabilities will also affect the cell's ability to engulf the particles. NPs may have the ability to attract and bind with other materials to coat and therefore may be "hidden" and be unidentifiable by the cell's bilayer. This may allow the particle to enter the cell by endocytosis when it ordinarily would be avoided. The small pore size of a few Å for ion-channelling transportation of NPs suggest that only the smallest of particles may enter the cell by this mechanism. Ions however, released from the surface of a NP during dissolution may enter the cell via ion channelling routes. Therefore dissolution rates are vital to be determined when identifying and understanding the fate, behaviour and transportation of NPs during cellular and organism exposures.

2.5.3 Hazard and toxicity

Hazard is the potential to cause harm and is an intrinsic property of a material (Lauwerys, 1998). Some of the knowledge of colloidal species has been transferred to the understanding behind the potential hazards associated with NPs, although systematic trends of colloidal systems are often not observed with NP interactions. There is emerging literature reporting the toxic effects of MNPs in organisms, although the mechanism of exposure and effects are still poorly understood (Handy *et al*., 2008a). The toxicity caused by some NP dispersions often show few trends. Particle characteristics of NPs including crystallinity, shape, SSA as well as dose, may be attributed to the toxicity observed from NP exposures assessments although no actual mechanisms has been deemed responsible for toxic effects observed from these studies.

2.5.4 Nanoecotoxicity

Ecotoxicity involves the identification of a chemicals risk to the environment by measuring the effects of that chemical on crustaceans, algae, aquatic plants (UNECE, 2004), fish, terrestrial plants (USEPA, 2007) and other environmental communities. Research encompassing UFPs by Oberdörster *et al*., (2004) largely laid the foundation for the emerging field of nanoecotoxicology. From such previous efforts however, a paradigm has emerged suggesting the cytotoxic effects associated with NP exposures to cells and aquatic organisms is due in large to oxidative stress (OS) discussed below. OS from C_{60} exposures for example was highlighted by Oberdörster *et al*., (2006) during exposures to *D.*

magna, and predicted as the mechanism of toxicity observed during exposures to *D. rerio* by Usenko *et al*., (2008) and also shown during exposures to *C. carpio* by Zhu *et al*., (2008), all with little or no evidence supporting OS production. With increasing technological advances in instrumentation to measure interactions of NPs to organisms, more recent publications have identified OS as true effects of some NP exposure to organisms through hydroxyl radical (OH) generation (Reeves *et al*., 2008).

Opposing the negative toxic effects associated with NP exposure studies is observed with research investigating transportation (Hassellöv and Kammer, 2008), bioavailability (Lee *et al*., 2008), aggregation and contaminant speciation (Kammer *et al*., 2005) of NPs in aquatic systems. These studies offer evidence of reduced bioavailability of NPs due to their specific behaviour and characteristics, under environmental conditions. Particular behavioural characteristics exhibited by NPs may reduce the exposure experienced by biota, regardless of initial NP concentrations being released. The mobility of ceria NPs for example, has been investigated by Thill *et al*., (2006) who concluded NPs as being highly mobile and rapidly transported in the environment or inside the body. In contradiction to this however, Borm *et al*., (2006) suggested other NPs do not move far in environmental conditions due to adsorption and immobilisation. Both reports were published following various preparation techniques and the use of different particles. Lecoanet *et al*., (2004) showed transportation of NPs will vary depending upon the particle type, with fullerenes

predicted to travel up to 10 m through sand aquifers, posing a real threat for the commercial use of fullerenes in the future. The toxicity of NPs therefore differs with particle type and specifically with particle preparation (Lovern *et al*., 2007), making it difficult to compare results from such research. Consumers of products containing NPs may become sceptical towards potential hazard of NPs as the dissemination of relevant information is offered. C_{60} for example has been found to be either harmful (Oberdörster *et al*., 2006), neutral (Jia *et al*., 2005) or have no significant (Robichaud *et al*., 2005) biological consequences under exposure conditions. C_{60} suspensions have been shown to be toxic to human cells (Sayes *et al*., 2004), toxic to bacteria (Lyon *et al*., 2006) a danger to fathead minnows (Zhu *et al*., 2006) and a danger to zebrafish embryos (Usenko *et al*., 2008). There is evidence to suggest NPs can penetrate deeply into the lung (Nemmar *et al*., 2001) where their large numbers of particles overwhelm defensive mechanisms.

2.5.4.1 Oxidative stress

The possible mechanisms for cytotoxicity observed with NP exposures to cells maybe described using Figure 2-4. Changes associated with the surface properties of NPs compared with their bulk counterparts may lead to toxicity observed due to the interaction of electron donor or acceptor active-sites with molecular oxygen (O_2). The subsequent formation of the superoxide radical (O_2^-), can generate reactive oxygen species (ROS) as described extensively in the literature. Under conditions of excess ROS production, OS occurs in cells. This is

essentially referred to as a state in which glutathione (a produced antioxidant) is depleted while oxidised glutathione accumulates (Nel *et al.*, 2006) by creating free oxygen radicals ($O2^-$). The outcome of this can result in damage to DNA. Carbon nanotubes for example have been shown to bind to DNA (Zhao *et al.*, 2005) which could either induce cancerous cells from cellular nucleotide mutations or ultimately cell death either from cell membrane rupture or mitochondrial damage (Li *et al.*, 2003).

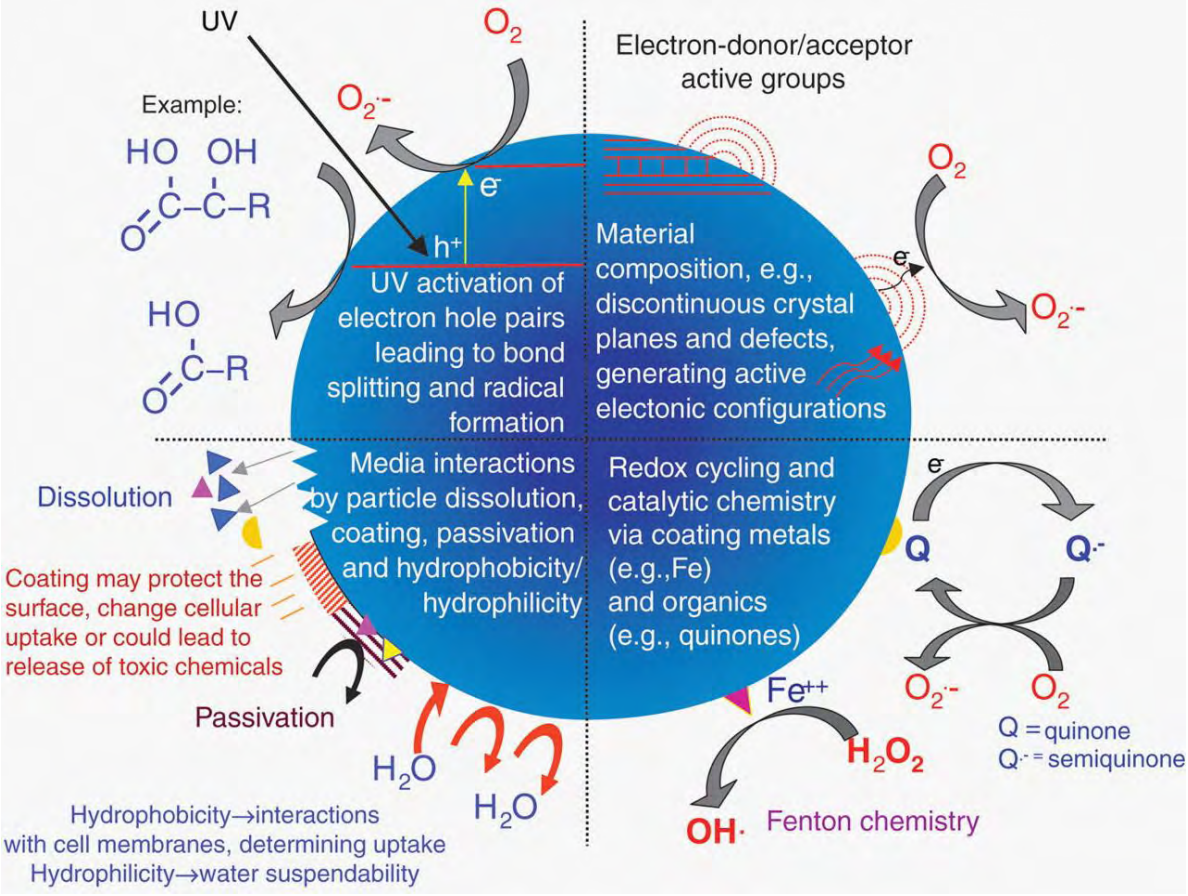

Figure 2-4 Possible mechanisms by which nanomaterials interact with biological tissue. Examples illustrate the importance of material composition, electronic structure, bonded surface species, surface coatings and solubility and the contribution of interactions with other environmental factors (e.g. UV activation). Taken from Nel *et al.*, (2006).

2.5.4.1.1 Measuring oxidative stress

Indicators of OS often include measuring total ROS, reduced glutathione levels, and increased malondialdehyde (indicator of lipid peroxidation) and lactate dehydrogenase (indicator of cell membrane damage) levels (Weisheng *et al*., 2006). These can be quantitatively assessed using a range of techniques and assays. Reduced glutathione levels for example can be determined by spectrofluorometric measurements of *o*-phthalaldehyde which reacts with reduced glutathione to produce a strong fluorescent intensity (Jia *et al*., 2010). Increase production of malondialdehyde can be measured by determining the associated thiobarbituric acid-reactive substances, (TBARS assay) which is often measured fluorometrically. The lactate dehydrogenase assay measures the reaction velocity as a decrease in absorbance at 340 nm, resulting from the oxidation of NADH.

Other indicators of OS can be measured by the aactivities of antioxidant enzymes such as superoxide dismutase (SOD). The SOD assay is measured spectrophotometrically by the formazan produced during SOD production. The measured activity of the antioxidant enzymes catalase can also be measured spectrophotometrically by the rate of H_2O_2 decomposition during a reaction (Kakkar *et al*., 1998). Although OS from NP exposures is often made from the determination of ROS, stress can be caused by other environmental factors (Choi and Hu 2008) including heat, drought and flood tolerances. Therefore, results from multiple tests are also important when assessing NP toxicity.

2.5.4.2 Toxicological studies

Data from toxicological studies will refer to the concentrations at which the chemical shows inhibitory growth, by using effective concentrations (EC) and high, low and no observable toxic effect concentrations. These measurements allow the regulatory authorities to support the registration and/or approval of new chemical products. Tests can be specific for particular effects e.g. unknown chronic effects to new substances. Acute toxicity tests are often conducted first, to identify likely biological outcomes from a short exposure. Sub-chronic tests help to determine the effects from biota when exposed to substances over several weeks, where chronic toxicity tests offer an insight into an organism's behaviour when exposed to a substance for a long period of time.

2.5.4.2.1 Effective Concentration

The EC_x estimations should be considered as the preferred type of analysis for toxicity assessments. The EC_x can be applied at any exposure period to show an organisms effect. For example, the EC_{50} is the concentration of a pollutant at which 50% of the test specie display non-lethal effects, (Singleton, 1989) compared against the control. The EC_x value however differs depending upon exposure time, species, contaminant and other biological factors.

2.5.4.2.2 No and low observable effective concentration

The NOEC (no observable effective concentration) is defined as the highest tested concentration that gives no significant deviation from a control without the

toxicant (Shieh *et al*., 2001) with respect to the effect that is studied. The LOEC (lowest observable effective concentration) is the lowest concentration at which a toxicant causes a significant growth effect compared against the growth of the control in a given system. The LOEC and consequently the NOEC have several disadvantages as summary measurements. The LOEC and NOEC are dependent on the test concentrations used and no statement of precision can be obtained for them (OECD, 2002).

2.5.4.2.3 PEC/PNEC

The predicted environmental concentration (PEC) is based on models for the degradation or distribution of a substance in the environment (between water, air and solids) using physicochemical and biodegradation data (DCS, 2011). The predicted no effect concentration (PNEC) is based on environmental effect data, such as toxicity to fish, Daphnia or algae and is determined by applying a safety factor (DCS, 2011) for nanoecotoxicological studies. PNEC values are typically gained from toxicological studies where the expected concentrations have been extrapolated to the point at which there is no adverse effect on organisms. For acute studies for example, the safety factor of 1000 is applied divisible by the EC_{50} value (Table 2-3). The ratio of PEC/ PNEC can be used as an indicator of risk, allowing risk to be quantitatively labelled (Table 2-4). If the PEC/PNEC ratio is <1, risk can be considered low (Mueller and Nowack, 2008). A PEC/PNEC ratio >100 suggests the risk of that substance needs reducing immediately.

Table 2-3 Safety factors for PEC/PNEC estimations

Toxicity test	Term (d/example)	Division made
Acute	Short (4 d fish)	EC_{50} / 1000
Sub-acute	Medium (21 d fish)	EC_{50} / 100
Chronic	Long (pond work)	EC_{50} / 100

Table 2-4 PEC/PNEC ratio values
Taken from DCS, (2011).

PEC/PNEC value	Suggested outcomes
<1	No immediate concern
1-10	Of concern if supply volumes increase
10-100	Further data required
>100	Reduce risk immediately

2.5.5 Risk

Risks, unlike hazards, can be managed and minimised. For example, a hazardous material poses low risk if the chances of exposure are low (Lauwerys, 1998). Risk also considers the magnitude and frequency of the toxicant dose that might be received by an organism. If the dose is low, or the discharge infrequent, exposure will be reduced and the risk of the toxicant will be lowered. For NPs to present a risk, there must be a potential for exposure and a hazard which results after exposure (Wiesner *et al*., 2006) e.g. toxicity.

Natural NPs have always been present in the environment and in higher concentrations compared with likely concentrations of MNPs (Nowak and Bucheli, 2007). The apparent risk from MNPs however, comes not from their expected release concentrations but from their novel characteristics (Ju-Nam and Lead, 2008). Risk of NPs in aquatic systems is poorly expressed and is

essentially unknown, increasing the concern for environmental systems. Results from nanoecotoxicological studies show that certain NPs have effects on organisms under environmental conditions, although these effects are mostly at elevated concentrations. The assessment of risk associated with aquatic species under NP exposures is therefore one of the major concerns of environmental research.

Quantifying the human health risks associated with a material requires answers to many questions, as identified by Maynard, (2009) as;

'How can the material enter a (organism/cellular) body'?

'Where does it go'?

'How does it change once it gets to a particular location'? And

"What is the human exposure from the environment"?

Understanding environmental risk of NPs therefore requires understanding into the exposure, toxicity, composition, dispersion, fate, transportation and behaviour of a NP under a range of conditions. To ensure the successful and continued application of nano-enabled products, there requires an active exchange of information to consumers, the general public and across the scientific community regarding the safety and potential toxic effects of NPs.

2.6 Benefits of nanoparticles

With some literature often focusing towards the negative effects observed from biological interactions of NPs, the use and therefore the benefits of NPs can often be neglected. For example, NPs have been found to prolong the life of brain cells (Rzigalinski, 2006), and gold MNPs are being developed for the used as drug delivery systems (Birnwar *et al*., 2011). The same inhalation and transport properties identified as negative NP properties can allow for rapidly delivery of medicines through the lungs (Chow *et al*., 2005). Ceria for example is being exploited as a diesel fuel by Oxonica (2003; 2005) due to its redox capabilities, reducing particulates from fuel combustion processes. Information regarding NP characteristics and behaviours therefore can be used as positive outcomes to further NP research and development. NPs have also been found to be transported through the bloodstream or lymphatic system to vital organs (Oberdörster *et al*., 2004) which can in turn be beneficial for medical applications. Therefore, unless the risk associated with NPs are understood and carefully managed, the potential benefits of this technology could be needlessly undermined due to public opinion, as observed during the genetically modified food debate (Gimbert *et al*., 2007).

2.7 Reason for choosing nano-ceria to study

Nano-ceria is being manufactured for current and future use in a number of commercial and industrial applications (Table 1-1). Nano-ceria may be persistent in biological and aquatic systems, due to its low solubility and may provoke a

range of long-term effects involving carcinogenic, mutagenic or teratogenic influences on specific aquatic organisms (Brunner *et al*., 2006). Ceria NPs are therefore currently one of 14 nanomaterials identified on the OECD, (2008) list of priority nanomaterials required for immediate testing. The overall environmental impact of nano-ceria particles is dependent upon understanding how environmental conditions such as solution chemistry, redox potential, heat, pressure, biochemical reactions over time and the presence or absence of coatings may affect NP stability and behaviour (Guzmán *et al*., 2006). At present, little or no ecotoxicity data are available for the determination of NP interactions, particularly with nano-ceria and biological matter, (algae, bactiera, viruses etc) resulting in limited risk assessments being made (Hoecke *et al*., 2009). The work this thesis supports investigated commercially available manufactured and in-house synthesized ceria particles for characterisations in a range of aquatic test systems and toxicity assessments to *P. subcapitata*.

2.7.1 Cerium dioxide

The element cerium, a member of the lanthanide series, is the most abundant of the rare earth elements (REE) and the 26th most abundant element in the Earth's crust. Cerium was discovered in the form of an oxide in 1803 by Klaproth, Hissinger and Berzelius (Cotton, 1991) and isolated in 1839 by Carl Gusteav Mosander (Hampel, 1968). Cerium was named in honour of the asteroid Ceres, discovered in 1801 and can be found in ores such as monazite as cerium dioxide. Cerium dioxide can be refered to as ceria or its chemical form, CeO_2.

2.7.2 Chemistry of cerium dioxide

Cerium has a melting point of 795^{o}C and a boiling point of 3,257^{o}C. Cerium is ductile, malleable and has a density of 6.78 g/cm^{3}. Ceria was found to emit complex spectra of beta and gamma radiation by Johnson and Kyker (1961) and has a number of known isotopes from cerium-119; to 157.

2.7.2.1 Redox state

Ceria has important redox chemistry with oxidation states of +4 and +3 and the ability to cycle between the two (Conesa 1995; Herman 1999), under ambient conditions (Hampel, 1968) (Equation 2-5). The reduction of Ce^{4+} (CeO_2 or cerium (IV) dioxide) to Ce^{3+} (Ce_2O_3 or cerium (III) oxide) is accompanied by the creation of an oxygen defect (Suzuki *et al*., 2002) or vacancy, (Schubert *et al*., 2006; Baalousha *et al*., 2010). This property is responsible for the interesting redox chemistry exhibited by ceria NPs and makes it attractive for catalytic applications discussed in the next section. The antioxidant properties associated with nano-ceria exposures that allow for the scavenging of free radicals (Perez *et al*., 2008) along with the contradictory hydroxyl radical formation associated with toxic responses observed with nano-ceria exposures (Lin *et al*., 2006) are thought to be due to the presence of the mixed valence states of ceria. For example, Ce^{3+} can react with oxygen to form Ce^{4+} and oxygen free radicals (Equation 2-6) which in turn can form hydrogen peroxide (H_2O_2) (Equation 2-7), a major contributor to oxidative damage within cells. H_2O_2 reacts with Ce^{3+} to produce hydroxyl free radicals (OH^{-}) and Ce^{4+} ions (Equation 2-8). The valence

and defect structure of ceria is dynamic and may change spontaneously or in response to physical parameters such as size or temperature, (Korsvik *et al*., 2007).

Equation 2-5 Ce^{4+} reacting with hydroxyl radicals
Taken from Karakoti *et al*., (2008).

$$Ce^{4+} + e^{-} \leftrightarrow Ce^{3+}$$

Equation 2-6 Ce^{3+} oxidation
Taken from Lin *et al*., (2006).

$$Ce^{3+} + O_2 \rightarrow Ce^{4+} + O^{-}_2$$

Equation 2-7 Hydrogen peroxide formation
Taken from Lin *et al*., (2006).

$$O^{-}_2 + O^{-}_2 + 2H^{+} \rightarrow O_2 + H_2O_2$$

Equation 2-8 Ce^{3+} reaction with H_2O_2
Taken from Lin *et al*., (2006).

$$H_2O_2 + Ce^{3+} \rightarrow Ce^{4+} + OH^{-} + OH$$

The redox property of ceria is responsible for the interesting chemistry exhibited by ceria NPs and makes ceria attractive for catalytic applications and medical uses (Karakoti *et al*., 2008). By releasing for example, fuel-rich (excess fuel present, where air is the limited reactant) and lean-fuel (excess oxygen with complete combustion of fuel and air) conditions, an optimal oxygen pressure for the catalytic removal of harmful exhaust gases can be maintained, achieved by partial reduction/oxidation of ceria (Equation 2-9). Ceria is also currently being used in diesel fuels (Zhang *et al*., 2005) as it reduces the temperature at which carbon combusts (Park *et al*., 2007), thus increasing the performance of the

engine. Most importantly, and specifically for environmental implications, nano-ceria addition to diesel results in reduced particulate emissions from the exhaust (Park *et al*., 2007).

Equation 2-9. Oxidation and reduction of ceria

$$CeO_2 \underset{\text{Oxidizing}}{\overset{\text{Reducing}}{<\text{----------}>}} CeO_{2-y} + y\ O_2$$

2.7.2.2 Chrystal structure

Bulk-ceria crystallises in the fluorite structure (Figure 2-5a) in which the Ce^{4+} cation is surrounded by eight equivalent O_2^- ions forming the corner of a cube (Deshpande *et al*., 2005) with each O_2^- coordinated to four Ce^{4+} (Skorodumova *et al*., 2001).

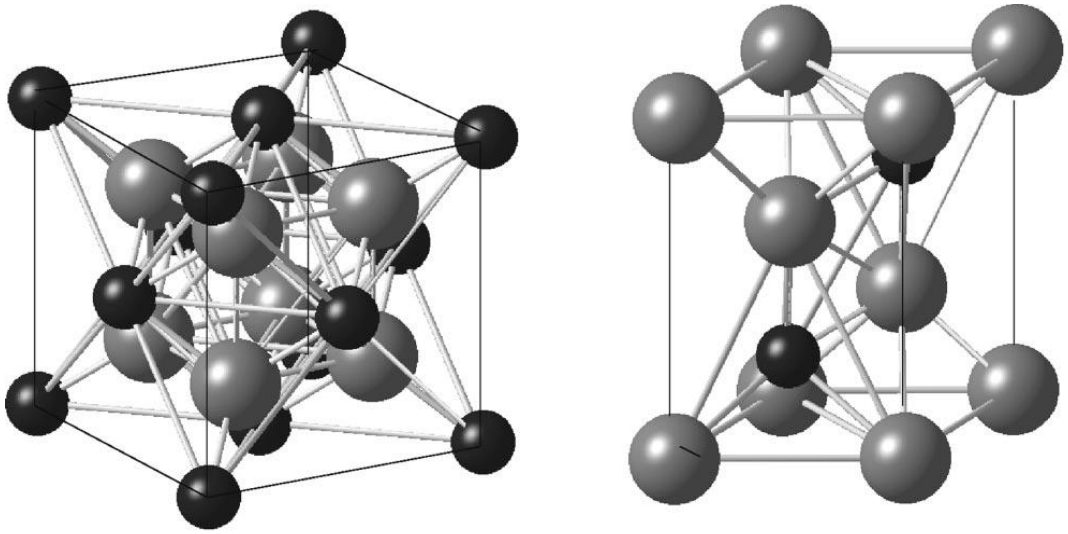

Figure 2-5 CeO_2 and Ce_2O_3 crystal structures
Crystal structures of the cubic fluorite lattice of CeO_2 and the hexagonal lattice of Ce_2O_3.
Ce and O atoms are shown by black and gray circles, respectively.
a) Bulk cerium (IV) dioxide (CeO_2) structure. b) Distorted crystal structure of cerium (III) oxide due to oxygen vacancy creation. Taken from Skorodumova *et al.,* (2001).

Ce^{3+} ions have higher ionic radius (1.034 Å) compared to Ce^{4+} ions (0.92 Å) producing a more distorted crystal structure of cerium (III) oxide (Figure 2-5b). The introduction of oxygen vacancies when considering nano-ceria and accompanying Ce^{3+} ions can lead to a distortion of the local symmetry. This causes the change in the Ce-O bond length (lattice disorder) and a change in the overall lattice parameter (Deshpande *et al*., 2005). The ratio of the two oxidation states may be size dependent (Zhang *et al*., 2002) with increasing Ce(III) being observed at the lower nanometer sizes (Baalousha *et al*., 2010).

2.7.3 Uses of nano-ceria

Ceria NPs are technologically important materials with remarkable properties used in a number of applications (Skorodumova *et al*., 2001). Numerous commercial applications use ceria, (Table 2-5) including metallurgy, ceramics, and phosphors (Oxonica, 2005). One company embracing nano-ceria use is Onoxica producing Envirox™. Envirox™ is a ceria based fuel borne catalyst supplied as a dispersion of 2% w/v cerium oxide in a hydrocarbon carrier. Envirox™ is diluted with diesel for delivery to the vehicle at a ratio of 1:4000, yielding a final nano-ceria concentration in the vehicle diesel fuel of 5 mg/L (Park *et al*., 2007). Current research focusing on further uses of ceria NPs are ongoing e.g. solid oxide fuel cell electrolyte material and for gas sensors, optical coatings, high storage capacitor devices (Zhang *et al*., 2003).

Table 2-5 Applications and properties of nano-ceria particles

Applications	Properties	References
Additives in polymers and dental materials	Fluorescent properties	Brunner *et al*., 2006
Polishing glass	Reacts chemically with the glass	Masui *et al*., 2002
UV absorption	Strong UV absorption High optical transparency in the visible region	Morimoto *et al*., 1999; Korsvik *et al*., 2007 Elidrissi *et al*., 2000
Cosmetics (although the surface and the size of particles, must be modified).	UV-absorption efficiency	Tago *et al*., 2003
Catalyst in automobile catalytic converters	High-active facets Reductions/oxidation capacity	Masui et *al*., 2003 Herschend *et al*., 2005
Diesel fuel additive	Reduces temperature carbon combusts and reduces particulate emissions	Zhang *et al*., 2005 Park *et al*., 2007

2.7.4 Risks associated with ceria

2.7.4.1 Bulk-ceria

REE are not known to possess a functional role in living cells, (Cotton, 1991) but a clear physiological hazard from these elements exists. The REE have long been known to be toxic to various organisms like inhibiting respiration of fungi (Sobek and Talburt 1968). It has also been established that various plants and animals are able to concentrate REE from their environments. Uptake of REE by various organisms has resulted in drastic morphological changes in cells and tissues as well as the poisoning of some cellular systems (Sobek and Talburt, 1968). One of the major problems in working with the REE is that they rapidly form virtually insoluble phosphate and hydroxide compounds at slightly acidic, neutral and alkaline pH values and may also precipitate from solution (Sobek and Talburt 1968).

2.7.4.2 Nano-ceria

Nano-ceria has been shown to provide protection towards cells, against radiotherapy carried out during cancer therapies (Tarnuzzer *et al*., 2005) and has been shown to have very low or no toxicity when in the form of exhaust emissions (HEI, 2001). Table 2-6 however shows the opposing view of nano-ceria listing the toxic effects associated with commercial nano-ceria from recent literature. There is also an apparent protective response of nano-ceria particles compared to the bulk-particles, with contradictory evidence of OS being produced. This suggests nano-ceria particle effects are dependent upon the physicochemical properties of the particle which seem to be relatively independent of its size. These areas of research using commercially available powdered nano-ceria particles, however, do have limitations in their use as toxicity data. The referenced size distribution for example, must be taken into consideration as powdered particles do not dispense readily in solutions, reducing the quoted doses offered. Also, aggregation of NPs can take place during transit which can increase the registered manufacturer's size distribution.

When investigating synthesized nano-ceria particles of well-defined dimensions, a variable cytotoxic effect is apparent (Table 2-7), compared against commercial nano-ceria particles. Thill *et al*., (2006) showed how the toxicity of cells from nano-ceria exposures was largely due to the NP surface chemistry and associated attractive capabilities rather than concentration or particle number. The activity dependency relating to the size of the nano-ceria particles during a

study by Ivanov *et al*., (2008) has also been attributed to the increase volume and surface oxygen of ceria when particle size decreases. This study by Ivanov *et al*., (2008) suggests that as synthesized nanomaterials remain in suspension for a period of time, they may become more hazardous. However, large agglomerates of NPs can form in solution over time, without appropriate dispersion methods undertaken, leading to conclusions by Ivanov *et al*., (2008) relating to particle size being misrepresented without characterisation data available.

Based upon this short review it is evident that the inherent toxicity of commercial nano-ceria is low with growing evidence that ceria NPs demonstrate protection towards living cells. Size dependent toxicity by commercial ceria is also low, due to the dispersion of these low soluble particles. Synthesized ceria offers a greater toxic effect compared to commercial ceria particles largely due to their particle dimensions and stable dispersions. The molecular mechanism of the antioxidant properties of nano-ceria has, as yet, to be elucidated and full understanding of the mechanisms must be assessed (Korsvik *et al*., 2007). Many of these investigations highlighted have been carried out using various methods, synthesis and preparation of nano-ceria dispersions which must also be taken into account when assessing such work, as manipulations of NPs can have an effect on chemistry and bioavailability of such materials.

Table 2-6 Effects associated with commercial nano-ceria particle exposures

Biological system	Effect	Reason	Particle type	Reference
Cultured human lung cancer cells	Cell viability was seen to decrease significantly as a function of dose and exposure time.	Free radicals were generated by exposure to nano-ceria and produced significant cell OS.	20 nm ceria NPs	Lin *et al.,* 2006
Nerve cell line HT22	Little or no difference between the neuro-protective activity of 6 or 12 nm ceria particles and bulk-ceria.	Antioxidant properties that promoted cell survival under conditions of OS.	NP oxides, cerium nitrate and cerium chloride (0.0001 to 0.05 mg/L)	Schubert *et al*., 2006
Salmonella strain TA100 and *Daphnia magna*	No effect up to 5000 µg/plate. MIP value <0.8 (NP+MP) considers low *in vivo* skin irritant No *D. magna* immobilisation effect observed.	Protection of cells in culture from lethal stress.	9 nm nano- and 320 nm bulk-ceria	Park *et al*., 2008
Human mesothelioma and a rodent fibroblast cell line	Insoluble ceria showed comparable results to titania and zirconia, reduced cell activity and DNA content but no complete mortality, (<30 mg/L).	Solubility greatly affects the cytotoxicity observed. An initial stress arose from NP incorporation but sealing or detoxification of the NPs in compartments may have helped to recover full cell culture viability.	~8 nm particles	Brunner *et al*., 2006
Daphnia magna , *D. rerio* embryos and *Pseudokirchneriella subcapitata*	No size dependent toxicity was observed up to 1000 mg/L (bulk) or 200 mg/L (NP).	No dispersion preparation or characterisation determined.	14, 20 and 29 nm ceria particles	Hoecke *et al.,* 2009

Table 2-7 Effects associated with synthesized nano-ceria particles

Biological system	Effect	Reason	Particle type	Reference
Gram-negative bacteria	Neuro- and radiation-protective properties on cells.	NPs were positively charged at neutral pH and display a strong electrostatic attraction toward bacterial outer membranes reducing exposure of 'naked' particles. NPs where mainly located on the surface of the bacteria showing no effect on the bacteria survival rate.	CeO_2 NPs were gifted from a chemical company Rhodia. They were obtained as a powder through precipitation of $Ce^{4+}(NO_3^-)_4$ salt at very low pH. (~7 nm)	Thill *et al*., 2006
E. coli	The bioactivity of ceria considerably increased with decreasing NP size being more pronounced for the ceria suspension preliminary kept for a month.	The mechanism of the biological effects of ceria was assumed to be based on the capability of the material to directly bind active oxygen derivatives formed in the system due to the presence of dissolved molecular oxygen.	Precipitation with a 3 M aqueous ammonia solution from water–isopropanol solutions (1 : 1 v/v) cerium(III) nitrate (0.08 M). (~5-8 nm)	Ivanov *et al.,* 2008
Human lung fibroblasts	Strong dependence of ceria availability to cells as a function of size (25 – 500 nm).	Agglomeration properties of ceria. Cells were found to rapidly absorb ceria NPs from the culture medium.	Prepared by flame spray synthesis using chlorine-free carboxylate precursors. (25-500 nm by DLS)	Limbach *et al*., 2005
Cultured human lung epithelial cells (BEAS-2B)	NPs (5, 10, 20, 40 µg/ml) led to cell death, ROS increase, GSH decrease and the inductions of OS-related genes (heme oxygenase-1, catalase, glutathione S-transferase and thioredoxin reductase).	The increased ROS triggered the activation of cytosolic caspase-3 and chromatin condensation. Uptake was observed where NPs penetrated into the cytoplasm and located in the peri-region of the nucleus.	Prepared by supercritical synthesis method. (15, 25, 30, 45 nm)	Park *et al*., 2008

2.8 Summary

It is clear from the literature that data regarding the physicochemical and ecotoxicological properties of NPs, specifically ceria particles, are not plentiful. Most areas of NP research involve various methods of synthetic media preparation and NP synthesis to obtain desired outcomes, so comparative assessments between commercial and synthesized particles is difficult to interpret. Also, results from *in vitro* studies cannot be directly transferred to environmental conditions (Nowack and Bucheli, 2007) due to the controlled conditions present in laboratory settings. Equally, cell media used for such tests are not fully representative of natural corporeal systems due to variation in pressure, temperature and salt interactions. Also, many of the studies reviewed here were performed on small data sets, with subjective methodologies for the assessment of NP characteristics. The apparent lack of characterisation data from such studies limits the understanding and knowledge of environmental effects associated with ceria particles. Although there is some difficulty associated with measuring NPs in environmental systems, many techniques can be applied to obtain a good representation of particle size, shape and aggregation behaviour during toxicological tests discussed in the next chapter.

3 Analytical techniques and methods

3.1 Chapter summary

The environmental fate, mobility, bioaccumulation and ecotoxicity of MNPs can be influenced by the particles physical properties and chemical composition including size, shape, particle charge and the presence of impurities. As no single detection technique is without potential artefacts (Ju-Nam *et al*., 2011), correct interpretation of NP characterisation must be based upon a large number of observations, using a combination of several techniques (Baalousha *et al*., 2011). Using a range of analytical techniques provides greater accuracy, reduces bias, offers a more complete picture of the physicochemical status of the NPs (Ju-Nam and Lead, 2008; Handy *et al*., 2008a) and also makes the available data comparable between studies. This chapter describes the analytical techniques and associated methodologies used to determine the particle characteristics chosen for this study, in order of most frequently used technique. This chapter offers a review on the instrumentation chosen expressing the reasons for their choice and including a brief theory of each. The advantages and limitations of each instrument are also discussed in the appropriate sections. Details on the sample concentrations used for analysis are offered in Chapter 4. A second aim of this thesis was to determine the mechanism of toxicity attributed by ceria NPs to *Pseudokirchneriella subcapitata* by using mass spectrometry, which is discussed in detail in Chapter 8.

3.2 Hydrodynamic diameter by dynamic light scattering

Light scattering is a common method used to determine particle size. Dynamic light scattering (DLS) also referred to as photon correlation spectroscopy (Hoo *et al*., 2008), is performed routinely on NP dispersions (ISO, 1996). This technique can be used to estimate the relative agglomeration of NP dispersions under different conditions by comparing their hydrodynamic diameters (Jiang *et al*., 2009).

3.2.1 Theory

DLS measures time-dependent fluctuations in the scattering intensity arising from particles suspended in a liquid solvent, undergoing random Brownian motion (Kaszuba, *et al*., 2008). A laser beam can be applied to the particle solution (Peters, 2000) scattering the light from the particles back to a detector with a different frequency. Assuming the particles are spherical and non-interacting, (Karlsson *et al*., 2009) the particle size (an intensity-weighted Z-average), can be calculated from an autocorrelation of the Doppler shifts of the scattered light over time. The Z-ave is estimated from the Stokes-Einstein equation (Equation 3-1) used to obtain the particles hydrodynamic diameter (d_H). The Stokes-Einstein equation uses the Boltzmann constant (k), temperature (T) and viscosity (η) of the sample. The Z-ave can be further converted to a volume distribution and to a number distribution (Gonçalves and Gama, 2008). The DLS also produces a width parameter (polydispersity index (PdI)) representing the standard deviation about the Z-ave assuming a monomodal distribution (Darlington *et al*., 2009).

Equation 3-1 Stokes-Einstein equation

$$d_H = \frac{kT}{3 \pi \eta D}$$

3.2.2 Advantages and limitations

There are a number of advantages and limitations of DLS as summarised on Table 3-1.

Table 3-1 Advantages and limitations of DLS

Advantages/limitations	Conditions	References
Advantages	Rapid Little/no sample preparation Low sample volume Automatic computational data conversion	
Limitations	Cannot distinguish between different types of particles Poor results from polydispersed samples Does not factor in shape Mean diameters are weighted toward larger agglomerate sizes due to light scattering	Tiede *et al.,* 2009 Hassellöv *et al*., 2008 Powers *et al.,* 2006 Darlington *et al.,* 2009

A further limitation of DLS arises with the measured d_H interpretation. The d_H depends not only on the size of the particle "core", but also on any surface structure, as well as the concentration and type of ions in the medium. Increased PdI of a dispersion, which is particularly common with environmental samples, also limits the use of DLS to measure particle diameters. To reduce error with polydisperse samples the particle scattering needs to be increased by increasing the particle concentrations, although this may result in greater particle aggregation (Domingos *et al*., 2009a). Another limitation arises from larger

particles which move more slowly through the fluid reducing the frequency shift. Larger particles have a greater influence on the measured d_H than smaller particles in the same sample. For example, two sizes of particles (5 nm and 50 nm) but with equal numbers of each particle size can produce three results from DLS (Figure 3-1).

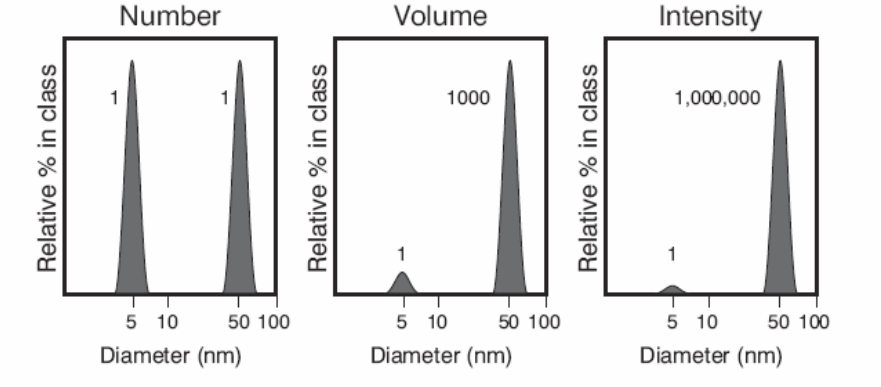

Figure 3-1 Influence of smaller particles on DLS measurements
An example of a sample containing equal amount of 50 nm and 500 nm particles showing a) number distribution, b) volume distribution and the c) intensity distribution
Taken from the Malvern (1997).

The number distribution (Figure 3-1a) shows the two peaks of the same size (1:1) as there are equal numbers of particles in solution. Figure 3-1b shows the peak for the 50 nm particles is 1000 times larger than the peak for the 5 nm (1:1000 ratios). This is because the volume of a 50 nm particles are 1000 times larger that the 5 nm particles. If the particles are small compared to the wavelength of the laser used, then the scattering from a particle will be essentially isotropic and Rayleigh approximation (Equation 3-2) can be applied using the intensity of light scattering (I), the particle diameter (d) and the laser wavelength (λ). The d^6 term shows that a 50 nm particle will scatter one million times as much light as a 5 nm

particle (Figure 3-1c). Hence there is a danger that the light from the larger particles will swamp the scattered light from the smaller ones.

Equation 3-2 Rayleigh approximations
Taken from Malvern (1997).

$$I \alpha d^6 \quad \text{and} \quad I \alpha \frac{1}{\lambda^4}$$

3.2.3 Method

Samples measured for size distribution were undertaken in accordance with ISO 13321, (1996), using a Malvern nanoseries Zetasizer (UK). A 1 ml aliquot of each sample was taken from the supernatant using a disposable syringe and needle. Approximately 0.5 ml was used to rinse a disposable cuvette and approximately 2 µl sample was used to load the cuvette. This was placed into the light scattering unit and ran automatically (Table 3-2) producing three repeated measurements for each sample. The refractive index (1.94) and absorption (0.1) for ceria samples (Khawaja *et al*., 2003) were used. The CONTIN algorithm was used to convert intensity autocorrelation functions to intensity-weighted particle d_H distributions, assuming the Stokes-Einstein relationship for spherical particles.

Table 3-2 DLS instrumental set-up details

Instrument	Malvern Zetasizer
Temperature (°C)	Variable[a]
Laser	4 mW, He-Ne
Laser position (mm)	633
Standards	Latex[b] 50nm, 80nm 125nm in 10 mM NaCl

a Specific temperatures used are outlined in Chapter 4
b Latex standards prepared under the guidance of guidelines ISO 13321 (1996 pp.18)

3.3 Zeta potential by electrophoresis

Environmental fate and reactivity of NPs can be controlled by their dispersion and agglomeration behaviour. NPs are affected by the weak physical forces of attractive van der Waals forces and repulsive electrostatic charges. The zeta potential (ζ) is an important parameter for a number of applications. The ζ is a function of the surface charge of a particle or any adsorbed layer at the interface and the natural composition of the surrounding medium, (Borm *et al*., 2006). Particles that are sterically stabilised can remain well dispersed even at high salt concentrations or where ζ is close to zero.

3.3.1 Theory

When a solid surface is in contact with an aqueous solution, ions of opposite charge to that of the particle are strongly attracted to the surface; (Figure 3-2) termed the stern layer (Shaw, 1980 pp55). The arrangement of the charges at the solid-liquid interface and the balancing counter ions in the liquid is usually referred to as the EDL. The ions in the stern layer are immobile due to the strong electrostatic attraction where ions outside the compact layer (diffuse layer) are mobile, (Sze *et al*., 2003). The ζ is the electrostatic potential at the boundary dividing the compact layer and the diffuse layer, called the slipping plane. When an electric field is applied across an aquatic dispersion, charged particles will move toward the electrode of opposite polarity. This phenomenon is called electrophoresis. If a laser beam is passed through the sample undergoing electrophoresis, the scattered light from the moving particles will be frequency

shifted (Jiang *et al*., 2009). By measuring the frequency shift, the electrophoretic mobility ($m^2V^{-1}s^{-1}$) can be determined given the laser wavelength and the scattering angle (Jiang *et al*., 2009).

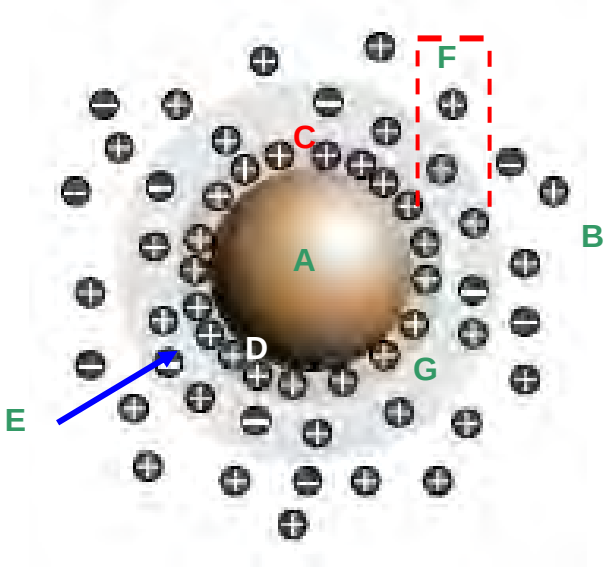

Figure 3-2 Charge arrangements at a particle surface
A) A negative particle in B) liquid medium with C) strongly attracted oppositely charged ions to the D) Stern layer between E) the slipping plane and F) the electric double layer supporting G) loosely attractive ions.

The ζ (Equation 3-3) is a measure of particle velocity in a liquid when a known electrical field (v) is applied. This can be determined by the electrophoretic mobility (UE) with the known dielectric constant (ε) of a sample when applying the Henry function (f(*k*a)) (Equation 3-4). The (f(*k*a)) can be expressed using the electric permittivity (μ) of the medium ($C^2N^{-1}m^{-2}$), the electrophoretic mobility (U) and the sample viscosity (η) measured in $kg/m^{-1}/s^{-1}$ (Jiang *et al*., 2009). The Henry function can be explained by the particle radius (a) and the ratio of the particle radius to the double layer thinness (*k*a), where *k* is detailed in Section 2.4.4.1. The *k*a value can be determined either by the Smoluchowski

approximation or by the Hückel approximation (Table 3-3) depending upon the particle being measured.

Equation 3-3 Zeta potential

$$UE = \frac{2\,\varepsilon\,\zeta\,f(ka)}{3\,v}$$

Equation 3-4 The Henry function

$$\zeta = \frac{\mu U}{\eta}$$

Table 3-3 The Smoluchowski and Hückel approximations

Approximation	Value	Application	Reference
Smoluchowski approximation	1.5	Based upon the electrophoretic mobility of rigid colloids or for particles in a polar medium	Ohshima, 1995
Hückel approximation	1.0	Based upon the electrophoretic mobility of 'small spheres'' or soft colloids' or particles in non-polar medium	Ohshima, 2002

A soft or permeable colloid relates to a particle coated with hydrodynamically permeable and often charged surface layers (Duval, 2007). Soft colloids may include adsorbed polyelectrolytes, biological cells (Makino *et al*., 1996), bacteria and humic substances. The electrophoresis of soft permeable systems is much less understood than that of hard spheres, (Duval and Ohshima 2006).

3.3.1.1 The Point of zero charge

The point of zero charge (Pzc) is an important interfacial parameter, which is used extensively in characterising the ionisation behaviour of a particles surface.

As the surface charge approaches zero, the interaction curve approaches the pure van der Waals curve (Figure 2-2) and the two surfaces may attract each other (Israelachvili, 1985). If all the particles have a mutual repulsion then the dispersion will remain stable preventing the particles from coming together. The DLVO theory (Section 2.4.4.1) describes the repulsive and attractive forces for particle-particle interaction and predicts that as EDL repulsion is lowered by pH or ionic strength changes, the particles can approach and adhere to each other, leading to flocculation (Eggleston and Jordan, 1998) and particle sedimentation.

3.3.2 Advantages and limitations

The measurement of ζ is relatively effortless with little to no sample preparation required. Calculations of ζ from electrophoretic measurements are fully computerised and standards are available for instrumental reliability checks. The ζ, unfortunately, offers no information on the chemical or elemental composition of the surface of a particle. The ζ also is not a measurement of the surface charge of the particle itself, but a voltage reflecting the effects of surface charge and flow dynamics near the surface (Handy *et al*., 2008a), which can be influenced by particle surface coatings.

3.3.3 Method

Two instruments were used for electrophoretic mobility measurements. The first instrument used was a Malvern zeta potential running at a constant temperature of 25 ^{O}C. This required the use of an electrolysis cell which was first removed

and sonicated in detergent and water for 10 min to ensure any previously deposited particles were removed. The system was flushed with 50 ml of deionised water (dH$_2$O) using a disposable syringe. A sample of dH$_2$O was then run as a control sample. A 4-5 ml sample was taken from the sample supernatant using a disposable syringe and needle and injected directly into the instrument. This was run automatically producing 10 analyses for each sample. Following each sample the instrument was purged using 20 ml dH$_2$O. The second instrument used was a Malvern nano Zetasizer. A disposable zeta cell was used, being rinsed with ethanol and subsequently three times with dH$_2$O. A 1 ml sample was taken from the supernatant using a disposable syringe and loaded into the disposable zeta cell. This was discarded and a further 1 ml sample loaded into the cell for analysis. This was placed into the Malvern Zetasizer and ran automatically three times. A Malvern instrumental standard solution of -68 mV ±6.8 mV was used. Measured electrophoretic mobility was converted to ζ using the Smoluchowski or Hückel approximation where appropriate. Surface charge is reported as the ζ and/or electrophoretic mobility.

3.4 Particle size and algal counts by microscopy

3.4.1 Optical microscopy

3.4.1.1 Theory

The optical, or light microscope (LM), has a multiple lens in which an image is obtained from a specimen and magnified. The LM (Figure 3-3) uses objectives on a turret that can be turned to selected powers of magnification. The objective lens

forms a real intermediate image, which is then greatly magnified by the eyepiece, typically with a power of 2 to 10 times magnification. The resultant magnification is calculated from the multiplication of the objective power by the eyepiece power. The objective lens and eyepiece are maintained at a fixed distance and focusing is achieved by moving the whole assembly up and down in relation to the sample.

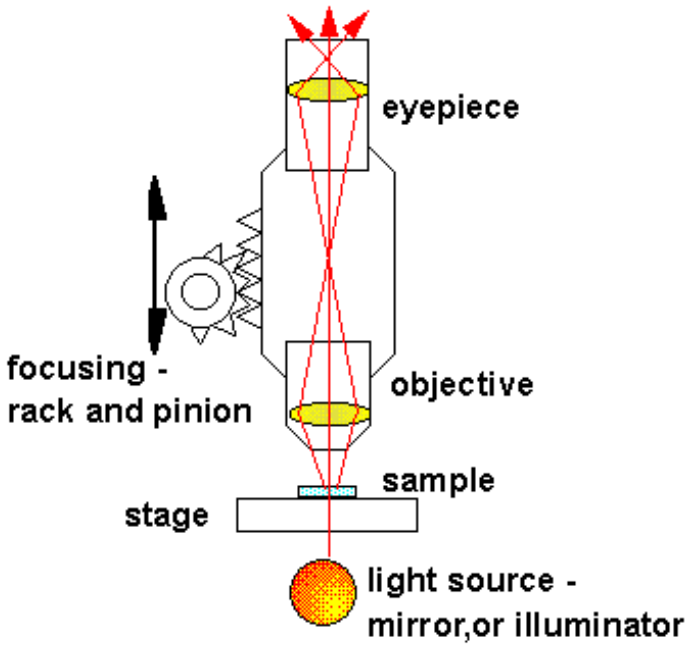

Figure 3-3 Schematic image of the optical light microscope

3.4.1.2 Advantages and limitations

The LM enables live specimens to be imaged in real time, with little to no sample preparation and only small sample volumes being required, making the process uncomplicated and rapid. The LM however does not have the magnification to extend beyond the micrometer (µm) range with a limited resolution in the order of 0.1 µm (Hassellöv and Kaegi, 2009).

3.4.1.3 Method

A Kyowa, (Tokyo) optical LM with 20W halogen light, was used to count algal cells at a magnification of 40X and an eye piece of 10X magnification. A 0.0025 mm^2 Neubauer haemocytometer (Neubauer, Superior Marienfield, Germany) with a depth profounder 0.100 mm was used as a counting chamber (Figure 3-4). The 200 µl algal samples were introduced into the V-shaped wells using a 200 µl pipette. Two main divisions separate the grid into nine large squares. Each square has a surface area of 1 mm^2 and chamber depth of 0.1 mm, with the entire counting grid under a volume of 0.9 mm^3. The cells were counted in the entire centre square comprising 5 X 5 1/25th mm^2. Counts taken across 25 squares, each with an area of 1/25 mm^2 and depth of 0.1 mm, (total volume 0.004 mm^3) equating to 0.1 mm^3 area. This was repeated with the opposite side of the counting chamber. Using Equation 3-5 the cell counts from both chambers were averaged and the cells/ml was obtained.

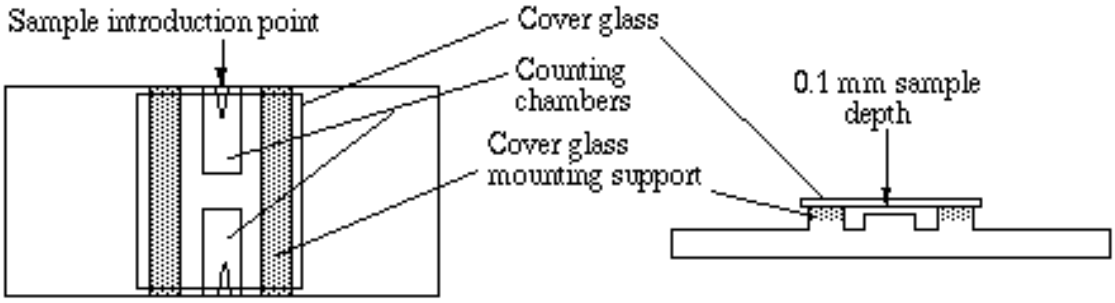

Figure 3-4 The haemocytometer counting chamber

Equation 3-5 Cell counts from haemocytometer calculations

$$\frac{\text{Counted cells}}{(0.1)} = \text{particles per mm}^3\ (\text{X } 1000) = \text{cells/ml.}$$

3.4.2 Transmission electron microscopy

Invented by Ruska in 1931, the transmission electron microscope (TEM) is arguably the single most powerful technique for characterising NPs. Because the wavelength of the electrons is much shorter than that of light, much higher spatial resolution is attainable for TEM images compared with that from a LM. Routine low-resolution TEM studies can permit a statistically significant, quantitative description of the size and shape of NPs in a sample (Murray *et al*., 2000). High resolution TEM (HRTEM) imaging can reveal the individual shapes and internal structures of particles and in some cases individual atoms. Furthermore, if the TEM is adequately equipped, qualitative chemical analysis (EDX) can be performed by exploiting the interactions of the electrons with the atoms in the sample. Elemental characterisations of specimens in TEM can also be performed using electron energy loss spectroscopy (EELS). EELS is based upon the inelastic scattering of the specimen and can be used to further determine elemental information on the sample.

3.4.2.1 Theory

Electrons can be generated in an EM by a process known as thermionic emission from a filament, usually tungsten (Hubbard, 1995) or from a lanthanum hexaboride source (LaB_6) using a field-emission gun (FEG). Connecting the

FEG to a high voltage source, (typically 100-300 kV), the FEG will begin to emit electrons by thermionic or by field electron emission into the vacuum (Egerton, 2005). Electrons produced by the FEG emit through the sample and magnetic lenses focus the image of the sample (Figure 3-5).

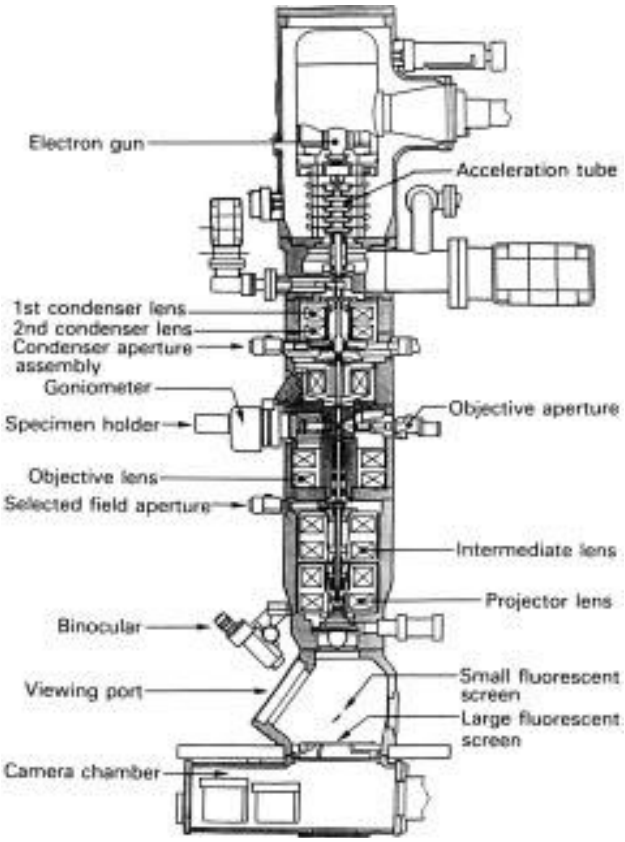

Figure 3-5 Schematic diagram of the transmission electron microscope

The surface topography of a specimen is revealed either by the reflected (backscattered) electrons or by electrons ejected from the specimen, as the incident electrons decelerate secondary electrons (RSRAEN, 2004). A visual image, corresponding to the signal produced, by the interaction between the

beam spot and the specimen is focused onto a fluorescent screen (Goodwin, 2004).

3.4.2.2 Advantages and limitations

Advantages and limitation of TEM instrumentation are highlighted in Table 3-4.

Table 3-4 Advantages and limitations of TEM

Advantages/ disadvantages	Conditions	Reference
Advantages	• Spatial resolution *ca* 1 nm • Drop deposition method easy to perform • Combine EDX to confirm the element composition • Only a small amount of sample is measured ideal for single particle measurements • Standards of silica particles at 0.1-1 µm with <90,000 particles can be utilised	Andrievsky *et al*., 1999; Chen *et al*., 2002 Yoshida *et al*., 2009
Limitations	• Expensive instrumentation • Drop deposition grid preparation causes artefacts and change the structure of the particles imaged • EDX requires adequate standards • Provides only 2D images causing orientation effects • Samples must be thin <100 nm • Large number of particles require counting to achieve a number average – time consuming • Biases due to the overestimation of particle sizes as the eye is drawn to easier-to-see particles • Electron scattering • Operates in a vacuum limiting its applicability and reduces accuracy away from the nature of the liquid the grid was made from • Only a small amount of sample is measured reducing representative analysis • Lack of standards available for particles <100 nm • Sample preparation • Electron scattering	Domingos *et al*., 2009a Nowack and Bucheli, 2007 Hassellöv and Kaegi, 2009 Powers *et al*., 2006 Fisker *et al*., 2000 Domingos *et al*., 2009a Porter *et al*., 2007 Requicha, *et al*., 2009; Mavrocordatos *et al*., 2007; Zattoni *et al*., 2007 Pecora, 2000 Porter *et al*., 2007

Further limitations of TEM analysis arise from the sample preparation methods employed. Sample preparation incorporating ‘drop deposition’ method can cause

difficulty in distinguishing NPs, NP impurities and salt contributions in a sample due to artefacts during the drying process. Other TEM sample preparation techniques have been developed such as cryo-techniques (Wang *et al*., 2004) and ultra-centrifugal (UC) harvesting (Hassellöv *et al*., 2008).

3.4.2.3 Method

Two methods for sample preparation were employed. The first 'drop deposition' method was conducted using a 50 µl sample aliquot using a 200 µl pipette, dropped directly onto the holey carbon-coated copper TEM grid. Drop deposition samples were allowed to air dry for 30 min in ambient conditions and were covered to reduce the occurrence of dust from the surrounding area. The remaining wet sample was removed by using absorbent paper and placed back into the grid holder.

The second UC method was also conducted for some samples. Using a Beckman L7 ultracentrifuge and plastic centrifuge tubes, 4 ml samples were centrifuged at 30,000 rpm for 1 h at 18 ^{O}C. The grids were subsequently rinsed for 3 s using *d*H_2O and dried using absorbent paper before being placed back into the grid holder. The images of the prepared TEM samples were obtained with a Philips (Tecnai Series) TEM operated at 200 kV with a lens of theoretical resolution 0.19 nm and images taken with Gatan 794 MSC digital camera, with an extension voltage of 4400 V. Support using TEM was obtained by Dr Ming Chu, Dr. Mohammed Baalousha and Dr. Ruth Merrifield; University of

Birmingham, UK. For particle size measurements, axes of individual particles were measured using DigitalMicroraph™ series 3.4.4 Gatan software 1999. Basic statistics for particle diameters and particle distribution histograms were calculated based on the percentage of total particles measured. Aspect ratios (*S*) were calculated by the division of the longest axis measured by the shortest axis measured using DigitalMicroraph™ where a value of 1.0 was considered spherical.

3.4.3 Atomic force microscopy

3.4.3.1 Theory

Atomic force microscopy (AFM) is a powerful tool for the determination of particle sizes down to the nm scale (Baalousha and Lead, 2007), but also to determine particle topography. Developed by Binnig, Quate and Gerber (1986), the AFM utilizes a piezoelectric effect to produce ultrafine focusing of optical assemblies at an atomic resolution. The AFM is designed to move a specimen in nanoscale increments in the X and Y surface and Z-axis directions (Hoo *et al*., 2008) using an oscillation movement. It is performed by mounting an AFM tip on a cantilever and positioning it above the specimen at a distance where the tip is either repelled (Pauli principle) during contact AFM imagery, or attracted (van der Waal forces) due to the interaction with the specimen surface. As the specimen is moved below the tip, the cantilever bends due to topography changes as the tip maintains a constant force from the surface (Hoo *et al*., 2008). The detector reads the deflection for the laser, processes it though the feedback loop and the

data acquisition software turns the measured detections into a 2D image. There are three methods to obtaining AFM topographical images through contact, non-contact or wet-cell mode. Contact mode (Figure 3-6a) can disturb loosely bound particles by the tip as it is moved across the sample. Non-contact mode (Figure 3-6b) has a lower force where the tip oscillates above the sample rather than touching it. Non-contact mode is more difficult to measure particles than that of contact mode but non-contact makes studying soft or elastic samples much easier.

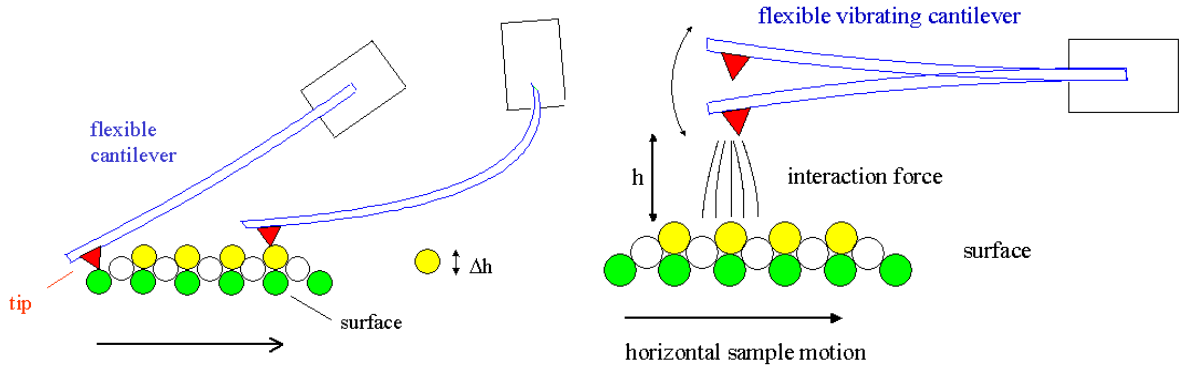

Figure 3-6 Schematic diagram of the AFM cantilever
a) In contact mode and b) non-contact mode

3.4.3.2 Advantages and limitations

The advantages and limitations of the AFM technique are highlighted on Table 3-5. Chemical characterisation of a sample is a limiting factor of AFM analysis but can be acquired by using techniques such as NanoIR. For the purpose of this work, the application of NanoIR was not used.

Table 3-5 Advantages and limitations of AFM

Advantages/limitations	Conditions	References
Advantages	Analysis is typically done at room temperature, in ambient air Relatively simple techniques for sample preparation Can be used as a comparative tool against other sizing techniques Suitable technique for precise 3D mapping of surfaces of cells The accuracy of particle height measurements, using standard gold particles are often reliable to 0.1 nm.	Ju-Nam *et al*., 2011; Wilkinson *et al*., 1999 Stoimenov *et al*., 2002
Limitations	Systematic bias can be introduced for NPs that are of sizes similar to (or smaller than) the radius of the curvature of the tip Need for locating the particles on the surface manually or 'blindly' Only possible for NPs that are sufficiently attached to the substrate can be moved around by the cantilever tip, disturbing the images obtained. Lateral dimension (x-y) measurements are often inaccurate for NP samples. Information about an ensemble of particles can often be poor	Requicha, *et al*., 2009 Hassellöv *et al*., 2008 Hassellöv and Kaegi, 2009 Borm *et al*., 2006

3.4.3.3 Method

Application of non-contact mode, on dried sample substrates was implemented supported by a number of staff at the University of Birmingham, (Table 3-6). For all samples, a freshly cleaved mica sheet of *ca* 1 cm^2 was prepared and placed into a sample aliquot horizontally. The adsorption method (Wilkinson *et al*., 1999) was used where the grid was left for a given time before being removed and rinsed with *d*H_2O for 3 s. For some samples, the bare mica sheets were not charged, (or rough enough) to sufficiently allow particle attachment. To counteract this, the absorption method was introduced. A specific charge on the mica surface was produced by soaking the cleaved mica sheet in 10 mM NaCl

before sample preparation. The measurements were imaged and analysed using a PSIA TIFF version 1.0.2 programme.

Table 3-6 AFM sample preparation

Mode	None contact
Image taken (µm)	10 X 10
Z-Scanner range	'Topography'
Low pass filter	0 (no flattening applied)
Data width and height (pxl)	256
Over scan (%)	10
Scan rate (Hz)	1
Set point (V)	1
Data gain (µm/step)	-132.46×10^{-6}
Measurements supported by	Dr. Yon Ju-Nam Dr. Ruth Merrifield

3.5 Dissolution by ICP-MS

Observed toxic effects of some NPs may be due to the dissolution of ions from the particles. Since many of the inorganic MNPs contain heavy metals that are known to be toxic in their dissolved form, it is important to measure the dissolution of such metals from NP solutions. Inductively coupled plasma (ICP) sources, especially when combined with mass-spectrometric (MS) detection, provide high sensitivity and robustness which are excellent tools for elemental analysis. ICP-MS is commonly applied during the synthesis of NPs, since it is perfectly suited to determine the total elemental concentration of a colloidal solution (Scheffer *et al*., 2007). ICP-MS can also determine the NP fraction of a sample along with the dissolved fraction, using a range of filtration steps.

3.5.1 Theory

When an analyte, in aerosol form, enters the central spray channel of the ICP-MS, (Figure 3-7) a number of processes occur. The sample desolvates, the matrix decomposes and the resulting analyte and solvent vapour undergo excitation to produce molecular atomic and ionic species in various energy states. Some of this energy is released in the form of electromagnetic radiation of a wavelength that is characteristic of the emitting species (Mermet, 1987). As a droplet of nebulised sample enters the central channel of the ICP it evaporates and any solids that were dissolved in the liquid vaporise and then break down into atoms. At the temperatures prevailing in the plasma a significant proportion of the atoms of many chemical elements are ionised where each atom loses its most loosely bound electron to form a single charged ion.

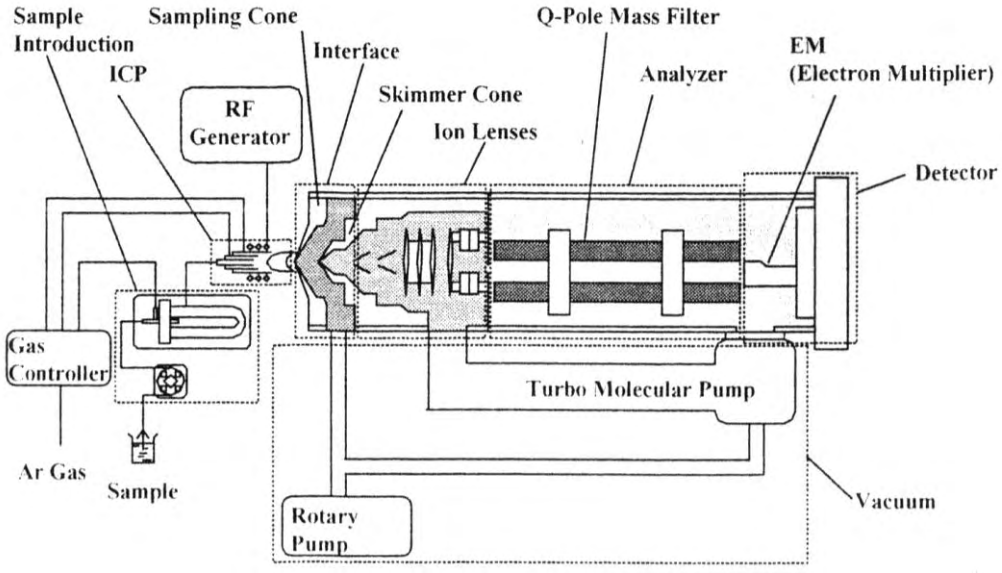

Figure 3-7 Schematic diagram of the Agilent 7500 ICP-MS

3.5.2 Advantages and limitations

Advantages and limitations of ICP-MS are given in Table 3-7.

Table 3-7 Advantages and limitations of ICP-MS analysis

Advantages/limitations	Conditions	References
Advantages	• Analyte concentrations can be measured to ppt • ICP-MS has a working range over 9 orders of magnitude • ICP-Ms easily vaporises, atomise and ionises NPs with radii typically of 5-25 nm • Aqueous or organic solutions and both colloidal and ionic solutions • Reliable with low detection limits	Scheffer *et al*., 2007
Limitations	• Atomisation may lead to clouds of metal atoms entering the detector increasing relative standard deviations of the measurements • Temperature fluctuations can cause severe instrumental drift • Isolation from vibration is requiring • Low efficiency of ICP-MS instrumentation *ca* 10-14 % • Limited speed, • Low signal levels (1 count/atom) • Low efficiency *ca* 1 atom in 107 detected • NPs may behave differently compared to the metal in solution • NPs may not fully atomise in the furnace causing a problem for agglomerated particles • Shear forces induced during ultrafiltration perturb the dispersion state of NPs leading to aggregation or particle disruption • Ultrafiltration membranes may have distribution of pore sizes • Concentration of sample, aggregation and hydration properties of humics can influence UF results	Barnes *et al*., 2003 Federici *et al*., 2007 Hassellöv *et al*., 2008 Bolea *et al*., 2006 Buffle *et al*., 1998

3.5.3 Method

To separate dissolved and NP fractions filters of 0.45 µm to 0.1 µm from Whatmann UK and regenerated cellulose UF membranes of 1 KD pore size from Cole-Palmer instruments Co. were used respectively. All filter papers were left overnight to soak in a 2% HNO_3 bath to remove any particular matter which may

interfere with the subsequent plasma analyses (Vonderheide *et al*., 2004). The filter papers were removed prior to use and placed into a 1 L beaker of *d*H_2O. Appropriate numbers of 25 ml polypropylene (PP) sample bottles were also left overnight to soak in 10% HNO_3 bath. The bottles were rinsed three times in *d*H_2O and left to air dry before use.

3.5.3.1 ICP-MS sample preparation

At low pH, most metal ions are soluble. All samples were therefore stabilised in nitric acid (HNO_3) to pH 1-2 by the addition of 1%/vol PrimarPlus HNO_3. HNO_3 also controls the NP dispersions and aggregation of the particle ions onto the surface of the collection vessel (Vonderheide *et al*., 2004). For *Daphnia magna* exposure samples, each filtered sample had sodium citrate at 10^{-2} M and ethylenediaminetetraacetic acid (EDTA) acid free at 10^{-4} M concentrations added, to help control the dispersions and reduce aggregation of particles in solution. All ICP-MS analyses were conducted using an Agilent 7500 ICP-MS instrument (Figure 3-8) housed in an air conditioned room. Cerium BDH ICP-MS standards from Aristar were used at 0, 1, 5, 20 and 50 ppb dilutions from 1000 mg/L stock solutions. An independent check was also made by using a multi-elemental standard solution. At the onset of analysis and between each sample measured, standards of 140-Ce and 142-Ce samples and terbium (159) were used. As cerium does not have any known polyatomic interferences, a sub-check was performed. Here, helium was added to one terbium standard and

omitted for a subsequent terbium standard to ensure results were acceptable. All samples were analysed by Dr. Steve Baker, University of Birmingham, UK.

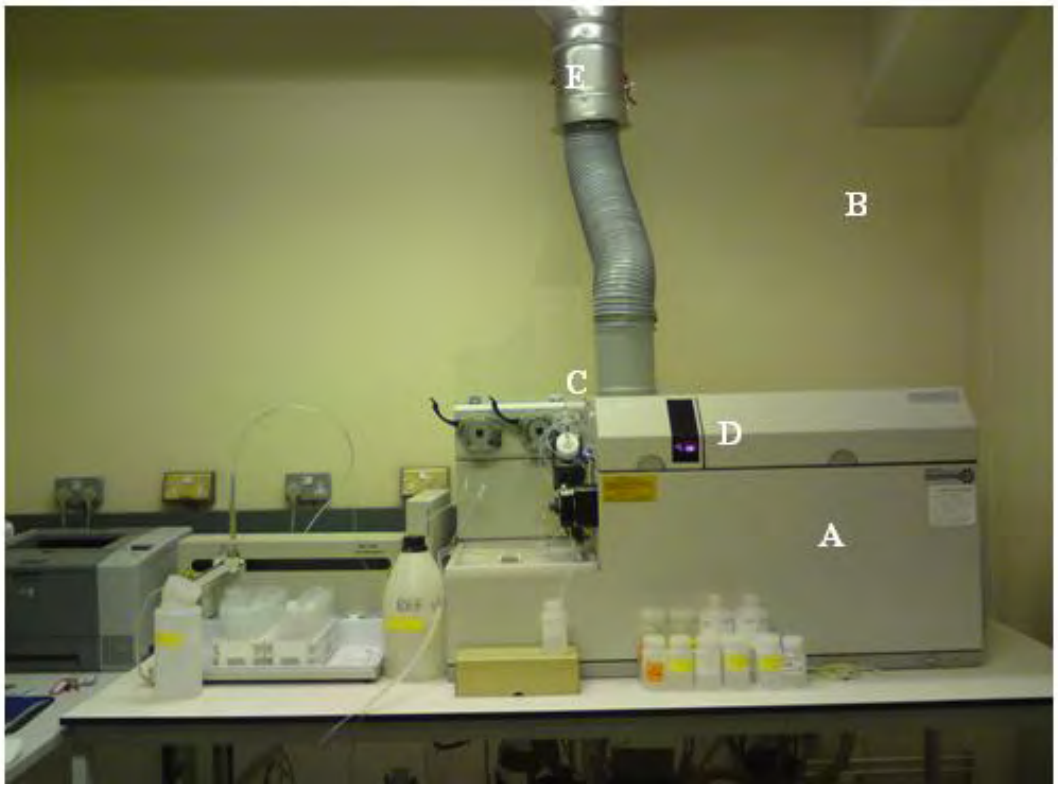

Figure 3-8 ICP-MS instrument used
A) Agilent 7500 ICP-MS instrument housed in an B) air conditioned room. C) sample is injected into D) flame nebuliser and excess gas removed by E) fume hood.

3.6 Particle absorption by UV-visible spectroscopy

Ultra-violet visible spectroscopy (UV-vis) is a useful tool in the detection of NP size changes, aggregation and surface chemistry (Ju-Nam and Lead, 2008) due to the specific position of the surface Plasmon (SP) band (Daniel and Astruc, 2004; Doty *et al*., 2005). SP is the oscillation of electron clouds, present at the metal-solution interface (Hassellöv *et al*., 2008). Both UV-vis absorbance and fluorescence spectrometry use the absorption of incident radiation causes the

excitation of loosely held electrons within double and triple bonds (Henderson *et al*., 2009). The interaction of UV light with liquids is related to electron polarisation which depends on the displacement of electrons with respect to the nucleus of an atom (Räty *et al*., 2004) and the strength of the electric field of the incident light. Ceria attenuates UV and scatters no visible light at all (Wang *et al*., 2010). Ceria also has the ability to be intrinsically excited by UV irradiation (Kydd *et al*., 2010) making UV-vis a useful tool to detect ceria particles in solution.

3.6.1 Theory

When light is absorbed by valence (outer) electrons, the electrons are promoted from their normal (ground) states to higher orbital energy (excited) states. The orbital energies involved in electronic transitions have fixed values. The energies of the photons in the region 200-800 nm permit excitation of outer valence electrons. SP resonance (SPR) bands are produced by the movement of the electrons around the particles, as a consequence of the incident electric field light. This results in a displacement of the negative and positive charges in the metal. This displacement gives origin to the particles polarisation as the positive charge acts as a restoring force to produce oscillations of the electrons (Slistan-Grijalva *et al*., 2005). Small metal NPs possess special SP effects which are particular absorption bands that do not show up in the larger metal particle dispersion or in metal salt solutions (Hassellöv and Kaegi, 2009). The observed shape and size of NPs can be distinguished from the UV-vis spectra obtained.

The absorbance spectra produced display a sharp peak called the first excitation peak at the upper wavelength of the absorption spectra, (Hassellöv *et al*., 2008).

The portion of the absorption peak can be correlated to particle size. The quantum confinement effect suggests the smaller particle size the lower wavelength of light absorbed. Aggregation of NPs can also result in band broadening and red shifting of the SPR band. According to Mie's theory, only a single SPR band is expected in the absorption spectra of spherical NPs. Anisotropic particles could give rise to two or more SPR bands depending on the shape of the particles. The number of peaks therefore increases as the symmetry of the NPs decreases (Stoimenov *et al*., 2002).

3.6.2 Advantages and limitations

Advantages and limitation of UV-vis instrumentation are given in Table 3-8. The area between where the deuterium and tungsten beam intensities decrease and increase cross, can result in low sample absorbencies being obtained, resulting in poor values calculated. NPs can also be more complicated than molecules to measure (Hassellöv and Kaegi, 2009) which also makes the UV-Vis technique less suitable for complex NP mixtures of different compositions and sizes.

Table 3-8 Advantages and limitations of UV-visible spectroscopy

Advantages/limitations	Conditions	References
Advantages	Instrumental set-up and application of UV-Vis is relatively straight forward Little to no sample preparation Analysis is rapid Spectral scans conducted in <1 min Effects from reflection, scatter and absorption by the solvent can be minimised by use of blanks	Clark *et al*., 1993
Limitations	Electronic drift, changes in voltage and effects of temperature, can induce electronic polarisation of charges Errors of method can often arise from the nonlinear behaviour of the sample material Deuterium source only measures below 320 nm and the tungsten source measures above 320 nm Fractional amount of light absorbed and light left for transmission related to the thickness and concentrations of the sample can cause errors.	Thomas, 1996 Swinehart, 1962

3.6.3 Method

UV–Vis absorbance was measured using a WPA lightwave UV–Vis diode-array spectrophotometer (S2000), using deuterium and tungsten filament lamps. Absorption spectra were obtained between 200 nm and 800 nm using a scanning method. A referenced cell, (Spencer *et al*., 2007) containing *ca* 4 ml *d*H_2O or relevant media in a 10 mm quartz cuvette was first conducted. A 1 ml aliquot of a sample was used to rinse the cuvette and subsequently discarded. A further aliquot *ca* 3 ml from the supernatant of a sample was placed in the cell using a disposable syringe and needle, placed into the spectrophotometer and ran

automatically. The cuvette was then rinsed three times in dH$_2$O, three times in 2% HNO$_3$ and three times again in dH$_2$O before addition of the next sample. Spectral scans were collected from at least three repeated measurements, averaged and blank corrected against the reverence cell, (Batchelli *et al*., 2009) to obtain the true absorbance of the sample at each wavelength.

3.7 Emission intensity by fluorescence correlation spectrometry

3.7.1 Theory

Particle fluorescence can be explained by the use of the Jablonski diagram (Figure 3-9).

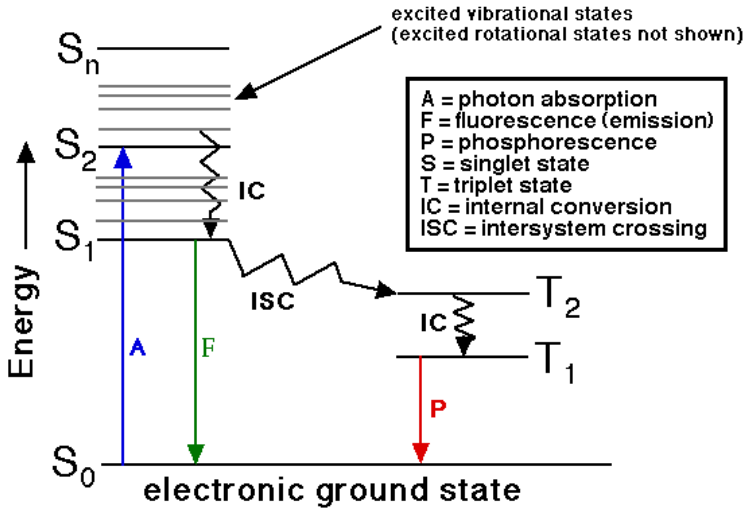

Figure 3-9 Jablonski diagram

Fluorescence is the phenomenon where the light absorbed by a molecule is emitted at a different wavelength than it is excited by. The absorption of light (A) energy (as photons) by a molecule excites if from its electronic ground state (So)

to an excited vibration state ($S_{1\text{-}n}$). The molecule will fall from this excited state to the lower orbital of the paired electron, (Lakowicz, 1983) by loosing energy through emitting radiation (Lakowicz, 1999). This excess energy is converted to vibration energy (IC) causing fluorescence of that molecule. If the spin of an excited electron is reversed, it will leave the molecule in an excited triplet state (T) called intersystem crossing (ISC). A light source from a xenon flash lamp is directed at a sample to excite it. The resulting emission spectrum, taken at right angles, is directed to a detector via a series of prisms. The emission spectrum can be converted to 3D 'excitation-emission matrix' (EEM). The EEM axes show the excitation and emission wavelengths and the observed intensity (Figure 3-10) of the fluorophores produced. A molecule in the T state may not use ISC to return to is ground state but emit a photon causing phosphorescence. A molecule which absorbs light is termed a chromophore, where molecules which absorb and emit light are termed fluorophores. The intensity and location in optical space of these fluorophore peaks can vary depending on sample character (Sierra *et al*., 2005) and changes from temperature, pH and salinity (Coble, 1996) fluctuations. Due to changes in optical space of the measured fluorophores, the regions at which specific known fluorophores are located on an EEM are therefore termed 'fluorophore'-like.

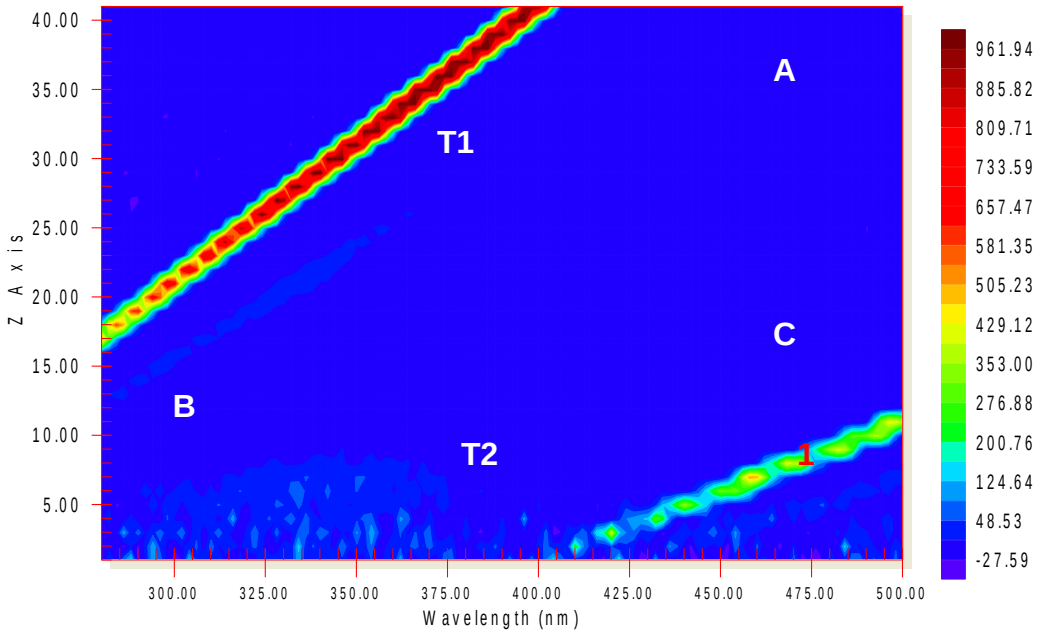

Figure 3-10 Regions of peaks on a typical EEM.
1) Rayleigh line, A) Humic peak, T1, T2) Tryptophan-like peaks, B) Tyrosine- like peak C) Fulvic-like.

The two straight lines (1) stretching diagonally across the EEM are not data and represent the scatter lines of the sample and the cuvette. Peak areas labelled A, B, C and T are typical fluorophores seen in natural and waste waters. Peak A is the region for humic acid and peak C the region for fulvic acid, termed humic-like and fulvic-like respectively. Peak A and Peak C will correlate to total organic carbon (TOC) found in water samples. Two peaks of tryptophan-like fluorophores (Peak 'T') are identified on the EEM, as they often emit in pairs. Peak B is where the protein tyrosine-like fluorophore emits. Tryptophan and tyrosine can be responsible for the protein-like fluorescence intensities correlating to microbial activity and biological oxygen demand (BOD) (Yamashito and Tanoue, 2003) and

amino acids found in water samples. Peak T and B are also present in waste waters and can be an indication of bacterial or faecal contamination. Identified fluorophore peaks, excitation and emission wavelengths, (Exλ and Emλ respectively) used during the NP fluorescence analysis of this work, are summarised in Table 3-9.

Table 3-9 Fluorescence peak excitation and emission regions

Peak	Related matter	Excitation wavelengths (nm)	Emission wavelengths (nm)
1	Raman scatter peak	275	303
T	Tryptophan-like	225 – 237 / 220* and 280*	340-381 / 350* and 350*
C	Fulvic-like	320-390	410-480
A	Humic-like	237-260	400-500
B	Tyrosine - like	225-237 and 275-220*	309-321 and 310-305*

*** Baker and Inverarity, (2004).**

Fluorophore A has undergone much less investigation that fluorophore C (Baker and Spencer, 2004), which is why fulvic acid was chosen, instead of humic acid, during the organic matter (OM) investigations in this work. Also, fulvic substances have a greater fluorescent signal than humic substances (Goslan *et al*., 2004; Sierra *et al*., 2005) which makes fulvic substances easier to distinguish than humic materials.

3.7.2 Advantages and limitations

Some advantages and limitation of fluorescence spectrometry are summarised in Table 3-10.

Table 3-10 Advantages and limitations of fluorescence spectrometry

Advantages/limitations	Conditions	References
Advantages	Rapid technique. Reagents not required. 10-1000X more sensitive than UV-Vis. Single molecule detection possible. None-intrusive method which does not interfere with particles molecular structure. Changes in fluorescent signatures can give information towards the agglomeration of NPs in a solution. Emission peaks tend to narrow and wavelengths are highly sensitive to NP size making it useful to use for NP size determination.	Henderson *et al*., 2009 Cumberland and Baker, 2007 Hassellöv *et al*., 2008
Limitations	Only ionic forms of molecules are fluorescent reducing the number of NPs which are fluorescent. Quantification and monitoring optical and special peak movement can be difficult. Affects of temperature, metal ions, pH and sample concentration can reduce intensity due to increased collision quenching, inner filtering effects and reduced intensity with increased NOM. Fluorophore peaks shifts to longer wavelengths with increases in molecular weight.	Clark *et al*., 1993 Hassellöv and Kaegi, 2009

3.7.3 Method

All fluorescence spectra of samples were recorded on a Varian Cary Eclipse spectrofluorometer equipped with a Peltier temperature controller. EEMs were generated using a method written by Professor Andy Baker, University of Birmingham (Table 3-11). For all samples, a quartz cuvette was first cleaned by three rinses of 2% HNO_3 followed by three rinses with dH_2O. A 1 ml sample was used to further rinse the cuvette which was subsequently discarded before the full sample of *ca* 4 ml was used. The sample was placed in the spectrophotometer and ran automatically. The spectrophotometer was calibrated by detecting the Raman intensity at 395/348 nm (Emλ/Exλ) with a 5 nm slit width, using a sealed water cell (Baker and Inverarity, 2004). These calibrations were

determined at the onset and end of the analytical process, to determine instrumental drift. Results are standardised to a mean Raman emission peak averaged at 20 intensity units, (Cumberland and Baker, 2007). Fluorescence results are reported as both excitation and emission wavelengths and intensity of the observed peaks.

Table 3-11 Fluorescence spectrometer methods

Parameters	Method*
Emission wavelength (nm)	200-400
Excitation wavelength (nm)	280-500
Excitation and emission increments (nm)	5
Slit widths (nm)	5
Voltage applied (V)	725
Temperature (^{O}C)	20 ± 0.1

***Written by Andy Baker, University of Birmingham, (UK) 2008**

3.8 Crystallography and particle size by x-ray diffraction

X-ray diffraction (XRD) is a method of measuring inter-particle spacing resulting from interference between waves reflecting from different crystal planes (Hassellöv *et al*., 2008).

3.8.1 Theory

An element in an alternating electromagnetic field will oscillate with the same frequency as the field it is in (Scintag, 1999). When an x-ray beam falls on an atom, the beam may be absorbed with an ejection of electrons (Warren, 1969). The electrons around the atom start to oscillate with the same frequency as the incoming beam. The atoms in a crystal are arranged in a regular pattern

therefore these waves will be in phase and there will be well defined x-ray beams leaving the sample at various directions. The highest electron densities are found around atoms so the intensities depend on what kind of atoms there are and where in the unit cell they are located thus the elemental composition can be determined. The mean particle sizes of NPs can also be calculated from x-ray line broadening of the (112) diffraction peak from x-ray diffraction by using the Scherrer equation (Equation 3-6).

Equation 3-6 The Scherrer equation

$$d_{XRD} = \frac{(0.94)\lambda}{\beta \cos \theta}$$

The mean crystallite diameter of the particle (d_{XRD}) is assumed to be spherical for this calculation. XRD patterns are used to apply the full-width half-maximum (FWHM) to the Scherrer equation using the radiation wavelength (λ) of the x-ray as 1.54178 and the diffraction peak angle (Cosθ), in radians (Ivanov *et al*., 2008). Instrumental broadening may arise from effects such as wavelength widths or superposition of the peaks, which has to be corrected for (Warren, 1969). The Warren's correction (β) is therefore applied to determine the experimental integral peak width FWHM by the averaged (112) peak from a standard silicon sample, averaged from three measured analysis. The obtained XRD ratio of peaks A(111)/A(200) also offers the probability that one plane will occur predominantly in a given sample (Clinton, 2008). Since the (111) ceria plane has a lower propensity for oxygen vacancies than the (200) ceria plane, (Yang, *et al*.,

2004) the sample with a higher concentration of Ce(III) should result in a higher ratio (Chen and Chang, 2005).

3.8.2 Advantages and limitations

XRD sample preparation is straightforward and rapid. The analysis is relatively easy and interpretation of results a simple process by computerised applications. Elemental composition of major elements can be obtained by XRD, although the sensitivity is much lower in comparison to other elemental techniques e.g. ICP-MS. Also, quite often a large amount of powdered sample is required for analysis using x-ray diffraction. There needs to enough dry powdered sample to cover *ca* 1 cm^2 area. This can be difficult to achieve if the sample is prepared in solution and requires drying.

3.8.3 Method

Powdered samples were prepared by loading into a 1 cm^2 disk holder using scotch tape (Figure 3-11). This disk was loaded into a Siemens D5000 Kristalloflex X-ray powder diffractometer with nickel-filtered CuKα radiation and set to run over a range of Bragg angles (25^o to 90^o) over 50 to 90 min at room temperature. Diffraction patters were obtained and analysed using ETA software. The Joint Committee on Powder Diffraction Standards (JCPDS) database holds over 500,000 XRD diffraction entries which allows for rapid peak matching. For cerium dioxide, the JCPDS matching card is often No. 75-0120. This peak identification confirms the formation of pure-phase CeO_2 powders

belonging to the face-centred cubic arrangement with a lattice dimensional length (a) 5.411Å.

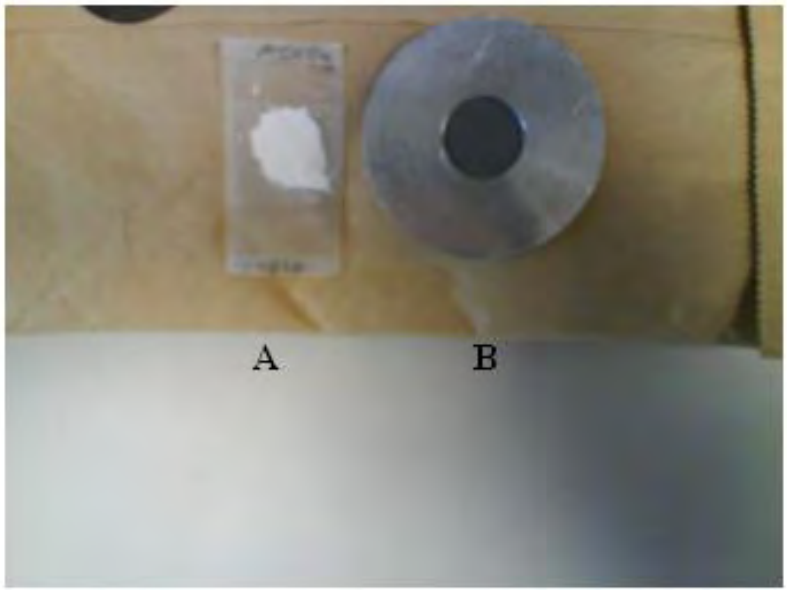

Figure 3-11 Powdered XRD sample preparation
Powdered particles are attached to scotch tape (A) and placed into the XRD disk holder (B).

3.9 Specific surface area by BET

Interactions between nanomaterials and biological organisms have recently been found to coincide with specific surface area (SSA) rather than NP mass (Donaldson *et al*., 1998; Oberdörster *et al*., 1992). This emphasises the need to determine such parameters of SSA for describing the possible chemical or biological reactivity of the particle surface. SSA therefore has particular importance in the reactions on particle surfaces (Nel *et al*., 2006).

3.9.1 Theory

Following the recognition that gases adsorb onto solids in multilayer's when the pressure is increased at the boiling point of a gas, Brunauer, Emmett and Teller, (BET) (1938) derived an adsorption equation termed the 'BET' Value. The BET value is calculated from the known amount of nitrogen atoms adsorbed on the surface of a particle and using the known size of the nitrogen atoms (Karlsson *et al*., 2009) assuming that the particles are spherical and non-porous at cryogenic conditions. Where SA is the measure of how much exposed area a solid object possessed (unit^2), SSA is a measure of the total SA per unit of mass, solid or bulk volume or cross-sectional area. SA measurements are calculated with varying equations depending upon actual material shape. For example, SA measurements for a cube (Equation 3-7) are quite different from that of a sphere (Equation 3-8). SSA can simply be measured from a particle size distribution making some assumption of the particle shape. SSA is derived by Equation 3-9 and Equation 3-10 as a mass or volume calculation respectively.

Equation 3-7 Surface Area of a cube

$$6\,a^2$$

Equation 3-8 Surface area of a sphere

$$\pi\, r^2$$

Equation 3-9 Specific surface area by mass

$$\text{SSA } (m^2/kg) = \frac{SA}{\text{Mass}}$$

Equation 3-10 Specific surface area by volume

$$SSA\ (m^2/m^3) \text{ or } (m^{-1}) = \frac{SA}{Volume}$$

The diameter of a particle can also be estimated from the SSA obtained from BET according to Equation 3-11, where d_{BET} is the diameter of the particles, ρ is the bulk density of the solid (7.132 g cm^{-3} used for CeO_2) and S_{BET} is the SSA measured.

Equation 3-11 Particle diameter measured from SSA obtained by BET analysis.

$$d_{BET} = \frac{6}{(\rho * S_{BET})}$$

3.9.2 Advantages and limitations

Although BET analysis can measure the surface of fine structures and deep textures, the results can differ markedly depending on the substance adsorbed. The SSA from BET analysis also assumes that N_2 has access to the complete surface of the particles (Hassellöv *et al*., 2008). The SSA measured by BET also uses dry samples which may not coincide with the apparent SSA in aqueous dispersions, especially for aggregating particles. The use of SSA is further complicated by the effect of shape on physical and chemical properties of NPs, reducing the precision of the technique. The SSA also assumes the particles measured are spherical in nature, which cannot always be accounted for.

3.9.3 Method

The BET SSA of the nanopowders used during this study was obtained by physical adsorption of N_2 at -196^{o}C using a Micromeritics Ltd, Surface Area Gas Porosimiter 2010. Samples *ca* 1 g powdered NP masses were conducted by Dr. John Wedderburn, University of Birmingham, UK.

3.10 Evaluation

To ensure a full representation of size, shape, crystal structure and chemical parameters during any environmental nanoecotoxicological test, it is important to use a range of techniques available, as summarised in Tables 3-12 and 3-13. One major drawback of using any of the outlined techniques is that only a minute fraction of material is characterised and essentially removed from its original context. Of course this is largely due to the sampling regime and only partially an analytical problem. Also, any sample preparation and certain measurement conditions can often change the structure of the NP being reported. A reduced sample volume makes it extremely difficult to ensure that a representative sample is examined and sample preparation must be taken into account during assessment procedures.

Table 3-12 Summary of instrumentation used for NP size determinations

Method	Optical microscope	AFM	TEM	BET	DLS
Measured parameter	Algae cell counts by haemocytometer	Particle height, shape and topography	Particle number, concentration, size and shape	Specific surface area and porosity	Particle hydrodynamic diameter (d_H) by intensity distribution (Z-ave), polydispersity (PdI), volume and number particle distributions
Principle	Passing visible light through a sample and magnifying it to image by eye	Scanning a probe on a mica surface containing a dry or a wet sample	Interaction of electrons with matter	N_2 absorption	Based upon ability of particles to scatter light.
Sample environment	Ambient air	Ambient air and liquid	Ultra high vacuum	Powdered sample	Aqueous sample, temperature controlled
Calibration method	None as standard	Gold standard	None as standard	None as standard	Polystyrene beads
Advantages	Easy to use Colour images and live specimens observed	High resolution performed in ambient temperatures and pressures	High resolution to offer visual observation of particles	Commercially available analysers with standard protocols	Uncomplicated and rapid Little sample preparation.
Disadvantages	2D imagery and low magnification	Time consuming, Lrge number of particles required	Time consuming, large number of particles required for quantitative particle evaluations	Assumes particles are spherical and full surface is available for gaseous absorption	Signals can be dominated by larger particles Mono-dispersity reliant.
Limit of detection	µm	ppb-ppm	ppb-ppm	SSA; 0.01>2000 m^2/g	~1000 particles present is Required
~size range (nm)	<200 µm	0.5 to >1000	1 to >1000	1 > 1000	3 > 1000

[@]Using quinine sulphate standard

Table 3-13 Summary of instrumentation used for NP chemical characteristics

Method	Electrophoresis	ICP-MS	UV-Vis	Fluorescence spectroscopy	XRD
Measured parameter	Electrophoretic mobility, zeta potential. Using a pH range - point of zero charge.	Dissolution	Estimation of soluble or colloidal organic substances. (SPR for Ag can be used to analyse concentrations)	Fluorophore excitation/emission/intensity/ Emission of light	Crystal structure phases, crystal size, lattice constants and parameters
Principle	Used for characterising biomedical polymers (Werner *et al*., 1999), Electro-kinetic particle transport (Ye *et al*., 2003) and Characterising micro fluids (Sze *et al*., 2003) by measuring velocity of particles in ionic solutions	Used for elemental determinations by vaporising elemental solutions	Used for the quantitative determination of different analytes by light absorbance or transmission of a suspended sample.	Analysis of frequencies emitted by excitation of species excited through photon emission.	Elastic interaction of x-rays with matter.
Sample environment	Liquid sample	Dilute liquid samples	Liquid sample	Aqueous sample	Ambient temperature.
Calibration method	Commercially available zeta potential calibration solutions (-68 mV ±6.8 mV).	BDH ICP-MS standards (Aristar) at 0, 1, 5, 20 and 50 ppb dilutions. Independent check by multi-elemental standard solution. Polyatomic interferences internal standardisation and sensitivity checks performed by standards terbium (159) for cerium (140 and 142).	Referenced samples against water or 'blank' sample cell.	Raman sealed cell	Automated software
Advantages	Uncomplicated and rapid, little/no sample preparation	Concentrations of ppt can be measured	No sample preparation. Simple, quick technique. None evasive	Uncomplicated and rapid No sample preparation	Non-destructive and fast
Disadvantages	Only representation of the calculated zeta potential with limited charge heterogeneity	Destructive technique isobaric. Molecular and doubly-charged ion interferences. Matrix effects.	Signal depends on concentration and extinction coefficient. Interferences from turbidity by particles.	Sensitive to fluctuations in pH, sample concentrations and to temperature	Low sensitivity and spatial resolution compared to TEM. Large sample mass required.
Limit of detection	ppm	0.0005 µg/l (ppt-ppb)	1 pg/ml	1 ng/mL[@]	Dry powder
~ size range (nm)	3 to >1000	<150	Depends on fractionation	Concentration sensitive	0.5 to >1000

4 Laboratory methods

4.1 Chapter summary

This chapter offers the detailed operation of particle preparations conducted during this work and as directed by the collaborative institutes. The chapter begins with a brief background covering safety precautions and choices of containers used. The details of the preparation methods, for each individual media and particle dispersion, are then discussed. The metabolomic analysis and protocols along with the use of MS is discussed in Chapter 8.

4.2 Central methods

4.2.1 Safety

Gloves were always worn during any particle handling along with laboratory coats along with eye protection and laboratory coats. Laboratory coats were never used across laboratories to reduce contamination of other workspaces. During NP powder handling, a face mask was always worn as a precautionary approach to reduce particle inhalation of airborne materials.

4.2.2 Containers

Although there is little evidence to suggest specific vessel material (glass, Teflon, plastic) increase adsorption or contamination of water samples (Reimann *et al*., 1999), PP vessels were chosen for characterisations and ICP-MS analysis

(Figure 4-1a-d) and glass was used for *P. subcapitata* growth and toxicity tests (Figure 4-1b) (Rogers *et al*., 2010). Centrifuged samples conducted in sterile plastic vessels (Figure 4-1c) and Pzc samples in 8 ml glass vials (Figure 4-1d). During sample transportation from collaborative institutes samples were housed in darkened bottles (Figure 4-1e) to reduce any photo-reactivity effects of the particles.

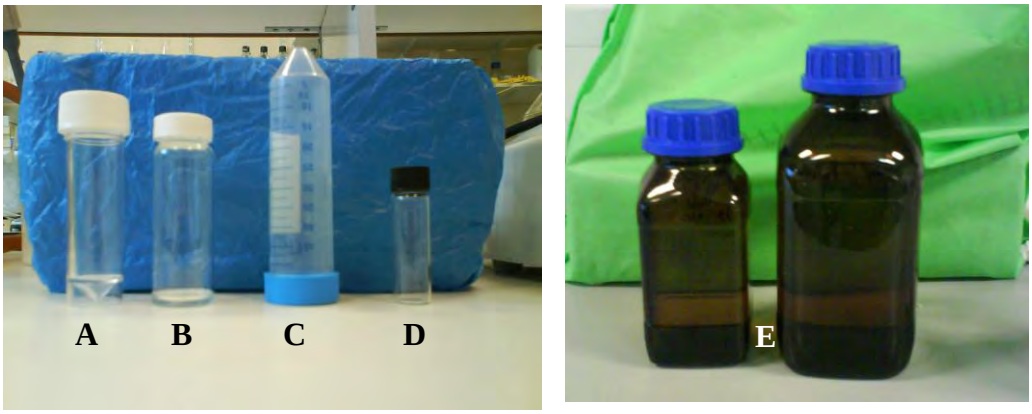

Figure 4-1 Containers used during the study.
A) PP 30ml vessels, B) glass 30ml vessels, C) PP centrifuge vessel, D) 8ml glass vial, E) brown glassware.

All glass and plastic-ware used was pre-acidified for 24 h in 10% HNO_3 and rinsed three times with *d*H_2O. The glassware was left to dry overnight in a dust free oven at ~33^{O}C. All plastic materials were left to air dry in a pre-acidified container covered with foil. For algal work, all new glassware was soaked for 24 h in 5% decon solution, rinsed three times in *d*H_2O. The glassware was then soaked for 24 h in 10% HNO_3 bath and rinse three times again using *d*H_2O. Glassware was again dried overnight in a dust-free oven. All glass equipment for

algal work was autoclaved using a Boxer microprocessor to 123^{O}C for 15 min prior to use.

4.2.3 Weighing

All powdered particles were weighed using a tarred, plastic weighing boat, on a pre-calibrated Satørius MC5 balance after static was removed. A balance was also housed in an XIT powder weighing still air cabinet (Figure 4-2) especially designed for the capture of fine particles. Calibration of the balance was conducted weekly by Dr. Gillian Kingston, Laboratory Manager.

Figure 4-2 XIT still-air cabinet

4.2.4 pH measurements

All pH measurements were conducted using a PHM 240 PH/ION meter lab probe. The probe was calibrated before use, using the standard calibration buffers (pH 4, pH 7 and pH 10) at room temperature. Calibration instructions were followed until a calibration curve >97% was met. Solution pH values were adjusted, where required, by the addition of dilute HNO_3 or sodium hydroxide (NaOH), at 0.01 *M*, 0.1 *M* and 1 *M* solutions.

4.2.5 Pipette calibrations

Pipette calibrations were performed using Milli-Q water and a calibrated mass balance, where 1 ml distilled water = 1 g.

4.2.6 Disposal

Waste NP solutions were placed in a 10 L high density plastic container. Calcium nitrate $Ca(NO_3)_2$ at 1 *M* was added to the vessel and left for 24 h. The suspension was filtered using 0.45 µm Whatman filter, which was subsequently disposed of via incineration. The filtrates were sent to the University of Birmingham disposal service (PHS Waste management), and treated as hazardous waste. Algal waste solutions were collected at the end of a test period and autoclaved to ensure all cell death. Calcium nitrate at 1 *M* was added to the container and left for 24 h, filtered and sent for disposal as discussed above.

4.2.7 Statistical analysis

Statistical tests were selected using a one way ANOVA and student's t-test using Excel statistical package. A *p* value <0.05 was considered significant in all occasions.

4.3 Preparation methods

Nano- and bulk-ceria particles were received from various collaborators with a variety of speculative properties, (Table 4-1). The ceria particles obtained from Sigma Aldrich, UK are termed ceria[a], particles from Alga Aesar are termed ceria[b] and particles obtained from Sigma Aldrich USA, are refred to as ceria[c] particles.

Table 4-1 Commercial nano- and bulk-ceria particle suppliers

Particle Used	Manufacturer	Manufacture size (nm)	Collaborator	Use
Ceria[a]	Sigma Aldrich, (UK) S26.	<25 nm (Nano) <5 µm(Bulk)	Napier University	Cell lines, *D. rerio* and *D. magna* exposures None-exposure characteristics in Exeter's determined *C. carpio* media and in NaCl solutions.
Ceria[b]	Alfa Aesar, (UK)	<35 nm (Nano) < 25 µm (Bulk)	Exeter University	35 and 10 day *C. carpio* exposures and none-exposure characteristics in NaCl solutions.
Ceria[c]	Sigma Aldrich (St Louis, MO, USA).	10-20 nm (Nano) (SA 80 m^2g^{-1} by manufacturer BET) Uncoated cerium (IV) oxide nanopowder < 5 µm (Bulk) Macro-particulate cerium (IV) oxide powder (99.9%)	CSIRO, Sydney Australia	*P. subcapitata* exposures and NaCl solution tests

Following discussions with collaborators, individual methods of particle preparation were established. Particles were prepared in relevant media at given stock concentrations, pH conditions and temperatures (Table 4-2). Cell culture mediums were also used for NP characterisations in the absence of cells using nano- and bulk-ceria[a] under specific conditions (Table 4-3).

Table 4-2 Guidelines for media preparation
Electrolyte solution concentrations and guidelines as given by collaborators

	Organism	***D. magna***	***C. carpio***	***C. carpio***	***P. subcapitata***	***D. rerio***
	Particles	ceria[a]	ceria[a]	ceria[b]	ceria[c]	ceria[a]
	Guideline	EPA (2002), ISO 6341, OECD 202.	OECD 204	ISO/DIS 7346-1.	ISO 8692, OECD 201	OECD 210
	$NaHCO_3$	192.0				
E	KCl	8.0	0.5175	0.5175		0.4
L	$MgSO_4$	120.0			3.675	0.5
E	$CaSO_4$	6.120				
C	NaCl		2.0675	2.0675		2.0
T	$MgCl_2$		1.095	1.095	3.040	
R	$CaCl_2$		6.125	6.125	1.10	3.0
O	H_3BO_3				46.40	
L	$MnCl_2$				104.0	
Y	$ZnZl_2$				0.820	
T	$FeCl_3$				40.0	
E	$CoCl_2$				0.360	
	Na_2MoO_4				1.820	
(mg/L^{-1})	$CuCl_2$				0.003	
	$NaNO_3$				6.375	
	KH_2PO_4				0.261	
	$NaHCO_3$				3.750	
	Sodium citrate			0.5		
	Temp (^OC)	20	10	10	24-27	12-15
	pH	7.9	7.3-7.6	7.3-7.6	6.5	7.3-7.6

Table 4-3 Additional materials in Eagle media for cell tests used for ceria[a]

	Details		
Cell lines	**Primary Trout hepatocyte**	**Human Hepatocyte C3A**	**Intestinal M cell Caco-2**
Media reference	Sigma Media M199	Sigma media M2279	Sigma media MEM (D6171)
$CaCl_2$ (mg/L)	0.0005		
$NaHCO_3$ (mg/L)	0.000344		
ADDITIONS	100 Units/mL penicillin/0.1 mg/mL streptomycin 0.834g/L Hepes, 0.344g/L 10% foetal calf serum	2mM L-glutamine 100Units/mL penicillin/0.1mg/mL streptomycin 10% foetal calf serum 1mM 28 sodium pyruvate 1% non-essential amino acids (Sigma M7145)	5ml Glutamax (Bibco 35050) 5ml non-essential amino acids (Sigma M7145) 50ml foetal calf serum 0.6ml Gentamcyin (Sigma G1272)
Temp (^{O}C)	12	37	37
pH	7	7	7

To further understand the likely fate and behaviour of NPs, it is also essential to understand their interaction with natural water components (Baalousha *et al*., 2008), such as natural organic material (NOM). NOM is known to play a critical role in controlling the biogeochemical uptake of trace elements (Guo *et al*., 2001) and be used as a carbon and energy source by organisms (OU, 1996).

To represent NOM in comparative synthetic media samples, Suwannee River Fulvic Acid (SRFA) purchased from the International Humic Substances Society

was used as received (Diallo *et al*., 2005; Hyung *et al*., 2007). DOC can be found at 0.54 to 20.9 mg/L between the Gulf of Mexico and Sabine-Neches estuary respectively (Guo *et al*., 2001). From this, a representative concentration of 10 mg/L SRFA (unless stated) was added in some media solutions, as conducted by Cumberland and Lead, (2009).

4.3.1 Pzc

For samples requiring Pzc analysis, at least six aliquots of 8 ml from each 10 mg/L particle solutions prepared were taken in 10 ml glass vessels with plastic screw lids, (Figure 4-1d). The pH of each six individual aliquots, were converted to between pH 2 and pH 10. These were pH monitored after 24 h being left in the dark at 4^{O}C prior to electrophoretic analysis.

4.4 Media preparations

4.4.1 Electrolyte solutions

Electrolyte stock solutions of 10 *mM* and 500 *mM* NaCl were prepared by filtering Milli-Q water using a pre-acidified 0.45 µm filter (Chapter 3) in the presence and absence of SRFA (Table 4-4). A 100 mg/L ceria dispersion was prepared from these stocks and sonicated for 30 min. A variety of particle concentrations were prepared using aliquots from the stocks using the remaining electrolyte stock solutions for dilutions. All samples were housed at 4^{O}C in the dark for 24 h before characterisation assessments.

Table 4-4 NaCl stock solutions preparation
In 1 L volumetric flasks using filtered Milli-Q water at pH 7, NaCl solutions were sonicated for 30 min. Using the appropriate NaCl stock solutions, 100 mg/L stock solutions of nano-and bulk-ceria were prepared in 50 ml volumetric flasks. These were stored in 30 ml volumes in PP vessels. Using appropriate NaCl stock solutions, aliquots of ceria particle stocks solutions were used to prepare 20, 10, 5, 1, 0.1 and 0.01 mg/L concentration at 20 ml volumes.

NaCl Stock solution (*mM*)	NaCl mass (g) in 1 L	SRFA mass (mg)	Ceria particle mass (mg/L)
10	0.58	0	50
10	0.58	10	50
500	29	0	50
	29	10	50

4.4.2 Cell culture exposure media

Three cell culture media termed 'Trout' 'Caco-2' and 'C3A' (Table 4-3) were sent courtesy of Dr. Birgit Gaiser at Napier University and were used as received, for dilutions and stock preparatory solutions (Table 4-5). All aliquots prepared were sonicated for 30 min and housed at $4^{O}C$ in the dark for 24 h before characterisation assessments. One specific concentration, as used for exposures by collaborators of 62.5 µg/L was also investigated.

Table 4-5 Cell culture media particle dispersion preparation
Cell mediums were used as received at pH 7. Nano- and bulk-ceria[a] particles were weighed to prepare 100 mg/L stock solutions directly dispersed in all cell mediums and sonicated for 30 min. Using the appropriate cell medium solutions, aliquots of particle stocks were used to prepare 20, 10, 5, 1, 0.1 and 0.01 mg/L at 20 ml volumes. A further concentration 62.5 µg/L was also prepared for all particles.

Cell media solution	Ceria particle mass (mg/L)
C3A	100
Trout	100
Caco-2	100

4.4.3 *C. carpio* exposure media

Both commercially available Alfa Aesar (ceria[b]) and Sigma Aldrich (ceria[a]) particles were used to compare commercial particles of the same chemical form, from different manufacturers, in *C. carpio* exposure media. The *C. carpio* media salt solution was prepared (Table 4-2), in the presence and absence of 10 mg/L SRFA, with sodium citrate at 0.005%/vol used as a stabilisation agent (Table 4-6).

Table 4-6 *C. carpio* media stock solution preparations

In 1 L volumetric flasks using Milli-Q water, *C. carpio* media was prepared and filtered to 0.45 µm along with a combination of SRFA and sodium citrate additions. Using the appropriate media solutions, nano-and bulk-ceria[a+b] particles from both Alfa Aesar and Sigma Aldrich manufacturers at 100 mg/L stock solutions were prepared in 50 ml volumetric flasks and sonicated for 30 min. These were stored in 30 ml volumes in PP vessels. Using appropriate media solutions, aliquots of these ceria particle stocks solutions were used to prepare 20, 10, 5, 1, 0.1 and 0.01 mg/L at 20 ml volumes, in 30 ml PP vessels.

C. carpio solutions	SRFA mass (mg)	Sodium citrate 0.005%/volume	Ceria particle mass (mg/L)
Media 1	0	No	100
Media 2	10	No	100
Media 3	0	Yes	100
Media 4	10	Yes	100

All ceria particle stock solutions (100 mg/L) were sonicated for 30 min prior to aliquot preparation (0.01-50 mg/L) and stored at 4^{O}C in the dark for 24 h prior to characterisation tests.

4.4.4 *D. magna* exposure media

The *D. magna* media salt solution was prepared (Table 4-2), in the presence and absence of 10 mg/L SRFA. Stock samples of ceria[a] particles were prepared at 100 mg/L and sonicated for 30 min. Stock solutions were then diluted using appropriate *D. magna* media to produce a range of particle aliquot solutions (Table 4-7). Samples were kept at 4^{O}C in the dark prior to characterisation assessments.

Table 4-7 *D. magna* media stock solution preparations

***D. magna* media in 1 L volumetric flasks were prepared using Milli-Q water at pH 7 and filtered to 0.45 µm. A further media solution was prepared with the addition of 10 mg/L SRFA additions. Using the appropriate media solutions, nano- and bulk-ceria[a] at 100 mg/L stock solutions were prepared in 1 L volumetric flasks and sonicated for 30 min. These were stored in 30 ml volumes in PP vessels at pH 7. Using appropriate media solutions, aliquots of ceria[a] particle stock solutions were used to prepare 20, 10, 5, 1, 0.1 and 0.01 mg/L at 20 ml volumes, in 30 ml PP vessels.**

D. magna solutions	SRFA mass (mg)	Ceria particle mass (mg/L)
Media 1	0	100
Media 2	10	100

4.4.5 *D. rerio* exposure media

Media used for *D. rerio* exposures were sent by collaborators at Exeter University consisting of salt concentrations shown in Table 4-2. The nano- and bulk-ceria[a] particles were weighed to 50 mg and made to 500 ml volume by using these sent solutions and sonicated for 30 min. Aliquots were prepared from the media and stock solutions to prepare 0.01-50 mg/L particle concentrations. Samples were left in the dark at 4^{O}C for 24 h prior to analysis.

4.4.6 *P. subcapitata* exposure media

P. subcapitata growth media was prepared as suggested by the collaborators at CSIRO as modified from Stauber, Franklin and Adams, (2005). EDTA is known to interfere with organic ligands, in respect to metal complexation (Guéguen *et al*., 2003) and has been found to release lipopolysaccharides in the bacterium *E. coli* (Amro *et al*., 2000). EDTA is therefore omitted during metal toxicity exposures and thus during characterisation investigations. For *P. subcapitata* growth however, EDTA is added to the media to aid metal elimination which may be present in solution. Five stock solutions were required for *P. subcapitata* exposure media preparation, (Table 4-8).

Table 4-8 Liquid Growth Medium for the stock *P. subcapitata* culture.

Stock Solution	Compound	Amount Dissolved in 250mL Milli-Q® Water (mg)
1~	$MgCl_2.6H_2O$	3040
	$CaCl_2.2H_2O$	1100 (g)
	H_3BO_3	46.4
	$MnCl_2.4H_2O$	104.0
	$ZnCl_2$	0.82[a]
	$FeCl_3.6H_2O$	40
	$CoCl_2.6H_2O$	0.36[b]
	$Na_2MoO_4.2H_2O$	1.82[c]
	$CuCl_2.2H_2O$	0.003[d]
	*$Na_2EDTA.2H_2O$	150
2	$NaNO_3$	6375
3	$MgSO_4.7H_2O$	3675
4	K_2HPO_4	2610
5	$NaHCO_3$	375

a $ZnCl_2$ at 164 mg is weighed out and diluted to 100 mL. From this, 0.5 mL is added to Stock #1.
b $CoCl_2.6H_2O$ at 71.4 mg is weighed out and diluted to 100 mL. From this, 0.5 mL is added to Stock #1.
c $Na_2MoO_4.2H_2O$ at 36.4 mg is weighed out and diluted to 10 mL. From this, 0.5 mL is added to Stock #1.
d $CuCl_2.2H_2O$ at 60.0 mg is weighed out and diluted to 1000 mL. 1 mL of this solution was added into a 10mL volumetric flask and made to volume. From this second dilution, 0.5 mL is added to Stock #1.
*** omitted during chemical tests and exposures.**
~For stock solution 1, each salt was dissolved prior to adding the next chemical according to the specific instructions

PIPES Buffer (Piperazine-1,4-bis(2-ethanesulfonic acid) $C_8H_{18}N_2O_6S_2$) at 0.5 *M* was prepared by weighing 17.315 g into a tarred polycarbonate vial. Milli-Q water was added at *ca* 50 mL and *ca* 500 µL of 3 *M* HCl then further diluted with additional Milli-Q to 100 ml and brought to *ca* pH 8.5. The final concentration of nutrients in the culture medium is given in Table 4-9.

Table 4-9 Final concentration of nutrients in stock *P. subcapitata* culture

Macronutrient	Concentration (mg/L)
$NaNO_3$	25.5
$MgCl_2.6H_2O$	12.2
$CaCl_2.2H_2O$	4.41
$MgSO_4.7H_2O$	14.7
$K_2H_2PO_4$	1.04
$NaHCO_3$	15.0
H_3BO_3	185
$MnCl_2.4H_2O$	416
$ZnCl_2$	3.27
$CoCl_2.6H_2O$	1.43
$CuCl_2.2H_2O$	0.012
$Na_2MoO_4.2H_2O$	7.26
$FeCl_3.6H_2O$	160
$Na_2EDTA.2H_2O$	300
pH	7.5 ± 0.1

This medium has an alkalinity of 9 mg $CaCO_3$/L and water hardness of 15 mg $CaCO_3$/L.
PIPES buffer addition of 1 ml in 1 L had a final concentration of 2 *mM*. Values assume no complexation due to PIPES buffer taken from Stauber, Franklin and Adams, (2005).

For *P. subcapitata* exposure media, 1 ml from each of the five stock solutions (Table 4-8) was added to approximately 900 mL of Milli-Q water and made up to 1 L using Milli-Q water. Four *P. subcapitata* media were prepared for ceria[c] characterisation assessments as described in Table 4-10. All media prepared were used immediately for characterisation studies.

Table 4-10 Nano- and bulk-ceria[c] preparation in *P. subcapitata* media
Media 1 is prepared with 1 ml of each 5 stock solutions. This was repeated with 1 ml PIPES as media 2. A third media solutions had the addition of along with 10 mg/L SRFA and a fourth media had 10 mg/L SRFA and 1 mL PIPES buffer additions. All media were adjusted to required pH (between 7.5 and 6.5 ± 0.1) by drop wise addition of 3 *M* HCL. Each of the four media solution were then filtered to 0.20 µm and used immediately for particle preparations. Using the appropriate media solutions, nano- and bulk-ceria[c] at 100 mg/L^{-1} stock solutions were prepared in 1 L volumetric flasks and sonicated for 30 min. These were stored in 30 ml volumes in PP vessels. Using appropriate media solutions, aliquots of ceria[c] particle stock solutions were used to prepare 20, 10, 5, 1, 0.1 and 0.01 mg/L at 20 ml volumes, in 30 ml PP vessels.

*M*edia solutions	SRFA mass (mg)	PIPES buffer (ml)	Ceria particle mass (mg/L)
Media 1	0	0	100
Media 2	0	1	100
Media 3	10	0	100
Media 4	10	1	100

4.5 Exposure methods

Collaborators from Napier University and Exeter University contributed ceria particle dispersion samples taken during their exposure assessments to *D. magna* and *C. carpio* respectively. Exposure assessments on *P. subcapitata* were carried out independently under the training and advice of the collaborative institute, CSIRO.

4.5.1 *D. magna* exposures

Daphnia magna exposures were conducted by Phillip Rosenkranz under the guidance and supervision of Dr. Birgit Gaiser and Professor Vicky Stone, at the University of Napier, Scotland. For *D. magna* exposures, all glassware was washed through a dishwater using *d*H_20 and then soaked for 24 h in 20-30% HCl, then rinsed three times in *d*H_20 again. Media salt concentrations (Table 4-2), were prepared and stored in a 100 L tank to reduce variation in readings of

conductivity (mean 430 µS and pH 7.9). The vessels were housed in a climate chamber at a constant 20 ^{O}C ± 0.5 ^{O}C and a 16 h light/ 8 h dark cycle.

Each ceria[a] particle treatment (Table 4-11) consisted of 120 ml media in 1 L glass beakers. A 75 ml sample was taken and replaced with fresh media and appropriate spiked particle treatments and termed Day 0 (D0). A further 75 ml sample was taken from each test vessel (D1 to D3) every day throughout the exposure period. Silver exposures were also conducted using *D. magna* (tank 2-5) and *C. carpio* by the collaborators at Napier University, but particle characterisation results are not represented in this thesis (Appendix A).

Table 4-11 Tank set-up for *D. magna* exposures.
[`]Six neonates were added to each treatment vessel of 120 ml media spiked with appropriate ceria[a] particle treatments after 'Day 0' sample taken (tanks 6-11).
The 1 mg/L^{-1} nano-silver treatments showed 100% mortality, so no 1 mg/L nano-silver treatments after 96h (D4) were produced and processed (tanks 2-5).
^ Particle stock solutions of 10 mg/L were prepared and sonicated for 30 min before inoculating.
[#]Nanoparticle
[*]Bulk particle

Tank[`]	Ceria (mg/L) ^
1	0
2	0
3	0
4	0
5	0
6	0.01[#]
7	1[#]
8	10[#]
9	0.01[*]
10	1[*]
11	10[*]

4.5.2 *C. carpio* exposures

Nano- and bulk-ceria[b] were used in exposures to *C. carpio* in duplicate studies at Exeter University. The first of these studies was conducted by Dr Blair Johnson over a 35 d exposure period using twelve separate treatments. The second repeated test was conducted by Rhys Goodhead over a 10 d exposure, under the same conditions. All work was overseen by Professor Charles Tyler.

4.5.2.1 Test 1

Twelve 60 L fish tanks were prepared at Exeter University by Dr. Blair Johnson. Nano- and bulk-ceria[b] solutions were prepared with the additions of 0.005%/vol sodium citrate. A stock concentration of 30 times higher than the highest dose was prepared at 1.5 mgL and sonicated for 30 min. Two 100 ml stock bottles of nano- and bulk-ceria[b] were added to the adjusted amount of sodium citrate solution and sonicated again for 30 min. For representative NOM samples, 10 ml of the correct concentration (50-250 µgL) of SRFA (not sonicated) was added to the tank before the particle and sodium citrate solution was added. Nano- and bulk-ceria[b] stocks were prepared in 1 L doses and added to the 29 L of water in the tank. Both nano- and bulk-ceria[b] were prepared at concentrations of 5 and 50 μgL^{-1} and added to tanks with and without SRFA. One tank remained with no particles or SRFA, only containing sodium citrate as a blank control. The particle concentrations in each tank are shown in Table 4-12.

Pre-exposure samples were taken (D0) followed by a sample extracted from the tanks 1 h after *C. carpio* were exposed (D1). Samples were taken from the base of the tank and placed in a labelled darkened 125 ml sample bottle. Further samples were taken on D7, D14, D21 and D35. These samples were sent to the University of Birmingham for immediate characterisation analysis. The water within the fish tanks was removed by half (15 L) every two days and replaced with the same volume of water, including the addition of appropriate particles, SRFA and sodium citrate where required.

Table 4-12 Tank set-up for nano- and bulk-ceria exposure to *C. carpio* for 35 days.
[’] 60 L tanks used with 30 L media, each with 18 fish. Fish were of a small size around 20 g and approximately 1 year old having been bred at Exeter University, fed once a day during exposures. The temperatures of the tanks were kept to an average daily temperature of between 11 ^{O}C to 12.6 ^{O}C. The average charges on the tanks were recorded at 190 µs (between 219 µs and 269 µs) and each tank was kept at an average of pH 7.85 (between 7.14 to 7.57).
*** Nano-ceria[b] mass**
 # Bulk-ceria[b] mass
[@] Cerium nitrate solution
^ All fish died within tank by end of investigation

Tank[’]	Sodium citrate (µg/L)	SRFA (µg/L)	Ceria (µg/L)
1	0.005	0	0
2	0.005	50	0
3	0.005	250	0
4	0.005	0	5*
5	0.005	50	5*
6	0.005	250	5*
7	0.005	0	50*
8	0.005	50	50*
9	0.005	250	50*
10	0.005	50	50[#]
11^	0.005	50	50[@]
12	0	0	0

4.5.2.2 Test 2

The second test was conducted by Rhys Goodhead one year after Test 1 following the same protocol. The only variation between Test 1 and Test 2 was the number of test tanks used (Table 4-13). A sample of the stock solution (30X higher than the dose) was also supplied for TEM preparation.

Table 4-13 Tank set-up for nano- and bulk-ceria exposure to *C. carpio* for 10 days.
[,] 60 L tanks used with 30 L media, each with 18 fish. Fish were of a small size around 20 g and approximately 1 year old having been bred at Exeter University, fed once a day during exposures. The temperatures of the tanks were kept to an average daily temperature of between 11 ^{O}C to 12.6 ^{O}C. The average charges on the tanks were recorded at 190 µs (between 219 µs and 269 µs) and each tank was kept at an average of pH 7.85 (between pH 7.14 to pH 7.57).
*** Nano-ceria[b] mass**
 # Bulk-ceria[b] mass

Tank[,]	Sodium citrate (µg/L)	SRFA (µg/L)	Ceria (µg/L)
1	0.005	50	0
2	0.005	250	0
3	0.005	0	5*
4	0.005	50	5*
5	0.005	250	5*
6	0.005	0	50*
7	0.005	50	50*
8	0.005	250	50*
9	0.005	50	50#
10	0.005	0	0

4.5.3 *P. selenastrum* exposures

P. selenastrum exposure samples could not be sent for analysis from the collaborators at CSIRO. *P. selenastrum* exposures were therefore conducted independently at Birmingham University under the same conditions as set out by the collaborator. Six weeks training was given on site at CSIRO to ensure *Modus operandi*.

4.5.3.1 *P. selenastrum* growth cultures

All handling and transferring of *P. selenastrum* during culturing procedures was carried out using aseptic techniques, in a biohazard cabinet. *P. selenastrum* growth media (Table 4-8) was prepared by adding 1 ml of each five stocks (stock 1 with EDTA) to 1 L Milli-Q water (Section 4.4.6). Growth media was then filter sterilised (Figure 4-3). Aliquots of 50 mL filter-sterilised medium were then dispensed into a pre-sterilised 250 mL Erlenmeyer flask, capped with loose fitting lids ready for algal inoculation.

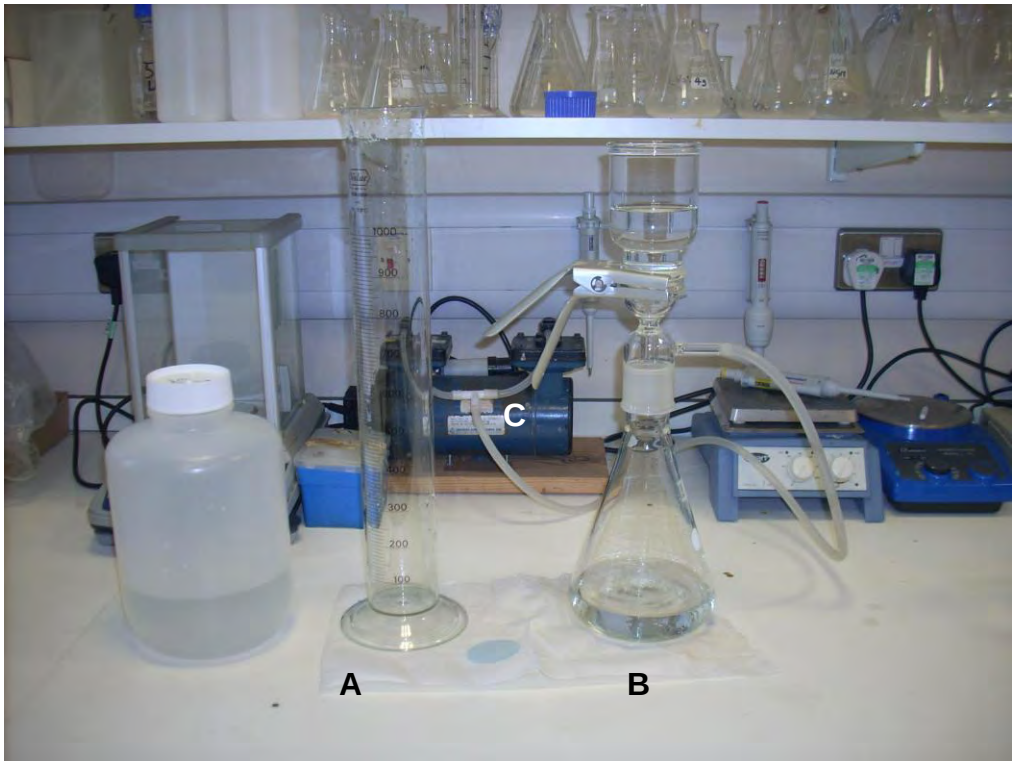

Figure 4-3 *P. selenastrum* media preparation set-up
1 L glass measuring cylinder (A), and the sterile filter system (B) with pump (C).

P. subcapitata was obtained from the ATCC culture (22662) UK. From this initial vial, 2 ml of *P. selenastrum* was removed by using a sterilised 5 mL pipette tips in a biohazard flow cabinet and placed into 50 mL filter sterilised growth media (with EDTA) at room temperature. Subsequent *P. subcapitata* stock cultures were prepared weekly, with each flask aseptically inoculated with 1 mL of the previous week's culture of using sterile 5 mL pipettes. The flasks were capped and stored in an incubation cabinet with fluorescent tubes providing standard conditions (Table 4-14), with a fitted agitation table at 100 rpm.

Table 4-14 Summary of culture conditions for *P. subcapitata*.

Temperature	$24 \pm 1°C$
Light quality	"Cool White" fluorescent lighting
Light intensity	65 ± 5 µmol s^{-1} m^{-2}
Photoperiod	Continuous illumination
pH	7.5 ± 0.1

4.5.3.2 *P. subcapitata* exposure suspensions

P. subcapitata inoculums were prepared and used within 2 h. The algal inoculums were prepared by decanting *ca* 25 mL of an exponentially-growing stock culture of 4-5 days old of *P. selenastrum* (Section 4.5.3.1) into two centrifuge tubes (Figure 4-1c) and centrifuged at low speed (~2500 revs/min) for 7 min. The supernatant was removed in each tube and the algal pellet gently re-suspend in *ca* 25 ml exposure media (without EDTA), vortex and then centrifuging again. The centrifuging and rinsing process was repeated twice more resulting in a concentrated algal suspension in fresh test media (without EDTA). This was then diluted in *ca* 15 ml of test media, ready for counting and

inoculating into the toxicity test containers. Each test vial was then secured with a screw lid and loosened by ¼ turn to allow gas exchange during the test period and placed on a shaker. The pH measurements were recorded on D0 and at test completion after 72 h (D3). The test conditions are based on the OECD Test Guideline 201, (1984) summarised in Table 4-15.

4.5.3.3 Cell counts

The required initial cell count volumes for each mini-vial was a density of 2-4 $\times$ 10^4 cells/ml (Rogers *et al*., 2010). This was calculated and checked by inoculating a "counting vial" with 10 ml media and *ca* 50 µL of the *P. subcapitata* exposure suspension. The density of *P. subcapitata* cells in the counting vial was determined by haemocytometer. The calculated volume of *P. subcapitata* inoculums is not to exceed 0.5% of the total media volume (e.g. 50 µl in 10 mL). To check calculated cell counts, a further counting vial is inoculated for validation. Upon validation this volume was then added to all sample vessels requiring *P. subcapitata* cells. To ensure the suspension remains homogenous, the *P. subcapitata* exposure suspension was covered and vortex between every 3 inoculations. The confirmation and recording of D0 cell density in three replicates of each test concentration was conducted using a haemocytometer and in some cases confirmed by spectroscopic means (Section 3.6) using UV-visible spectroscopy.

Table 4-15 Summary of growth inhibition test conditions to *P. subcapitata* Revised from OECD 201 (1984) guidelines

Test type:	Shaking
Temperature:	24 ± 2°C
Light quality:	"Cool white" fluorescent lighting
Light intensity:	4000 ± 10% lux (65 µmols photons/m^2/s)
Photoperiod:	Continuous illumination
Test chamber size:	30 mL minivial
Test solution volume:	10-15 mL minivial
Renewal of test solutions:	None
Age of test organisms:	4 - 5 days (in exponential phase of growth)
Initial cell density:	10,0000 cells/mL
No. replicate vessels / concentration:	8 vials (3 vials for daily cell counts, 4 vials for chemical analysis).
Shaking rate:	100 rpm
Dilution water:	Algal culture medium (without EDTA)
pH range:	6.5
Test duration:	72 h
Effect measured:	Cell growth inhibition, measured as inhibition of exponential growth rate
Test acceptability[#~]:	Cell density in the control to increase by a factor of 16 after 72 h.

#Quality assurance by reference toxicant is often used to ensure that the algae are responding in a reproducible way to a known toxicant (e.g. copper). During training at CSIRO, a dilution series of copper (40, 20, 10, 5 and 2.5 µg/L) prepared from a copper sulphate stock solution was calculated. Quality assurances were further conducted using commercial ceria powders during synthesized ceria particle exposures.

~Turbid samples can alter light quality and quantity available to the algal cells in the growth rate inhibition test, potentially causing decreased algal growth, unrelated to sample toxicity. To overcome this problem, additional turbidity controls at various dilutions of sample can be prepared. The turbid sample (e.g. highest concentration of the nanoparticle suspension) is poured into clear polycarbonate containers and the mini-vial containing control water (culture medium only) is placed inside the container on the shaking platform. Cells are counted daily as usual and any effect of light reduction on algal control growth can be compared to normal controls. This was conducted at CSIRO with no significant effect compared with the controls observed and therefore not repeated.

4.5.3.4 Growth inhibition determination

The growth inhibition test measures the decrease in growth rate of treated *P. selenastrum* over 72 h compared against controls. Ordinarily growth rates in test solutions are compared statistically to that of controls, enabling a calculation of

NOEC, LOEC, EC_{20} and EC_{50} values. The growth rate value however, does not take into consideration algal cells which are dead within the sample. Therefore, the 'growth rate' which is often used to define the growth of cells over the period of an exposure assessment, is in fact a measure of cell density difference between the treated samples compared against the control sample. The 'growth rate' determined during this study is therefore the calculated cell number difference in comparison to the control samples of that test.

The average specific growth rate was calculated as the slope of a linear regression of the natural logarithm of the measured cell density versus time (Hoecke *et al*., 2009). The $\log_{10}$ cell density for each replicate in each treatment is plotted against time (d). Lines of best fit are then calculated for each test treatment where the slope of the line is equivalent to the growth rate. The specific growth rate is calculated by multiplying the slope by 2.303 for each treatment and control. Growth rates in each treatment as a percentage of the mean control growth (the specific growth rate) can be calculated as shown in Equation 4-1 using μC as the mean value for average specific growth rate in the control and μT as the average specific growth rate for the treatment replicate. The growth rate (μ) at time t and can be expressed as Equation 4-2.

Equation 4-1 Specific growth rate
Taken from Stauber *et al,* (2005)

$$\text{Growth rate (\% of control)} = \frac{\mu T \times 100}{\mu C}$$

Equation 4-2 Growth rate
Taken from Stauber *et al,* (2005)

$$\mu = \frac{(\ln Nt - \ln N_0)}{(t-t_0)} \quad (day^{-1})$$

N_0 is the cell density at time t_0 where the cell density (Nt) can be calculated as Equation 4-3 at time (t) days.

Equation 4-3 Cell density

$$Nt = N_o \exp [\mu t (t-t_0)]$$

Percent growth compared to control results in each individual replicate should be plotted against the logarithm of the test substance concentration. This is the concentration-response curve. The EC_{50} and EC_{20} cell growth compared to the control were calculated from the concentration response curve.

4.5.3.5 Nano-ceria particle preparation in algae exposure media

4.5.3.5.1 Commercial ceria particles

Commercial nano- and bulk-ceria[c] particle powders were prepared in *P. subcapitata* exposure test media (Table 4-16). Ceria[c] particles prepared in *P. subcapitata* test media were sonicated for 30 min. Aliquots of 50, 20, 10 and 5, 1, 0.1 and 0.01 mg/L were prepared with the 100 mg/L stock solution. Aliquots of 1, 0.1 and 0.01 mg/L were prepared with the 10 mg/L stock solution.

4.5.3.5.2 Synthesized nano-ceria particle preparation

Four discrete ceria NP particle dimensions were also used for *P. subcapitata* toxicity assessments. Ceria particles were synthesized using various chain lengths of poly(N-vinylpyrrolidin-2-one) (PVP) as the stabilising agent for specific dimensions required (Table 4-16) thanks to Dr. Ruth Merrifield, University of Birmingham following a protocol previously described by Zhou *et al*., (2007). The redox state of the ceria particles were not measured following synthesis, so no definitive state of Ce(III) or Ce(IV) can be offered during this study.

Table 4-16 Synthesized nano-ceria particle preparation
PVP was dissolved in 40 ml Milli-Q water along with cerium nitrate in 20 ml water. After heating, solutions were cooled before centrifugation with acetone. After centrifugation, 5 ml Milli-Q water was used to dissolve the ceria particle pellet.

Particle	A	B	C	D
PVP Chain (K)	10	40	160	360
PVP (g/60ml water)	3	1.5	1	0.233
Cerium(III)nitrate (g/60ml water)	130	130	130	130
Heat (min)	180	180	180	180
Re-suspended in Milli-Q water (ml)	5	5	5	5

The PVP solution was prepared in 60 ml Milli-Q water and added to a stirred 1800 mg/L cerium nitrate solution in Milli-Q water. This mixture was allowed to stir at 100^{O}C for 3 h and allowed to cool to ambient temperature. Following cooling, the solution was washed three times by centrifugal force using acetone. The final ceria pellet was re-suspended in 5 ml Milli-Q water as a stock nano-

ceria particle solution. Four particle dimensions (A-D) between 5 nm and 40 nm were prepared as a batch of samples. Three individual batches (1-3) were prepared several months apart from one another. Each particle stock solutions were diluted directly in *P. subcapitata* test media (Table 4-8) for toxicity testing and characterisations as discussed in Chapter 6.

5 Nanoparticle characterisations in aquatic ecotoxicological test media

5.1 Chapter Summary

There is increasing research addressing the uptake, accumulation and toxic fate of biota during nanoecotoxicological exposures. Many of these studies however do not consider potential changes in the NPs physicochemical characteristics within the test media, from the onset to the end of an exposure investigation. Changes of specific NP characteristics due to the presence of biota are also rarely considered or documented. This chapter investigates the physicochemical characteristics of three commercially available nano- and bulk-ceria particles from samples dispersed in a range of aquatic media both before and after exposure investigations. Results imply different MNPs of the same chemical form will exhibit variations in physicochemical characteristics such as increases in d_H (up to 7.5%) and UV-visible absorption, when dispersed in the same media. Collaborators repeated samples varied up to 2 fold in d_H measurements reducing the reliability of such samples. The presence of the test organism can cause increases in particle d_H by up to 80% and increase Ce dissolution up to 63%, specifically after 1 h of exposure. To obtain a reasonable appreciation of particle characterisation in test media, it is advised that future nanoecotoxicological work includes vigorous particle characterisation assessments using accurate test conditions, sample preparation methods and appropriate analytical techniques.

5.2 Chapter organisation

This chapter begins with the experimental design including the aims and objectives, (Table 5-1) of this work. This experimental design precedes a brief introduction to the project, setting the scene of this chapter's relevance in nanoecotoxicological research.

Table 5-1 Aims and objectives for Chapter 5

Aim
▪ To determine and compare the physicochemical characteristics of commercial ceria particles in a range of aquatic ecotoxicity test media. ▪ Determine the physicochemical characteristics of commercial ceria particles in a range of aquatic ecotoxicity test media, when in the presence of test species
Objectives
▪ Conduct a series of analyses to determine commercial ceria particle characteristics in a range of aquatic ecotoxicity test media; ▪ Discuss comparatives observed in particle characteristics in the presence and absence of test species; ▪ Compare the physicochemical characteristics of the same particles in different media in the presence and absence of biota.

Samples were produced during separate but parallel collaborative studies investigating NP toxicity. It was not the rationale of this chapter to investigate or discuss in detail the uptake or any toxic effect of the associated NPs as much of this work is published. It was however considered relevant to include a short passage of the results which were obtained from the collaborators' exposure investigations, which follows the brief introduction. The characterisation results obtained are subdivided between the individual commercial particles tested (ceria

a-c). The associated trends and variations in the particles physicochemical characteristics measured are then further discussed collectively in the subsequent section. Due to the amount of data accompanying this work, Figures A1-A33 and Tables A1-A13 can be accessed via Appendix A, using the CD-ROM. Some of this work has also been published, as listed in Appendix B. Figures A50-63 and Tables A16 in Appendix A represent characterisation data conducted using silver NPs, not represented during this study.

5.3 Introduction

One widely used strategy to monitor the 'health' of an ecosystem is to monitor one or more organisms that are particularly sensitive to the presence of a pollutant or other environmental contaminants (Griffitt *et al*., 2008). Experiments to determine biota sensitivity range from *in vitro* cellular toxicology and 'omics' to more traditional measurements of growth response investigations (Bar-Ilan *et al*., 2009). Over the past two decades, increasing numbers of aquatic nanoecotoxicological studies have been published using a range of test species from *Pseudokirchneriella subcapitata*, (Aruoja *et al*., 2009) and *Daphnia magna* (Lovern and Klapper, 2006), to *Cyprius carpio* (Hao *et al*., 2009) and more recently *Danio rerio* (Zhu *et al*., 2009). Many of these studies have reported the effects of NP exposure to specific organisms without any indication of particle characteristics from the onset to the end of the test period.

Three individual research groups were involved in investigating uptake and accumulation of three individually purchased commercial ceria particles (nano and bulk) on a range of aquatic biota (Table 4-1). In collaboration with these groups, NP characteristics were conducted using extracted exposure samples, sent via the collaborator, during their studies. These results were compared against independently conducted NP characterisations in equivalent test media, prior to these exposure tests, (pre). This offered a cross-comparison relating to inter-laboratory NP characterisations and effects of NP characterisations due to the direct exposure to an organism.

5.4 Collaborative nanoecotoxicological exposure results

5.4.1 Effects of ceria on cells and aquatic species at Napier University

Investigations into the nanoecotoxicological effects to a range of aquatic organisms and cell lines using commercially available nano- and bulk-ceria[a] (and silver) particles were conducted under the supervision of Professor Vicki Stone and Dr Birgit Gaiser, at Napier University, UK. The test subjects included *in vitro* cell cultures of human hepatocytes (C3A), primary trout hepatocytes (Trout) and human intestinal cells (Caco-2), and organism exposures using *D. magna* and *C. carpio* (Gaiser *et al*., 2009; 2011 Appendix B). Ceria[a] particles did not exhibit significant toxicity at equivalent doses to that of silver particles and did not cause significant toxicity in C3A cells or to *D. magna* (Gaiser *et al*., 2011)[Ж]. Nano-sized particles were found to be more toxic than their bulk equivalents in all conditions measured.

5.4.2 Effects of ceria on *Cyprius carpio* at Exeter University

The effects of uptake and accumulation of nano-ceria[b] to the freshwater fish *C. carpio* was investigated at Exeter University by Professor Charles Tyler and Dr. Blair Johnson. A repeated investigation was conducted 12 months later by Rhys Goodhead. The aim of this work was to determine the toxic effects of ceria[b] particles to *C. carpio* in the presence and absence of SRFA once stabilised with sodium citrate (Goodhead *et al*., 2011_1 Appendix B). Cerium concentration measurements taken of the gill, brain and kidney tissues, demonstrated significant uptake of higher nano-ceria[b] concentrations (50 µgL) with the addition of SRFA, compared to controls (Goodhead *et al*., 2011[1]). The tissue data indicated how the presence of SRFA can significantly affect the bioavailability of commercial nano-ceria[b] to *C. carpio.*

5.4.3 Effects of ceria on *Pseudokirchneriella subcapitata* at CSIRO

A research group lead by Dr. Simon Apte and Dr. Nicola Rogers were investigating the toxic effects and mechanisms associated with commercial ceria[c] particles to *P. subcapitata* at the CSIRO laboratories Sydney, Australia. Nano-ceria[c] particles were found to be 6 times more toxic per Ce mass than the bulk equivalent to *P. subcapitata*, (Rodgers *et al*., 2010). Nano-ceria[c] showed an inhibitory mode of action caused by ceria[c] particles interacting with the algal cells. Cell membrane damage was observed along with increasing hydroxyl radical generation by the ceria[c] particles. Hydroxyl species were found to be caused by

[1] Information obtained from Rhys Godhead prior to data being prepared for publishing.

photo-catalytic activity of nano-ceria[c] particles produced due to light illumination during the algal exposure conditions.

5.5 Results

The following is an account of the findings for each ceria (a-c) particle dispersion characteristics under both pre- and exposed conditions.

5.5.1 Ceria A

Ceria[a] particles (Table 4-1) were used in exposures to Caco-2, C3A and Trout cell cultures and to *D. magna* and *D. rerio* (Table 4-2). *D. magna* exposures were conducted at Napier University, with samples sent for characterisation assessments following 24 h exposures. Pre-exposure tests were conducted using appropriate media solutions (Table 4-3) in the presence and absence of 10 mg/L SRFA. Tables of results are offered in Appendix A, (Tables A1-A2).

5.5.1.1 Powdered particle analysis

XRD diffractograms were obtained for nano- (Figure 5-1) and bulk-ceria[a-c] (Figure A1) particle samples. BET results show a low variation in the repeated SSA measurements (Table 5-2). Calculated particle sizes (d_{BET}) of nano- and bulk-ceria[a] were found to be within the nominal particle distribution range as determined by the manufacturer (<25 nm and <5000 nm respectively), although bulk is much less.

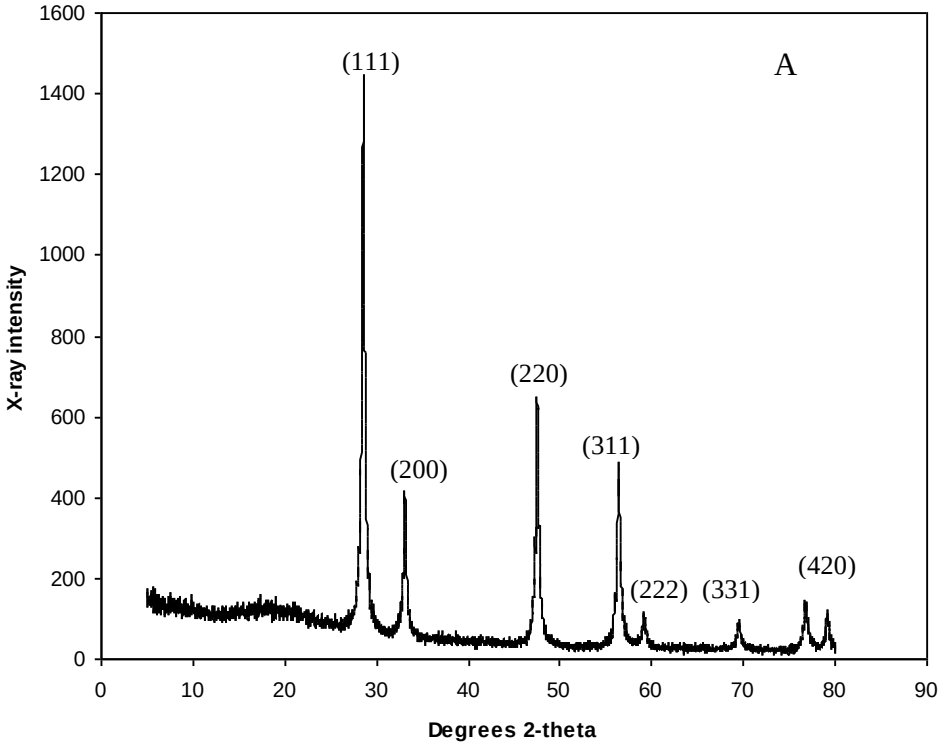

Figure 5-1 XRD diffractogram of nano-ceria[a]
Obtained from powdered commercial nano-ceria[a] particles at room temperature

Ceria[a] particles are well matched with that of CeO_2 JCPDS Card No. 75-0120 confirming the formation of pure-phase CeO_2 powders belonging to the face-centred cubic arrangement with lattice constant *a*=5.411 Å. The measured nano-ceria[a] (111)/(200) XRD absorption plane ratio is greater than that of bulk-ceria[a] (111)/(200) plane ratios, suggesting a greater number of (111) sites exposed in nano-ceria[a] and thus a greater proportion of Ce(III) to Ce(IV) compared with bulk-ceria[a] powdered samples.

Table 5-2 Nano- and bulk-ceria[a] powdered BET and XRD analysis
Specific surface area and associated particle diameter by BET were obtained and further calculated size distributions were made using XRD analysis using the Scherer equation.

Particle	Particle diameter by manufacturer (nm)	BET SSA. (m^2/g) units	d_{BET} (nm)	d_{XRD} (nm)	*(111/200) ratio*
Nano-ceria	<25	53.81± 2.4	15.9	15.3	1.12
Bulk-ceria	<5000	0.37 ± 0.4	2316.6	1155.5	0.982

n=2 for BET analysis
n=1 for XRD

5.5.1.2 Charge – pH relationship

As the electrolyte solution concentration and viscosity increases from *D. magna* to cell culture media, the pH at which the calculated ζ is zero (Pzc) increases from pH 2 to pH 4 for both nano- and bulk-ceria[a] particles (Table 5-3).

Table 5-3 The pH at which zeta potential is zero
pH of nano- (black) and bulk-(blue) ceria[a] at 62.5 µg/L in cell mediums and at 10 mg/L in *D. magna* media with the additions of 10 mg/L SRFA where shown.

Media	Cell media			*D. magna* media	
Conditions	C3A	Caco-2	Trout	Pre-Exp	Pre-Exp + SRFA
Zero charge (pH)	4.3 4.2	4.3 4.1	3.5 4.6	<2 2.2	<2 <2

The Pzc of nano- (Figure A2) and bulk-ceria[a] (Figure A3a), at 62.5 µg/L in cell culture mediums is consistent at pH<5. The Pzc of nano- and bulk-ceria[a] in *D. magna* media at 10 mg/L, (Figure A3b) is pH<2. The addition of SRFA to *D. magna* media has no effect on the pH at which ζ is zero.

5.5.1.3 Particle hydrodynamic diameter

Nano-ceria[a] have low PdI (<0.5) in all cell mediums (Tables A1-2). Using calculated hydrodynamic diameters (d_H) from Z-ave results using DLS analysis, nano-ceria[a] dispersed in cell mediums >10 mg/L show similar d_H as calculated by d_{BET} and d_{XRD}. Nano-ceria[a] particles in Trout media have up to 47% larger d_H compared to equivelant nano-ceria[a] dispersions in C3A media, (Figure 5-2) although these results are not significantly different ($p>0.05$). Bulk-ceria[a] dispersions in cell media have no obvious trend in measured d_H (Z-ave). Nano-ceria[a] dispersions in *D. rerio* media show increased d_H with increasing concentration.

With the addition of SRFA to *D. rerio* media, d_H increases in nano-ceria[a] by up to 85%. In the highest ionic strength media (*D. magna*) the d_H of nano-ceria[a] dispersions generally increases as concentration increases (Figure A4a). This increase in d_H of nano-ceria[a] in *D. magna* media is significantly reduced ($p<0.05$) in the presence of SRFA (Figure A4b) up to 86% across the dispersions 0.01-100 mg/L. As electrolyte concentration increases (*D. rerio*<*D. magna*) d_H for equivalent dispersion of nano-ceria[a] generally increase. During exposures to *D. magna*, nano-ceria[a] <1 mg/L show a significant increase ($p<0.05$) in d_H, up to 80% compared against equivalent pre-exposure measurements.

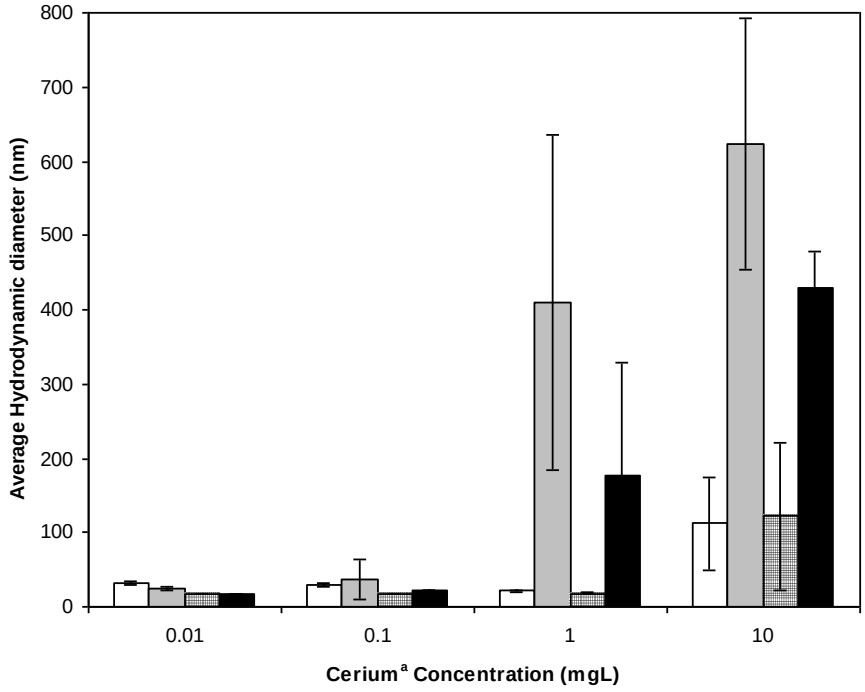

Figure 5-2 Average Z-ave of nano- and bulk-ceria[a] in cell media
Using DLS analysis as a function of concentration. Nano-ceria[a] in Trout media, white; bulk-ceria[a] in Trout media, grey; nano-ceria[a] in C3A media; bulk-ceria[a] in C3A media.

5.5.1.4 Particle zeta potential

Ceria[a] dispersions in cell culture media were not conducted due to corrosion of the zeta-cell by the media. As nano- or bulk-ceria[a] concentrations increase in *D. magna* media, ζ decreases (away from zero) although this is not systematic (Figure 5-3). Significant differences are observed, ($p<0.05$) between nano- and bulk-ceria[a] in *D. magna* media at equivalent concentrations where bulk-ceria[a] appears to be less negatively charged (-ve) than nano-ceria[a] dispersions. The ζ is significantly reduced (-ve) with the addition of SRFA when compared to equivalent dispersions in *D. magna* media alone. There are no trends associated with ζ between exposure and pre-measured samples, (Table A1-2). There are

significant differences observed between equivalent concentrations ($p<0.05$) of exposure and pre-measured ceria[a] dispersions in *D. magna* media, where exposed samples are generally lower (+ve) in measured ζ than pre-exposure samples. As nano- and bulk-ceria[a] concentration increases in *D. rerio* media at pH 7, the ζ decreases (-ve).

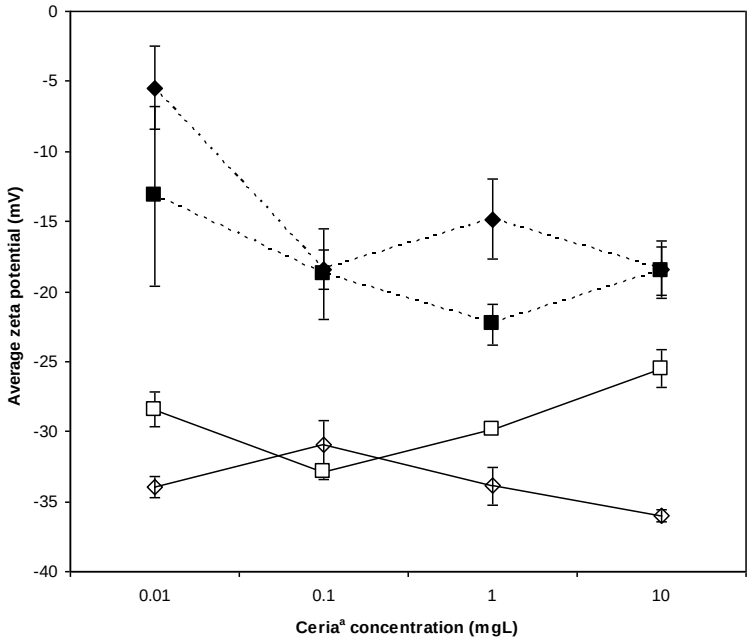

Figure 5-3 Average zeta potential for nano- and bulk-ceria[a] in *D. magna* media
Measurements in the presence and absence of 10 mg/L SRFA as a function of concentration were also taken. Nano-ceria[a] dispersed in *D. magna* media, black square; bulk-ceria[a] dispersed in *D. magna* media, black diamond; Nano-ceria[a] dispersed in *D. magna* media with SRFA, white square; bulk-ceria[a] dispersed in *D. magna* media with SRFA, white diamond.

Bulk-ceria[a] produces a significantly ($p<0.05$) more -ve ζ than nano-ceria[a] at equivalent concentrations in *D. rerio* media. The addition of SRFA to *D. rerio* media at pH 7 significantly reduces (-ve) the ζ of nano-ceria[a] dispersions. As media electrolyte concentrations increase, the ζ of equivalent nano-ceria[a] dispersions increases (-ve) significantly ($p<0.05$).

5.5.1.5 TEM

Images of nano- and bulk-ceria[a] at 1 mg/L dispersed in deionised water were received courtesy of Dr. Birgit Gaiser, University of Napier. TEM images were independently conducted taken from grids prepared by the drop method for particles dispersed in *D. rerio* media at 500 mg/L and at 1 mg/L in *D. magna*. The UC method (Chapter 3) for TEM grid preparation was used for all cell medium particle dispersions at 62.5 µg/L. Particles were counted and their aspect ratios (*S*) calculated (Table 5-4).

Table 5-4 Nano-ceria[a] particle diameters by TEM
Particle diameter calculated from TEM (d_{TEM}) particles counts along with agglomeration and aspect ratios (*S*) across a range of media and dispersions.

Media	Conditions	Dispersion (mg/L)	d_{TEM} (nm/No particles)	Range (nm)	Agglomeration (nm)	*S* (range)
Milli-Q	Pre-Exp	0.1	57.7 ± 54.1 / 96	9.6 - 556	1237.5 ± 279.9	0.82 ± 0.2
	Sent	1.0	11.3 ± 25.3 / 148	3.02 - 222.9	75.2 ± 42.7	0.80 ± 0.1
D. magna	Pre-Exp	1.0	28.6 ± 25.5 / 146	3.2 - 145	350.6 ± 202	0.87 ± 0.2
	Pre-Exp + SRFA	1.0	5.47 ± 3.5/116	1.2 - 21.9	21.9 ± 3.5	0.63 ± 0.2
	24 h Exp	1.0	18.1 ± 11.5 / 80	3.9 - 69	1335.4 ± 1384.4	0.86 ± 0.1
D. rerio	Pre	500	487.4±640.8 / 38	3.9 - 1909.1	2909.1± 618.8	0.69 ± 0.2
Cell media	C3A	0.0625	1021 ± 1369/1305[#]	10 - >10,000	52.6 - 13,750	1.4 ± 0.4 (1-2)
	Caco-2	0.0625	1072 ± 1305/1739[#]	10 - >10,000	615 - >10,000	1.5 ± 0.4 (1-2)
	Trout	0.0625	611.3 ± 44.6/2264[#]	10 - 5000	<4521.7	1.8 ± 1.1 (1-4)

 # conducted courtesy of Dr. Mohammed Baalousha

At relatively low, environmentally relevant concentrations (0.1 mg/L) nano-ceria[a] particles in Milli-Q water, (Figure 5-4) appear to form truncated octahedron with

rectangular features (Lin *et al*., 2011; Getzlaff, 2008) supported by a calculated *S* <1.0. A ten fold increase in concentration (1 mg/L) shows larger aggregates of nano- and bulk-ceria[a] dispersions (Figure A5a+b) and equivalent calculated *S* in Milli-Q water.

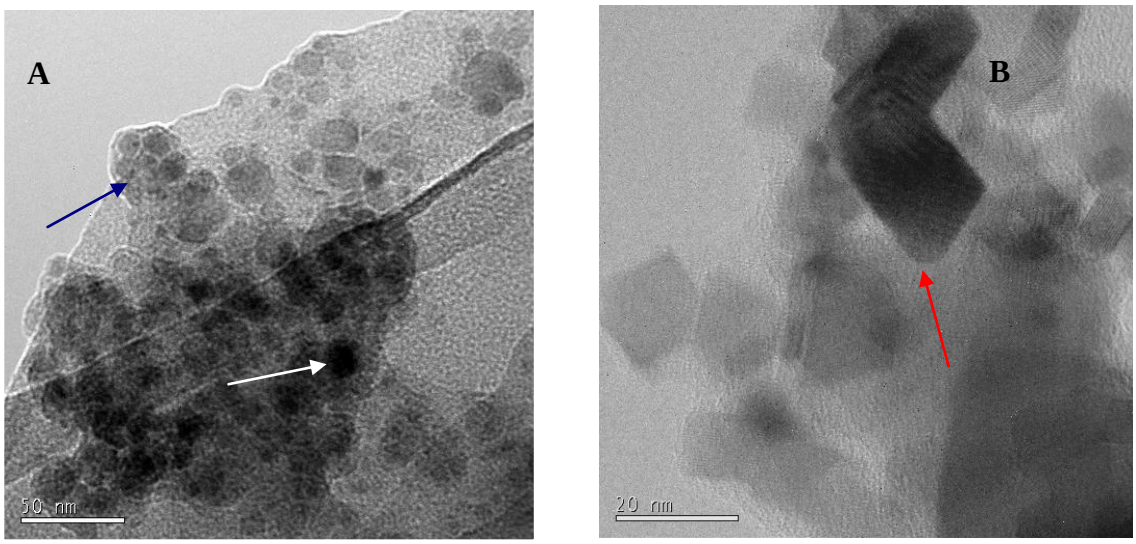

Figure 5-4 TEM micrographs of nano-ceria[a]
a) Dispersion at 0.1 mg/L in Milli-Q water. b) Dispersed in C3A media at 0.06 mg/L.
Blue arrow indicates octahedral forms, white arrow highlights more rectangular features and red arrow highlights rhombus forms.

Nano- and bulk-ceria[a] dispersed in C3A, (Figure 5-4b) at 62.5 µgL show similar structures as nano- and bulk-ceria[a] in Caco-2 (Figure A6) and in Trout cell media (Figure A7). Cell media dispersions (Figure A8) show the formation of large agglomerates with higher *S* (1.4-1.8) suggesting more rod-like shapes (Lin *et al*., 2011) or rhombus forms with unequal sides (Baalousha *et al*., 2010). Nano-ceria[a] d_{TEM} in trout media (Figure A9) are nearly two fold smaller than that measured in equivalent dispersions in C3A and Caco-2, opposing DLS measurements. At the lowest electrolyte solution of *D. rerio* media the particle

images (Figure A10) shows the highest rate of aggregation at 500 mg/L of rectangular shaped nano aggregates (*S*=0.69, Figure A11). In higher electrolyte *D. magna* media, nano-ceria[a] form relatively well dispersed particle distributions at 1 mg/L (Figure A12). With the addition of 10 mg/L SRFA particle size reduces supporting trends observed by DLS measurements for *D. magna* dimensions. After 24 h exposures to *D. magna*, particle size reduces as particle number reduces and aggregation occurs. Particle shape is equivalent in Milli-Q water, pre- and exposure dispersions (*S*=0.80 to 0.87).

5.5.1.6 Particle UV-visible absorption

Spectra obtained across the λ 200-800 nm showed two significant peaks at 420 nm and at 580 nm for both nano- and bulk-ceria[a] in all cell media at 62.5µg/L, (Figure A13). Nano-ceria[a] produces greater absorption peak intensities than equivalent bulk-ceria[a]. There is a significant difference ($p<0.05$) in UV-visible absorptions measured in Trout and Caco-2 media between nano- and bulk-ceria[a]. Maximum UV-visible absorption λ is red-shifted with increasing concentrations of nano- and bulk-ceria[a] in *D. magna* media from 368 to 377 nm (Figure 5-5). With the addition of SRFA, nano-ceria[a] dispersions show a blue-shift in peak absorption λ compared to in media alone. After 24 h exposures to *D. magna*, nano- and bulk-ceria[a] UV-visible absorption λ is red-shifted compared to equivalent pre-exposure analysis. Nano- and bulk-ceria[a] exhibit significantly higher ($p<0.05$) UV-visible spectra intensty in exposure samples compared to

equivalent pre-exposure samples. Higher concentrations (10 mgL) of nano-ceria[a] offer greater UV-visible peaks than lower concentration (0.01 mgL).

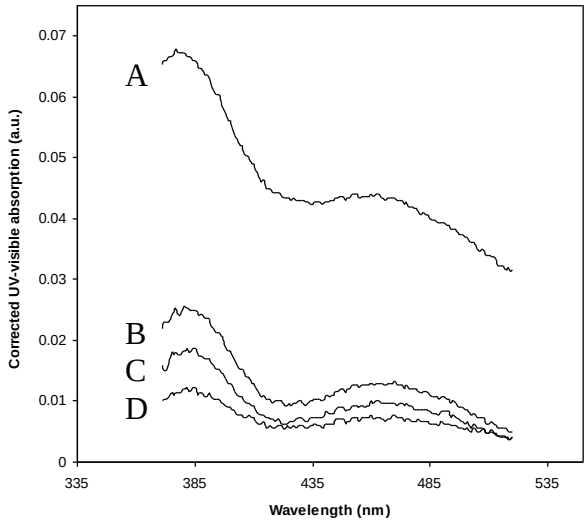

Figure 5-5 UV-Visible spectrum of nano-ceria[a] in *D. magna* media
After 24 h exposure to *D. magna* UV-visible spectroscopy was performed, as a function of concentration; a) 10 mg/L, B) 1 mg/L, C) 0.1 mg/L, D) 0.01 mg/L.

5.5.1.7 Emission intensity by fluorescence spectrometry

Fluorescence analysis was not used for the determination of any particular particle but to identify if any fluorophore changes occur under the influence of ceria particles. Cell media were found to be highly fluorescent without dilution (Figure A14a) and were considered unsuitable for fluorescence spectroscopy analysis. Representative EEM's (Figure A14b-c) of nano- and bulk-ceria[a] dispersions in *D. magna* were used to determine maximum absorptions and associated Emλ and Exλ of five frequently quoted fluorophores (Table A3). As ceria[a] concentration increases in *D. magna* media in the presence and absence of SRFA, a significantly greater ($p<0.05$) number of Emλ decrease in bulk-ceria[a]

compared to equivalent nano-ceria[a] dispersions. SRFA significantly increases ($p<0.05$) the fluorescence intensity observed across all ceria[a] dispersions compared to in media alone. Tryptophan-like Emλ are lower in bulk-ceria[a] dispersions compared to equivalent nano-ceria[a] dispersion. T1 fluorophore peaks (Figure 5-6) increase significantly ($p<0.05$) in exposure samples compared to none-exposure samples for both ceria[a] particle dispersions.

5.5.1.8 Total particle concentration

Calculations against measured ICP-MS concentrations of nano- and bulk-ceria[a] dispersions in *D. magna* media were compared against initial particle concentrations applied and offered as a percent of initial mass added (Table 5-5). Nano- and bulk-ceria[a] have low solubility in the absence (<0.2 % and <1.8% original mass added respectively) and presence (<0.6% and <0.2% original mass added respectively) of *D. magna*.

Table 5-5 ICP-MS measurements of ceria[a] particles in *D. magna* media Samples taken in the absence (0 h) and presence (24 h) of *D. magna*.

Time (h)	Initial ceria Concentration (ppb)	Control (ppb)	Nano-ceria (ppb)	Nano-ceria (% added)	Bulk-ceria (ppb)	Bulk-ceria (% added)
0	100	<0.2	<0.2	0.2	<0.2	0.2
24	10		<0.2	2.00	1.73	17.3
	100	0.21	0.44	0.44	0.21	0.21
	1000		5.74	0.57	<0.2	0.02
	10000		16.2	0.16	2.22	0.02

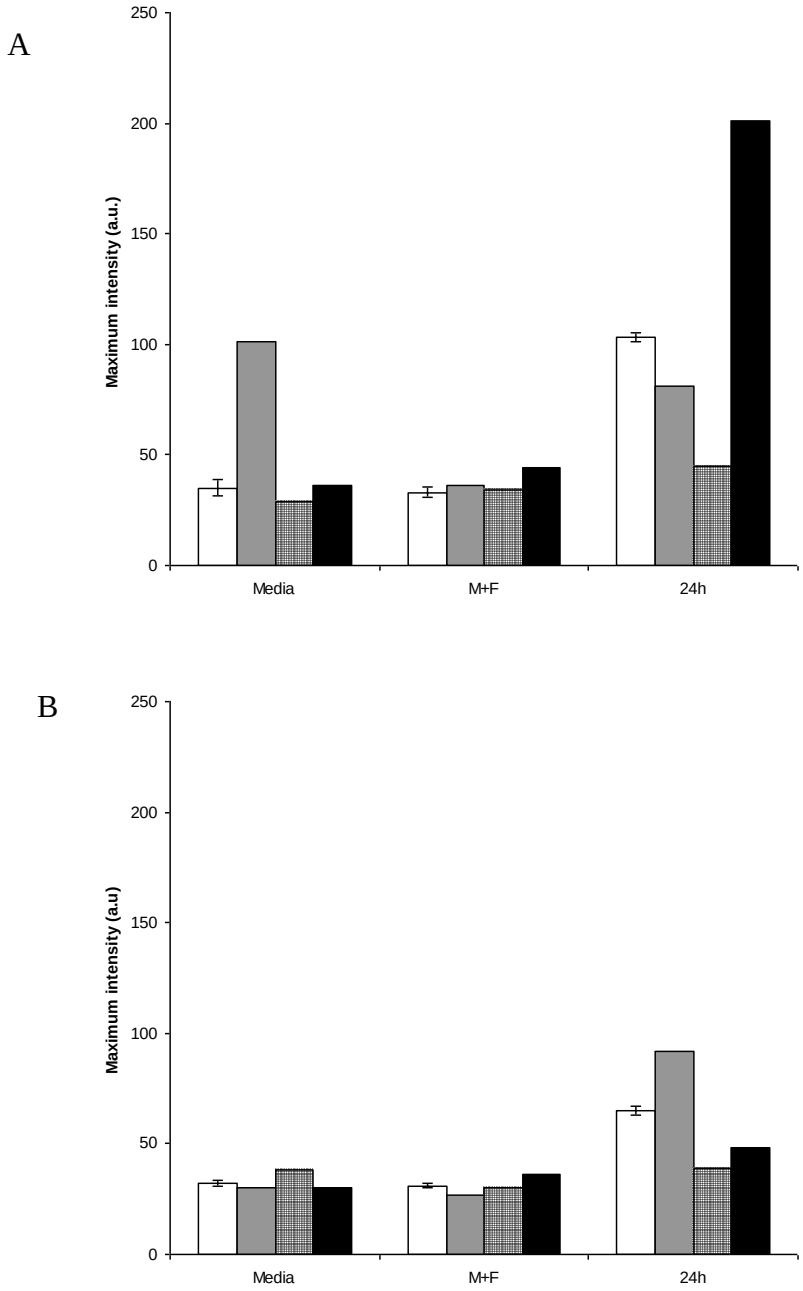

Figure 5-6 Maximum ceria[a] peak-T fluorescence intensity in *D. magna* media
Peak T (tryptophan-like) fluorescence in media, media with SRFA and after 24 h exposures to *D. magna*. Samples taken in the presence and absence of SRFA and under pre- and exposure conditions across a concentration range. A) Nano-ceria[a] in *D. magna* media conditions; B) Bulk-ceria[a] in *D. magna* media conditions. 0.01 mg/L, white; 0.1 mg/L, grey; 1 mg/L chequered; 10 mg/L, black; dispersions in pre-exposure media - (media); dispersions in pre-exposure media with SRFA - (M+F); dispersions in exposure after 24 h – (24 h).

5.5.1.9 Summary

Seven general observations were made following characterisation studies using ceria[a] particle dispersions in cell and aquatic test mediums.

- Ceria[a] particle dispersions display low solubility, form rectangular, octahedral and rhombus structures and have Pzc <pH4 in all media.
- Bulk-ceria[a] dispersions have greater d_H, generally more negative (-ve) ζ, have blue-shifted UV-visible maximum λ, reduced UV-visible peak intensities and generally have lower fluorophore intensities than equivalent nano-ceria[a] dispersions.
- As concentration of nano- and bulk-ceria[a] increases, d_H increases, ζ decreases (–ve), aspect ratios remain stable and UV-visible λ red-shifts. Fluorophore Emλ red-shift and fluorophore intensity increases in nano-ceria[a] dispersions.
- As media electrolyte concentration (and viscosity) increases, (*D. rerio* < *D. magna* < Cell media) ceria[a] particle d_H increases, Pzc pH increases from pH 2-4, ζ increases in negativity (-ve) and TEM images suggest a greater dispersity of particles in solution.
- Addition of SRFA to any media produces a more negative ζ (-ve), reduces d_H, and reduces d_{TEM}, increases fluorophore intensity and UV-visible peak λ blue-shifts.

- The presence of organisms generally increases d_H, reduces d_{TEM}, decreases ζ (+ve), red-shifts UV-visible peak wavelengths and increases tryptophan-like fluorophore intensity of nano-ceria[a] particle dispersions.
- Independent pre-exposure sample analysis differs by increased measured Ce solubility and reduced d_{TEM} compared to equivalent samples sent by collaborators.
-

5.5.2 Ceria B

Ceria[b] particles were used for *C. carpio* exposures at Exeter University. Exposure samples were sent throughout the 35 day test period and at the end of the repeated 10 day exposure period. Ceria[b] was also dispersed into electrolyte solutions of 10 *mM* and 500 *mM* NaCl, in the presence and absence of 10 mg/L SRFA, as a further comparative study (Table A4-6).

5.5.2.1 Powdered particle analysis

Each sample measured using BET and XRD calculated size (Table 5-6) were found to be within the nominal particle distribution range as determined by the manufacturer. Ceria[b] particles are well matched with that of CeO_2 JCPDS Card No. 75-0120 (Figure 5-1 and Figure A1).

Table 5-6 Nano- and bulk-ceria[b] powdered BET and XRD analysis
Specific surface area and associated particle diameter by BET were obtained and further calculated size distributions were made using XRD analysis using the Scherer equation.

Particle	Particle diameter by manufacturer (nm)	BET SSA. (m^2/g)units	d_{BET} (nm)	d_{XRD} (nm)	(111/200) ratio
Nano-ceria	<35	59.4± 1.1	14.4	15.5	0.87
Bulk-ceria	<2500	0.66 ± 0.1	1298.7	554.6	0.683

n=2 for BET analysis
n=1 for XRD

5.5.2.2 Charge – pH relationship

Using 10 mg/L ceria[b] particle dispersions, (Table 5-7) an increase in NaCl concentration (10 *mM*<500 *mM* NaCl) reduces the Pzc from pH 4.5 to 2, (Figure A15). The addition of 10 mg/L SRFA further reduces the Pzc to pH<2. The Pzc is a physiological pH 6.3 in C*. carpio* media with 0.05% sodium citrate, (Figure A16). The addition of SRFA to *C. carpio* media reduces the Pzc to pH 2.4. With the addition of SRFA to *C. carpio* media with sodium citrate, the pH is further reduced to <2.

Table 5-7 The pH at which nano-ceria[b] zeta potential is zero

pH of nano-ceria[b] at 10 mg/L in 10 *mM* and 500 *mM* NaCl and in *C. carpio* media in the presence and absence of 10 mg/L SRFA where shown.

Media	**NaCl media**				***C. carpio* media**		
Conditions	10 mM	10 mM with SRFA	500 mM	500 mM with SRFA	Media with SRFA	Media with sodium citrate	Media, sodium citrate and SRFA
Zero charge (pH)	4.5	~3	<2	<2	2.5	6.3	<2

5.5.2.3 Particle hydrodynamic diameter

The mean d_H measured by DLS (Table A4-6) increases with increasing concentrations of ceria[b] particles in all media tested with up to 47% decrease in PdI. PdI is further reduced with the presence of SRFA in all NaCl solutions. Nano-ceria[b] d_H are generally lower than the equivalent bulk-ceria[b] dispersions. Nano-ceria[b] d_H measurements increase up to 7.5% in 500 *mM* NaCl media compared against equivalent dispersions in 10 *mM* NaCl (Table A4-6). With the presence of SRFA in NaCl solutions, the d_H is seen to decrease significantly ($p<0.05$) by 79% with increasing particle concentrations >0.1 mg/L (Figure 5-7). The d_H is reduced by between 65-88% in *C. carpio* media with the addition of 0.05% sodium citrate in the presence and absence of SRFA, compared to equivalent dispersions in media alone (Figure A17).

During exposures to *C. carpio*, there is a significant increase ($p<0.05$) in measured d_H between pre-exposure measurements and equivalent D0 sent samples. Between D0 and 'D0 repeated' samples, there is a noticeable two fold decrease in measured Z-ave, which are significantly variable ($p<0.05$). Significant differences ($p<0.05$) are observed across all tanks, between D0 and D1, by a measured reduction in d_H. The d_H measurements decrease between D0 and D35 showing statistically significant differences ($p<0.05$) within tanks 5, 6, 7, and 8. Significant increases ($p<0.05$) in d_H between independent (pre) and equivalent collaborators (D0) measurements were also observed.

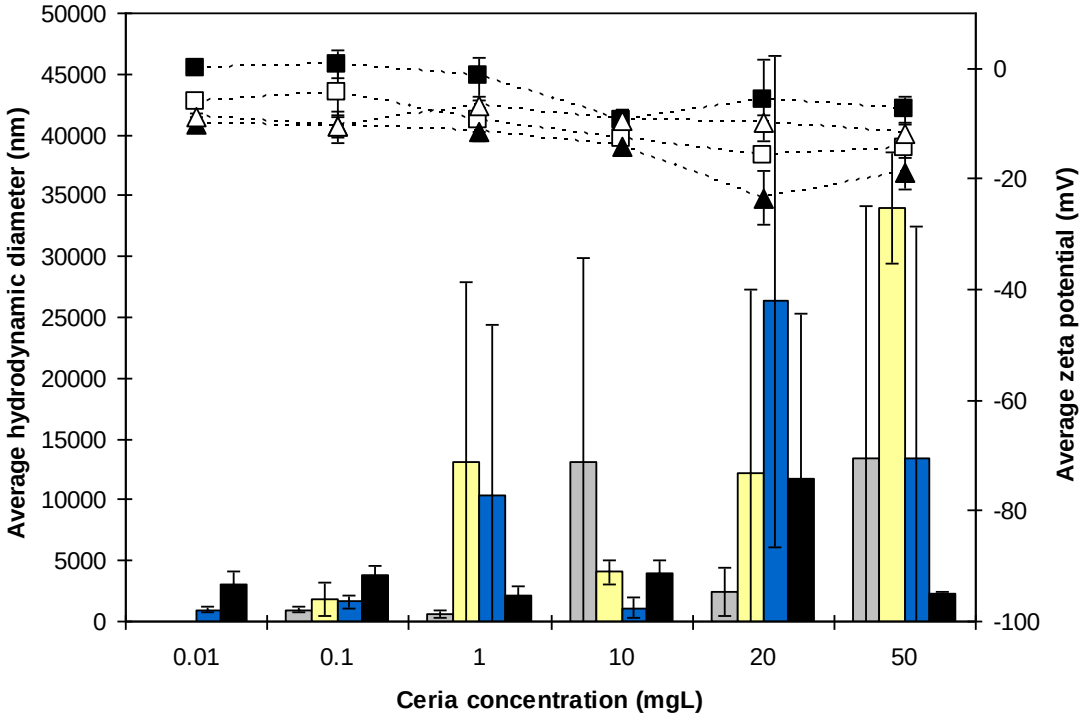

Figure 5-7 Average Z-ave (d_H) and zeta potential for nano-ceria[b] in NaCl media
Average particle hydrodynamic diameters (d_H) by DLS and zeta potential of nano-ceria[b] in NaCl mediums as a function of concentration. *Z-ave*: 500 *mM* NaCl with SRFA, grey; 10 *mM* NaCl with SRFA, yellow; 500 *mM* NaCl, blue; 10 *mM* NaCl, black. *Zeta:* 500 *mM* NaCl with SRFA, white square; 10 *mM* NaCl with SRFA, black triangle; 500 *mM* NaCl, black square; 10 *mM* NaCl, white triangle.

5.5.2.4 Particle zeta potential

Nano- and bulk-ceria[b] dispersions are –ve charged in all NaCl media dispersions at pH 7 (Figure 5-7). Nano-ceria[b] dispersions are less –ve charged than equivalent bulk-ceria[b]. Ceria[b] particles exhibit a general decrease in ζ (-ve) with increasing particle concentrations in all NaCl solutions. The addition of SRFA to any NaCl media increases the negativity of measured ζ ceria[b] dispersions. In *C. carpio* media with 0.005% sodium citrate, in the presence and absence of SRFA, ζ reduces (-ve) compared to equivalent dispersions in media alone (Figure A17). Nano-ceria[b] dispersions in *C. carpio* media show a more negative ζ (-ve) in the

presence of organisms (D1) compared against the absence of organisms (D0) at pH 7. Recorded ζ are however not significantly different ($p>0.05$) between D0 and D1 in tanks 4, 7 and 9. Nano-ceria[b] exhibits a decrease in ζ from D0 to D35 at pH 7, of which is only significant ($p<0.05$) for tanks 6 and 7. D0 exposure samples offer a more negative ζ compared with equivalent pre-exposure particle sample ζ, although these results are not significant ($p>0.05$).

5.5.2.5 TEM

Table 5-8 offers particle counts obtained from TEM images. Dispersed in Milli-Q water, nano-ceria[b] form large aggregated material, many found to be elongated (Figure 5-8) supported by a high *S*=3.5 (Lin *et al*., 2011).

Table 5-8 Nano-ceria[b] particle diameters by TEM
Table offers maximum agglomerates average particle diameters (d_{TEM}) and calculated particle aspect ratio (*S*).

Media	conditions	Dispersions (mg/L)	d_{TEM} (nm/No)	Range (nm)	Agglomeration (nm)	*S* (range)
Milli-Q		500	17.1 ± 13.1 / 34	5.9-43.2	-	3.5 ± 1.5 (1.1-5.0)
10 *mM* NaCl	Pre	1.0	14.9 ± 6.3 / 125[ж]	14.6-67.2	1720.0 ± 749.8	1.7 ± 0.6 (1.1-3)
	Pre + SRFA	1.0	44.8 ± 40.5 / 20	11.4-170.7	5190.5 ± 1545.1	2.7 ± 1.2 (1.6-4.4)
C. carpio	Pre	1.0	74.7 ± 107.2 / 134	3.9-618.6	8065.7 ± 2802.5	1.8 ± 1.8 (1.0-15.7)
	Pre + SRFA	1.0	16.5 ± 22.7 / 204	2.8-139.1	5970.0 ± 1777.3	1.5 ± 1.1 (1.0-11.4)
C. carpio	(D0)	Tank 7	103.3 ± 146.0 / 142	1.6-703	2593.5 ± 504.6	1.8 ± 0.9 (1.0-4.2)
	(D0)	Tank 9	23.3 ± 18.4 / 134	5.2-80.7	1700.8 ± 392	1.4 ± 0.4 (1.0-3.0)
	(D1)	Tank 7	873.1± 44.7 / 58	31-237	783.0 ± 214.4	2.0 ± 1.7 (1.0-10.9)
	(D1)	Tank 9	35.9 ± 19.8 / 124	3.75-136	3420.0 ± 735.2	1.5 ± 0.4 (1.0-3.6)

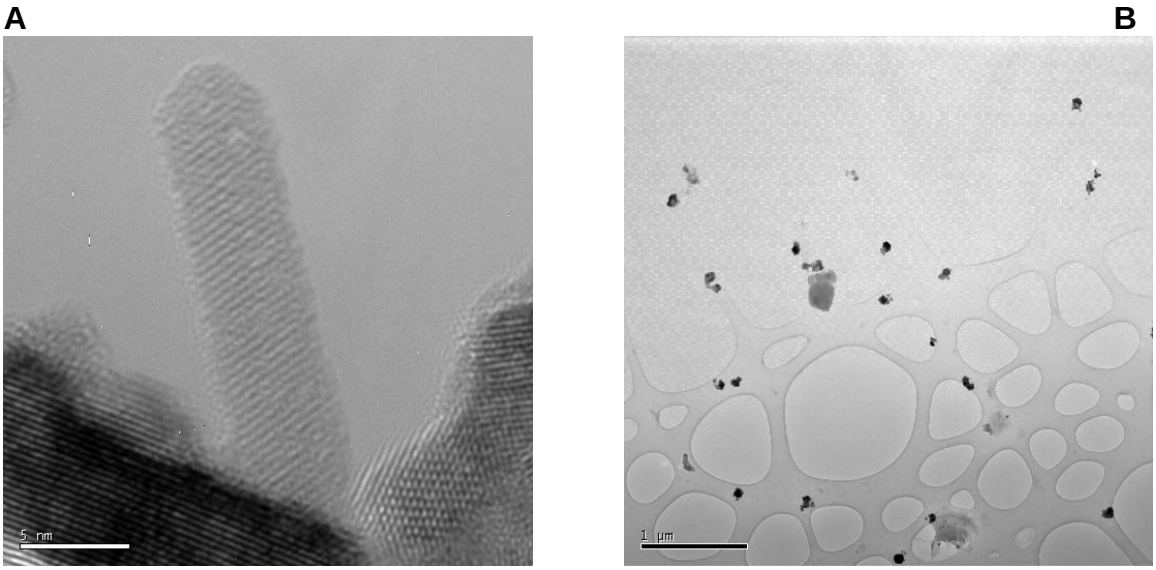

Figure 5-8 TEM micrographs of nano-ceria[b]
a) Dispersion of 500 mg/L in Milli-Q water, b) dispersions in 10 mM NaCl with 10 mg/L SFRA.

Average particle diameters are equivalent to calculated d_{XRD} and d_{BET} albeit obtained from low number of particles (<35) of which were only present on the TEM images for representative counts. In 10 *mM* NaCl, nano- and bulk-ceria[b] (Figure A18) looks more variable forming semi-porous aggregates. Particles appear to form less elongated shapes in 10 *mM* NaCl solutions (Figure A19) than when just dispersed in Milli-Q water, supported by a lower *S*=1.7. In the presence of SRFA, nano-ceria[b] dispersions in 10 *mM* NaCl appear to be more distributed than in 10 *mM* NaCl solutions alone (Figure 5-8b). Particle diameters are increased in 10 *mM* with SRFA compared to without SRFA (Table 5-8) due to surface coating of SRFA in particles. Agglomeration increases in 10 mM media with SRFA by *ca* 26% with increased *S* being measured.

In *C. carpio* media, there appears to be a greater dispersion of nano-ceria[b] particles compared to images from Milli-Q water dispersion, possibly due to four times the number of particles available for counts (Table 5-8). There are more dispersed particles present in *C. carpio* dispersions with SRFA than equivalent samples without SRFA (Figure A20). Pre-exposure and equivalent collaborative samples (D0) are comparable in *C. carpio* media (Figure A21-22) with respect to d_{TEM} (Figure A23). Maximum agglomerates are greater in independent pre-exposure samples than equivalent collaborator samples. Only one image of nano-ceria[b] was obtained in equivalent pre-exposure tank 7 reducing reliability in particle counts measured. D1 exposure images show (Figure A22) what appears to be organic substance on the grid. This increases the d_{TEM} also observed by DLS analysis. Particle shape does not change as the *S* is comparable from D0 to D1. There are larger agglomerates in tank 9 TEM images after 1 h exposure compared against equivalent TEM images from tank 7, due to the fulvic addition in the sample.

5.5.2.6 Particle UV-visible absorption

As the concentration of nano-ceria[b] dispersed in all *C. carpio* media conditions increases, the maximum absorption λ remains unchanged, (259-261 nm). The UV-visible absorption of ceria[b] dispersions in *C. carpio* media at relatively high concentrations (10 mg/L) is low (<0.1 a.u.) with no trend in absorbance with concentration observed (Table 5-9). As absorption measurements are so low for

ceria[b] concentrations <1 mg/L, the UV-vis analysis is difficult to interpret for exposure samples obtained.

Table 5-9 Maximum UV-Visible absorption data for nano-ceria[b] in *C. carpio* media
Maximum peaks and wavelengths for nano-ceria[b] in various *C. carpio* media under a range of conditions at 10 mg/L.

Dispersion media	Conditions	Maximum absorption peak λ (nm)	Maximum peak absorptions[#] (a.u.)
C. carpio	Media	259-261	>0.0
	Media with citrate	259-261	>0.0
	Media with SRFA	259-261	0.05
	Media with citrate and SRFA	259-261	0.035

[#]**Measured from highest absorption peak using 10 mg/L particle concentrations.**

5.5.2.7 Emission intensity by fluorescence spectroscopy

Representative EEM's are presented for the raw fish mucus sample offered by Dr. Blair Johnson, Exeter University, as requested (Figure A24a) and 0.1 mg/L nano-ceria[b] present in media with citrate in the absence (Figure A24b) and presence of SRFA (Figure A24c). Tank 4 and Tank 6 on D0, D1 and D35 EEMs are also given in Figure A25 and A26 respectively. Maximum peak fluorophores with Emλ and Exλ are offered in Tables A7-8. In *C. carpio* media with citrate, only T_1-T_2 peaks increase with an addition of SRFA, where other fluorophores decrease in media dispersions with SRFA (Figure 5-9). Fluorophore intensity increases with associated blue-shifts in Emλ when nano-ceria[b] is dispersed in *C. carpio* media with 0.005%/vol sodium citrate compared to equivalent dispersions in media alone. D0 measurements show an increase in fluorophore intensities with increased Emλ compared to equivalent independent samples.

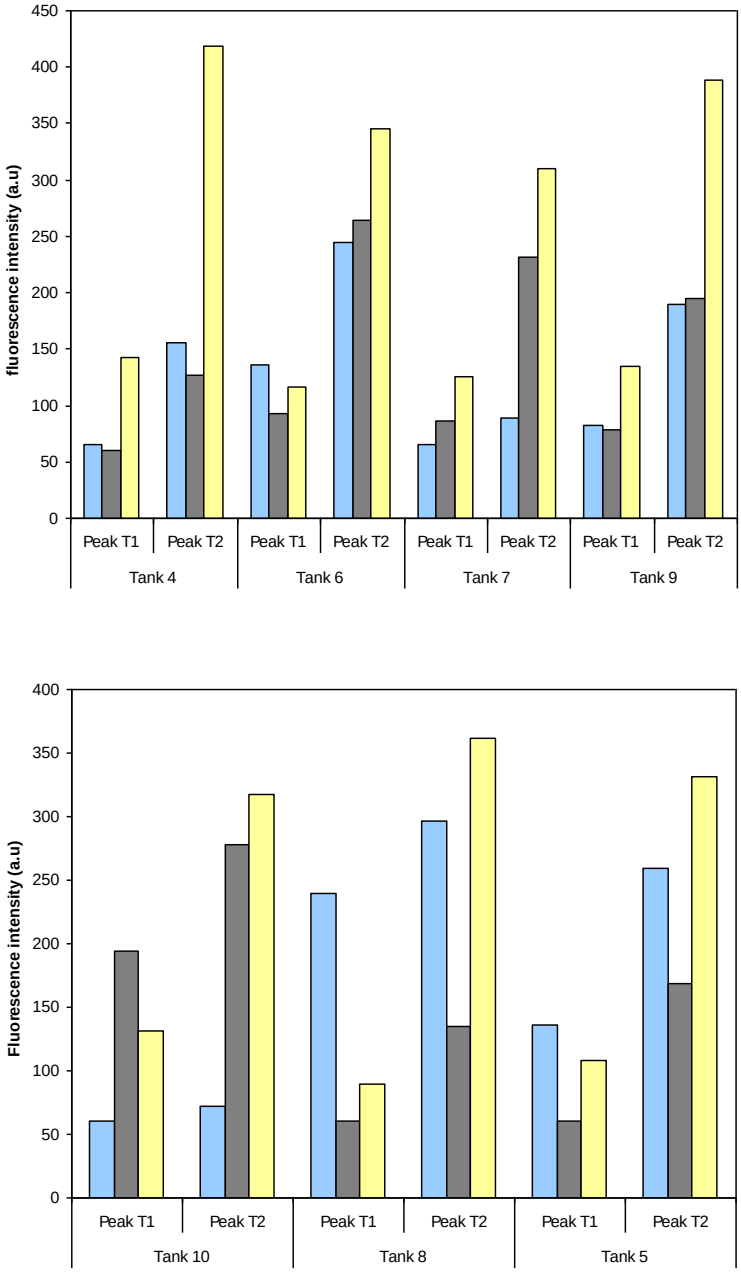

Figure 5-9 Maximum ceria[b] peak T fluorescence intensity in *C. carpio* media
Peak T tryptophan-like fluorescence of exposure conditions of nano- and bulk-ceria[b] to *C. carpio*. Day 0, blue; Day 1, grey; Day 35, yellow. Tank 4 (5 µg/L nano-ceria in media with citrate); Tank 5 (5 µg/L nano-ceria in media with citrate and 50 µg/L SRFA); Tank 6 (5 µg/L nano-ceria in media with citrate and 250 µg/L SRFA); Tank 7 (50 µg/L nano-ceria in media with citrate); Tank 8 (50 µg/L nano-ceria in media with citrate and 50 µg/L SRFA); Tank 9 (50 µgL nano-ceria in media with citrate and 250 µg/L SRFA); Tank 10 (50 µg/L bulk-ceria in media with citrate and 250 µg/L SRFA).

Nano-ceria[b] dispersions have higher tryptophan-like fluorescence than bulk-ceria[b] on D0 which is reversed following 1 h organism exposure. Nano-ceria[b] dispersions at 0.1 mg/L significantly reduce Peak T fluorophore intensity of the fish mucus samples measured from a maximum intensity of the fish mucus 1000a.u at 284/339 nm (Em/Ex) to 363 a.u 281/338 nm. This suggests ceria[b] may quench the fluorophore signals of protein (tryptophan-like) fluorophores. Between D0-D1, a decrease in T_1-T_2 fluorophores is observed in 5 out of 7 tanks. A general increase in T_1-T_2 peak intensities between D0 and D35 is observed across all tanks measured. The decreased fluorophores observed are found in samples with lower (50 µg/L) SRFA additions compared to higher SRFA concentrations (250 µg/L).

5.5.2.8 Total particle concentration

Nano- and bulk-ceria[b] dispersions show low solubility across all conditions measured with <0.4% and <5% Ce mass added, respectively being measured after D35 exposures (Table 5-10). Across all tanks, nano-ceria[b] concentration increases up to 63% from D0 to D1 and decreases overall from D0 to D35 by up to 12% of mass added. Lower concentrations of nano-ceria[b] (5 µg/L) show up to 20% more Ce being measured between D0 and D1 than higher nano-ceria[b] concentrations (50 µg/L) under the same conditions. The higher SRFA concentrations (250 µg/L) show up to 2 % more Ce being detected than in lower SRFA concentrations (50 µg/L) under the same conditions. With an increase of SRFA concentrations from 0-250 µg/L there is a greater recovery of Ce in

solutions from 7 to 16% of nano-ceria[b] mass added in lower nano-ceria[b] concentrations (5 µg/L) than with higher nano-ceria[b] concentrations (50 µg/L) with 4 to 7 % mass added being measured. The repeated test results comparing D7 from the first test and D10 from the second test vary by between -13.2 % up to +14.8% by mass added. Replication from ICP-MS is *ca* 5-10%, so these results are not significant. NPs have been found not to fully atomise in the ICP-MS furnace which can cause some inaccuracies in analysis.

Table 5-10 ICP-MS measurements of ceria[a] particles during *C. carpio* expsosures

Day	Tank Number Ce Dissolution / % mass added (Ce ppb/%)						
	4	5	6	7	8	9	10
(D0)	0.38±3.64 / 7.6	0.47±28.7/9.4	0.90±11.0/18	2.39±13.0/4.78	2.84±6.31/5.68	3.47±4.11/6.94	<0.2/<0.4
(D0 Repeat)	~	~	~	~	~		~
(D1)	1.38±10.2 / 27.6	1.42±9.27/28.4	0.84±18.4/16.8	4.88±4.37/9.76	4.50±34.9/9	3.64±8.29/7.28	<0.2/<0.4
(D7)	1.12±2.6 / 22.4	0.97±28.4/19.4	0.56±20.3/11.2	3.72±13.2/7.4	6.17±2.94/12.3	6.03±7.49/12.1	<0.2/<0.4
(D10 Repeat)	0.46±0.83 / 9.2	1.3±2.51 / 26	1.3±1.42 / 26	9.57±5.93 / 19.1	0.64±0.72/1.28	1.55±1.24/3.1	3.07±1.05/6
(D35)	0.25±9.74 / 5	<0.2/<0.4	<0.3±26.1/6	3.58±5.69/7.2	2.11±4.20/4.2	3.16±2.27/6.3	<0.2/<0.4

Tank 4-media with citrate and 5 µgL nano-ceria[b]. Tank 5-media with citrate and 50 µgL SRFA and 5 µgL nano-ceria[b]. Tank 6- media with citrate and 250 µgL SRFA and 5 µgL nano-ceria[b]. Tank 7-media with citrate and 50 µgL nano-ceria[b]. B) Tank 8- media with citrate and 50 µgL SRFA and 50 µgL nano-ceria[b]. Tank 9- media with citrate and 250 µgL SRFA and 50 µgL nano-ceria[b]. Tank 10 representing media with citrate and 50 µgL SRFA with 50 µgL bulk-ceria[b].

5.5.2.9 Summary

The general observations made following characterisation studies of ceria[b] particle dispersions in *C. carpio* test media are offered below.

- Ceria[b] particles have low solubility, form elongated/rectangular aggregates with *S*>1.4 and Pzc pH<6 and reduced peak-T fluorescence intensity of fish mucus samples.
- Nano-ceria[b] has lower d_H, less –ve charge, greater UV-visible absorption and higher tryptophan-like fluorescence intensity with red-shifting UV-visible peak λ compared to equivalent bulk-ceria[b] dispersions.
- As concentration of ceria[b] increase d_H increases, PdI increases up to 47%, ζ decreases (-ve) and 20% less Ce concentration is detected by ICP-MS.
- As media electrolyte concentration increases Pzc reduces, d_H increases up to 7.5%, UV-visible absorption and fluorescence intensity increases.
- The addition of SRFA reduces the Pzc, the ζ becomes more negative and d_H decreases up to 88%. The d_{TEM} increases up to 26% and Ce solubility, UV-visible and tryptophan-like fluorophores absorptions increase.
- Presence of *C. carpio* increases d_H after 1 h exposure but over 35 d d_H decreases. The ζ becomes more negative and tryptophan-like fluorophores intensity decreases with 63% increases in Ce measured after 1 h exposure.
- Independent samples have higher d_H, higher d_{TEM}, are less -ve charged and have lower measured UV-visible and florescence intensity than equivalent collaborators' samples. Ce concentration by ICP-MS differed by between -13 to 15% mass added between independent and collaborator samples with collaborators repeated samples differing in d_H up to 2 fold.

5.5.3 Ceria C

Ceria[c] particles were gifted by the collaborative group at CSIRO. Results of nano- and bulk-ceria[c] characterisations are offered in Tables A9-10. Once *P. subcapitata* growth curves (Figure A27) were verified, (Rogers *et al*., 2011) characterisation assessments were conducted under the appropriate toxicity conditions, in the presence and absence of 10 mg/L SRFA.

5.5.3.1 Powdered particle analysis

Calculated d_{BET} of nano- and bulk-ceria[c] were found to be within the nominal particle distribution range as determined by the manufacturer (Table 5-11) and bulk being much smaller. Ceria[c] particles are well matched with that of CeO_2 JCPDS Card No. 75-0120 (Figure 5-1 and A1).

Table 5-11 Nano- and bulk-ceria[c] powdered BET and XRD analysis

Nano- and bulk- ceria[c] purchased from a number of manufacturers were analysed for specific surface area and associated particle diameter by BET. Further calculated size distributions were made using XRD analysis using the Scherer equation.

Particle	Particle diameter by manufacturer (nm)	BET SSA. (m^2/g)units	d_{BET} (nm)	d_{XRD} (nm)	(111/200) ratio
Nano-ceria	<25	53.23 ± 0.8	16.1	16.3	1.092
Bulk-ceria	<5000	0.56± 0.1	1530.6	324.3	0.863

n=2 for BET analysis
n=1 for XRD

5.5.3.2 Charge – pH relationship

The pH at which nano-ceria^c ζ dispersions at 10 mg/L are zero (Table 5-12) decreases with increasing electrolyte solutions (10 *mM* < 500 *mM*) (Figure A28). The addition of 10 mg/L SRFA further decreases the Pzc pH<3.5. In *P. subcapitata* media, irrespective of PIPES buffer or SRFA additions, the nano-ceria^c at 10 mg/L dispersions have Pzc pH<2 (Figure A29).

Table 5-12 The pH at which ceria^c zeta potential is zero
pH of nano-ceria^c at 10 mg/L in NaCl media and in *P. subcapitata* media with the additions of 10 mg/L SRFA where shown. Test media includes PIPES buffer.

Media	NaCl				*P. subcapitata*	
Conditions	10 *mM*	500 *mM*	10 *mM* + SRFA	500 *mM* + SRFA	Test media	Test media with SRFA
Zero charge (pH)	6.6	4.3	3.2	<3	<2	<2

5.5.3.3 Particle hydrodynamic diameter

Nano-ceria^c dispersions have lower d_H than equivalent bulk-ceria^c dispersions. As the electrolyte concentration increases, (10 *mM* NaCl< *P. subcapitata* media<500 *mM* NaCl) the d_H of nano-ceria^c significantly increases, ($p<0.05$) across equivalent concentrations (Figure 5-10), although this trend is not systematic. The increasing d_H signifies an increase in aggregation of the particles in solution. As particles aggregate, they will become denser, fall out of suspension and settle, reducing the dimension of material present in solution to be detected by DLS. This will offer a reduced d_H as shown by the more concentrated solutions. There is a significant reduction in d_H measurements ($p<0.05$) in nano-ceria^c 500 *mM* NaCl dispersions with SRFA compared to in

500 *mM* NaCl alone. As ceria^{c} particle concentrations increase, the d_H increases in *P. subcapitata* media in the presence and absence of SRFA. The majority of the particles in *P. subcapitata* media however are found as aggregates (vol) which are greatly reduced in *P. subcapitata* media with SRFA. Individual nano-aggregates (No) are however reduced to as low as 31 nm in the presence of 10 mg/L SRFA.

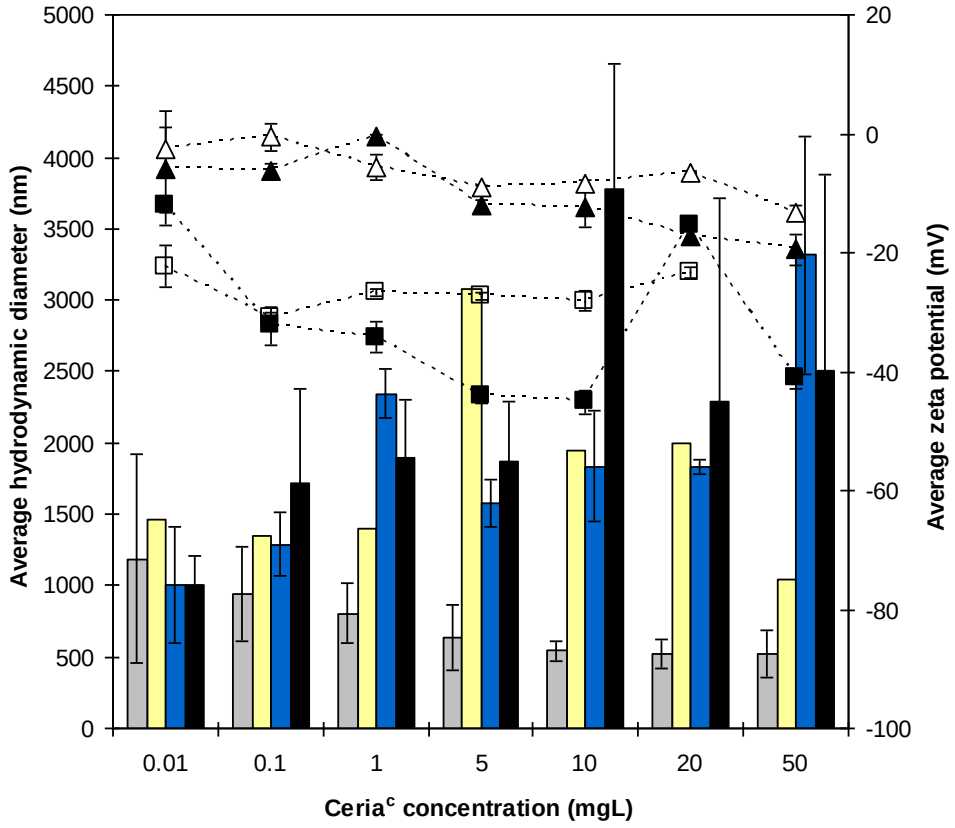

Figure 5-10 Average Z-ave and zeta potential measurements of ceria^{c} in NaCl solutions
Average hydrodynamic diameters (d_H) by DLS and average zeta potential of nano-ceria^{c} in NaCl media as a function of concentration. d_H: 10 *mM* NaCl with SRFA, grey; 500 *mM* NaCl with SRFA, yellow; 10 *mM* NaCl, blue; 500 *mM* NaCl, black. *Zeta potential*: 500 *mM* NaCl with SRFA, black triangle; 10 *mM* NaCl with SRFA, black square; 500 *mM* NaCl, white triangle; 10 *mM* NaCl, white square.

There are no significant differences ($p>0.05$) in d_H observed at the onset (0-24 h) of exposure between equivalent samples in the presence or absence of *P. subcapitata* ($p<0.05$). Throughout the 72 h exposure period nano-ceria^c dispersions without *P. subcapitata* cells do not significantly change in d_H measured.

5.5.3.4 Particle zeta potential

As nano- and bulk-ceria^c concentration increase at pH 7 in either NaCl solutions, ζ becomes more –ve (Figure 5-10). With the addition of 10 mg/L SRFA, ζ decreases (-ve) in both NaCl media. As the NaCl concentration increases (10 *mM*< 500 *mM*) nano-ceria^c dispersions of 10 mg/L at pH 7 increase ζ (+ve). In the presence of *P. subcapitata*, ζ of nano-ceria^c dispersions becomes more positively charged (+ve) irrespective of SRFA addition compared to equivalent samples absent in *P. subcapitata* cells, although this is not significant ($p>0.05$).

5.5.3.5 TEM

Particle counts from TEM images (Figure A30) are presented in Table 5-13. All TEM grids were prepared from 0.1 mg/L ceria^c solutions using the drop method supported by frequency curves (Figure A31) determined from particle counts. Nano-ceria^c appear to form rectangular assemblages when dispersed in Milli-Q water, (Figure A30a-b), although with *S*=1.3 this suggests more rod-shaped particles (Lin *et al*., 2011) or rhombus forms (Baalousha *et al*., 2010) dominate. In *P. subcapitata* media, single nano-ceria^c particle counts are equivalent to

dispersions in Milli-Q water with *S*=2.2. However, much fewer particles are present in *P. subcapitata* media samples. Agglomerates are much greater in *P. subcapitata* media images (Figure A30c-e) than in Milli-Q water dispersions offering higher *S*=2.2. After 72 h exposure to *P. subcapitata*, the only image obtained shows small particle agglomerates on the TEM image obtained (Figure A30f), reducing reliability in this measurement but offering support with DLS measurements obtained.

Table 5-13 Nano-ceria^c particle diameters by TEM
Average particle diameters (d_{TEM}) calculated from TEM images for nano-ceria^c dispersion in Milli-Q water, *P. subcapitata* media and NaCl solutions with aspect ratio (*S*) calculated.

Media	Conditions	Concentration (mg/L)	d_{TEM} (nm/No)	Range (nm)	Max Agglomeration (nm)	*S* (range)
Milli-Q	Pre	0.1	11.9±4.2 / 112	4.5-30.9	215.7±95.6	1.3±0.2 (0.9-1.9)
P. subcapitata media	Pre	0.1	7.1±4.1 / 10	1.0-15	1000±518.8	2.2±1.0 (1.1-4)
	72 h	0.1	2.1±1.2 / 22	0.5-4.8	26.8±11.6	1.3±0.2 (1.1-1.6)

5.5.3.6 AFM

The average dimension of 0.1 mg/L nano-ceria^c dispersed in 10 *mM* NaCl, (Table 5-14) after the mica grid was left for 30 min, was ~15 nm diameter (Figure 5-11). This is equivalent to TEM dimensions measured in Milli-Q water. After the grid was left for 1 h, these dimensions doubled. An increase in nano-ceria^c concentration to 10 mg/L obtained further increased measured particle diameters by AFM, increasing again with increasing mica adsorption time (Figure A32). Nano-ceria^c particles show agglomerated features from AFM images with

diameters up to 0.5 µm in *P. subcapitata* media, (Figure A33) relative to d_H data obtained.

Table 5-14 Ceria[c] particle counts in NaCl from AFM images
Grids were removed form the sample after 30 min adsorption at 0.1 mg/L dispersions

Ceria[c] particle	Particle diameter (nm)	Standard deviation	Number particles counted
Nano	14.9[Ж]	6.3	157
Bulk	62.1[Ж]	48.4	117

[Ж] Appendix B

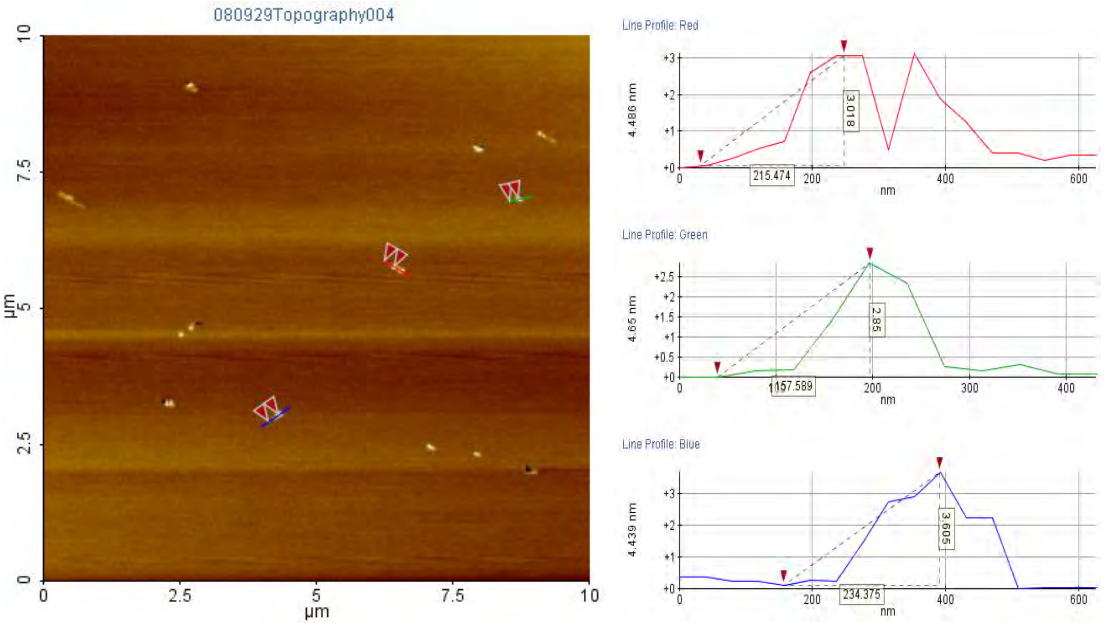

Figure 5-11 AFM images of nano-ceria[c] in NaCl media
Dispersion at 0.1 mg/L in 10 *mM* NaCl after 30 min in solution

5.5.3.7 Particle UV-visible absorption

There is an overall increase in ceria[c] particle UV-visible absorption intensity with increasing concentration in all media observed. The UV-visible absorption spectra for nano-ceria[c] in NaCl mediums are always larger by nearly double than observed with the bulk-ceria[c] in equivalent dispersions (Table 5-15).

Table 5-15 Maximum UV-visible absorption peaks ceria[c]
Maximum UV-visible absorption peaks and wavelengths for nano- (black) and bulk-ceria[c] (blue) in NaCl media.

Dispersion media	Conditions	Maximum absorption peak wavelengths (nm)	Maximum peak absorptions[#] (a.u.)
10 *mM* NaCl	Media	340	0.048
		257	0.008
	With SRFA	291	0.108
		290	0.08
500 *mM* NaCl	Media	211-214	0.111
		207-214	0.219
	With SRFA	211/340	0.052
		208/352	0.018

There is a red-shift in peak λ in all nano-ceria[c] samples with increasing concentration in all NaCl solutions. This trend is reversed for bulk-ceria[c] where there is a blue-shift in peak λ with increasing concentration in all NaCl solutions. As NaCl electrolyte concentration increases there is a blue-shift observed in UV-visible peak λ obtained in equivalent nano-ceria[c] dispersions. The peak λ is further blue-shifted with nano-ceria[c] dispersions in NaCl solutions in the presence of 10 mg/L SRFA. The absorption peaks of nano- and bulk-ceria[c] in *P. subcapitata* media do not change significantly with changes in concentrations in the presence (Figure 5-12) or absence of SRFA.

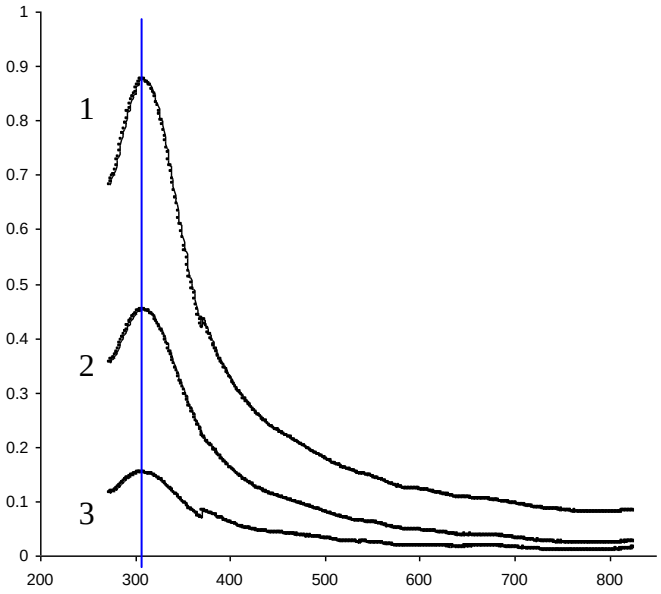

Figure 5-12 UV-Visible spectrum of nano-ceria^c in *P. subcapitata* media
The addition of PIPES buffer and 10 mg/L SRFA to aglae media at; 1) 100 mg/L, 2) 50 mg/L, 3) 20 mg/L. Blue line shows no spectral shift in UV-visible peak.

5.5.3.8 Emission intensity by fluorescence spectrometry

Table A11-12 offers the maximum fluorophore peak absorptions along with Emλ and Exλ for particles in *P. subcapitata* media in the presence and absence of SRFA and in the presence and absence of *P. subcapitata*, across a 72 h exposure period. Results show as nano-ceria^c concentration increase, fluorophore intensity increases. Fluorophore intensity generally increases with the addition of SRFA than in media alone with the exception of tryptophan-like (Peak T_1) fluorophore (Figure 5-13). With the addition of *P. subcapitata*, fluorophore intensity further increases with the exception of tryptophan-like

fluorophores. Fluorophore intensity increases between 0 h and 72 h exposures in the presence of *P. subcapitata*.

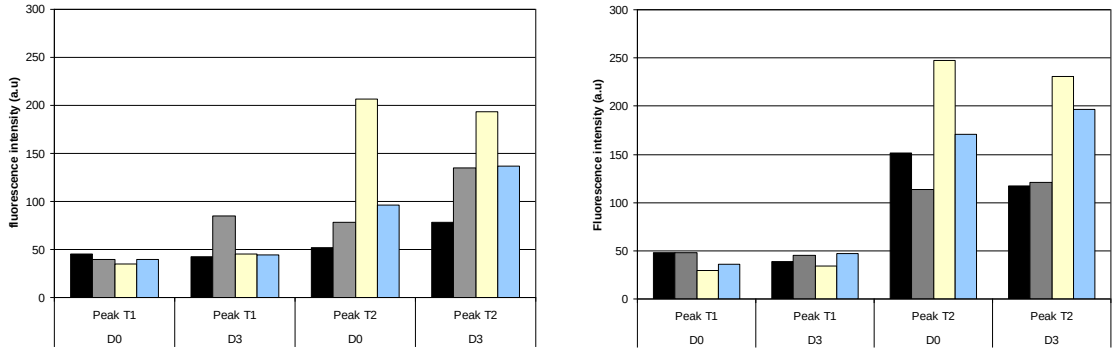

Figure 5-13 Maximum peak T fluorescence intensity for ceria[c] in *P. subcapitata* media Nano-ceria[c] fluorophore tryptophan-like peaks T_1 T_2 maximum at; A) 0.01 mg/L, B) 1.0 mg/L Absorption in *P. subcapitata* media (black) and in *P. subcapitata* media with *P. subcapitata* exposure (grey) and in media with 10 mg/L SRFA (yellow) and in media with 10 mg/L SRFA with *P. subcapitata* exposure (blue).

5.5.3.9 Total particle concentration

ICP-MS analysis was conducted under exposure conditions using ceria[c] particles, by the collaborator at CSIRO. Results showed ceria particle dispersions have low solubility with >0.003 mg/L nano-ceria[c] dissolving in *P. subcapitata* media (Rogers *et al*., 2010) over 72 h.

5.5.3.10 Summary

Six observations were made following characterisation studies using ceria[c] particle dispersions in *P. subcapitata* and NaCl test media.

- Ceria[c] particles have low solubility, form elongated and rectangular particles with aspect ratios >1 and have variable Pzc in all media tested.

- As concentration of ceria^{c} increases, d_H and d_{AFM} increases, ζ decreases (-ve) and UV absorption and fluorophore intensity increases with red-shift in nano-ceria^{c} UV-visible peak intensity λ and fluorescence Emλ.
- As media electrolyte concentration increases (10 *mM* NaCl< *P. subcapitata* media< 500*mM* NaCl) Pzc pH decreases, d_H increases, ζ increases (+ve), TEM particle counts decrease, UV-visible absorption increases and UV-visible λ blue-shift. The UV-visible absorbance and peak λ do not change as ceria^{c} concentration increases or as SRFA is added to *P. subcapitata* media.
- Addition of SRFA reduces the Pzc, reduces Z-ave and ζ (-ve), increases UV-visible and fluorophore absorption and blue-shifts UV-visible peak λ.
- The presence of organisms increases ζ (+ve), increase fluorophore intensity and decreases d_{TEM}.
- Some analytical techniques compliment others in measurements obtained including AFM, TEM and DLS although the preparation methods used e.g. AFM grids can alter the measured particle diameters.

5.6 Discussion

The first aim of this chapter was to use a range of analytical techniques to determine and compare the physicochemical characteristics of three nano- and bulk-ceria particles in a variety of synthetically prepared ecotoxicity test media. The second aim was to determine if the physicochemical characteristics of the particles in synthetic aquatic media varied when dispersed in test media in the

presence and absence of test organisms. The main trends were identified (Table A13) and discussed under the trend headings below.

5.6.1 Nano and bulk particle characteristics vary in equivelant media

NPs exhibit variable measured characteristics compared to equivalent MP dispersions, a phenomenon common throughout the literature. NPs were found to have a greater SSA by BET, where the proportion of atoms on the surface compared to interior of the particle is much greater compared to the MPs. This increased SSA can increase the surface reactivity of NPs compared to MPs in solution and may affect the variable characteristics observed and associated toxicity attributed with NPs. Powdered NP samples also show a greater broadening of obtained XRD diffraction peaks, as a result of NPs nanocrystalline behavior (Sharma *et al*., 2010). Variations in the NP surface coordination can also lead to changes in the surface acidity constants (Bullard and Cima, 2006) as shown by the reduced pH at which ζ becomes zero with NP dispersions compared with MP dispersions. NP dispersions also appear to generally have a more reduced ζ (+ve) compared to equivalent MP dispersions. As a NPs electrical double layers overlap, electrolytes build up in this overlap. This concentration imbalance causes a rush of solute into the area producing a more neutral charge on the particles, reducing the negative charge of ζ observed. In some cases, NPs exhibit more negatively charged dispersions than equivalent MPs, which has also been observed in the literature (Tang *et al*., 2007; Chen *et al*., 2011).

NPs have a greater UV-visible and fluorescence intensity compared to the MP dispersion measured. The confinement of electrons in NPs changes the wavelengths absorbed compared to MPs of the same chemical form. More Ce(III) predicted as being present in nano-ceria creates more electrons that can be excited and increases the florescence intensity observed (Clinton, 2008). UV-visible peaks of NPs will shift to regions of greater intensity and wavelengths, (red-shift) due to the higher ratio of Ce(III) ions within the crystal lattice and the defect states associated with oxygen vacancies (Clinton, 1998). From these results the trends appear to be media dependent, discussed next**.**

5.6.2 Variation in media composition alters particles characteristics

As the media electrolyte concentration increases, general trends are observed across the ceria[a-c] particle dispersions. Such changes include an increase in d_H, and increased UV-visible absorption. The ζ trends are particle dependent where ζ decrease (-ve) with ceria[a] particle dispersion as electrolyte increase and ζ increase (+ve) with ceria[c] particle dispersions as electrolyte increases. Increasing the ionic strength of a solution compresses the EDL layer (Jiang *et al.,* 2009) and causes opposite charges to attract. Some of the salt ions will accumulate in the EDL and screen some of the surface charge of the NPs, reducing the negative charge observed, (Suttiponparnit *et al*., 2011). When the electrolyte concentrations increase, the surface charges of the NPs are completely screened allowing attractive van der Waals forces to dominate, causing fast aggregation (Chen and Elimelech, 2006). This increases the particle

attachment behaviour and subsequently increases the d_H obtained. The larger particles in turn possess higher scattering coefficient for visible light, (Liu *et al*., 2009) increasing the UV-absorption measured. The increased d_H will allow sedimentation of particles increasing the dispersity observed by TEM and reducing counts measured.

The dispersion media can have a profound effect on the particle characteristics measured. There is evidence to suggest a direct influence of some mediums e.g. the cell culture mediums, acting upon the ceria particle dispersions measured, as shown by the d_H, ζ and UV-visible absorption peak wavelengths using largely unchanged, irrespective of particle concentration. Protein adsorption from cell culture medium can dominate the surface charge of oxides (Limbach *et al*., 2005) and can shift the ζ in a more negative direction than would be obtained in aquatic mediums**.** Additional material in the cell media like amino acids along with the variation in temperatures are also contributing factors against particle characteristics measured. Both calcium and phosphorus have been found to destabilise and subsequently increase aggregation of TiO_2 NPs by Domingos *et al*., (2010), likely to be the cause of increased aggregation in ceria[a] particles observed in d_{TEM} measurements from Trout cell media. With no cell media dilution made, there is no significant difference between the particles UV-visible absorption peak wavelengths and that of the control media measured showing a direct effect of media on particle measurements. This makes predictions and

further investigations difficult when using such media and may infer predications made against real scenarios.

5.6.3 Different nanoparticles in equivalent media exhibit variable characteristics

When different ceria particles are dispersed in the same aquatic media, (e.g. NaCl) variations across the measured characteristics were obtained. No significant systematic trends were observed in any analyses conducted, as previously observed in the literature (Xia *et al*., 2008). There were no trends observed in the d_H data obtained from ceria[b] and ceria[c] particle dispersions in either 10 *mM* or 500 *mM* NaCl media. There were more discrepencies in the data observed with larger standard deviations obtained, across the repeated data with ceria[b] dispersion compared to ceria[c] dispersion in equivelant media. The reduced significance observed in these samples may in large be due to the manufacturer's processing procedures, producing the variences in the NP powder analyses being produced.

5.6.4 Particle concentration varies the measured characteristics

As the concentration of nano- and bulk-ceria[a-c] particles increases, d_H and d_{AFM} increases, PdI and ζ increases (-ve) and Ce concentration measured by ICP-MS reduces up to 20% mass added. The NP dispersions also exhibit a UV-visible intensity increase with UV-visible λ being red-shifted.

The increase in particle concentration will increase the number of particles in solution. The frequency of particle collision is a strong function of particle number concentration (O'Melia, 1995) suggesting greater number of particles present in solution, the greater chance of collision and subsequent increased d_H measured from DLS analysis. As NPs agglomerate, they decrease the surface-to-volume ratio thus decreasing the free energy of the particle dispersion (Simakov and Tsur, 2007) and changing the stability of the particle solution. The stability of colloidal systems is dealt with by the DLVO theory (Section 2.4.4.1). DLVO suggests decreases in ζ (+ve) reduces the electrostatic repulsive force and subsequently increases the agglomeration (Suttiponparnit *et al.,* 2011) and associated increase in d_H measured. DLVO theory therefore predicts that as the particle charge increases, (-ve) stability of NPs should increase, and d_H should reduce, opposing that observed in this study with nano-ceria[a-c] particle dispersions. The DLVO theory however is reliant on particle measurements being from spherical shapes, which is not the case with these observed particle dispersions showing elongated and rectangular assemblages. Particle shape appears to be a governing characteristic which requires further investigation and modelling for future nanoecotoxicological tests.

5.6.5 The addition of SRFA alters the particles characteristics

The presence of SRFA leads to a significant increase ($p<0.05$) in measured ζ (-ve) for ceria[b+c] dispersions, decreases the pH of Pzc and increases the Ce concentration detected by ICP-MS analysis by 2% mass added. UV-visible peak

intensity λ blue-shift and d_H reduces up to 88% with SRFA addition to a media. Since the SRHA bears a particular average charge of its own, the SRHA "masks" the charge of the particles with its own (Pelley and Tufenkji, 2008), reducing (-ve) the measured ζ and reducing the pH at which ζ is zero. In the presence of SRFA, NP suspensions can be effectively stabilised (Chen and Elimelech, 2007) through steric repulsion of the particle dispersions exerted by the SRFA, resulting in reduced d_H and PdI measured. A reason for the generally observed reduced d_H measurements with SRFA can be explained due to the high electrostatic energy barrier caused by SRFA producing a protective layer of adsorbed chains (Kallay and Žalac, 2002). At lower ceria concentration dispersions with SRFA, reductions in UV-visible absorption suggest ceria is dissolving due to the presence of the SRFA, as observed by Domingos *et al*. (2009b), and shown by a 2% increase in Ce detected by ICP-MS. The effects of SRFA on particle dispersions however are largely due to media dispersion and particle type (a-c).

5.6.6 The presence of test species alters the particle characteristics

The presence of organisms in a test solution was found to have variable characteristic differences depending on particle type and organism exposed. General decreases in the measured ζ (-ve) of nano-ceria[a-c] dispersions are observed with fluorescence intensities increasing and UV-visible peak λ red-shift. Up to 63% more Ce can be measured by ICP-MS (ceria[b]) after 1 h *C. carpio* exposure. Measured d_H increased up to 80% in exposures to *D. magna* increases and after 1 h exposure to *C. carpio*, but reduced in exposures to *C.*

carpio after 35 d. No significant changes in d_H were recorded during exposures of ceria[c] to *P. subcapitata*.

Aquatic organisms will produce natural defences to reduce effects of environmental pollutants and contaminants from exudates e.g. mucus from fish (Coello and Khan, 1996). Fish mucus can aid in the removal of particles and other environmental contaminants away from their bodies, (Handy, 1989). Heavy metals like cadmium and mercury are known to bind to mucus glycoprotein's (Handy and Eddy 1989). If NPs bind to fish body mucus, the mucus will form an organic layer around the particles in the same way as SRFA can, causing increased agglomeration resulting in the increased d_H. The particles will be well dispersed in the mucus layer, creating an increase in individual particles, as was identified by TEM imagery and reduced d_{TEM} measured during exposure investigations with ceria[a+c] particles. The organic fish mucus and *P. subcapitata* exudates will have a more negative charge as with other organic molecules as with SRFA. This reduces the particle charge measured by ζ being measured on the particles in *D. magna* and *C. carpio* media under exposures and increase the fluorophore intensity measured. With an increase in organic material from predicted fish mucus production, this will increase the aggregation of particles and allow settlement in the sample. The supernatant of the sample used for analysis therefore will only measure particles left in suspension resulting in the reduced d_H observed with ceria[b] particle dispersions under exposures to *C. carpio*.

5.6.7 Collaborator and independent particle characteristics vary under equivalent conditions

Independent samples show greater reductions in measured d_H, more variable ζ values and had decreased fluorophore intensities than equivalent collaborators samples. This variation between sent samples compared against independently conducted samples maybe due to a number of factors. The change in personnel and therefore laboratory practices may be a contributing factor. Also, the time from which samples were taken and transported for analysis may cause some error in readings taken due to settlement of particles during transit. There are also larger volumes of collaborative samples offered. Therefore, taking a small 1 ml sample from 15 L tank sample may offer a more unrepresentative sample for analysis than e.g. 1 ml from a 20 ml sample. The reproducibility of the collaborators repeated test samples was also poor, with up to two fold variations in measured d_H, a phenomenon observed in the literature (Lanone *et al.,* 2009). Future protocols and further inter- and intra-laboratory investigations on particle characterisations are therefore required.

5.6.8 Using a range of analytical techniques increases the understanding of particle characteristics

The true size of a particle dispersed in cell or aquatic media vary considerably across the techniques applied. Variations in pH, temperatures and salt concentrations will also alter observed particle characteristics measured. Variation between calculated diameters (d_{TEM}, d_{XRD}, d_{BET}) and manufacturers

average estimates range between 41-65% across some measurements made. This phenomenon was also observed by Darlington *et al*., (2009) who found up to 38% difference in particle diameter of aluminium between calculations made from d_{BET} and sizes quoted by the manufacturer. Aggregation of NPs during mechanical process such as milling is inevitable and it is difficult to overcome the strong forces holding NP clusters together (Hoecke *et al*., 2009). BET also works on the premise of a particle being spherical and thus having equidistant pore space for N_2 dispersion.

Clusters of NPs tend to form during TEM sample preparation, particularly from the 'drop-method' employed. As a result, particle dimensions calculated from TEM imagery were larger than crystallite sizes obtained from XRD, as observed by Pike *et al*., (2006) and Ju-Nam *et al*., (2011). Using the centrifugal method for cell media TEM grid preparation also showed artefacts during the use of higher concentrations of particles with increased particle material on the images obtained. Using the adsorption method for AFM grid preparation can also give various images depending upon particle concentrations and length of time the mica grid is left in solution (Ju-Nam *et al*., 2011). Both the AFM and TEM images suggest the method preparation is vital to the observed particle effects. Some techniques for predicting and calculating particle diameters were found to be comparative across results obtained. AFM particle dimensions for example, support those obtained by TEM particle counts measured and in some cases, were found to be in good agreement with particle sizes calculated by d_{BET} and

d_{XRD} analysis. The measured (111)/(200) XRD plane ratio values were also in good agreement from PEELs data obtained by Gaiser *et al*., (2011) and Baalousha *et al*., (2011) for equivalent samples measured. All particle diameters in test mediums estimated by d_H measurements were larger that predicted by the manufacturer in all aquatic media measured also observed in the literature, [e.g. Adams *et al*., (2006); Jiang *et al*., (2009)]. The ceria particle dispersions measured are poorly soluble resulting in poor particle dispersions in solution. Due to this, DLS was found not to be conducive as a suitable instrumental technique for determining particle diameters in some mediums, particularly at low concentrations (<0.1 mg/L) due to low scattering of light of the particle suspension. The unpredictability of DLS d_H results could also be due to the particle shape not being spherical producing the over averaged and highly variable results. At these low concentrations the polydispersity of the samples is high in all aquatic media measured (>0.5) and DLS quality control is low.

From this study, it is important to determine the best analytical techniques to use prior to characterisation for chosen working concentrations. The low trend in d_H data maybe due to a greater volume of arbitrary sized and shaped particles, produced in the media. In the course of aggregation of NPs the overlap of the diffuse layers is practically compete, so that one also cannot apply the common DLVO theory (Kallay and Žalac, 2002). DLVO theory also does not include the effects of particle shape, charge, heterogeneity and surface roughness which, looking at TEM images, is an important factor and requires further investigations.

5.7 Conclusion

It was the aim of this chapter to determine if and how the characterisations of ceria particles may or may not change in various ecotoxicity test mediums in the presence and absence of exposure species. Using three separately purchased commercially produced nano- and bulk-ceria samples, a series of physicochemical characterisations were carried out under a range of dispersion conditions. Three cell culture media along with aquatic mediums appropriate for *P. subcapitata*, *D. magna*, *C. carpio* and *D. rerio* exposure assessments were used for particle dispersions. It is evidence from this short account that NP behaviour in some media still has not been fully addressed. Results show NPs behave significantly differently ($p<0.05$) in comparison to their bulk form and most interestingly, to each other in different media. The same particle may also significantly increase in d_H by up to 7.5% and increase in UV-visible absorption in various media. Cell media offer a unique environment eliminating the ability to determine the changes in nano- and bulk- particles under exposure conditions due to the media composition. The effects therefore, on the particles in contact with cell media are not conclusive. It is also evident that the use of different test media for different aquatic test organisms, introduces an additional variable when addressing nanoecotoxicological results to a test design, even when the commercial particle remains the same. It is evident that the preparation of NP solutions may project different NP characteristics experienced during exposure to different organisms. The presence of organisms can also increase measured d_H up to 80% and increase measured Ce solubility by 63%.

The DLVO theory is not applicable during commercial NP characteristic studies largely due to particle shape. As yet, there is no theory or model to support commercial NP dispersions in aquatic ecotoxicity test media at environmentally relevant concentrations, an area required for future work. Using a range of analytical techniques is invaluable in ascertaining the characteristics of a particle dispersions in a given media used. The reduction of particle concentrations (<1 ppm) reduces the reliability of some analysis including the TEM, UV-visible spectroscopy and DLS. This highlights the difficulty in reliably detecting and understanding NP distributions in aquatic suspensions at environmentally relevant concentrations but supports the need to conduct a full range of particle characteristics under such conditions to obtain a better idea of the particles in solution.

Weighing out samples and attempting to disperse poorly soluble powders in aquatic mediums can cause loss of material when producing aliquots from stock solutions and must be taken into account during such activities. Reproducibility in some tests was reduced by changes in laboratory personnel; volumetric changes in sample measurements, sample transportation and length of time between sampling and measurements taking place. Repeated collaborative samples differed in measured d_H up to 2 fold and Ce dissolution differed by between -13 to 14% mass added between independently produced and equivalent collaborative samples. It would be fitting to conduct a full characterisation assessment of particles under exposure conditions at the

exposure site and use a greater volume of sample than that suggested by the analytical method requirements. This would of course increase costs and time in the analytical procedure. Identifying toxicity hazards in new chemicals and NPs, to trophic-level organisms is an increasing area of research. It is therefore essential that NP dispersions be characterised in test media before such investigations take place, using appropriate techniques.

5.8 Evaluation

The inconclusive data obtained and therefore the weaknesses relating to this study were largely derived from the inconsistency in particulate material used. Increasing the variables being measured by incorporating a number of variously supplied commercial particles, makes the comparative assessments of commercial cerium dioxide NP characteristics difficult to evaluate. It is unrealistic therefore to determine the comparative effects of measured particle characteristics across and within a range of aquatic media when the particles being measured are from various manufacturers. Sub-samples of the particles purchased by the collaborators were sent from their specific institutes for this independent research to be carried out, with little consideration of potential contamination or further transportation effects of the particles. It would be fitting for example, if all three collaborators had used the same particles from one manufacturer to compare the particle interactions across their trophic studies. It would also have allowed for comparative characterisation assessments to have been made of one particular particle across the range of conditions measured.

Further to this, it would have been beneficial for the study if the particles that were used by the collaborators for their exposure assessments and therefore during this characterization assessment, to have been from a 'real' source e.g. nano-ceria from Envirox as used in their additives for diesel products, or nano-ceria particles derived from the combustion of such ceria particle additives, to offer a real environmental scenario to resolve.

5.9 Further work

During natural environmental conditions, turbidity of aquatic systems will aid displacement of particles, making them small and un-agglomerated. Dissolution and rapid removal of NPs will also take place under such environmental conditions. With turbidity factors at play, it is likely that exposed particles to natural aquatic systems will become smaller, more spherical in shape and dissociate rapidly. It is therefore vital to further investigate size and shape factors of NPs in environmental systems at environmentally relevant particle concentrations. Further to this, it is important to determine toxic effects of NPs as a factor of size and shape to a range of taxonomic groups. Producing spherical particles of a discrete size is a difficult yet obtainable challenge. In the next chapter, particle characteristics and associated toxicological assessments were carried out on freshwater algae *Pseudokirchneriella subcapitata* using spherical, synthesized nano-ceria particles at discrete particle diameters.

6 Size dependent toxicity of nano-ceria to *Pseudokirchneriella subcapitata*

6.1 Chapter summary

A number of nanoecotoxicity tests have been carried out using commercially available nano-ceria particles to identify the associated toxic effects to aquatic organisms such as algae, (Rodea-Palomares *et al.,* 2011). The interactions between nano-ceria and biological targets are however, somewhat paradoxical, with some publications highlighting the benefits (Silva, 2006) and others the potential risks (He *et al*., 2010) of nano-ceria. Recent nanoecotoxicological tests have highlighted the increased risks of commercial nano-ceria particles compared to commercial bulk-ceria particles to *P. subcapitata* (Rogers *et al*., 2010) directly reflecting the effect of particle size. To date however, nano-ceria toxicity as a function of size has not been fully addressed. With current and future uses of nano-ceria being engineered at low particle diameters to purposefully enter cells, (Cerion, 2011) associated size-dependent toxicity assessments are required. This study investigated the effects of four synthesized nano-ceria particles to *P. subcapitata*. Results suggest a size dependent toxicity of synthesized particles showing over a 600 fold EC_{50} increased toxicity with 5 nm ceria particles compared against commercial nano-ceria particles. 5 nm ceria particles show a 4% and 20% greater risk to *P. subcapitata* by EC_{50} than dissolved copper and PCP respectively.

6.2 Chapter organisation

This chapter begins with the experimental design (Table 6-1) reviewing the aims and objectives addressed in Chapter 1. This leads onto a short introduction followed by the results obtained from synthesized nano-ceria particle exposures to *P. subcapitata* with related discussions.

Table 6-1 The aims and objectives for Chapter 6.

Aim
1. Determine the physicochemical characteristics of a range of synthesized ceria nanoparticle sizes in *P. subcapitata* test media. 2. Determine the toxic effects associated with nano-ceria to *P. subcapitata* as a function of particle size.
Objectives
▪ Produce and characterise a range of discrete synthesized nano-ceria particle sizes. ▪ Conduct toxicity tests using *P. subcapitata* and OECD 201, (1984) growth inhibition test using well characterised synthesized nano-ceria particles. ▪ Determine if any, the size related toxicity effect of ceria NPs to *P. subcapitata*.

6.3 Introduction

Nano-ceria is being exploited in a number of commercial and industrial uses including medical applications (Karakoti *et al*., 2008) and healthcare practices (Pierscionek *et al*., 2011). Due to its unique redox capabilities, nano-ceria has also been found to protect normal cells against radiation damage during cancer treatments (Tarnuzzer *et al*., 2005). Nano-ceria has been found to be able to prevent vision loss due to light-induced degeneration of photoreceptor cells (Chen *et al*., 2006) and has been found to

be able to repair spinal cords by increasing the survival of the neurons against OS related damage (Das *et al*., 2007). Due to the potential medical applications of nano-ceria, synthesized dimensions of 3-20 nm are becoming more widespread (Karakoti *et al*., 2008). Although nano-ceria is considered as having negligible effects to cells (Pierscionek *et al*., 2011) and a number of aquatic organisms, (HEI, 2001 pp15) smaller nano-ceria particles have been found to be more toxic than their bulk counterparts (Roh *et al*., 2010). It is imperative therefore that nanoecotoxicological studies are performed on nano-ceria particles as a function of their size.

6.4 *Pseudokirchneriella subcapitata*

The most common micro-alga used in aquatic nanoecotoxicological studies (OECD 201, 1984), is the green alga *Pseudokirchneriella subcapitata*, (Figure 6-1) formally known as *Selenastrum capricornutum*. From the kingdom Plantae; phylum Chlorphyla and class Chlorphyceae, *P. subcapitata* is considered a model organism for freshwater algal toxicity tests. This species is a 'sensitive', pelagic organism (Ward *et al*., 1995) with a rapid exponential growth rate under optimal conditions, making it an ideal species for well controlled investigations. *P. subcapitata* also has a familiar crescent shape making it easy to identify under microscopic investigations (Figure 6-1). *P. subcapitata*, has been used in a number of studies including investigations into cell surface absorbance efficiencies, (Casiraghi *et al*., 2005) metal toxicity (Koukal *et al*., 2007) and more recently, effects of growth due to NP exposures as a single organism (Rogers *et al*., 2010) and as a trophic level specie (Hoecke *et al*., 2009).

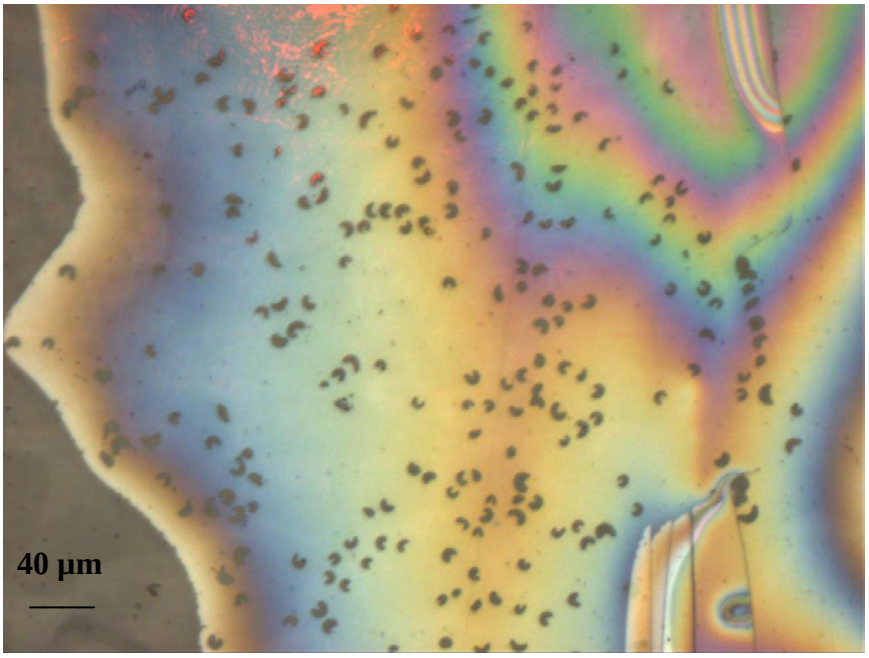

Figure 6-1 *Pseudokirchneriella subcapitata* under the light microscope
Optical light microscope imagery taken from an AFM grid of *Pseudokirchneriella subcapitata* used during size dependent toxicity assessments under control conditions after 72 h.

6.4.1 Cell structure and reproduction

The cell structure of *P. subcapitata* is usual for most Chlorphyceae, although the shape varies within this class. The nucleus of *P. subcapitata* lies near one end of the cell with the inner side of the nucleus having a Golgi apparatus (Hoek *et al*., 1995). The single chloroplast usually lies at the tip of the cell and contains pyrenoids with high levels of rubisco (Hoek *et al*., 1995). Cell walls are composed of cellulose and many Chlorophyceae are calcified (South and Whittick, 1987). A long mitochondrion stretches along the inner face of the chloroplast. Flagella are usually apically inserted (South and Whittick 1987) and the entire cell is surrounded by a thin cell wall (Hoek *et al*., 1995). *P. subcapitata* propagate asexually (South and Whittick, 1987) through the formation of autospores (Hoek *et al*., 1995).

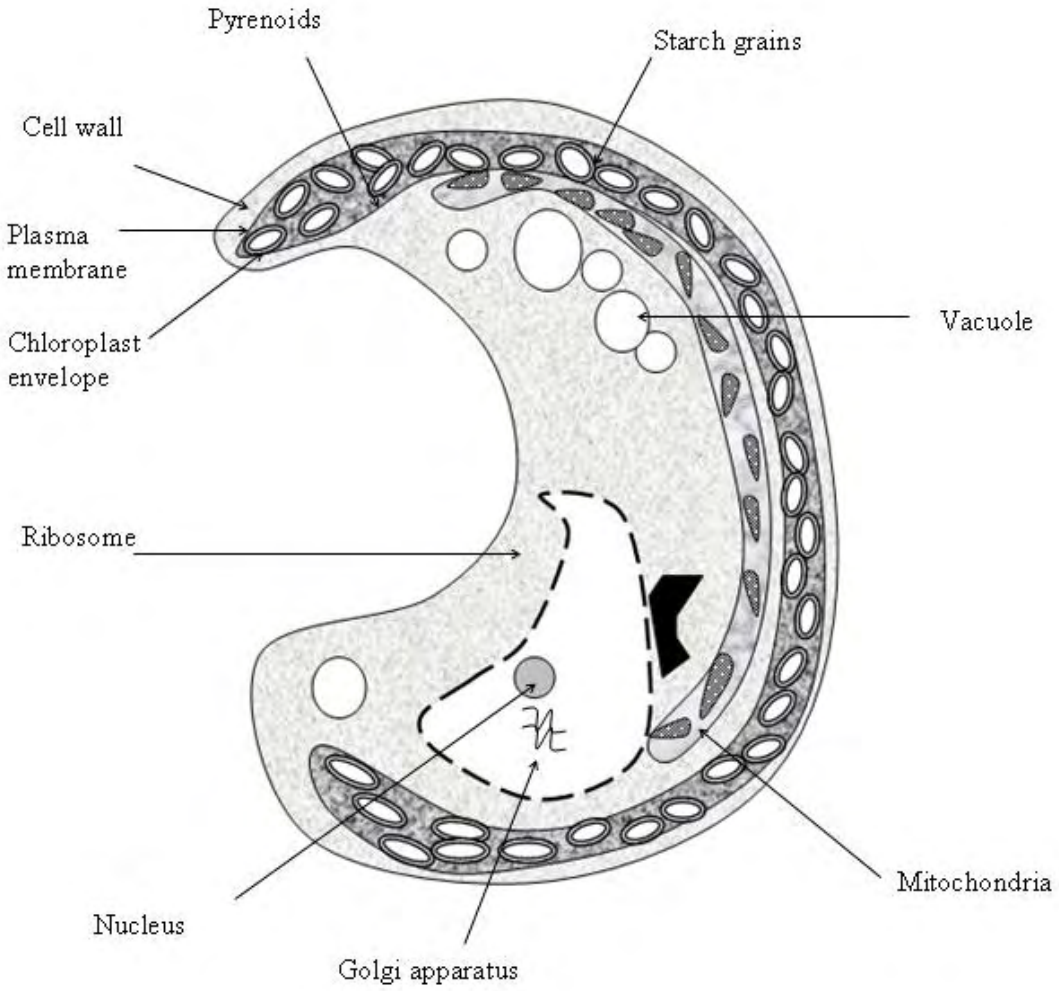

Figure 6-2 Cell structure of *Pseudokirchneriella subcapitata* Adapted from Hoek *et al*., (1995) not drawn to scale.

6.5 Results and discussion

Nano-ceria particles were synthesized using an aqueous method by Dr. Ruth Merrifield, University of Birmingham (Chapter 4). Four discrete particle sizes were obtained and characterised using a range of techniques (Chapter 3). These particles were exposed to *P. subcapitata* using OECD 201, (1984) guidelines (Chapter 4). The

results of these exposures were repeated with three separate batches of synthesized nano-ceria particles to ensure reproducibility across particle batches obtained. Batch one was also repeated at the CSIRO laboratories to ensure inter-laboratory reproducibility.

6.5.1 Synthesized particle characterisations

A summary of synthesized nano-ceria characterisations preparation in Milli-Q water is offered in Table 6-2.

6.5.1.1 Dynamic light scattering

From the d_H measurements obtained, the particles A-D in Milli-Q water may be addressed as mean diameters 5, 7, 12 and 43 nm respectively, (Figure A34) across all three batches made. The d_H obtained for each particle (A-D) measured are similar showing reliability in batches produced across each particle batch (1-3).

6.5.1.2 Electrophoresis

Across all three synthesized nano-ceria particle batches, each particle (A-D) prepared were found to have different ζ ranging from -0.28 mV to -33.2 mV with variable pH values from pH 4 to pH 9 making it difficult to compare the ζ of the four nano-ceria particles measurements under these 'as made' conditions. The increase in ζ measurement (+ve) with increasing particle dimension, (Figure A35) is a phenomenon previously observed [Ofir *et al*., (2007); Suttiponparnit *et al*., (2011)].

Table 6-2 A summary of synthesized nano-ceria particle characterisations
Nano-ceria particle size distributions by DLS and TEM, electrophoretic measurements and associated zeta potential values taken from at least three repeated values. Three batches (1-3) of four synthesized nano-ceria particles (A-D) obtained.

		Synthesized nano-ceria particles			
Analytical technique	**Measurement**	**NP A**	**NP B**	**NP C**	**NP D**
DLS	*Z average* (nm) 1~	6.5 ± 0.3#	9.8 ± 1.7	12.8 ± 1.0	32.2 ± 3.1
	Z average (nm) 2~	5.5 ± 0.2	5.2 ± 0.6	7.6 ± 0.6	13.9 ± 1.9
	Z average (nm) 3~	3.2 ± 0.2	8.2 ± 1.5	15.4 ± 6.5	83.5 ± 27.5
TEM	Size distribution (nm)	3.2 ± 0.2	8.1 ± 1.4	11.1±2.1	14.1 ± 4.7
	Particles counted (no)	114	26	104	126
	Shape factor (ratio)	1.4±0.2	1.4±0.4	1.4±0.4	1.4±0.3
Electrophoresis	ζ (mV/~pH)	-33.2±6.4 / 7.8	-5.3 ± 0.7 / 4.3	-11.9±2.10 / 9.3	-0.98±0.4 / 6.4
	Conductivity (mS/cm)	0.19	0.26	0.3	0.2
ICP-MS+ 1		18.4 ± 3.8	128.1± 5.29	92.5 ± 1.5	22.6 ± 1.3
2	Ce concentration (mg/L)	40.34	65.26	57.84	~
3		19.3 ± 678.5	585.2 ± 219.8	215.8 ± 32.3	32.7 ± 10.4
UV-vis	Max Absorption λ (nm)	267	264	262	260

~Representing batchnumber
#Mean taken from only two results.
+Following 0.1 µm filtration and acidification using HNO_3 to ~pH 2.

Using electrophoretic measurements alone would suggests the 35 nm particles are more likely to aggregate under these conditions due to charge neutralisation effects (Baalousha *et al*., 2008). However the particles are sterically stabilised with PVP, which has a high dielectric strength, good charge storage capacity and is hydrophilic, which protects the surface of NPs (Gasaymeh *et al*., 2010) from attractive forces.

6.5.1.3 Transmission electron microscopy

TEM imaging was conducted under the supervision of Dr. Ruth Merrifield, Birmingham University. TEM grid preparation for all samples was conducted using the drop deposition method. Figure 6-3 shows representative images of particles A-D. Nano-ceria particles were clearly visible and distinct from the dispersion media due to the high electron density of CeO_2. It is evident that all particles are well dispersed due to the PVP coating used during the synthesis process and show little aggregation and few defects. TEM images show that there are relatively low particle numbers resulting in fewer particles to count for a representative size distribution. The particle size distributions obtained from TEM do however coincide with the d_H results obtained from DLS analysis. TEM particle counts suggest particles A-D are between 3, 8, 11 and 14 nm in diameter respectively. The particles A-D show a similar particle shape, irrespective of particle dimensions, all with an S=1.4. This suggests rhombus and octahedral forms (Baalousha *et al*., 2010) of particles were produced.

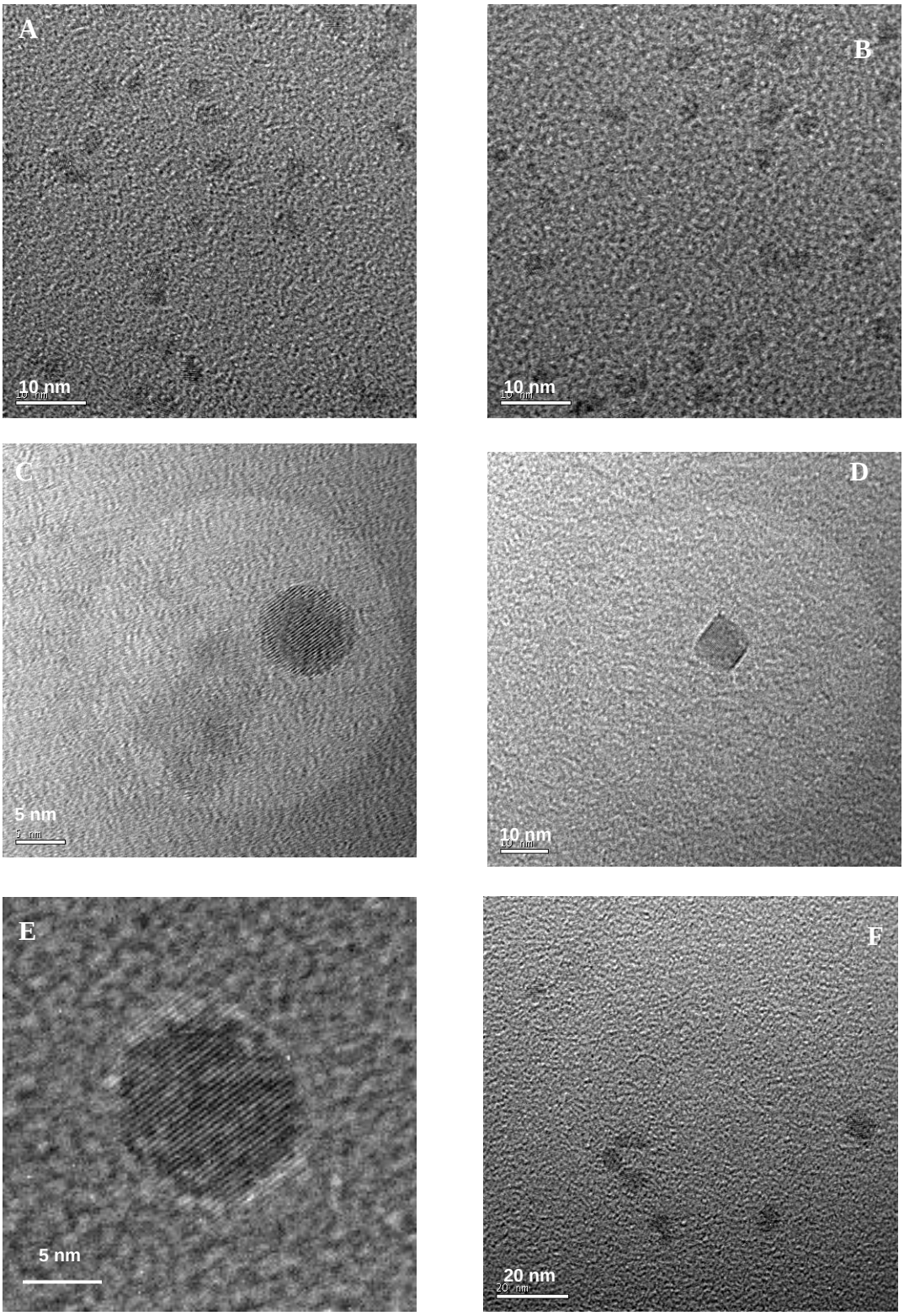

Figure 6-3 TEM images of synthesized nano-ceria particles
a-b). Ceria particle A, c-d) Ceria particle B, e) Ceria particle C, f) Ceria particle D.

6.5.1.4 UV-visible spectroscopy

As particles A-D increase in size, by measured d_{TEM} and d_H, the UV-visible maximum peak absorption wavelength reduces from 267 nm to 260 nm, although this shift is not significant but suggests particles may in large be Ce(III), (Roa and Sahu, 2001).

6.5.1.5 Summary

From the particle characterisations it is reasonable to speculate that the synthesized nano-ceria particles A-D prepared across three separate batches (1-3) are within nominal dimensions of 5, 7, 11 and 35 nm, which is how they are depicted from herein. The particles have a range of ζ at various pH's 'as made' in Milli-Q water. Although the low ζ measured indicates a potential instability of the particles, the PdI by DLS and TEM images suggest well dispersed particle solutions due to them being sterically stabilised by the PVP coating. These measured parameters however, may change upon dispersion into *P. subcapitata* test (OECD) media. Therefore further characterisations in OECD media were performed during exposure conditions.

6.5.2 Synthesized particle characterisations in OECD media

Additional physicochemical characterisations of each of the four synthesised nano-ceria particles were carried out in diluted stock solutions of 1:100 representing nano-ceria stock solutions used for dosing during the *Pseudokirchneriella subcapitata* exposures. Dilutions were made using *P. subcapitata* test media. A summary of results obtained are given in Table 6-3.

Table 6-3 A summary of synthesized nano-ceria characterisations in OECD media
Point of zero charge, (Pzc) maximum absorbencies and size distributions of all synthesized ceria particles dispersed in OECD media at 1:100 dilutions at pH 7.

		Synthesized nano-ceria particle termed sizes (nm)			
Analytical Technique	Measurement	5	7	10	35
Electrophoresis	ζ pH7 (mV)	-25	+12.7	-12.1	-0.9
	Pzc (pH)	4.34	7.59	5.5	<2
	Z-ave (nm)	34.6 ± 45.2	21.7 ± 6.8	34.3 ± 0.9	50.5 ± 0.7
	Polydispersity	0.26	0.2	0.25	0.35
DLS	Vol (nm)	7.52 ± 1.8	23.5 ± 21.7	83.78 ± 5.7	430.8 ± 91.3
	Nom (nm)	4.4 ± 0.2	9.1 ± 0.5	15.8 ± 1.1	23.4 ± 1.4
UV-Vis	Maximum Absorbance (nm)	263	260	259	258

6.5.2.1 The point of zero charge

The Pzc for the nano-ceria particles in *P. subcapitata* media (Figure A36) at 1:100 stock dilution is pH <5.5 for 5 nm, 10 nm and 35 nm particle dimensions. The Pzc for 7 nm particles is *ca* pH 7.5 which is the dispersion pH used for *P. subcapitata* exposures. Results suggest 5, 10 and 35 nm synthesized nano-ceria particles at 1:100 stock dilutions should be negatively charged when under *P. subcapitata* exposure conditions. This will reduce any associated algal cell interactions by reducing charge based reactions with negatively charged algae cells. Nano-ceria at 7 nm diameters has the potential to interact with algae cells given by a positive surface particle charge at relevant exposure pH 7.5.

6.5.2.2 Dynamic light scattering

There is an increase in d_H observed across all the particles in 1:100 algae media dilutions at ~pH 7, compared to original readings taken prior to dilution (Section 6.5.1.1). A 1.7 fold increase is observed for 35 nm diameter ceria particles and *ca* 2.8 fold increases for 7 and 10 nm diameters with a 7 fold d_H increase for 5 nm ceria

particle dimensions. The increased d_H is due to the EDL being reduced in the high electrolyte concentration of *P. subcapitata* media, allowing particle interactions and increased aggregation observed. The associated PdI is however low (<0.4) with size distributions calculated by number from DLS reflecting those originally made, (between 5-23 nm) suggesting the majority of particles are still present in their original dimensions when dispersed in the *P. subcapitata* test media.

6.5.2.3 UV-Visible absorption

The maximum UV-visible absorption peak of each particle size at 1:100 dilutions at pH 7 is observed at the same wavelength of ~270 nm (Figure 6-4). The 5 nm particles have a smaller peak area compared against 35 nm particles, possibly due to the 5 nm particles being so small and present in such low quantities at this chosen dilution. This reduces the absorption of light detected by the WPA lightwave UV-Visible spectrometer used. There is a decrease in maximum absorption peak wavelength with increasing particle size suggesting a red-shift in larger sized particles as observed by Clinton (2008) and being consistent with previous work by Elechiguerra *et al*., (2005).

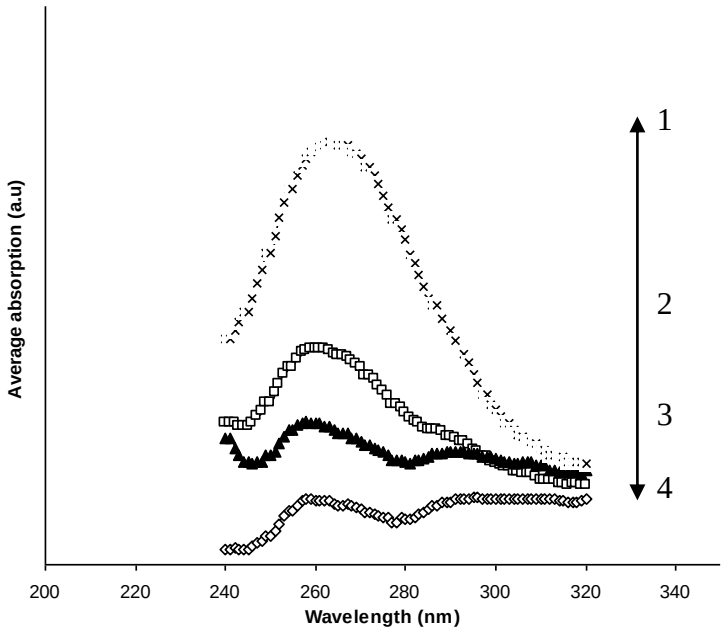

Figure 6-4 UV-Visible absorption spectra of nano-ceria in *P. subcapitata* test media
Batch three ceria particles, in *P. subcapitata* media at ~pH 7 following 1:100 dilution - in order 1-4 showing maximum peak absorption wavelengths; 35 nm, 7 nm, 10 nm, 5 nm.

6.5.2.4 Summary

Synthesized nano-ceria particle dimensions 5-35 nm will easily disperse into *P. subcapitata* media at 1:100 dilutions at pH 6.5. Particle dispersions under these conditions will occur largely as single particles with few agglomerates, maintaining a stable formation. Nano-ceria particles of 5, 10 and 35 nm diameters will have a negative charge in *P. subcapitata* media at stock dilutions of 1:100 at pH 6.5, where nano-ceria particles of 7 nm dimensions will have a positive charge, which may increase the *P. subcapitata* cell interactions during exposure assessments. During exposure investigations, these stock dilutions of 1:100 will be further diluted by up to 1% prior to exposure conditions. This may infer further particle changes in dimension,

ζ and maximum UV-visible peak wavelengths. This advocates the need to continue physicochemical characterisations under *P. subcapitata* exposure tests, as conducted.

6.5.3 Exposure assessments

P. subcapitata cell density measurements were determined using a linear regression plotted from UV-Visible absorption measurements at 680 nm for *Pseudokirchneriella subcapitata* (Molot *et al*., 2010) calibrated against cell counts conducted using a haemocytometer (Section 3.4.1.3). Growth curves are given as a percentage of growth over 72 h compared against the control sample under the same conditions.

6.5.3.1 Growth curves

Commercial nano-ceria growth curves obtained for *P. subcapitata* (Figure A27) were in good agreement with previously conducted work at CSIRO laboratories and as published (Rogers *et al*., 2010), increasing confidence in the growth curves from synthesized nano-ceria particles. Representative growth curves from each nano-ceria particle dimensions (A-D) across all three batches (1-3) are offered in Figure 6-5 to 6. A further representative growth curve from each particle size distribution is offered in Figure 6-7 compared against commercial ceria particles. Using Figure 6-7, the associated EC_{50}, EC_{20}, NOEC, PNEC and LOEC values were obtained for each particle dimension (Table 6-4).

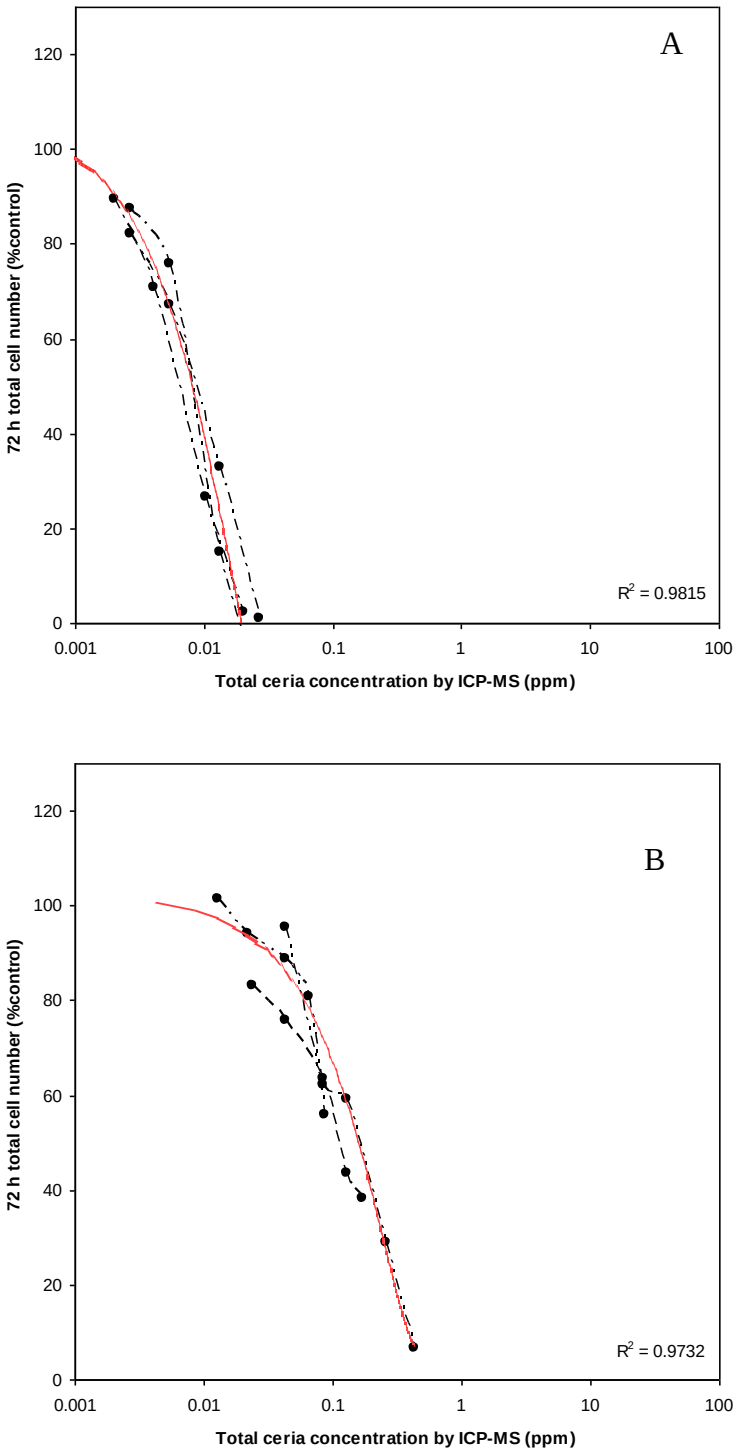

Figure 6-5 *P. subcapitata* growth curve of synthesized 5 nm and 7 nm ceria particles Growth curves taken across all three particle batches compared to the control, both with an associated gradient (red line) A) 5 nm ceria; B) 7 nm ceria.

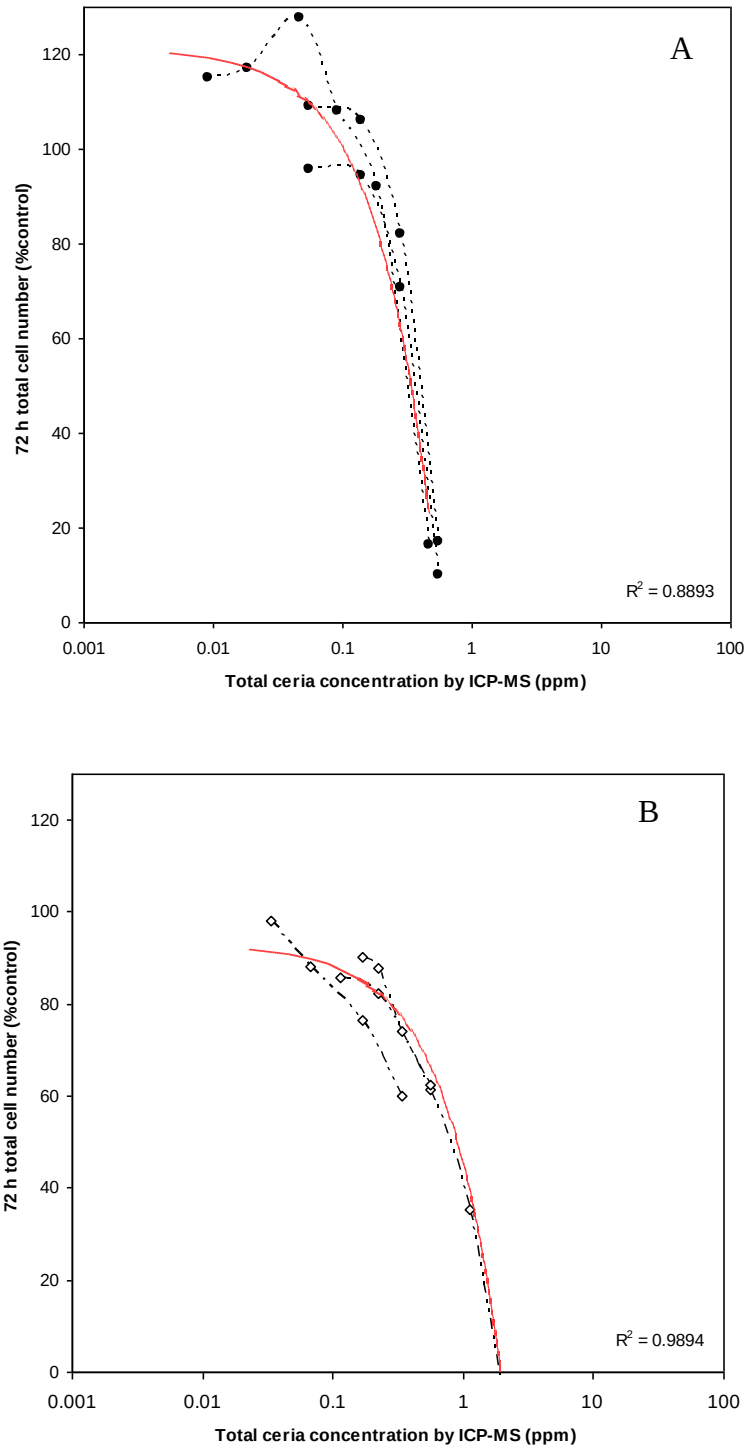

Figure 6-6 *P. subcapitata* growth curve of synthesized 10 nm and 35 nm ceria particles
Growth curves taken across all three particle batches compared to the control, both with an associated gradient (red line) A) 10 nm ceria; B) 35 nm ceria.

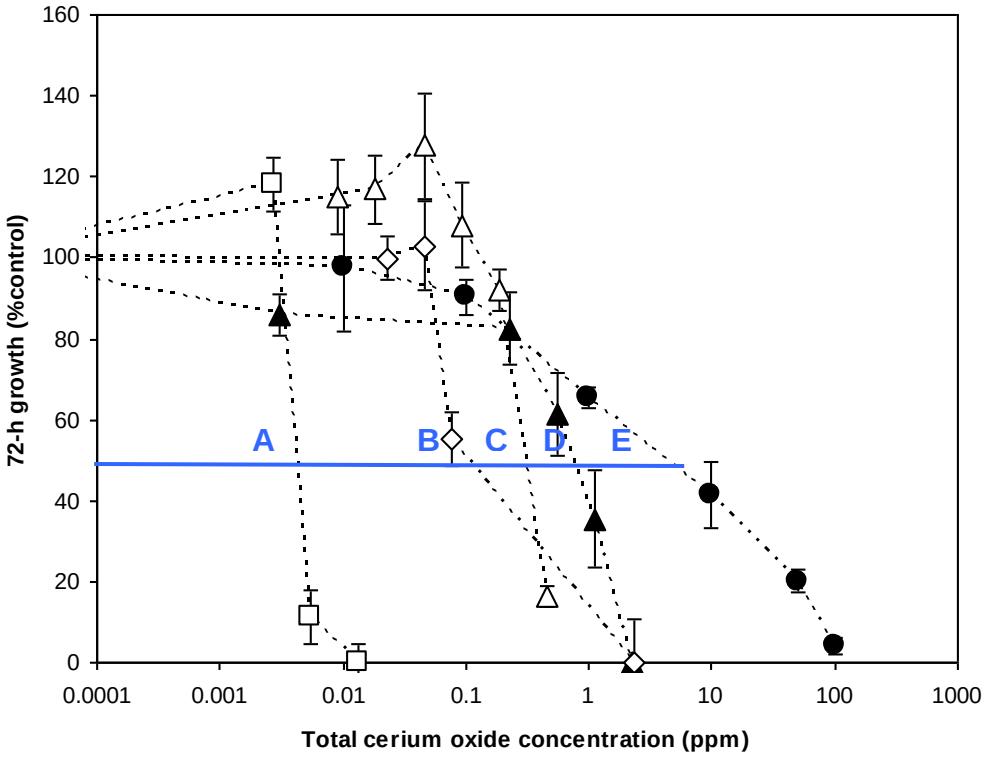

Figure 6-7 Representative growth curves of nano-ceria exposures to *P. subcapitata*
One representative growth curve from Figure 6-5 to 6-6 showing synthesized nano-ceria and commercial nano-ceria particle growth curves to freshwater algae *Pseudokirchneriella subcapitata*. A-E across the blue line representing the EC_{50} value associated with particle toxicity in order from 5 nm (White Square), 7 nm (white diamond), 10 nm (white triangle), 35 nm (black triangle) and commercial nano-ceria[c] NPs (black circle).

Some growth curves show an increase in *P. subcapitata* cell growth compared to the control as a function of increased nano-ceria dose. This may be due to the speculative hormesis effect. Hormesis is a term used to describe the phenomenon of biphasic dose- or concentration-response relationships (Cedergreen, 2008). Stimulation of *P. subcapitata* cell growth has been observed following TiO_2 NP exposures to algal cells by Hartmann *et al*., (2010) although the hormesis effect often occurs below contaminant concentrations often measured, or below the LOEC in toxicity tests, and is therefore rarely

documented during environmental nanoecotoxicity tests, with little understood by this phenomenon.

6.5.3.2 Effective concentrations

EC_{50} values are used in ecotoxicity studies as a measure of comparable toxicity of a contaminant against that of the control. Commercial nano- and bulk-ceria[c] EC_{50} values along with positive controls of cerium nitrate solutions (Table 6-4) correlated well with those obtained by Rogers *et al*., (2010).

Table 6-4 Average toxicity data from ceria particle exposures to *P. subcapitata*
Toxicity assessment values of EC_{50}, EC_{20}, NOEC and LOEC obtained during size toxicity investigations of synthesized nano-ceria particles to *Pseudokirchneriella subcapitata* showing commercial powered nano- and bulk-ceria[c] particle exposures conducted in Chapter 5.

				~EC values (mg/L)		~Growth rate inhibition range (% control/mg/L)				Other values
Ceria Particle	**~NOEC (mg/L)**	**~LOEC (mg/L)**	**PNEC (mg/L)**	**20**	**50**	**0.01**	**0.1**	**1.0**	**10**	**Gradient value**
Commercial Bulk[c #]	3[+]	~	0.003	~	60[+]					~
Commercial Nano[c]	0.5[+]	0.81	0.0005	0.16-0.8	8	81.2–91.5	82–86.1	73.5-78	27–47	-1.8225
Cerium Nitrate[#]	0.03[+]	~	0.00003	~	0.3 0.15[+]	~	~	~	~	~
35 nm	<0.034	0.23	0.000034	0.14-0.28	0.3-0.8	>100	83.5-91	39.5	~	-48.137
10 nm	<0.010	0.14	<0.00001	0.23-0.29	<0.35	>100	>95	~	~	-212.1
7 nm	0.013	0.043	<0.000013	0.03-0.065	<0.14	>100	48.5-57.5	~	~	-221.22
5 nm	<0.001	0.002	<0.000001	0.003-0.0045	0.0013	26.5-45	~	~	~	-4346.8

Gradient taken from individual growth curves, shown by red lines on individual growth curves.
[+]Data received by collaborative work in Rogers *et al*., (2010) or during training at CSIRO
[#] Growth curves not shown
[~] Data not conducted.

As the measured nano-ceria particle size decreases from 35 nm to 5 nm the EC_{50} value also decreases suggesting a size dependent toxicity of synthesized nano-ceria particles to *Pseudokirchneriella subcapitata* of 0.8, 0.3, 0.1 and 0.001 mgL respectively.

6.5.3.3 Gradient values

The gradients derived from Excel software applied to the growth curves obtained offer a further indication of particle toxicity. The steeper the gradient, as a function of particle dose, can be assigned to a more rapid toxic effect. The least gradient measured was -1.8, obtained from commercial nano-ceria[c] particle exposures. The gradient is shown to reduce from -48 to -4346.8 with decreasing calculated synthesized nano-ceria particle diameters (35 nm to 5 nm). This trend supports the decrease in nano-ceria particle's growth effect to *P. subcapitata* compared to controls, with decreasing particle size as obtained from EC_{50} values.

6.5.3.4 LOEC, NOEC and PNEC values

The LOEC values calculated from Figure 6-7 were found to follow the trends observed by the EC_{50} where as the synthesised nano-ceria particle size decreased from 35 nm to 5 nm the calculated LOEC also reduces. The NOEC values however do not present this linear trend. The NOEC values obtained are derived largely from approximate values from the growth curve, as particle concentrations below this were not measured. Therefore, the NOEC values are

only offered as a guide as concentration below which a no observable effect will occur. The PNEC was derived from the NOEC using an extrapolation factor of 1000. As a guide, the PNEC values are between 0.0005 mg/L for commercial nano-ceria[c] to 0.000001 mg/L for synthesized nano-ceria particles at a dimension of 5 nm, although further work is required to fully determine these values.

The PEC has yet to be set for cerium particles, due to water quality data being required (ENV, 2007). The predicted maximum exposure to humans via inhalation, based on general environmental atmospheric data, is *ca* 0.0078 µg/m^3 where the predicted maximum oral exposure is estimated to be *ca* 0.45 µg//kg/day based on calculations from data for soil (ENV, 2007). Using the PEC value 0.00045 mg/L the PEC/PNEC ratio calculation for risk is presented on Table 6-5.

Table 6-5 PEC/PNEC values for commercial and synthesized ceria exposures to *P. subcapitata*

Particle	Commercial MP	Commercial NP	Cerium nitrate	5 nm	7 nm	10 nm	35 nm
PNEC (mg/L)	0.003	0.005	0.00003	0.000034	0.000001	0.000013	0.000001
PEC/PNEC ratio	0.15	0.9	15	13.2	450	34.6	450

Using PEC/PNEC ratio values (Table 2-3) it is evident that commercial nano- and bulk-ceria[c] particles offer no immediate concern (<1 value). However, all synthesized particles are of some concern with a PEC/PNEC ratio value 1-10 in the concentrations measured. Further data is required for 5 nm and 10 nm particles where PEC/PNEC ratio values were 10-100. The 7 nm and 35 nm ceria

particles are of great risk to *P. subcapitata* with a PEC/PNEC ratio value >100 value based upon this risk assessment model.

6.5.3.5 Dose-response semi-log plot

Synthesized nano-ceria particle EC_{50} values were plotted against commercial ceria particle EC_{50} values (Figure 6-8) to obtain a comparative understanding of size related toxicity. Previously determined d_H results by DLS (Section 5.5.3.3) for commercial bulk- and nano-ceria dimensions in OECD test media, of 4209 nm and 2662 nm respectively were used for the commercial ceria particle size values. From this log-plot distribution, it is evident that the apparent toxicity associated with synthesized nano-ceria particles follows a typical dose-response sigmoidal profile. There are however, some limitations using the dose determinations for this model when using commercial ceria particle dimensions determined from DLS. It is difficult to determine whether the initial commercial nano-ceria^c stock solution used for dosing is an accurate measure of dissolved nano-ceria. Also, the dose referenced from the synthesized nano-ceria particles are also reduced as the initial concentration is only measured from ICP-MS analysis which can be subject to errors when measuring NP concentrations.

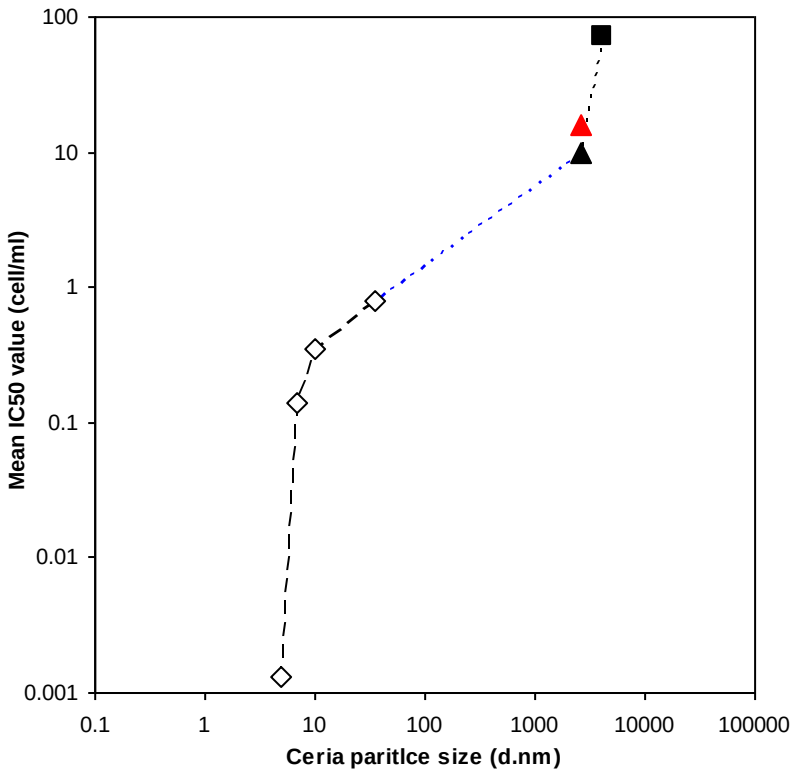

Figure 6-8 Dose-response semi-log plot of EC_{50} ceria particle exposures
Synthesized (white diamond) and commercial (black symbols) nano- (triangle) and bulk-ceria (Square) particles associated EC_{50} values following toxicity assessments to *Pseudokirchneriella subcapitata*. Blue dotted line signifies potential predicted EC_{50} values for particle sizes which have yet been conducted. Red triangle indicates an example of an average EC_{50} commercial nano-ceria result taken from Rodea-Palomares *et al.*, (2011).

Future tests using increased synthesized nano-ceria particle sizes >35 nm to *Pseudokirchneriella subcapitata* maybe projected upon this sigmoidal trend, using EC_{50} values. Such results may be plotted along the red line as indicated in Figure 6-8. For example, a recent study using commercial ceria NPs of 2632 nm (by DLS) on *Pseudokirchneriella subcapitata* was conducted by Rodea-Palomares *et al*., (2011) resulting in an average EC_{50} value of 16 mg/L. This result plotted shows a direct relationship to the EC_{50} values obtained during the commercial ceria particles used during this independent study.

6.5.3.6 Comparative toxicity to other investigations

Table 6-6 shows related EC_{50} values obtained by previous 72 h exposure studies to *Pseudokirchneriella subcapitata* using a range of toxicants.

Table 6-6 Comparative EC_{50} values for exposures to *P. subcapitata* Using a range of documented EC_{50} values following 72 h growth inhibition tests in OECD test media, for a range of toxicants.

EC_{50} (mg/L)	Contaminant specie	Reference
0.0013	5 nm synthesized ceria	Chapter 6
0.0067	Pentachlorophenol (PCP)	Yeh and Chen 2006
0.03	Cu (dissolved)	Schamphelaere *et al*., 2003
0.06	2,3,4,6-tetrachlorophenol	Chen and Lin 2006
0.13	Cu^{2+}	Pereira et al., (2005)
<0.14	7 nm synthesized ceria	Chapter 6
0.15	Cerium nitrate	Rogers *et al*., (2009)
0.3	Cerium nitrate	Chapter 6
<0.35	10 nm synthesized ceria	Chapter 6
0.3-0.8	35 nm synthesized ceria	Chapter 6
8	Commercial nano-ceria	Chapter 5
60	Commercial bulk-ceria	Rogers *et al*., (2009)
0.2-20	Bromoxynil octanoate	Ma *et al*., (2007)

From these previous studies, it is evident that the smallest synthesized nano-ceria particle dimension of 5 nm offers a greater toxicity (using EC_{50}) by *ca* 20% than that obtained by PCP exposures (Yeh and Chen 2006). The synthesized nano-ceria particles of 5 nm dimensions also show a 4% greater risk to *Pseudokirchneriella subcapitata* than that of dissolved copper (Schamphelaere *et al*., 2003). This suggests nano-ceria particles as a function of size offers a greater risk to *Pseudokirchneriella subcapitata* than previously determined contaminants.

Oxidation of ceria NPs have been considered as being a cause for algal toxicity observed during previous nanoecotoxicological tests. With 6% Ce^{3+} found in 6 nm particles and 1 % Ce^{3+} found in 10 nm particles, (Amin *et al*., 2011) there is reason to believe the proportion of Ce^{3+} has a profound effect on toxicity. Using cerium nitrate (III) as a positive control for Ce^{3+} tests, EC_{50} values of 0.3 mg/L were obtained during work at CSIRO (Table 6-4) with EC_{50} values of 0.15 mg/L previously being determined by Rogers *et al*., (2009). Cerium nitrate results therefore show less toxic effect on the growth of *P. subcapitata* compared to results from synthesized nano-ceria particles <10 nm. This indicates that there are further effects attributed to the observed size dependant toxicity than the effect of dissolved ceria ions alone.

6.5.3.7 Effects of PVP on *Pseudokirchneriella subcapitata* toxicity

Although synthesised nano-ceria particles used in this independent study were washed three times in acetone before exposure assessments, (Chapter 4) there remains the possibility that residual PVP may remain in solution which may be attributed to the toxicity observed. Surface modifiers on e.g. gold NPs have been found to significantly increase cellular toxicity (Connor *et al.*, 2005). To eliminate the possibility of the PVP coating being the potential cause of observed toxicity, PVP solutions were prepared without cerium nitrate addition, during the synthesis process and used for comparative toxicity tests. Pure PVP samples were used as stock solutions and diluted to the same concentrations as the nano-ceria stock solutions of particles, to obtain a growth curve representing

maximum possible PVP concentration in solution. The growth curves associated with these PVP concentrations are given in Figure 6-9 and were conducted at CSIRO laboratories during training.

The growth curves of the tests for PVP toxicity, across the dilutions made, were found to have no apparent toxic effect towards *Pseudokirchneriella subcapitata* compared to the control samples, at the highest solution concentration of PVP possibly present in the samples of synthesized nano-ceria particles prepared. Equivalent results from PVP toxicity tests have also been found [Elechiguerra *et al*., (2005); Benhra *et al*., (1997)] during *P. subcapitata* exposures.

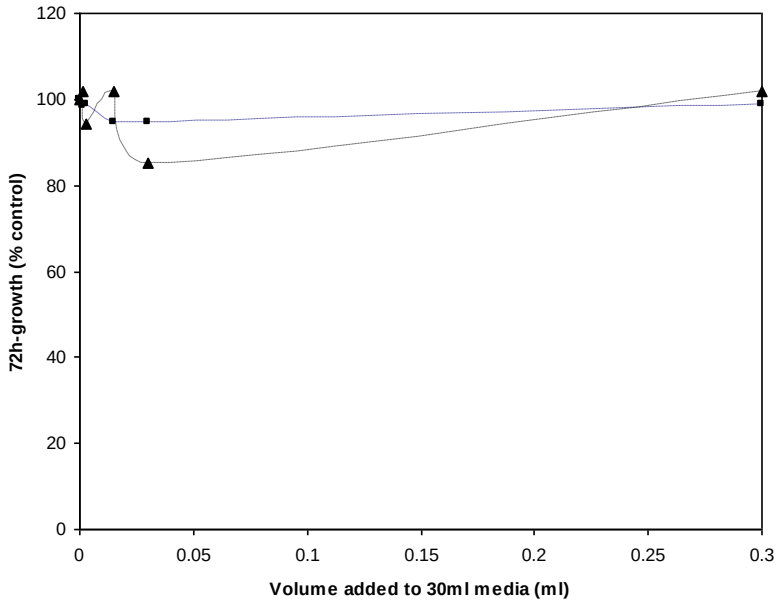

Figure 6-9 *P. subcapitata* growth inhibition curve using PVP
10K PVP chain (black square) and 360 PVP chain lengths (black triangle) at the same concentration of synthesized nano-ceria stock solutions, compared to the control.

6.5.3.8 Synthesized nano-ceria particle exposure characterisations

To further understand any associated mechanisms of nano-ceria particle toxicity, the physicochemical characterisation of the particles under the test conditions, in the presence and absence of *P. subcapitata*, was also carried out. Under exposure conditions, a range of size distributions were undertaken using DLS and TEM analysis at the associated EC_{50} values of each particle size, (Table 6-7) along with maximum UV-visible absorption wavelengths and ζ measurements.

Table 6-7 Synthesized nano-ceria particle characterisations during exposures
Particle characterisations at concentrations representing EC_{50} dose under exposure conditions to *Pseudokirchneriella subcapitata* after 72 h in the presence (blue) and absence (black) of *P. subcapitata*.

Concentration of particles measured at EC_{50} doses (mg/L)	Determined nano-ceria particle size (nm)	d_H (nm)		ζ (mV)		Maximum UV-visible absorption wavelength (nm)	
	Exposure time (h)	0	72	0	72	0	72
0.0013	5	2.5±2.5 4.5±1.9	4.3±1.7 4.1±13.3	-32.7±9.0 -19.8±1.2	-35.2±3.1 -7.4±1.2	260/294 259/296	260/298 261/297
0.14	7	12.6±2.0 9.0±3.4	9.9±2.1 13.3±2.3	-18.1±7.6 -12.1±0.5	-31.5±4.8 -4.1±1.7	263 261	259/294 259/291
0.35	10	13.6±1.3 10.2±4.0	18.8±5.2 9.4±4.9	-4.5±4.4 -1.2±3.1	-3.1±0.8 -1.5±0.6	261/293 259/293	260/295 260/297
0.8	35	23.9±9.4 26.1±2.2	22.5±10.5 22.1±7.8	-12.9±8.9 -4.4±2.0	-19.2±6.8 -1.9±1.5	265 265	262/290 261/291

6.5.3.8.1 Dynamic light scattering

From d_H results (Z-ave) using DLS analysis (Figure A37) it is evident that synthiezed nano-ceria particles do not significantly change ($p>0.05$) in diameter during the test period, either in the presence or absence of algae at the associated EC_{50} values. This suggests the particles are stable under the 72 h *P. subcapitata* toxicity test conditions. This also suggests that *P. subcapitata* cells

do not have any significant effect on the particle diameters which could otherwise be attributed to changes in solution pH, algal exudates (Hartman *et al*., 2010) or removal of phosphates from solution by algae cellular processes (Vanderborough and Buyers, 1974).

6.5.3.8.2 Zeta potential

All nano-ceria particle dimensions at associated EC_{50} measured had negative ζ (Figure A37) suggesting no charge related interactions are applicable with *P. subcapitata* cells. The ζ did not significantly alter ($p<0.05$) between the onset (0 h), to the end (72 h), of the exposure period in the presence or absence of *P. subcapitata* across all particle sizes measured. The ζ measurements for all nano-ceria particle sizes become more negatively charged in samples containing *P. subcapitata* cells compared with samples without. This result would infer a direct effect of *P. subcapitata* cell present in solution. All samples, however, were syringe filtered to 0.45 µm prior to analysis, to eliminate *P. subcapitata* cell signal interferences. The associated charge decrease over time maybe a direct relation with negatively charged *P. subcapitata* exudates being produced in solution (Pan *et al*., 1998). The increased control growth rate obtained over 72 h can be directly attributed to the further negative charge in ζ measured.

6.5.3.8.3 UV-Visible spectroscopy

At the onset of exposure (Table 6-7) the *P. subcapitata* cells do not appear to have any effect on the UV-visible absorption maximum peak intensity of nano-

ceria particles measured (Figure A38). The nano-ceria particles both in the presence and absence of *P. subcapitata* also increase in broadening the secondary UV-visible absorption peak shoulder observed at ~290 nm, throughout the test period (Figure A39-41). This may suggest an increase in Ce^{4+} ions (Roa and Sahu, 2001) over 72 h across all particle sizes in *P. subcapitata* test media both in the presence and absence of *P. subcapitata*.

6.5.3.8.4 ICP-MS

At EC_{50} doses, ICP-MS analysis shows lower Ce concentration detected for all synthesized ceria particle dimensions in *P. subcapitata* test media with *P. subcapitata* compared to Ce concentration in media alone (Table 6-8). ICP-MS values also indicate some reduced dissolution of ceria particles under the exposure conditions after 72 h shown by a reduction in Ce concentration after 72 h in the presence and absence of *P. subcapitata*.

Table 6-8 ICP-MS analysis of synthesized nano-ceria during exposures
Synthesized nano-ceria particle ICP-MS measurements in algae media at onset (0 h) and end (72 h) of exposure assessments, at EC_{50} doses, in the presence and absence of algae

Nano-ceria Particles	0 h		72 h		Ce loss after 72 h	Ce loss after 72 h
Size (nm)	With algae Ce(ppb)	No algae Ce(ppb)	With algae Ce(ppb)	No algae Ce(ppb)	With algae (%)	No algae (%)
5	1.08	4.09	0.32	0.86	30	21
7	0.87	0.96	0.52	0.61	60	64
10	62.3	46.6	42.9	39.2	69	84
35	68.2	70.8	13.2	4.5	19	6

Up to 13% more Ce is lost from the *P. subcapitata* test media in samples with 5 nm and 35 nm synthesized nano-ceria particles in the presence of *P. subcapitata* (30 and 19 % respectively) compared to without *P. subcapitata*, (21

and 6% respectively) over the 72 h exposure period. More than double Ce is lost in 7 nm and 10 nm ceria particle dispersions (60 and 69% respectively) with *P. subcapitata* after 72 h exposures compared to equivalent 5 nm and 35 nm particle dispersions. The reliability of the ICP-MS data however is somewhat questionable and can range in reproducibility of up to 10% observed from previous measurements made.

6.5.3.8.5 TEM

Nano-ceria samples, in the absence of *P. subcapitata*, were further investigated using TEM imagery under the same 72 h test conditions, using the drop method for TEM grid preparation (Figure 6-10) at relevant EC_{50} values. TEM images were supported by Dr Ruth Merrifield, University of Birmingham. Although there are a small number of particles present in these sample images, there is evidence to suggest 7 nm, 10 nm and 35 nm ceria particles may aggregate in the *P. subcapitata* media following 72 h exposure conditions. Although the TEM suggests some aggregation of the particles in *P. subcapitata* test media, there is no further evidence to support this from UV-Visible absorption, DLS or electrophoretic measurements conducted, which may be due to the low sensitivity of such measurement methods.

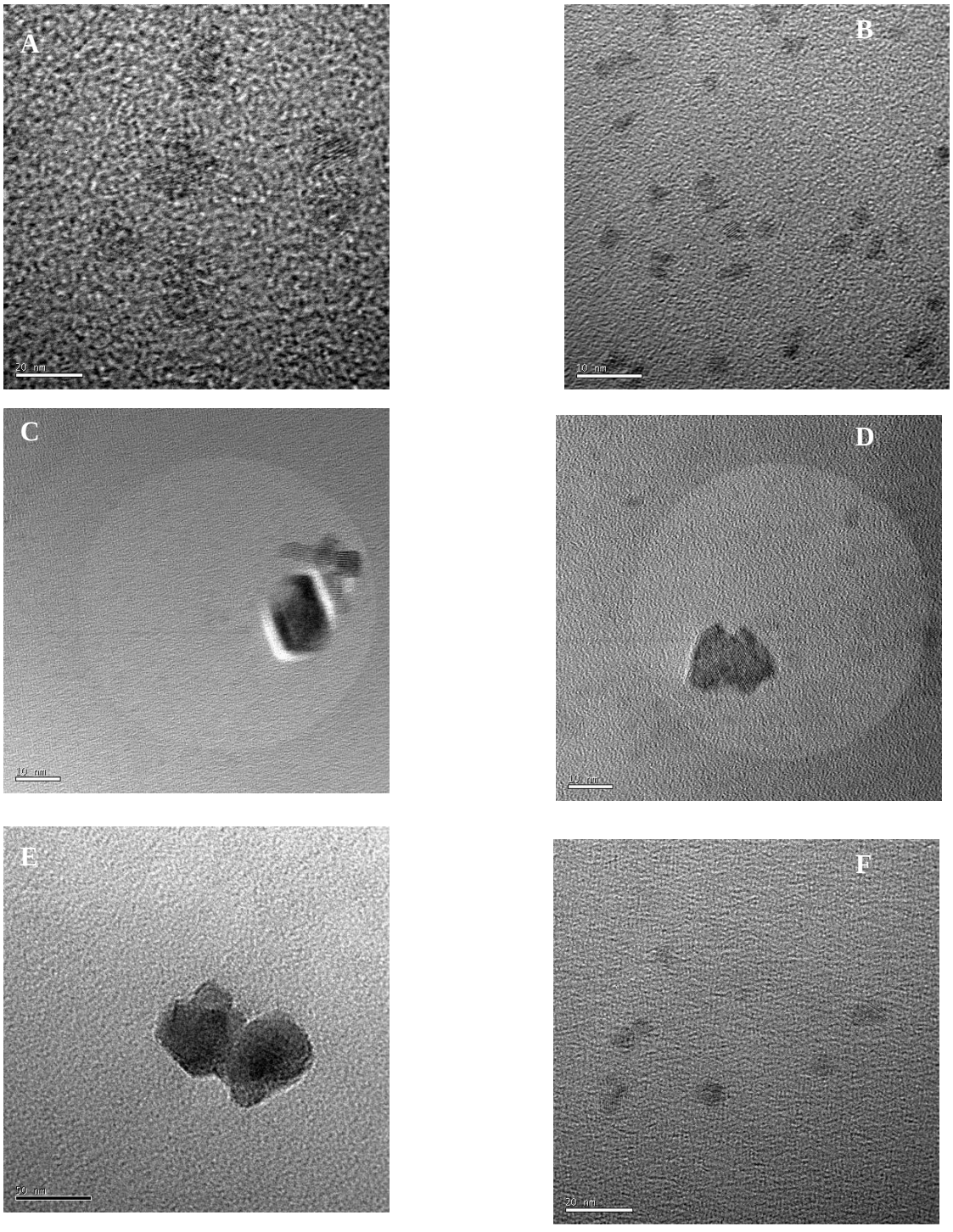

Figure 6-10 TEM images of synthesized nano-ceria particles after 0 h exposure
TEM images of nano-ceria particles on 0 h of exposure in the absence of algae. a-b) 5 nm ceria particles, scale bar 20 nm and 10 nm respectivley; c-d). 7 nm ceria particles, scale bar 10 nm; e) 10 nm ceria particles, scale bar 10 nm; f) 35 nm ceria particles, scale bar 20 nm.

Alternatively, the TEM images of agglomerates may be artefacts of drying during the TEM grid preparation process.

6.5.3.8.6 AFM

To investigate external *P. subcapitata* cell conditions during exposure assessments, AFM analysis and imagery was conduced. Compared with control cells (Figure 6-11a), AFM images of commercial nano-ceria particle exposures to *P. subcapitata* at 0.5 mg/L (Figure 6-11b-c) show similar *P. subcapitata* cell morphology after 1 h exposure. Further analysis show *P. subcapitata* cells under these conditions are surrounded by a material, re-shaping the topography measured after 72 h exposures. Although there is no confirmation of particle internalisation or chemical analysis by AFM images it is evident that under exposures to commercial nano-ceria[c], compared against the control samples, the *P. subcapitata* cells are being coated by a material, hypothesised as being the ceria nano-powders. This apparent coating of commercial nano-ceria however does not reduce *P. subcapitata* growth rates from this sample, as shown by the growth curves obtained. Further AFM images investigating *P. subcapitata* cell morphology to the exposed synthesized 5 nm and 35 nm ceria particles at EC_{50} values are shown in Figures 6-12 to 6-13 respectively**.** The direct interpretation of these images is that the 5 nm particle treatments at EC_{50} concentrations created ‘holes’ or ‘pits’ in the cell wall, thus potentially reducing the cells’ ability to function naturally. The term ‘pits’ refers to the indentations observed on the

surface of the treated algal cells, which show a greater surface depression compared against that observed from the control algal cell sample.

There appears to be agglomeration of cells (Figure 6-12a) and the cells appear to collapse (Figure 6-12b-c). In some cases, cells exposed to 5 nm particles also seem to curl around themselves (Figure 6-12d). After only 48 h exposure to 5 nm particles, the typical crescent shape of some *P. subcapitata* cells become more spherical in shape (Figure A42). The 'pitted' cell shows a significantly changed cellular profile, increased roughness and increased measured topography suggests greater SA compared to the control sample. The increase in topography can be attributed to some algal cells lying on top of adjacent cells or by a cell covering itself as it curls to form a spherical shape. The curling of *P. subcapitata* cells has also been observed using bright-field and fluorescence microscopy by Bouldin *et al*., (2008) following a 96 h quantum dot exposure to *P. subcapitata*. Such changes in the structural integrity of cells have been also been observed by Brunner *et al*., (2006) where human mesothelioma and a rodent fibroblast cells were found to change their shape in response to 7.5 mg/L crocidolite asbestos particles producing a nearly spherical shape gaining volume and loosing adhesion to the cell culture plate. After 72 h exposures to 35 nm particles, at EC_{50} values, pitting of the algal cells and swollen centres are observed (Figure 6-13a).

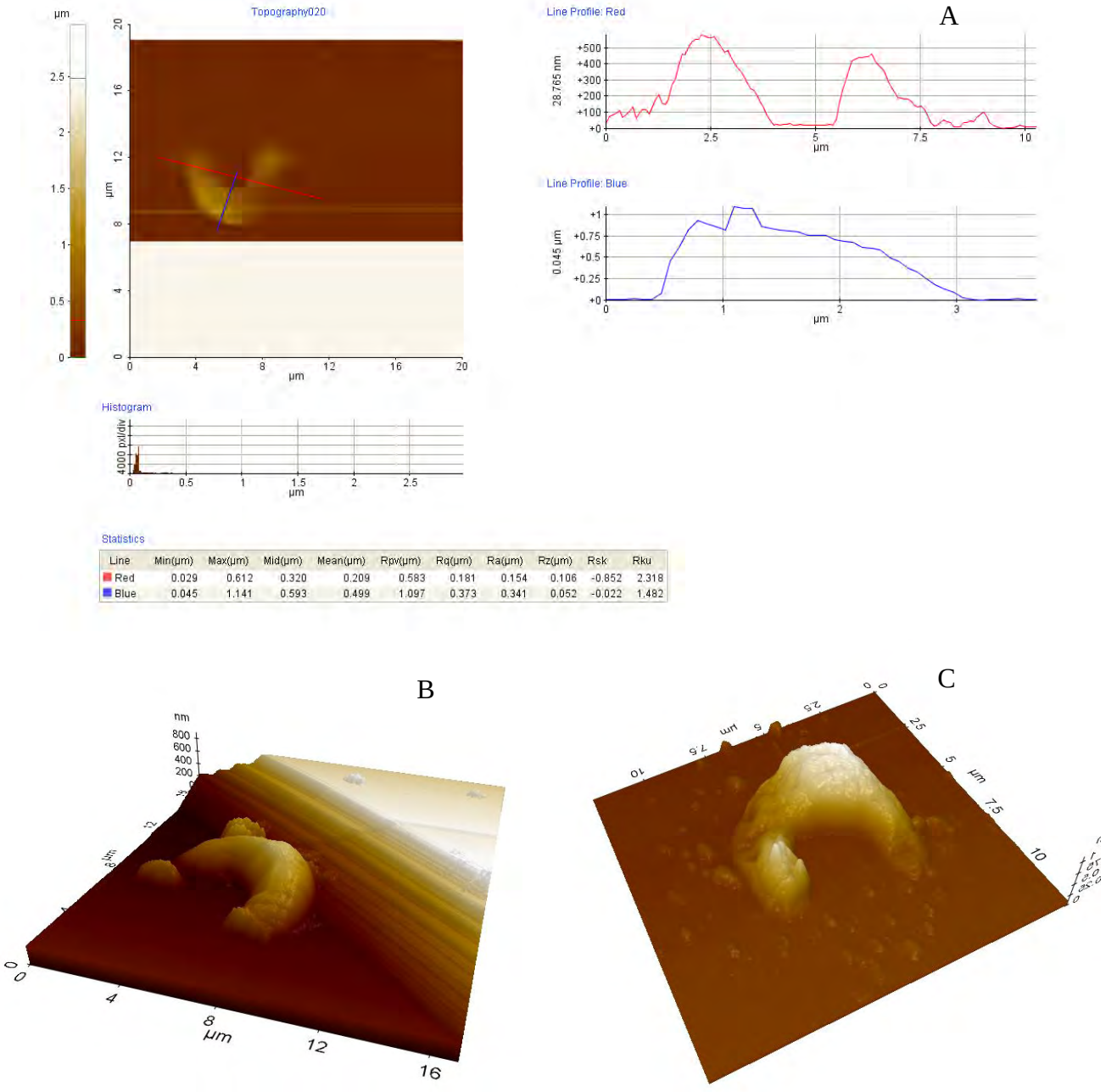

Line	Min(µm)	Max(µm)	Mid(µm)	Mean(µm)	Rpv(µm)	Rq(µm)	Ra(µm)	Rz(µm)	Rsk	Rku
Red	0.029	0.612	0.320	0.209	0.583	0.181	0.154	0.106	-0.852	2.318
Blue	0.045	1.141	0.593	0.499	1.097	0.373	0.341	0.052	-0.022	1.482

Figure 6-11 AFM images of *P. subcapitata* cells
A). AFM analysis showing typical dimensions of a control *P. subcapitata* cell after 1 h. B). *P. subcapitata* cell after 1h exposure to 0.5 mg/L commercial nano-ceria[c]. C). *P. subcapitata* cell after 72 h exposure to 0.5 mg/L commercial nano-ceria[c] under test conditions.

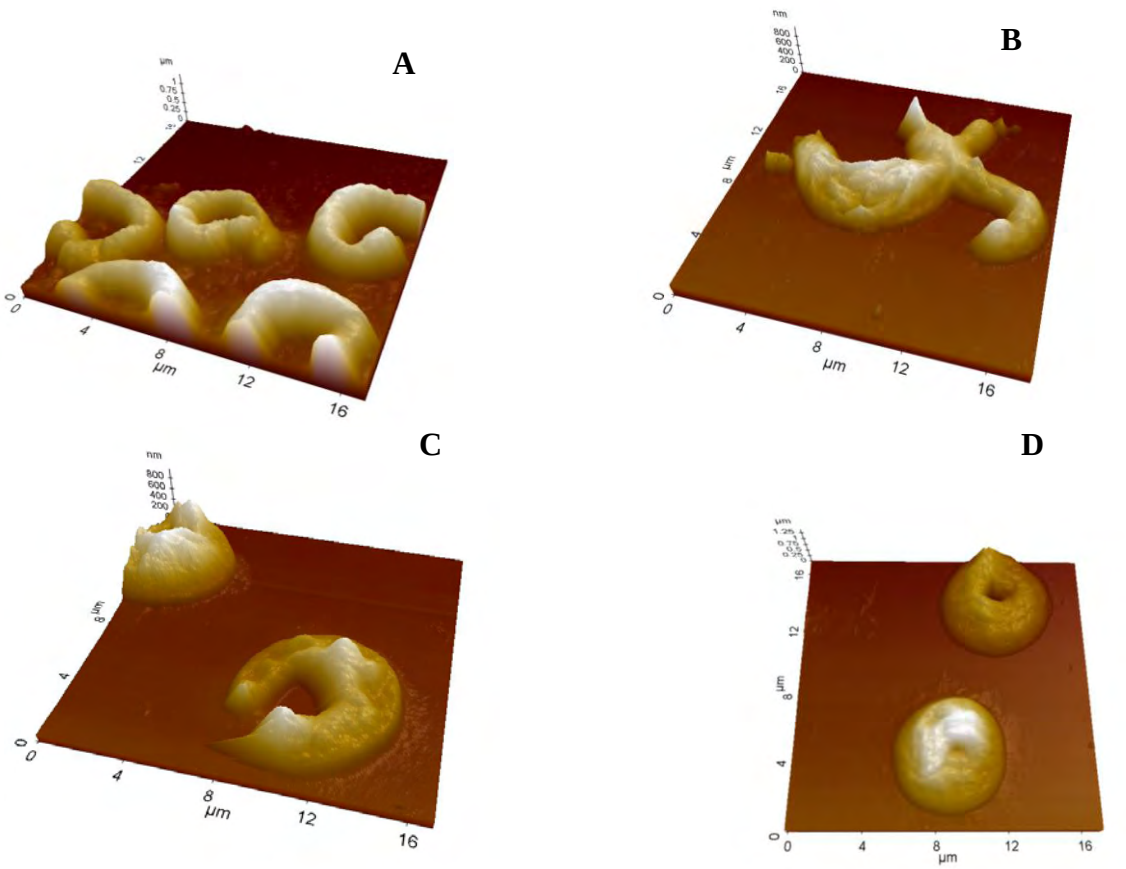

Figure 6-12 AFM images of *P. subcapitata* cells exposed to 5 nm ceria particles
a) Image after 30 min exposure at EC_{50} values; b) Image after 1 h exposure at EC_{50} values;. c) After 48 h at EC_{20} values showing pitted features; d) after 48 h at EC_{20} values showing cells curled over themselves.

Cell densities calculated suggest *P. subcapitata* cells can still reproduce, albeit at a lower rate compared to control samples suggesting this observation maybe due to the cells reproduction processes. This is shown by possible autospore evolution from the one cells' lateral side (Figure 6-13b) but which could also be particles accumulating in that area as this AFM analysis used does not allow recognition of chemical forms. The observed 'pits' may also be produced by the AFM cantilever, during analysis. As the cell membrane is free moving and much softer than the surrounding structure,

when the AFM tip applies force, a crack in the cell wall may bend easily causing the appearance of a depressed area (Stoimenov *et al*., 2002). However, as these structures are not observed in control samples, it is reasonable to suggest such artefacts from AFM imaging of these cells is negligible and in this case the observed images can be attributed to direct effects from nano-ceria exposure.

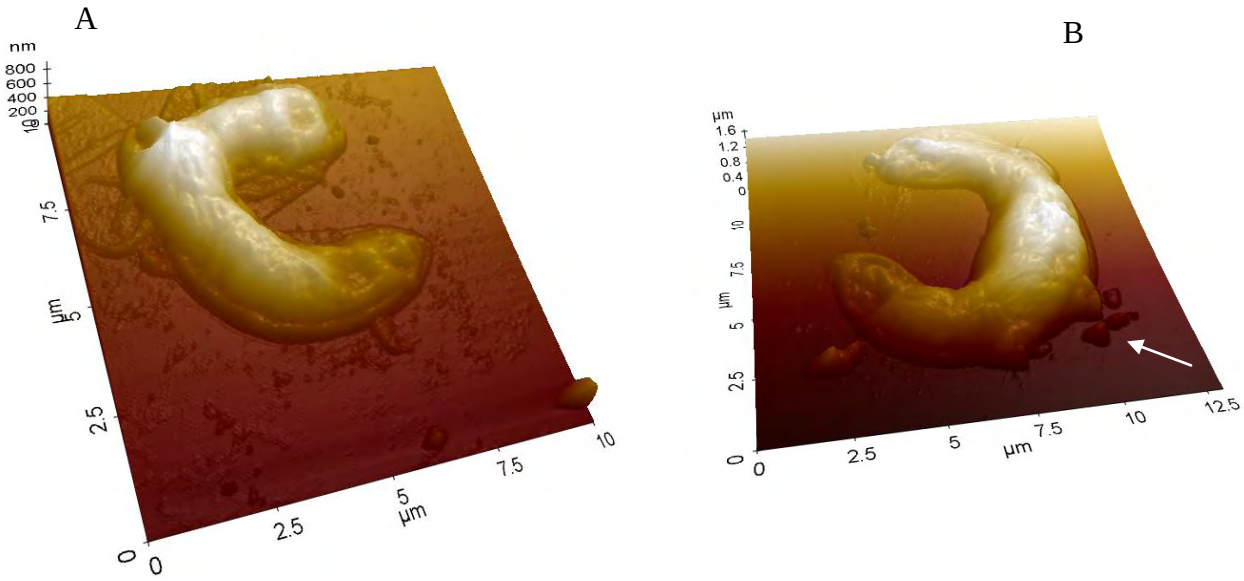

Figure 6-13 AFM images of *P. subcapitata* cells exposed to 35 nm ceria particles after 72 h exposure at EC_{50} doses.
Arrow indicating possible autospore formation or particle aggregation after 72 h at EC_{50} doses.

The 'pits' of the algal cells imaged can be quantified by direct observation of the treated or exposed algal cell samples compared against the control algal cell AFM images obtained. The number of 'pits' were counted by eye from the control; commercial nano-ceria; 5 nm and 35 nm synthesized nano-ceria particle exposure AFM images taken and are offered in Table 6.9. The 'depression pits' are those

observed as areas showing deeper surface indentations compared to those observed in the control algal sample images.

Table 6-9 Counted observed 'pits' from AFM images
AFM images used were from the control and exposed algal cells. Counted 'depressions' are those observed as areas more profound than the surface indentations observed with the control algal images.

Sample	Exposure (min)	Exposure concentration (mgL)	Counted 'Pit' number	Counted 'depression' number	AFM Images counted	Number algae cells counted within images taken
Control	60	0	11	0	1	1
Commercial	60	0.5	-75	0	1	1
Commercial	4320	0.5	37	33	1	1
5 nm	30	EC50	62.4 ± 14	3.4 ± 3.2	1	5
5 nm	60	EC50	41 ± 12.7	40 ± 12.7	1	2
35 nm	2880	EC50	21 ± 4.2	80.5 ± 7.8	2	2
5 nm	2880	EC20	70 ± 47.6	36 ± 42.8	2	4

Commercial samples refer to nano-ceria[c] exposures.
Negative counted 'pit' value from commercial nano-ceria[c] AFM image represents increases in surface topography. This suggests some material, considered the commercial powders, is coating the algal surface, compared against the control sample.

The additional surfaces observed with the commercial nano-ceria particle exposures are thought to be due to material coating the algal cell, shown on the Table 6.3 as a negative counted 'pits'. As the exposure time increases, in either the commercial or 5 nm synthesized nano-ceria particle exposures, the number of depressions counted from the AFM images obtained, also increases. There are more depressions and pits counted with 5 nm synthesized ceria particles after 60 min exposure compared against the commercial nano-ceria particle exposures after 72 h. This suggests greater cellular surface effects are occurring after a short exposure period to synthesized nano-ceria particles compared against commercial nano-ceria particle exposures.

The number of pits and depressions being counted are limited by the number of AFM images taken and also by the access available to observe the complete algal surface having been imaged, reducing the accuracy of this procedure. Also, the counts of 'pits' or surface coated material being viewed is also bias in the manor of counting by the individual, where the eye is known to be drawn to the more discernable regions. The counts can also only be as good as the images and any artefacts from the AFM imagery may account for a greater number of pit or depression counts taken. To improve this quantification, a greater number of images should be taken per sample being investigated and the SA of the algal cells should be calculated from a greater surface image where possible.

6.5.3.9 Summary

Following a range of particle characterisation assessments, it is evident that synthesized nano-ceria particles in the range 5-35 nm in dimension do not alter significantly in the presence or absence of *P. subcapitata* after 72 h exposure period, under test conditions. AFM images offer evidence of cellular interactions directly attributed to synthesized nano-ceria particle exposures to *P. subcapitata*. Such interactions cause pitting and other morphological changes to the *P. subcapitata* cells.

6.5.4 Conclusion

Four nano-ceria particle dimensions were prepared by synthesizing cerium nitrate and PVP to produce calculated mean particle dimensions of 5, 7, 10 and 35 nm as determined by DLS and TEM analysis. These particles were extensively characterised under three conditions: as made; in OECD test media and under appropriate test conditions in the presence and absence of *P. subcapitata*. These particles were exposed to *P. subcapitata* using OECD 201, (1984) tests guidelines. Evidence of a size dependent toxicity of *P. subcapitata* was observed under exposures to synthesized ceria particles between 5 nm and 35 nm dimensions. Physicochemical characterisation results showed all synthesized nano-ceria particles do not significantly change in the presence or absence of *P. subcapitata* throughout the exposure period and conditions. This suggests the toxicity observed is more likely to be directly attributed to the particles and not due to aggregation or surface particle changes associated with increases in media electrolyte solutions or exudates from *P. subcapitata* cells. Morphological changes of *P. subcapitata* cells were observed through AFM imagery indicate a 'pitting' of the cells, possibly caused by cellular interactions of the synthesized nano-ceria particles. The EC_{50} value for 5 nm particles was <0.001 mg/L, which is more than a factor of 10 below nano-ceria concentrations currently predicted in the environment from its use as a diesel additive (Prospect, 2010). This highlights a real effect which could be met if nano-ceria particles <7 nm diameters are released into the environment at concentrations predicted at <1 mg/L by Müller, (2007).

6.5.5 Future work

Many questions relating to the size-dependent toxicity of nano-ceria particles to *P. subcapitata* remain unresolved following this study. Further work to test particle size effects might include investigating the SSA effects of *P. subcapitata* cell membrane disruption by nano-ceria exposure or changes in osmotic pressure due to nano-ceria exposure. Measured glutathione levels, the production of malondialdehyde and the measured oxidation of NADH levels, would all have been useful parameters to have helped to identify potential mechanisms of reduced growth of algae cells observed, (Section 2.5.3.1.1.) and must be considered in future NP exposure assessments. Such parameters may help to identify stress factors associated with OS, which is considered the main cause of reduced algae cell growth during NP exposure assessments. Looking into the metabolomic changes from *P. subcapitata* cells as a direct result from the exposure to synthesized nano-ceria particles is also an important investigation to explore for future assessments.

Although this study would have benefitted from additional analyses to identify OS, which is considered the potential cause of NP toxicity, the opportunity to investigate and use the novel method of metabolomic analysis presented itself and was considered better use of time and resources at this point of this project. To further this study it was therefore proposed to help determine the mechanism of toxicity, attributed to synthesized nano-ceria particles as function of size, by using a novel method of metabolomic analysis, discussed in the following chapter.

7 Investigating *P. subcapitata* toxicity using a metabolomic approach

7.1 Chapter summary

With the ever increasing commercial use of ceria NPs, particularly of well defined shapes and dimensions, there is a greater threat of exposure, specifically in aquatic systems. Toxicological effects associated with nano-ceria maybe superficial, acute or chronic and may occur at the cellular level. It is therefore essential not only to understand the fate, behaviour and ecotoxicity of NP exposures but to understand the mechanism of nanotoxicity associated with aquatic biota. To date, no metabolic responses induced by NPs are so far understood (AshaRani *et al*., 2009). This chapter investigates the appropriate use and associated outcomes of metabolomic analysis using *P. subcapitata* as a test species, under previously determined toxic responses from synthesized nano-ceria particles as a function of size and dose. The metabolomic signals obtained indicated exposure of *P. subcapitata* to >EC_{50} values of 5 nm and 35 nm ceria particles contributed most to the separation of samples in the PCA scores plots, suggesting significant metabolic differences exist between control and exposure *P. subcapitata* cell samples. Although extraction methods are sensitive to cell density and temperature fluctuations, metabolomic analysis has huge potential in future environmental nanoecotoxicological applications using *P. subcapitata* as a test species, although further knowledge of the metabolic peak locations are required.

7.2 Chapter organisation

This chapter opens with the aims and objectives (Table 7-1) followed by an introduction to the topic and methods of metabolomic analysis used. The rationale of this work is largely underpinned by the hypotheses developed from the previous experimental conclusions made.

Table 7-1 Aims and objectives of Chapter 7

Aim
Identify and quantify the metabolomic responses of *Pseudokirchneriella subcapitata* exposed to synthesized nano-ceria particles.
Objectives
1. Develop appropriate methods for the quenching and extraction of metabolites from Pseudo*kirchneriella subcapitata*. 2. Provide preliminary evidence that metabolomic analysis will be appropriate for identifying cellular processes in *Pseudokirchneriella subcapitata* exposed to synthesized nano-ceria particles compared to control samples as a function of cell density. 3. Identify any significant variations in metabolomic signals obtained from *Pseudokirchneriella subcapitata* when exposed to nano-ceria particles as a function of size and dose. 4. Ascertain the use of metabolomics as a tool for environmental nanotoxicology analysis for future assessments.

Following some of the more recent literature on this topic, the experimental design and subsequent progress for this work is discussed. The results section encompasses the experimental design and is supported by appropriate discussions. Chapter 7 is brought to a close by a summary of the findings and evaluation of the work conducted.

A grant application to the NERC Biomolecular Analysis Facility – Birmingham Node, was successfully approved to allow this study to take place.

7.3 Introduction

To date, very little is known about the toxic effects associated with ceria NPs to aquatic biota, irrespective of the volume of published work related to this topic. Following previously derived data (Chapter 6) it is evident synthesized nano-ceria particles exhibit size-dependent toxicity to *Pseudokirchneriella subcapitata*. The reason for this apparent toxicity is still not established. Considerable effort is however, currently being invested in cellular, genomic and computational models to meet this need for toxicological effects of specific contaminants. Recently, 'Systems Biology' approaches (e.g. genomics and proteomics) have been widely applied in the toxicology research field and have provided valuable information in toxicology assessments. Among them is the novel approach of metabolomic analysis, which is a rapidly developing new discipline. This new approach was initiated for this study, to help ascertain the toxicity observed by nano-ceria particles as a function of size and dose, to *Pseudokirchneriella subcapitata*.

7.3.1 What is metabolomics?

Metabolomic analysis is a relatively new approach for quantitatively (Fiehn, 2002) assessing the interactions of living organisms with their environment (Viant *et al*., 2009). Metabolomic analysis measures the changes of an organism's phenotype. An organism's phenotype is the observed biochemical or physical characteristics of an

organism determined by its genetic and environmental influences. Under conditions of stress, like drought or disease, molecular changes will take place within a cell and essentially change the original phenotype measured. Metabolomic profiles therefore reflect the dynamic response of biochemical reactions to environmental, genetic or development signals as a valuable measure of how a living system adjusts to a changing environment (Bölling and Fiehn, 2005) and to understand the biology of an organism and its response to environmental stimuli (Roessner and Bowne, 2009).

7.3.1.1 Metabolism

Metabolism consists of hundreds of enzymatic reactions which change the concentrations of metabolites on a rapid timescale, (seconds). Figure 7-1 shows a representative metabolic pathway of energy, carbon and oxygen during photosynthesis and growth of an alga. All organisms possess similar metabolic pathways by which they synthesize and utilise certain essential compounds such as sugars, amino acids and lipids and the polymers derived from them e.g. polysaccharides, proteins and lipids, (Mann, 1987). This is termed primary metabolism and these compounds are classed as primary metabolites. Most organisms utilise other metabolic pathways which produce compounds that usually have no apparent utility. Such 'natural products' are termed secondary metabolites (Mann, 1987). These pathways are as much a product of genetic make-up of the organism as are the primary pathways, but they are only activated during particular stages of growth and development, or during periods of stress caused by nutritional limitation or microbial attack, (Mann, 1987). Secondary metabolite profiles may better reflect the

differentiation of species and their complex response to environmental factors and to other organisms (Roessner and Bowne, 2009).

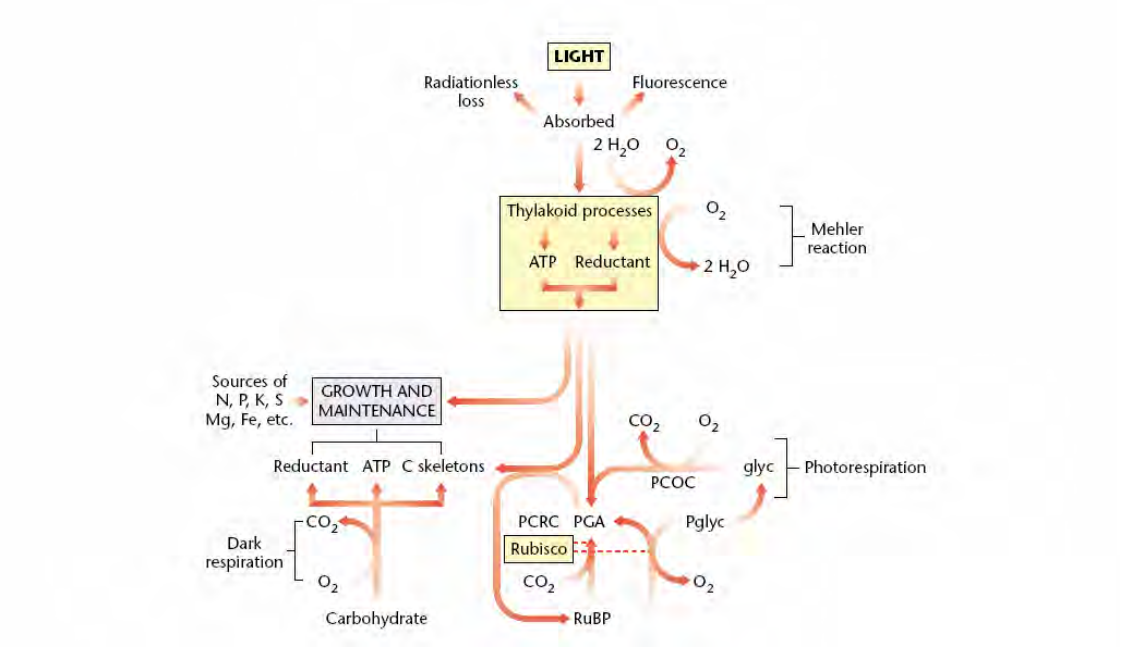

Figure 7-1 The pathways of energy, carbon and oxygen in photosynthesis of an alga.
Abbreviations: Glyc, glycolate; PCOC,photorespiratory carbon fixation cycle; PCRC, photosynthetic carbon reduction cycle; PGA, 3-phosphoglycerate; Pglyc, phosphoglycolate; RuBP, ribulose bisphosphate; Rubisco, ribulose bisphosphate carboxylase-oxygenase. Taken from Raven (2001).

7.3.1.2 Metabolites

Inside the cell, DNA is first transcribed to mRNA which is then translated into proteins. Proteins can catalyse reactions that act on, and give rise to, metabolites (Jamers *et al*., 2009). In the living organism chemical compounds are synthesized and degraded by means of a series of chemical reactions, each mediated by an enzyme (Mann, 1987). These processes are known collectively as metabolism, which comprise of catabolism (degradation) and anabolism (synthesis). The suite of secondary metabolites in an organism can be highly complex, and while similar compounds may be found in different organisms a vast number of compounds are very species-specific

(Roessner and Bowne, 2009). For most secondary metabolites, the exact functions in plants and algae still remain unknown. Carotenoids for example, are important metabolites which comprise a large and diverse group in plants and algae (Rao and Rao 2007). In photosynthetic organisms, carotenoids play important roles in many biological processes such as pigmentations and protection against oxidation (Liu *et al*., 2009). One drawback with measuring a metabolite as carotenoids is that there are more than 600 kinds which have so far been identified in nature (Britton *et al*., 2004).

7.3.2 Established 'omic approaches

Currently available 'omic analysis (Figure A43) provide high data content, offering a comprehensive description of nearly all components within the cell. While the genome gives rise to a blueprint to any living organism, the transcriptome is the result of the transcription factors responding to stimulus from upstream receptors (Khoo and Al-Rubeai, 2007). The proteome can be determined in a number of ways for example by measuring the corresponding levels of mRNA transcripts (Khoo and Al-Rubeai, 2007). Metabolite concentrations are determined by enzymes, which form a part of the proteome. Metabolomics is therefore a complementary method to transcriptomics and proteomic analysis (Khoo and Al-Rubeai, 2007; Viant *et al*., 2009). Despite the 'omics being relatively young technologies they have taken up a very important position in the biological and biomedical scientific landscape during the last decade, (Jamers *et al*., 2009).

7.3.3 Previous metabolomic studies

Metabolomics has successfully been applied across the environmental sciences, briefly sumerised in Table 7-2.

Table 7-2 Summary of previous environmental metablolomic analysis carried out

Test specie	Investigation	Reference
Algae	Stress physiology for studying nutrient depletion.	Bölling and Fiehn 2005
Fish	Aquatic toxicity analysis.	Viant *et al*., 2006a; 2006b Turner *et al*., 2007
Molluscs	Marine toxicity analysis.	Viant *et al*., 2003
Cereal plants	Determine novel mechanisms for adaption and tolerance to abiotic stresses like drought, salinity, frost and mineral deficiencies.	Roessner and Bowne (2009)
Plants	Distinguishing between silent plant phenotypes.	Weckwerth *et al*., 2004
Plants	Freezing tolerances.	Cook *et al.,* 2004
Plants	Temperature stresses.	Guy *et al*., 2008
Earthworms	Ecotoxicological work	Mckelvie *et al*., 2009

7.3.3.1 Metabolomic studies using algae

Light-induced synchronous cultures of microalgae are ideally suited to investigate cell cycle related metabolic events (Kluender *et al.,* 2008) as all individuals of the population are in an equivalent developmental stage and will reproduce within a similar period of time. Intra-specific variation at a given developmental stage is considered to be minimal in colonial populations of genetically identical algae (Kluender *et al*., 2008). *Pseudokirchneriella subcapitata* are remarkably robust in terms of substances affecting metabolism in organisms (Munkegaard *et al*., 2008) and have been used extensively in previous environmental nanoecotoxicological studies. Although *Pseudokirchneriella subcapitata* are genetically identical, they can reproduce at different stages in a given sample and this must be taken into consideration during

metabolomic analysis. Only a very small number of metabolomic studies on algae have been performed. Most algal studies have been focused on the quantification and identification of secondary metabolites with economical value in food science, pharmaceutical industry and public health, including fatty acids; steroids; carotenoids and polysaccharide investigations, (Jamers *et al*., 2009). Lee and Fiehn, (2008) and Boyle and Morgan (2009) used *Chlamydomonas reinhardtii* to study the control of metabolism. Their results showed that a number of responses can be stress related and/or plant-specific.

7.3.3.2 The need to use metabolomics for nanoecotoxicology studies

Karakoti *et al.,* (2008) found ceria NPs have a radical-savaging role under environmental conditions. Nano-ceria has also been found to suppress ROS production and induce cellular resistance to an exogenous source of OS by Xia *et al.,* (2008). In other studies, nano-ceria has also been found to exert toxicity through OS production *in vitro* to human bronchial epithelial cell, (Beas-2B), by Eom and Choi, (2009). Such contradictory reports make it difficult to interpret the actual mechanism by which nanotoxicity is induced. These data underscore the need to develop a more comprehensive understanding of toxicological pathways induced during NP exposures. Metabolomic analysis offers a potential to unlock such uncertainties offering it as a viable contribution for this independent study.

7.4 Experimental work

Metabolomics is a relatively new area of research incorporating techniques which require time to develop, particularly for metabolite quenching, extraction and analysis. A range of methods were therefore deployed particularly for the use of environmentally relevant *P. subcapitata* cell density *ca* 4 X 10^4 cell/ml (Rogers *et al*., 2010) used throughout this independent study. To obtain metabolomic data that correctly measures the amount of ceria to reflect the levels of intracellular metabolites, a multistep procedure was followed. This can conceptually be divided into three areas: cell quenching, cell homogenisation and metabolite extraction.

One aim for this work was to optimise the methods for metabolomic extraction of *Pseudokirchneriella subcapitata* cells for any future nanoecotoxicological studies. Extraction efficiencies have already been optimised for metabolomic profiling of a variety of matrices such as *E. coli* (Dwivedi *et al*., 2010), yeast cells (Villas-Boas *et al*., 2005) and blood plasma (Jiye *et al*., 2005) each yielding quite different protocols. These efforts document that sample preparation methods have to be carefully calculated and cannot be transferred from one field of application to the other without in-depth validation (Lee and Fiehn, 2008). Lee and Fiehn (2008) presented a method for algal metabolite profiling based on extractions from the *Chlamydomonas reinhardtii* using GC-TOF/MS. Kluender *et al*., (2008) presented a method for algal metabolite profiling using *Scenedesmus vacuolatus*. Improvements were made from these two diverse methods to facilitate using *P. subcapitata* and smaller culture volumes for this independent study.

7.4.1 Methods

7.4.1.1 Precellys tubes

Lee and Fiehn, (2008) found sample handling, reliability and metabolite extraction efficiency using glass beads was 30–40% lower than by metal ball grinding. Therefore, Precellys '24 hard tissue-grinding mix-lysing kit' tubes from Bertin Technologies were used for this study. The six steel balls present in each Precellys tube were removed and stored in the dark at -4^{O}C for the homogenisation process. The 1 ml volume of cold quenching solution (CQS) consisting of HPLC grade methanol (CH_3OH) and analytical grade water (H_2O_{agde}) at 70:30 ratio was added to each Precellys tube and stored at -80^{O}C for cell harvesting. The following methods are supported by Figures A44-45.

7.4.1.2 Cell harvest

The Precellys tubes with CQS were removed from -80^{O}C freezer and temperature maintained by placing them all on dry ice. Quenching of *P. subcapitata* metabolism was achieved by mixing 1 ml of a biological sample into one Precellys tube with the CQS. This was then centrifuged at 17,000 rcf at -9^{O}C for 3 min using a Sanyo Hawk 15/05 refrigerated centrifuge MSE. The supernatant was removed and the remaining algal cell sample pellet retained in the Precellys tube and stored at -80^{O}C for homogenisation.

7.4.1.3 Homogenisation

When using suspension cultures, mild quenching methods may unavoidably lead to some degree of metabolite leakage through the weakening of cell walls. In such cases, lyophilisation methods are employed to remove any remaining interstitial water, residual CQS and efficiently inhibit any enzymatic reaction during storage (Lee and Fiehn, 2008). During the homogenisation process, six to ten Precellys tubes containing the pellet algae samples were removed from the -80^{O}C freezer and temperature maintained on dry ice. Using a methanol-washed Hamilton syringe and 1 ml pipette, 500 µl CH_3OH and 200 µl H_2O_{agde} were added to each Precellys tube, respectively. Six cold-stored steel balls were added to the Precellys tube and subsequently homogenised using a Precellys Centrifuge Lysis and Homogeniser for 10 sec, twice. The homogenised sample was placed back onto dry ice for the metabolite extraction process.

7.4.1.4 Metabolite extraction

The homogenised sample was removed from the Precellys tube using a Pasteur pipette, into a pre-labelled 1.8 ml glass vial with plastic screw lid, placed on crushed ice. To the glass vial sample, 500 µl $CHCl_3$ and 250 µl H_2O_{agde} was added by use of a chloroform-washed Hamilton syringe and water rinsed 1 ml pipette, respectively. Each sample was vortex for 30 s and left in a polystyrene box of dry ice for 10 min. Centrifugation of these samples was performed at 4000 rpm at 4^{O}C for 10 min using a thermoelectric corporation Hercules Biofuge Primo R Centrifuge. The sample was

removed using forceps and left at room temperature for ten mins before metabolite fraction separation.

7.4.1.5 Metabolite separation

The polar layer was removed by using a methanol-washed Hamilton syringe and placed into a pre-labelled eppendorf. The non-polar (lipid) layer was subsequently removed by using a chloroform-rinsed Hamilton syringe. This sample was placed into a pre-labelled 1.8 ml glass vials with plastic screw lid. The eppendorf samples were dried using a Thermo SPD111V Speed Vac and RV14104 refrigerated vapour trap at 970 mbar. All samples were kept at -80^{O}C until MS analysis.

7.4.2 Analysis

All samples were analysed using a Fourier transform ion cyclotron resonance (FT-ICR) mass spectrometry was performed using an LTQ FT Ultra (Thermo Fisher Scientific, Bremen, Germany) equipped with a chip-based direct infusion nanoelectrospray ion source (Triversa, Advion Biosciences, Ithaca, NY) (Figure 7-2) by Dr. Ulf Sommer, University of Birmingham. Each dried sample had 50 µl spray solution added which consisted of 1:4 $CHCl_3$:H_2O_{agde} ratio with an additional 0.25%/vol formic acid (CH_2O_2) for positive ion analysis (non-polar samples were not measured). The sample was vortex for 10 s and subsequently centrifuged at 14000 rpm at 4^{O}C for 10 min to remove any particular matter. Each sample was analyzed in triplicate from a 96-well plate using the selected ion monitoring (SIM)-stitching method from m/z 70 to 590 in both ion modes.

Figure 7-2 HR-MS instrument used
A thermo LTQ FT ultra high resolution mass spectrometer used for metabolite profiling. All samples were conducted by Dr Ulf Sommer.

7.4.2.1 Putative identification of metabolites

Metabolites in the MS were identified using MI-Pack software (an in-house script), which provided putative identifications based upon the KEGG database. The initial peak lists were filtered for false negatives, artefact peaks and contaminants, conducted and interpreted by Dr. Ulf Sommer.

7.4.2.2 Principal component analysis plot

The principal component analysis (PCA) plots were prepared and interpreted by Dr. Ulf Sommer and used to identify the overall metabolic similarities and differences between the test samples and controls. Distances between the groups of samples give a measure of the overall differences between the metabolite signals, with greater distances corresponding to greater differences, obtained throughout different treatments (Bölling and Fiehn, 2005).

PCA was used initially to assess the overall metabolic differences between the sample groups in an unbiased manner, using the PLS_Toolbox (version 5.5.1, Eigenvector Research, Manson, WA, USA) within Matlab (version 7.8; The MathsWorks, Natick, MA, USA). Supervised multivariate analysis was performed using partial least squares discriminant analyses (PLS-DA), with internal cross-validation and permutation testing. The m/z signals with the largest weights (i.e. top-ranked) correspond to the metabolites that maximally discriminate the treatment groups. ANOVA were conducted using in-house R scripts in Excel (Microsoft). All contributions to MS and statistics were conducted by Dr Ulf Sommer.

7.5 Results and discussion

7.5.1 Hypothesis 1: Feasibility study

The metabolomic signals obtained during nano-ceria exposures to *P. subcapitata* will vary due to lower cell densities when compared against control samples.

7.5.1.1 Aim

The aim of this study was to investigate the potential use of metabolomic analysis for future environmental nanoecotoxicology assessments using *P. subcapitata* as a test subject and identify any changes in metabolomic profiles of *P. subcapitata* cells as a function of cell density.

7.5.1.2 Design

Six control samples (algal cells only) and six treated samples using 10 nm synthesized ceria particles at EC_{50} values, (*ca* 0.4 mg/L by ICP-MS) to *Pseudokirchneriella subcapitata* were prepared in 15 ml OECD test media. Initial *P. subcapitata* cell inoculations were *ca* 4 X 10^6 cell/ml and grown under the OECD 201, (1984) 72 h growth inhibition test guidelines. All samples were counted daily (24 h) using a haemocytometer and the final cell densities recorded. After 72 h, all *P. subcapitata* samples were harvested for metabolomic analysis and extracted the following day. Six further control samples were then prepared representing 'reduced control' (RC) *P. subcapitata* cell density samples at equivalent cell densities to those of the treated samples (*ca* 7 X 10^7 cell/ml).

7.5.1.3 Cell counts

The control cell counts are approximately double that obtained for the 10 nm ceria treated samples at expected EC_{50} values (Table 7-3). The RC cell counts are relative to that of the treated cell densities obtained, with one outlier.

Table 7-3 Cell counts after 72 h exposure

	Cell density counts (x 10^7 cell/ml)		
Sample	**Control**	**RC**	**Treated**
a	13.5	5.5	7
b	10	5.5	6
c	13.5	5	3
d	9	5	3
e	17.5	3	7.5
f	14.5	8	17.5[#]

[#] **Outlier**

7.5.1.4 Principal component analysis

The PCA plot (Figure 7-3) shows no significant difference in the metabolomic signals measured from the control and RC samples. This suggests cell density variance of up to half, does not infer metabolomic signals obtained from *Pseudokirchneriella subcapitata* under such growth conditions.

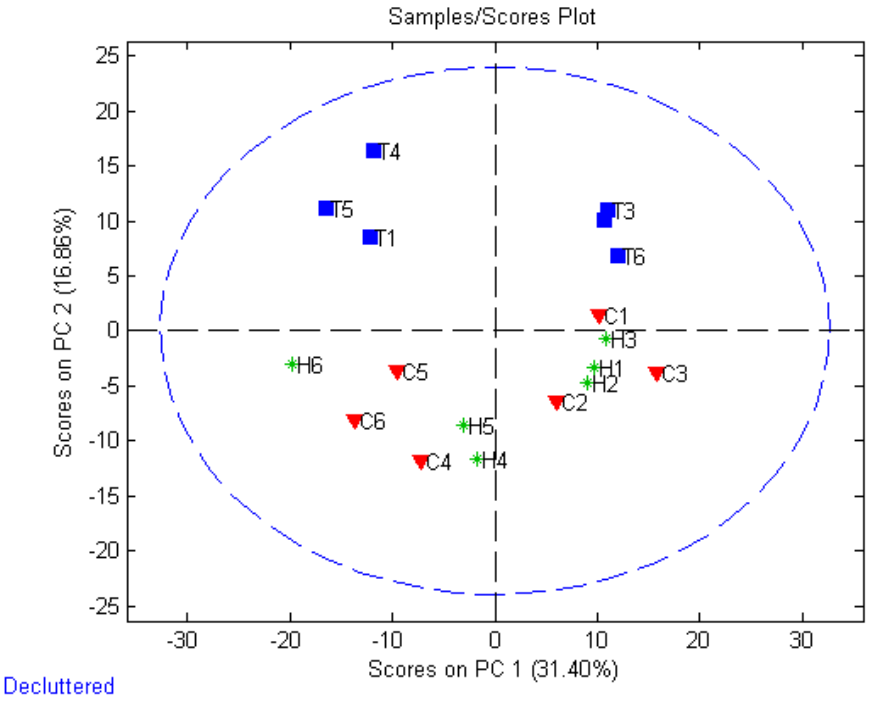

Figure 7-3 PCA plot for Hypothesis one
Treated cells; Control samples; Reduced control samples

7.5.1.5 Summary and evaluation

The hypothesis tested is rejected as *P. subcapitata* cell densities did not appear to significantly interfere with the metabolomic signal obtained from the control samples tested. There is evidence to suggest however, that the exposure of 10 nm synthesized ceria particles at EC_{50} values (c*a* 0.4 mg/L) to *P. subcapitata* results in a metabolic profile that is significantly different to the untreated *P. subcapitata* cell control samples.

Cell density does not have a significant effect of metabolic signals obtained. The no significant effect observed in metabolomic profiles by reduced cell density compared to control samples validates the use of metabolomic analysis for nanotoxicological investigations using *P. subcapitata* exposures to synthesized nano-ceria particles at EC_{50} values. This conclusion however is drawn from a limited scale experiment, (five repeats and three factors) with some signal variability obtained between biological repeats, as shown by the low clustering between repeated samples on the PCA plot. The results do however offer the use of *P. subcapitata* as a reliable species for nanoecotoxicological metabolomic analysis under these conditions. From this, the further investigation into the metabolomic profiles obtained from environmentally relevant *P. subcapitata* cell densities, exposed to synthesized nano-ceria particles compared to control samples, was considered plausible, at 10^6 cell/ml density.

7.5.2 Hypothesis 2: Effective concentration comparative study

P. subcapitata exposed to four synthesized nano-ceria particle dimensions, at previously obtained EC_{50} and EC_{20} values (Chapter 6), will produce comparable metabolomic signals, irrespective of the nano-ceria particle dimensions.

7.5.2.1 Aim

Identification of *P. subcapitata* toxicity is often assigned by EC_{50} and EC_{20} obtained after 72 h exposures compared against control samples. The aim of this work was to explore the metabolomic signals obtained during *Pseudokirchneriella subcapitata* exposures to four synthesized nano-ceria particle dimensions (5, 7, 10 and 35 nm

diameters) as a function of previously determined EC_{50} and EC_{20} dose, using OECD 201, (1984) guidelines.

7.5.2.2 Design

Each of the four determined nano-ceria particle sizes were prepared using five replicates at two concentrations, (EC_{50} and EC_{20}) (Table 7-4). In addition, five background samples (media only) along with five control samples (algae only) were also prepared. Cell density counts were conducted daily, using a haemocytometer. The investigation was then repeated 14 days later to demonstrate the reproducibility and reliability within the data set and associated analytical processes used. The cell sample replicates were inoculated with an approximate mean value *ca* 4 $X10^4$ cells/mL for Test 1 and an approximate mean value *ca* 3 $X10^4$ cells/mL for the repeated Test 2.

Table 7-4 Representative doses of each synthesized nano-ceria particle dimensions Based upon ICP-MS determination of stock solutions

	Mean synthesized ceria particle dimensions (nm)			
	5	7	10	35
EC_{50} (mg/L)	0.0027	0.13	0.37	0.45
EC_{20} (mg/L)	0.0009	0.044	0.18	0.15

7.5.2.3 Cell counts

P. subcapitata growth counts (Figure A46) and the 72 h growth inhibition results (Figure 7-4) compared against control samples for both tests as a function of dose was obtained. Test 1 growth rates showed cell densities outside that predicted for the

chosen mean EC_{50} and EC_{20} predictions. For Test 2, these concentrations were not changed in order to keep the investigation comparable. Test 2 growth rate therefore also show some variance (Figure A46) outside the predicted EC_{50} and EC_{20} values previously produced (Table 6-4). Although a size dependent toxicity was observed during this replicated study, (Figure 7-4) various EC_{50} values outside predicted values were obtained across all four nano-ceria particle size exposures (Figure A46).

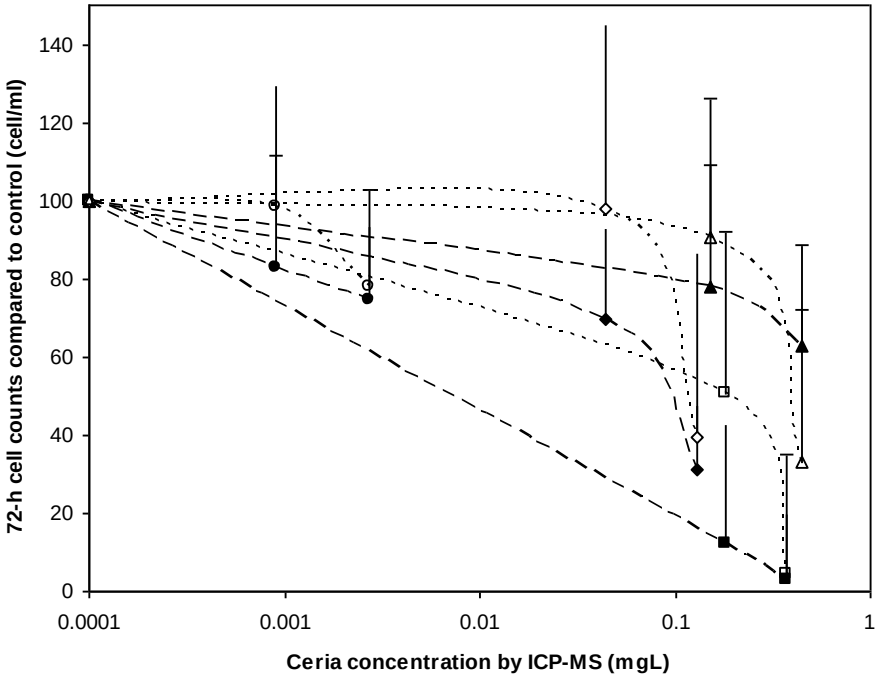

Figure 7-4 Growth inhibition semi-log plot for Hypothesis two
Growth curve of *Pseudokirchneriella subcapitata* after 72 h exposures to synthesized nano-ceria particles compared to the control, across two test periods.
Solid symbols represent Test 1, white symbols represent Test 2. Circles, 5 nm; diamond, 7 nm; square, 10 nm and triangle, 35 nm ceria particles. SD in growths shown by upper limits only.

The 5, 7 and 35 nm ceria particle dimensions at EC_{20} doses from Test 1 and 35 nm ceria particle dimensions at EC_{20} doses from Test 2 were within the predicated growth rate expected. There were also significant differences ($p<0.05$) in growth rates after

72 h for all *P. subcapitata* cell counts within biological repeats across both Test 1 and Test 2 shown by the large standard deviations obtained.

7.5.2.4 Principal component analysis

Figure 7-5 presents the PCA plot showing both Test 1 and Test 2 samples (labelled A and B respectively). From this plot, it is evident that the two tests are significantly different from each other, shown by the distinct separation from both tests. The quality control (QC) samples show little variance across the two test periods, eliminating the possibility that the results could be due to analytical drift from the MS.

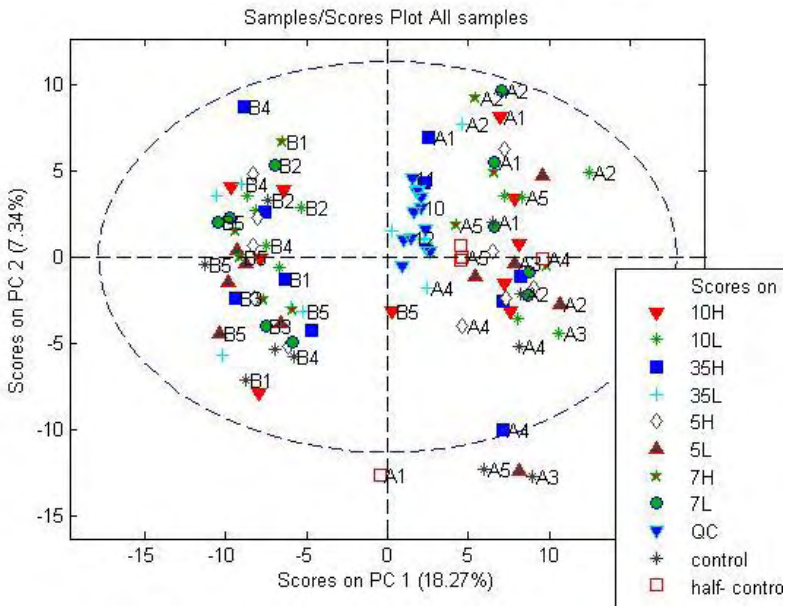

Figure 7-5 PCA plot testing Hypothesis two
The two repeated tests A and B.

Due to the variance in the growth curves across the two test periods, these metabolomic profiles are not comparable and appear as two separately conducted investigations. Unlike the conditions predicted from the testing of hypothesis 1, the

otherwise high precision of *Pseudokirchneriella subcapitata* growth rates were not equivalent during this investigation. This may be due to variance in starting cell densities, potential temperature variations, changes in light conditions and exposure preparations conducted during the tests. Test 1 (Figure A47) shows little grouping of the biological repeated samples, suggesting little difference in the overall metabolic profile/fingerprint compared to the controls. This high variation in metabolomic signals within biological repeats is observed in the cell counts, shown by the high standard deviations measured. Figure 7-6 represents the PCA plot obtained from each of the five biological repeated samples from each condition measured in Test 1. The PCA plot shows a drift in the data for Test 1, suggesting samples quenched or extracted in order show equivelant metablomic signals.

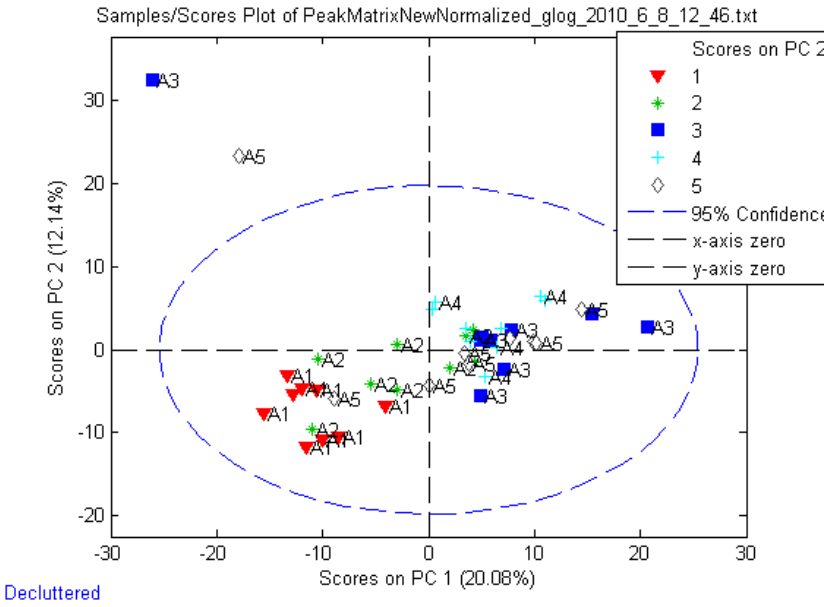

Figure 7-6 PCA plot of all extracted samples in Test 1 Hypothesis two
The variance across repeated samples (1-5) for each particle size (5 nm, 7 nm, 10 nm and 35 nm) across two doses represnting EC_{20} (L) and EC_{50} (H).

The PCA plot from Test 2 (Figure 7-7) also shows little clustering of biological repeated samples, suggesting variance within the same biological samples. This was observed in the cell density measurements obtained, shown by high error bars, as with Test 1. The Test 2 PCA plot show a pooling of the data (Figure A48) in order of extraction as observed with Test 1 (Figure 7-6). As the MS process was conducted in a block randomised order and conducted at the same time for Test 1 and Test 2, this ellimenates any pontential analytical error from the MS instrument. For both Test 1 and Test 2, the cell samples for each biological sample were harvested systematically and extracted chronologically. The drift of metabolomic signals in the PCA models therefore must be due to human error during the cell harvesting and extraction procedure.

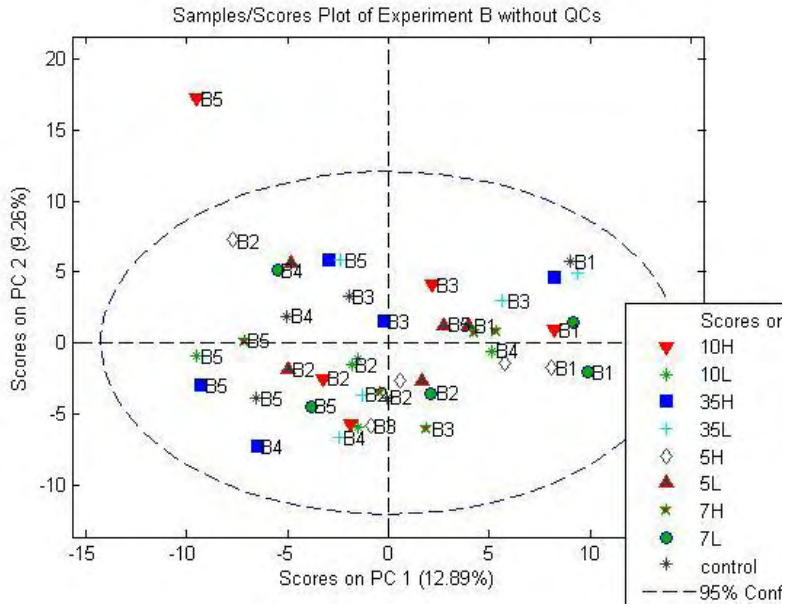

Figure 7-7 PCA plot of Test 2 Hypothesis two
The variance across repeated samples (1-5) for each particle size (5 nm, 7 nm, 10 nm and 35 nm) across two doses represnting EC_{20} (L) and EC_{50} (H).

7.5.2.5 5 nm ceria particles

From the PCA plots, the lack of clustering observed by the data points suggests *P. subcapitata* cells exposed to 5 nm synthesized ceria particles at either EC_{50} or EC_{20} shows no significant ($p>0.05$) metabolic differences compared to the control in either Test 1 (Figure 7-8a) or Test 2 (Figure 7-8b). From the cell counts (Figure A46) it is evident that the EC_{50} and the EC_{20} doses resulted in similar growth trends for both tests conducted. The scatter in the PCA plot would therefore suggest no significant variations in the metabolomic signals obtained due to little difference in toxicological change in the cell samples.

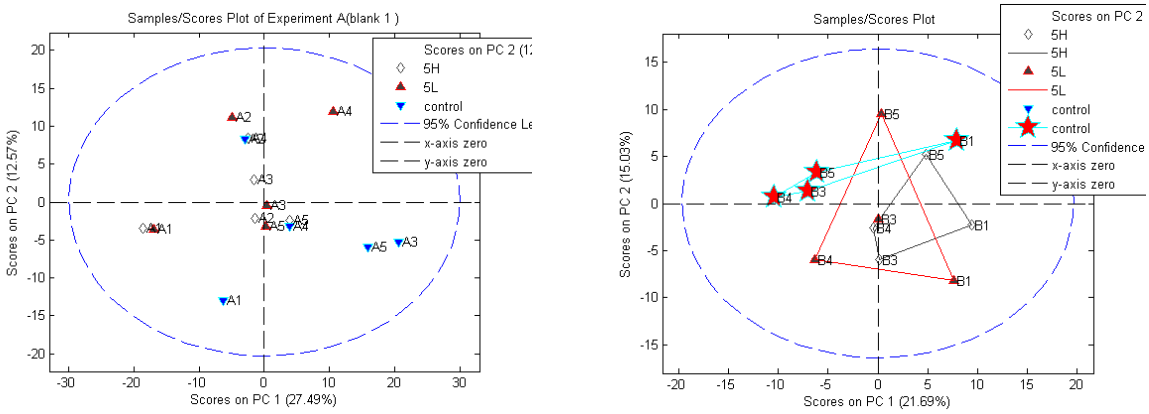

Figure 7-8 PCA plot of 5 nm ceria particles testing Hypothesis two.
EC_{50} values ($5nm_H$) and 5 nm EC_{20} values ($5nm_L$)
A) Test 1, B) Test 2.

7.5.2.6 7 nm ceria particles

There is a greater variance of metabolomic signals from 7 nm ceria exposures at EC_{50} doses in Test 1 (Figure 7-9a) compared against the control. These variations in metabolomic signals may be related to the variable cell counts obtained from the EC_{50}

(31.4 x 10^4 ± 16.5 x 10^4 cell/ml) doses compared to the EC_{20} (69.6 x 10^4 ± 23 x 10^4 cell/ml) dose cell density measurements. The variation of 7 nm ceria EC_{50} treatments in Test 1 is not as apparent in Test 2 (Figure 7-9b) where the clustering of both EC_{20} and EC_{50} metabolomic signals are close to the control. The 7 nm ceria particle PCA scores, in both Test 1 and Test 2, show a similar clustering around the centre of the PCA plot, although between the two tests, the clustering is in two directions. This suggests variation between the repeated tests.

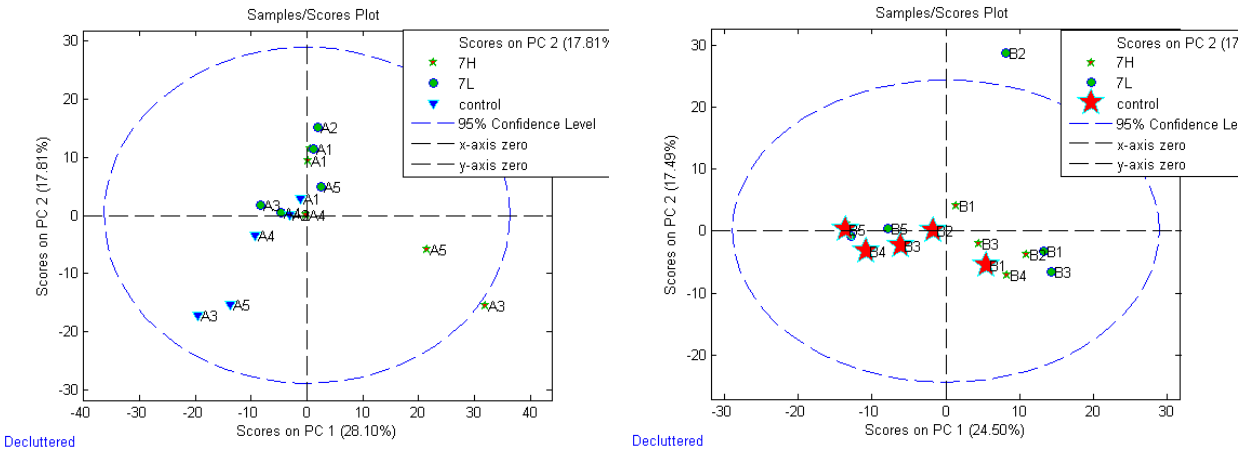

Figure 7-9 PCA plot of 7 nm testing Hypothesis two EC_{50} values ($7nm_H$) and 7 nm EC_{20} values ($7nm_L$) particles from A) Test 1, B) Test 2.

7.5.2.7 10 nm ceria particles

The 10 nm ceria particles show greater scatter across samples in Test 1 (Figure 7-10a) compared with controls than the clustering of samples compared against the controls observed in Test 2 (Figure 7-10b). The scattering of metabolomic signals from Test 1 PCA plots maybe due to the signals not being significantly variable between

EC_{50} and EC_{20} scores, as the cell counts were similar (EC_{50} 3.1 x 10^4 ± 16.8 x 10^4 cell/ml and EC_{20} 12.3 x 10^4 ± 30.6 x 10^4 cell/ml).

Test 2 metabolomic signals plotted show some trend across the PCA plot for both the 10 nm ceria doses compared against the controls. The cell densities for 10 nm ceria exposures for both Test 1 and Test 2 showed the most reduced cell count compared to any other particle dimensions measured. Also, the high cell count variability in Test 2 (EC_{50} 4.5 x 10^4 ± 30.5 x 10^4 cell/ml and EC_{20} 50.8 x 10^4 ± 47.1 x 10^4 cell/ml) would suggest some metabolomic impact, but this was not the case. As the cell counts were so low, it is possible that the metabolomic signals obtained were not from actual cells and possibly caused from background signals.

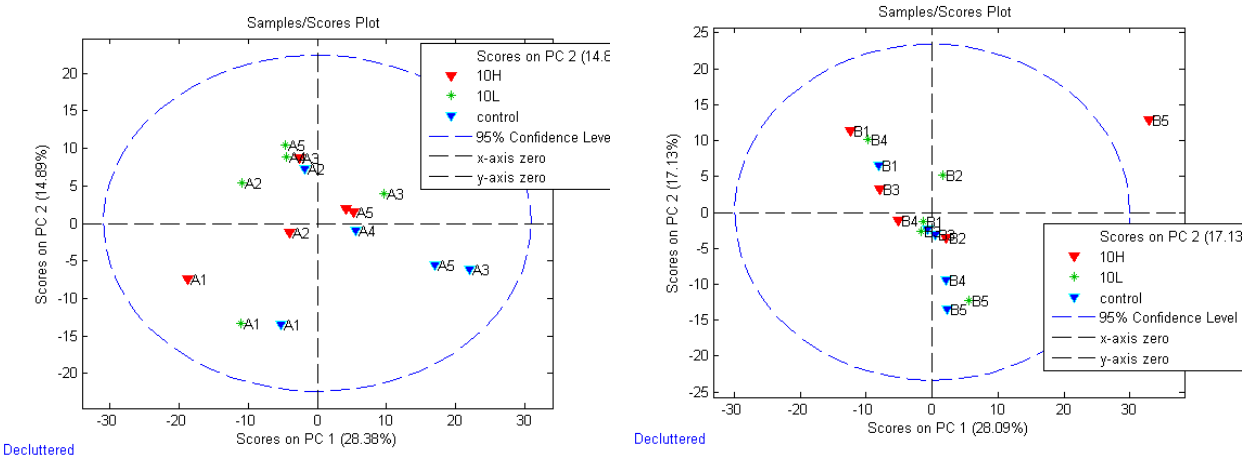

Figure 7-10 PCA plot of 10 nm testing Hypothesis two
10 nm at EC_{50} values ($10nm_H$) and 10 nm EC_{20} values ($10nm_L$)
A) Test 1. B) Test 2.

7.5.2.8 35 nm ceria particles

The metabolomic signals obtained from the 35 nm ceria particle exposures at the EC_{50} dose results from Test 1 show good reproducibility in the biological repeats compared to the 35 nm EC_{20} dose (Figure 7-11a). This reproducibility maybe due to the reduced variance observed in the cell counts with the EC_{50} dose ($63 \times 10^4 \pm 9.3 \times 10^4$ cell/ml) compared with the EC_{20} dose cell counts ($78 \times 10^4 \pm 31.3$ cell/ml) producing reduced clustering in the PCA plot. The PCA plot from Test 2 (Figure 7-11b) shows a closer clustering of metabolite scores plot obtained. Some outliers are observed in Test 2 which is an opposite trend to that found in Test 1, where more scatter in PCA scores are observed. This close resemblance to the control samples suggested by the PCA plot cannot be attributed to the cell counts which are significantly different and have a high variability (EC_{50} $33.1 \times 10^4 \pm 55.6$ cell/ml and EC_{20} $90.7 \times 10^4 \pm 35.6$cell/ml).

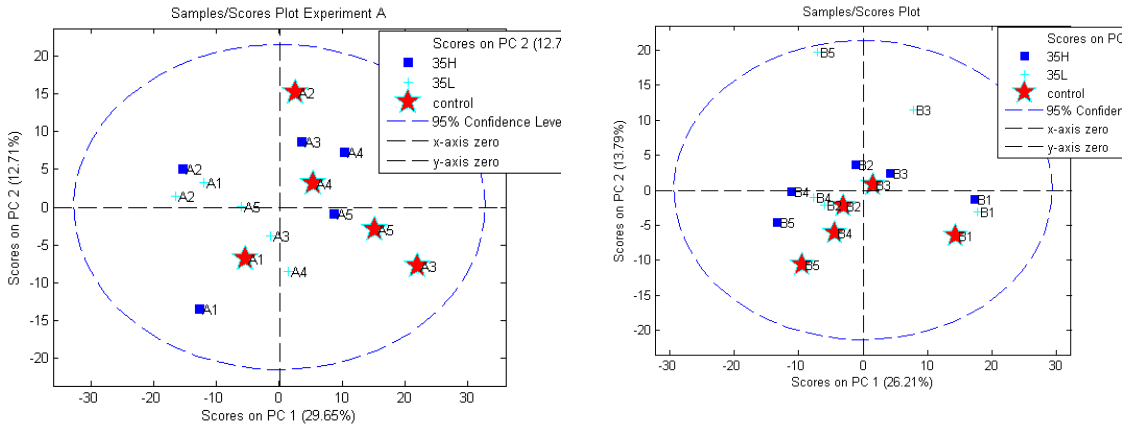

Figure 7-11 PCA plot of 35 nm ceria particles testing Hypothesis two
35 nm particles at EC_{50} values (35 nm_H) and 35 nm particles at EC_{20} values (35 nm_L)
A) Test 1, B) Test 2.

7.5.2.9 Summary and evaluation

The hypothesis tested "*P. subcapitata exposed to four synthesized nano-ceria particle dimensions, at previously obtained EC_{50} and EC_{20} values will produce comparable metabolomic signals, irrespective of the nano-ceria particle dimensions*" is rejected as EC_{50} concentrations across four synthesized nano-ceria particle dimensions did not produce equivalent metabolomic signals. The EC_{20} concentrations of four synthesized nano-ceria particles also did not produce equivalent metabolomic signals. The observations in metabolomic signals obtained from the PCA plots following synthesized nano-ceria particle exposures to *Pseudokirchneriella subcapitata* as a function of size and dose was found to incur many errors. The variability in repeated *P. subcapitata* cell growth rate for example, reduces the ability for an accurate cross-comparison across the metabolomic signals obtained. Reproducible growth rates from identically conducted *P. subcapitata* exposures are difficult to obtain and have been reported as being as variable as 25% by Mayer *et al*., (1998). Similarities in cell counts after 72 h exposures across the two tests for a range of particle sizes and doses also reduces the effectiveness to compare the tests, specifically across low numbers of biological repeats.

The test samples after 72 h may also contain dead algal cells, as well as algae cells at various stages of growth. Such factors complicate the metabolomic signals measured and must be taken into consideration during future studies. It is also evident from this work, that future extrapolation of algal cell samples must be conducted randomly to reduce the systematic error observed during this work. Although it would be

considered crucial to continue with and repeat this experimental design it was considered important to investigate whether the reduction of identified variables and cellular effects will aid in future nanoecotoxicity studies of this kind. Due to this and the time remaining for the study, a third and final hypothesis was developed.

7.5.3 Hypothesis 3: Onset of *P. subcapitata* cell toxicity to synthesized nano-ceria

Metabolomic signals from *Pseudokirchneriella subcapitata* will differ at the onset of toxicity when exposed to 5 nm and 35 nm ceria particles as a function of dose, compared to the controls.

7.5.3.1 Aim

The experimental design was altered from the testing of Hypothesis two in order to eliminate potential artefacts derived from various stages of algal cell growth during a 72 h exposure. Metabolite signals from synthesized nano-ceria particle exposed *Pseudokirchneriella subcapitata* cells at the onset of toxicity (calculated at 18 h) were therefore conducted. To reduce the number of factors in the experimental design, only two synthesized nano-ceria particle dimensions were investigated (5 and 35 nm). Initial starting cell densities were kept at environmentally relevant concentrations (4 X 10^4 cell/ml) and biological repeats were more than doubled from previous studies to address the problem of high metabolic variability.

7.5.3.2 Design

Twelve biological repeats of two synthesized nano-ceria particle dimensions of 5 nm and 35 nm, across six concentrations (Table 7-5) were prepared in 15 ml media and then used in 72 h growth inhibition tests (OECD 201, 1984) of *P. subcapitata*. Initial inoculations of *ca* 4 X 10^4 cell/ml were made and cell density counts were conducted using a haemocytometer and further supported by spectroscopic means.

Table 7-5 Nano-ceria dose measurements for Hypothesis three
Dose measurements based upon ICP-MS determination.

Synthesized ceria particle sizes	Exposure dose used (mg/L by ICP-MS)			
	1	2	3	4
5nm	0.00069	0.00231	0.00347	0.0069
35nm	0.0039	0.012	0.039	0.079

After 18 h exposure, ten of the twelve biological repeated samples were selected for metabolomic quenching. A 1 ml aliquot was removed from each sample for harvesting (Section 7.4.1.2). The biological sample was then placed back into the growth cabinet for continued growth for the remaining 72 h growth period.

7.5.3.2.1 Cell viability

To reduce the previous variation in metabolomic signals obtained during the testing of Hypothesis two, it was considered important to reduce the probability of dead *P. subcapitata* cells in a sample. Cell viability tests were therefore conducted prior to the test to ensure the *P. subcapitata* cells present in solution would be at least 80% viability after 18 h.

7.5.3.2.2 Cell viability method

Cell viability tests were conducted using a fluorescence activated cell sorter (FACS) facilitated and supported by Dr. Rachel Hayden, University of Birmingham. *P. subcapitata* toxicity test was prepared for three biological repeated exposures to 5 nm and 35 nm synthesized ceria particles at EC_{50} (*ca* 0.003 and 0.4 mg/L receptively) and EC_{20} doses (*ca* 0.001 and 0.2 mg/L respectively) along with three control samples. After 18 h the three biological repeats were centrifuged at 17,000 rpm for 10 min to obtain a pelted sample then re-suspended in fresh test media to obtain a cell count *ca* 30 X 10^4 cell/ml. The control sample was separated into two aliquots one of which was autoclaved to produce the 'dead cell' sample. A 500 µl aliquot of each sample was suspended in 100 µl of phosphate buffered saline (PBS). Propidium Iodide (PI) from Sigma Aldrich, UK was diluted to 50 µg/ml with a 5 µl aliquot used to stain *P. subcapitata* cells in each sample.

7.5.3.3 Cell viability tests

A distinctive peak observed for the 'dead cell' samples compared against the 'live cell' sample was obtained from FACS cytometry (Figure 7-12a). Results obtained suggest at least 81% viable cells were obtained in control samples (Figure 7-12b) after 18 h growth. This was also observed with treated *P. subcapitata* cell samples, exposed to 5 nm ceria particles at *ca* 0.002 mg/L and at *ca* 0.007 mg/L (Figure A49a) and to 35 nm ceria particles (Figure A49b-c) at *ca* 0.004 mg/L and 0.012 mg/L doses after 18 h.

7.5.3.4 Cell counts

The higher doses of 5 nm and 35 nm ceria particles (*ca* 0.007 mg/L and *ca* 0.08 mg/L respectively) showed a significant ($p<0.05$) reduction in growth compared against the control samples, after 18 h exposure (Figure 7-13a). Throughout the 72 h exposure period, the growth rates observed for both 5 nm and 35 nm ceria particles (Figure 7-13b) were comparative to those obtained in previous studies (Chapter 6).

7.5.3.5 Principal component analysis

Following harvesting and extractions, all samples were normalised against cell densities by Dr. Ulf Sommer based upon the 18 h cell counts obtained through spectroscopic calibrations. The total number of mass spectral peaks in the metabolomics dataset, obtained by Dr. Ulf Sommer, was 1375, with all blank signals removed. The MS contained a large number of unusually low intensity signals, most probably due to the relatively low cell densities used, following only 18 h of growth. The scatter obtained in the metabolomic signals across the PCA plot (Figure 7-14a) implies an increased variability in the signal obtained, which is not observed with the well placed QC plots.

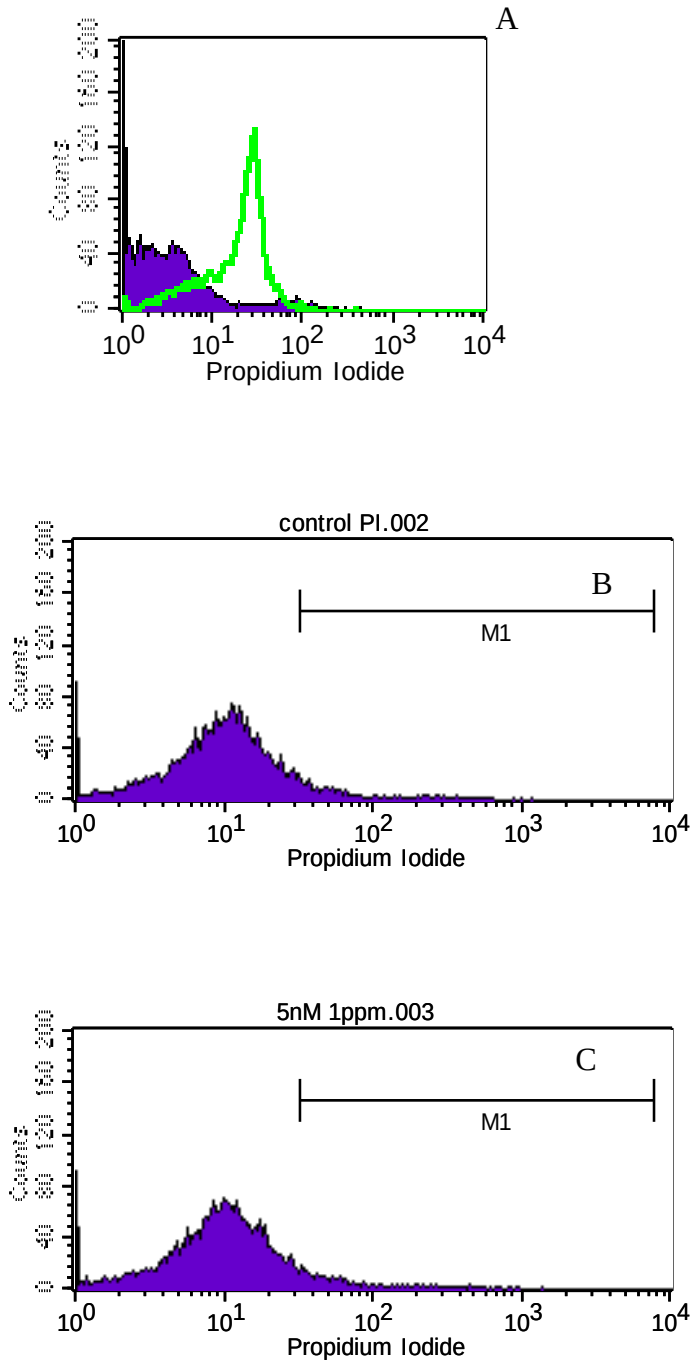

Figure 7-12 Stained algae cell counts obtained from FACS cytometry
Showing amount of PI against calculated algae cell counts. A) Overlay of live cells (purple region) V's "dead" cells (green peak) both with PI stain showing a distinct variation in positions with counts obtained. B) M1 showing < 7% (-2.92%) of cells in control sample potentially "dead" offering at least 81 % cell viability in control samples. C) M1 showing exposed cells to 0.002 mg/L 5 nm ceria particles after 18 h expressing < 7.5% (-2.92%) of cells in sample potentially "dead" offering at least 81 % cell viability.

A

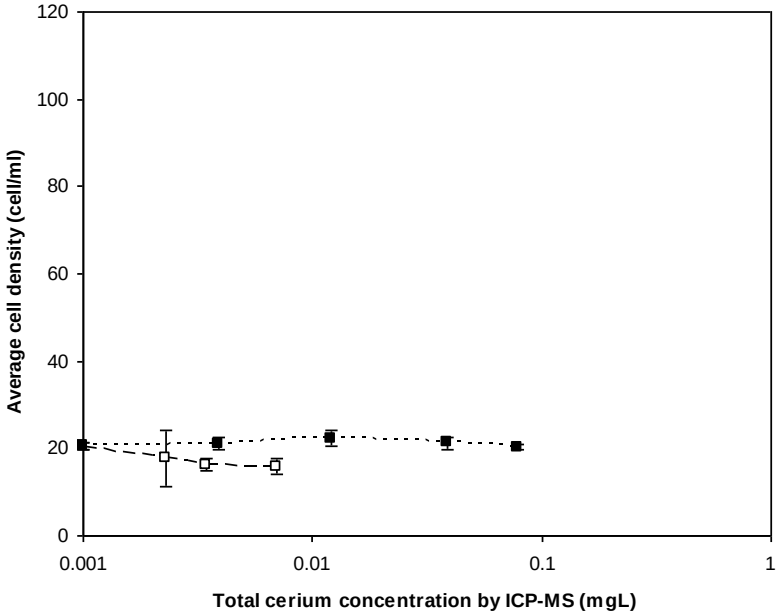

B

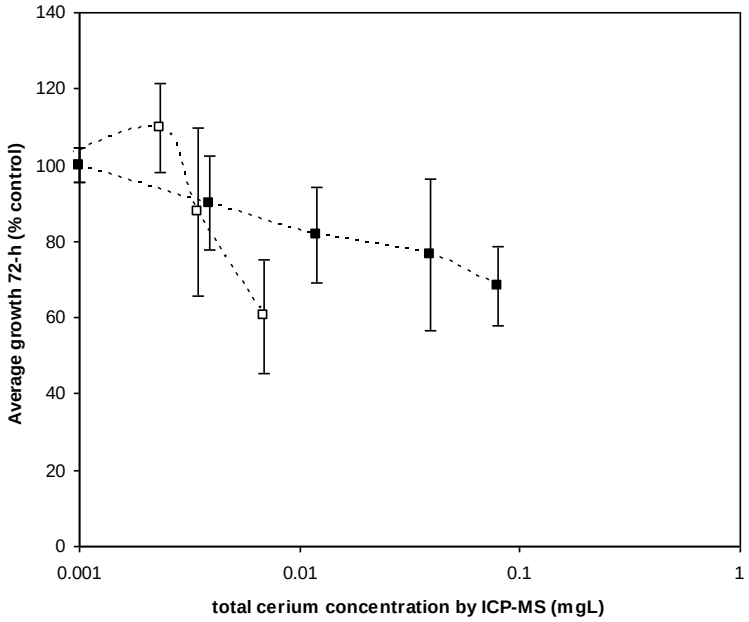

Figure 7-13 Daily cell counts after 18 h exposure testing Hypothesis three
35 nm (black square) and 5 nm (white square) synthesised nano-ceria particles.
A) After 18 h exposure, representing the time the samples were harvested for metabolomics analysis, B) growth inhibition graph, compared to the control after 72 h exposure.

7.5.3.5.1 5 nm ceria particles

With two outliers removed, the PCA scores plot shows a high degree of scatter between the control samples and the 5 nm ceria particle treated samples (Figure 7-14b). This maybe due to the biological variability or due to the low signal obtained from the MS analysis. It may also be due to the sample signals all being very similar to one another as cell densities at the lower particle doses are comparative to control cell densities after 18 h. In order to focus on the most discriminating peaks (e.g. between control samples and dosed samples), a multivariate statistical approach using partial least squares-discriminant analysis (PLS-DA) was used instead of PCA.

The PLS-DA models of the control and 5 nm treated samples produced by Dr. Ulf Sommer, built were subsequently "forward selected", which is another technique for determining which of the peaks in the MS are the most important for discriminating biological groups. In this data, only 17 of the most important peaks (*m/z* values) were chosen, reducing the significance ($p>0.02$) of this data, (Table A14). Statistical analysis on the 18 h cell growth counts revealed that only the highest dose (0.007 mg/L) was different from controls. Therefore, another PLS-DA model was built where forward-selection revealed 89 of the most discriminatory peaks between the highest 5 nm ceria particle dose and the controls (Figure 7-15).

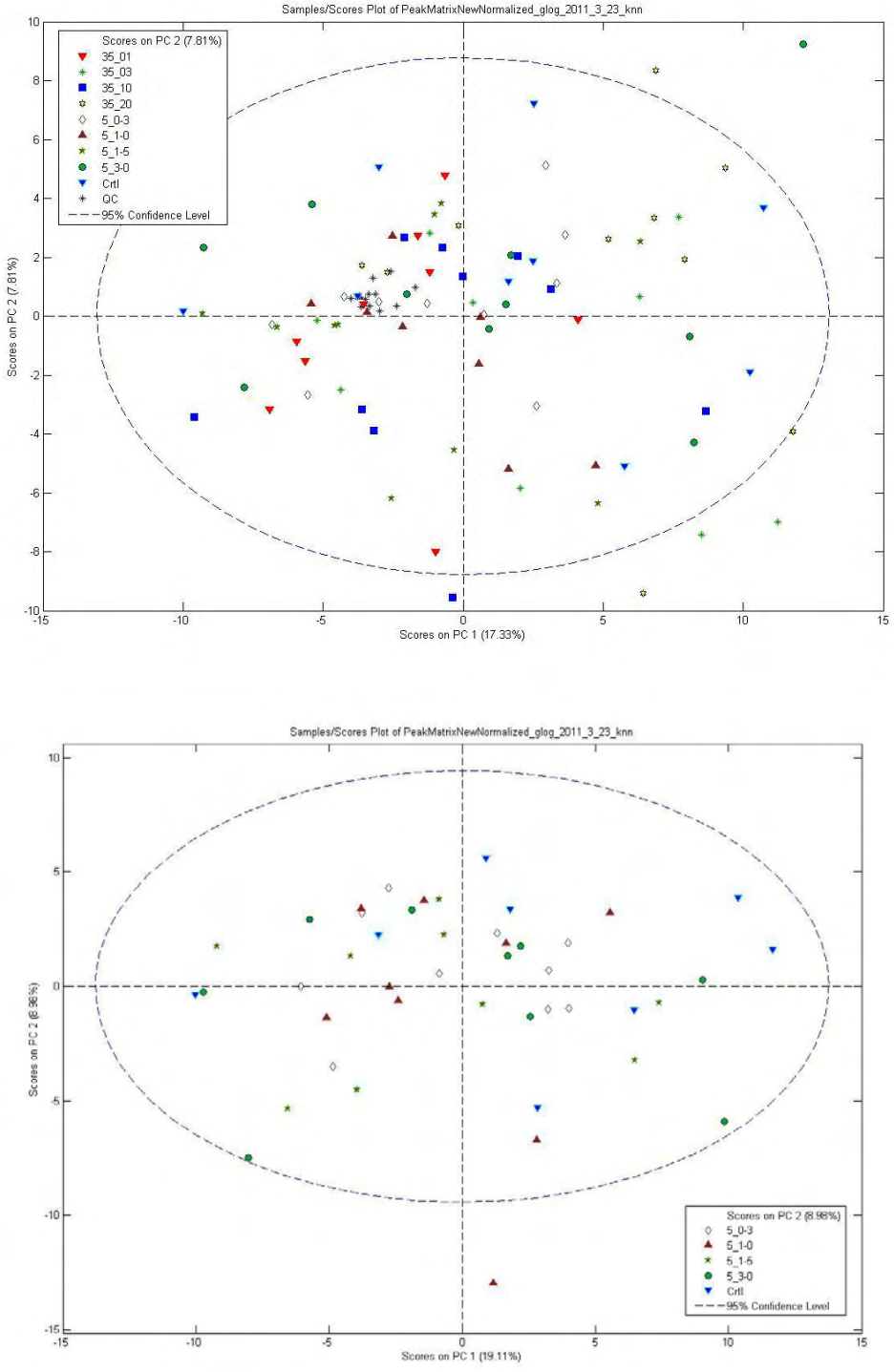

Figure 7-14 PCA scores plot from selected analysis testing Hypothesis three
A) All samples with quality controls and control samples included, with two outliers (35 nm 0.08 mg/L number 8 and Control number 7) removed. B) PCA of control and all 5 nm particle treated samples with 2 outliers removed. (Control sample number 7, 5 nm 0.003 mg/L sample number 2, and 5 nm 0.007 mg/L sample 8).

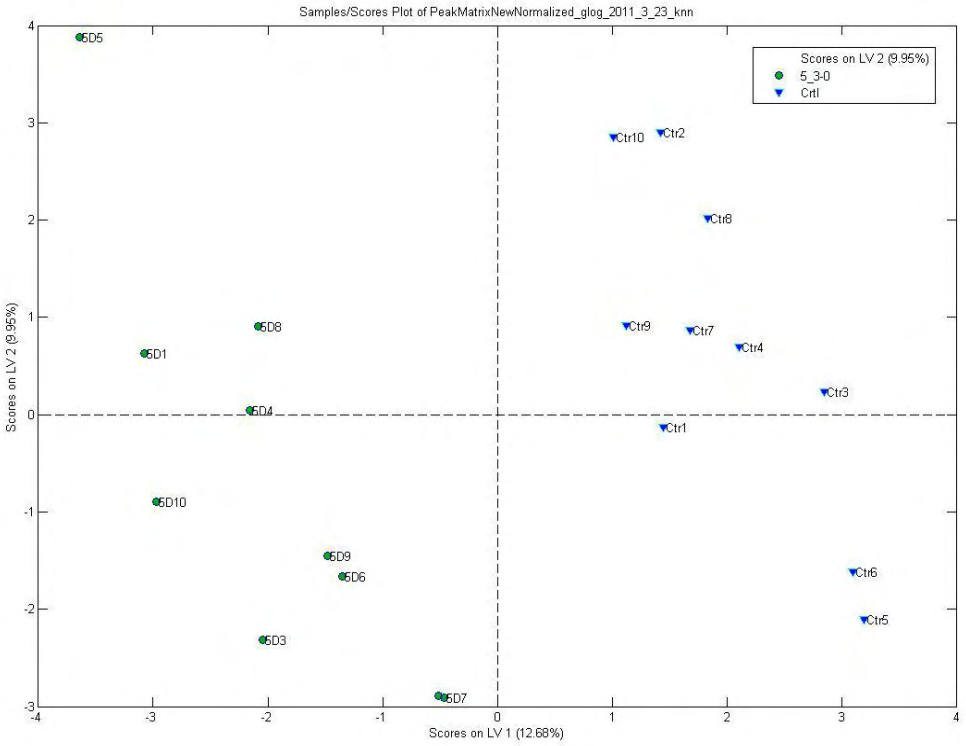

Figure 7-15 PCA plots from selected analysis testing Hypothesis three
A) PLS-DA forward-selected control and only 5 nm, 0.007 mg/L particles: Comparison of only these two groups shows a clear separation after forward election (3 LVs, 89 m/z variables). The model was initially built without four samples then rebuilt with them added back in.

Comparisons of the controls and treated samples show a clear separation in the PLS-DA plot obtained. It is however easy to over-fit the data in this instance with only 1/5th (20 data points) of the entire data set being investigated, so caution must be taken when interpreting these results. These data points fit well with good statistical significance ($p<0.01$). The class error rate of 0.06 infers 6% of the samples removed will be incorrectly predicted as being control samples when in fact they are treated samples (or vice versa) in the PLS-DA analysis. This shows that 94% of the predictions are correct and this equates to a highly predictive multivariate model.

7.5.3.5.2 35 nm ceria particles

When forward-selected control and 0.08 mg/L 35 nm synthesized ceria particle treatments were chosen for PLS-DA, the controls are shown to cluster well suggesting little variation between these samples compared to the treated samples. In this PLS-DA scores plot, large variability in the treated samples is observed compared to the controls, with a distinct separation between peaks selected. This suggests a variation in the metabolomic response when *P. subcapitata* are under exposure to 0.08 mg/L 35 nm ceria particles compared to control conditions. The 35 nm ceria particles at a 0.012 mg/L dose induces a growth above that of the control sample (Figure 7-14b), potentially related to the hormesis effect of cells (Calabrese, 2008). The PLS-DA plot investigating the metabolic profiles of the 0.012 mg/L dose group as well as the control group shows a clear separation (Figure 7-16). This separation suggests at this dose promoting a cellular response in growth, there is a clear change in the metabolic profile of exposed *P. subcapitata* relative to the controls.

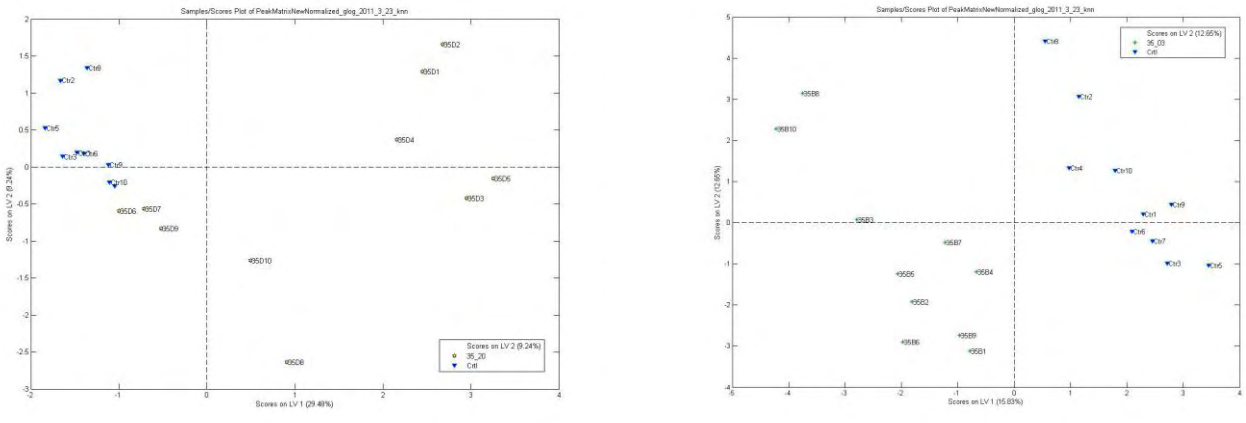

Figure 7-16 PLS-DA scores plot from selected analysis testing three
A) PLS-DA forward-selected control and 35 nm, 0.08 mg/L particles using 14 forward selected m/z variables: B) PLS-DA forward-selected control and 35 nm, 0.012 mg/L particles using 93 m/z variables.

7.5.3.6 5 nm and 35 nm ceria treatments overlap

When the most discriminating peaks from the highest doses of 5 nm (0.007 mg/L) and 35 nm (0.08 mg/L) ceria particles are collated and compared against the control peaks, there is a general lack in overlap of the peaks obtained (Figure A50). This poor overlap of metabolomic signals from the two particle sizes that are associated with the greatest toxic effect may be due to there being two separate mechanisms of toxicity observed between these two particle sizes. This mechanistic approach is beyond the scope of this work and requires further interpretation for future work.

7.5.3.7 Regression analysis for growth predictions

Further analysis, conducted by Dr. Ulf Sommer using the MS data, involved a regression analysis to determine whether any of the peaks in the MS data correlated with the cell count data. This was conducted for both particle dimensions (5 nm and 35 nm) after 18 h exposures compared against the 72 h growth rates obtained. Ultimately this analysis sought to determine if any MS signals could predict *P. subcapitata* cell growth. Forward selection of the *m/z* peaks was again pursued to produce a low number of predictive signals which led to significant PLS regression models (Appendix C). The results suggest a lower growth rate (and therefore cell count) is associated with specific metabolic signals. Higher cell counts over the same exposure period exhibit different metabolic signals than lower cell counts. These specific peaks however have not been successfully identified at this time, and requires further work for this analysis to be useful in future prediction models.

7.5.3.8 Summary and evaluation

The hypothesis tested can be accepted as metabolomic signals from high doses of 5 nm and 35nm synthesized nano-ceria particles (0.007 and 0.08 mg/L respectively) after 18 h showed distinctive PCA separation compared to controls. The metabolomic profiles from PCA and PLS-DA score plots showed that *P. subcapitata* exposed to the higher synthesized nano-ceria particle doses, at two particle dimensions (35 nm and 5 nm respectively), contributed most to the separation across the PLS-DA scores plots obtained. The results obtained suggest relatively small metabolic differences exist between none-exposed and exposed *P. subcapitata* cells to the lower doses of synthesized ceria particles. There is also reason to believe a possible homeostatic range for lower concentrations of synthesized nano-ceria particles at 35 nm diameters also exists although further work is required to determine this effect. As a large number of metabolites undergo marked changes in at least one condition, the (future) identification of these peaks would be adventitious but is beyond the scope of this work at present.

7.5.4 Conclusion and evaluation

This work was conducted with four objectives. The first objective was to develop the methods for quenching and extracting metabolites from *P. subcapitata cells*. This was conducted successfully following previously determined publications. From the method used it was evident that using the highest possible initial *P. subcapitata* cell density $>10^6$ cell/ml for future applications is imperative to ensure good MS signal intensities which will reduce interference and variability obtained from metabolomic signals obtained during analysis.

A second objective was to determine whether metabolomic analysis could be used effectively to understand the mechanisms of nano-ceria toxicity as a function of size and dose on exposures to *P. subcapitata*. The variation in *P. subcapitata* cell density between control and treated samples did not significantly alter the metabolomic signals obtained, which lead into the third objective of this study.

The third objective was to identify significant differences in metabolomic signals obtained from *P. subcapitata* when exposed to nano-ceria particles as a function of size and dose. It was evident that investigating a range of factors from nano-ceria particle size, various dose measurements and conducting parallel tests, at low initial *P. subcapitata* cell densities, ($<4X10^4$ cell/ml) can result in large variation with the metabolomic signals obtained. The metabolomic signals did show *P. subcapitata* exposure to higher doses of 5 and 35 nm nano-ceria particle diameters contributed most to the separation of samples in the PCA scores plots and therefore significant

metabolic differences do exist between the control and treated *P. subcapitata* cell samples.

From this study it is evident that *P. subcapitata* is a viable model organism for future environmental nanoecotoxicological studies using metabolomic analysis. Cell densities must be >20X10^6 cell/ml in order to produce reproducible results, which is also dictated by the finite sensitivity of the MS based metabolomics method. Metabolomic analysis can aid in the interpretation of nanoecotoxicological assessments for future work, fulfilling the final objective of this work, although identification of specific metabolic changes and their associated signals is required in order to learn more about the mechanisms of toxicity.

7.5.5 Future work

Following this short study, the mechanisms of observed synthesized nano-ceria toxicity to *P. subcapitata* have not been identified with any certainty. Due to time restraints and the sheer novelty of the metabolomic techniques employed, there is still a great deal of work which can be developed to enhance metabolomic analysis in the future. One area of work still to be developed is the identification of specific m/z peaks which may offer further insight into the possible mechanisms of toxicity by identifying the most discernable peaks and their associated chemical signature. However, at this developmental stage of metabolomic use, only 10% of the peaks obtained from MS analysis from this study are identifiable. A problem associated with peak identification however, is that specific peaks may be species dependent and was therefore beyond

the scope of this short project. With improvements in the peak identification for future metabolomic use, there is huge potential for better understanding of exposure effects of *P. subcapitata* to synthesized nano-ceria particles.

From this independent investigation, it is evident that metabolomic analysis can successfully be used for future nanoecotoxicology work, although variable signals obtained using *P. subcapitata* can dominate metabolomic signals produced. Although the genetic variation is reduced in algal samples, *P. subcapitata* maybe at different growth stages at metabolomic quenching, resulting in variable metabolomic signals. To reduce this variation, future nanoecotoxicological work using algae may consider the marine macro algae species *Ulva linza* which releases zoospores synchronously, thus reducing this potential variation in cell growth within a sample. Also, identifying MS signals relating to specific metabolites like pyruvate or glycerol phosphate, in algae cells will help to identify the mechanisms of toxicity, being another step in developing this analytical process as a viable tool for future nanoecotoxicological tests.

8 Conclusions and further work

8.1 Conclusion

This thesis aimed to investigate three areas of environmental nanoecotoxicity research outlined below.

8.1.1 Aim 1: Physicochemical characterisations of commercial ceria

The physicochemical characterisations of three commercial nano- and bulk-ceria particles showed variations across a range of media used, appropriate for *C. carpio*, *D. rerio*, *P. subcapitata* and *D. magna* exposures and including cell media. Variations in media electrolyte concentrations showed significant differences ($p<0.05$) in measured hydrodynamic diameters (d_H) of commercial nano-ceria particles. UV-visible intensity increased and Pzc changed from pH 6 to pH<2 as media electrolyte increased. A general trend showed that as the NP concentration in a given media increased, the measured d_H increased and the ζ become more negatively charged opposing the DLVO theory. Characterisations of different commercial nano-ceria particle dispersions in the same media obtained from collaborative institutes also showed significant differences in d_H, ζ and measured Ce concentrations compared to equivalent independently produced samples. In one instance, a collaborative institute repeated a nanoecotoxicological test using the same nano-ceria particle batch but using different personnel to conduct the particle dispersions. This resulted in significantly variable particle characteristics of ζ and UV-visible absorbance and a two fold difference in measured d_H. The addition of Suwannee River fulvic acid, (SRFA) to

a media also had variable effects on commercial nano-ceria particle characteristics measured, across all the media used. The addition of SRFA significantly reduced d_H up to 88% and increased the ζ negative charge measured. The dissolution of nano-ceria increased up to 2% with SRFA additions and fluorescence intensities significantly increased ($p<0.05$). There was also evidence to suggest the presence of the test biota has further effects on the commercial nano-ceria physicochemical characteristics, particularly at the onset of exposure (1 h). Decreases in measured d_H of up to 80% compared to none exposure samples were observed along with increased Ce dissolution of up to 63% in the presence of organisms. The polydispersity of the nano-ceria dispersion decreased up to 47% with increasing nano-ceria concentration and a 20% reduction in measured Ce dissolution was recorded in the presence of an organism. An increase in negative charge with the presence of organisms was also measured. The increased fluorophore measurements obtained from exposure assessments allow the prediction that organic material is produced by the organism (exudates) during exposure to NPs, contributing to the changes in particle characteristics observed.

The results from the NP characterisation study may have implications for future nanoecotoxicological tests. It was evident from this study, that a number of particle characteristics with comparative analysis from a variety of instruments are required to obtain an understanding of particle behaviour at the onset and post exposure test. The method of sample preparation can also have an effect on the outcome of results obtained and must be justified before use.

8.1.2 Aim 2: Physicochemical characterisations of commercial ceria

The next aim was to characterise the nanoecotoxicity effects of *Pseudokirchneriella subcapitata* under the exposure of four discrete synthesized nano-ceria particles. *P. subcapitata* showed a convincing size-dependent toxic effect to the well-defined synthesized nano-ceria particles. Nano-ceria particles of 5 nm dimensions were found to have a greater effect on cell growth compared to 7 nm, 10 nm and to 35 nm particle dimensions with EC_{50} values 0.0013, 0.14, 0.35 and 0.8 mg/L respectively compared against commercial nano-ceria dispersions (EC_{50} 8 mg/L). These results suggest there are still real challenges associated with the proposed future applications of synthesized nano-ceria in e.g. drug-delivery systems, which are purposefully produced at dimensions <30 nm. Associated disposal mechanisms for nano-ceria particles particularly at low particle dimensions also needs immediate consideration to ensure future environmental safety.

8.1.3 Aim 3: *P. subcapitata* toxicity using a metabolomic analysis

The final aim of this work was to investigate the novel approach of metabolomic analysis to further understand the observed toxicity of synthesized nano-ceria particles to *P. subcapitata*. The limitations of this technique were governed mainly by the extraction methods are which are sensitive to cell density volumes and temperature fluctuations. Cell densities of $>10^6$ cell/ml for *P. subcapitata* exposures were found as optimal to ensure good signal responses during MS analysis. The metabolomic signals obtained during *P. subcapitata* exposures to nano-ceria particles of 5 nm and 35 nm dimensions at $>EC_{50}$ values following 18 h exposure contributed most to the

separation of samples in the PCA scores plots, suggesting significant metabolic differences exist between control and treated cell samples under these conditions. From this short study, it is evident that metabolomic analysis has a huge potential for nanoecotoxicological investigations. Increasing our knowledge of the metabolic peak locations will further aid the future use and application of this technique.

8.2 Future Work

From this study it was evident that much more work is still required to help develop methods of NP characterisations and to further extend our understanding of the toxic effects of ceria NPs to a range of taxonomic groups. A number of questions regarding future investigations on nano-ceria are highlighted below.

8.2.1 Short and medium term studies

How should future nanoparticle characterisations be assessed?

It is important to monitor the changes in physicochemical characterisations of any NP in aquatic media during future exposure investigations. Defining a standardisation protocol to incorporate NP dispersion and physicochemical characterisation methods will reduce bias across laboratory tests and allow better comparative analysis of results.

What is the mechanism of action observed from nano-ceria toxicity?

It is evident from this work that full appreciation of the mechanisms associated with nano-ceria particle uptake in *P. subcapitata* cells and other biological test species are not fully understood. Understanding the mode of action relating to nano-ceria particle toxicity, across a range of species, is imperative to ensure the future use of nano-ceria at these low particle dimensions. Further developments in metabolomic analysis will aid in the understanding of NP toxicity.

Does nano-ceria shape have a contributing effect of toxicity?

It was evident that synthesized nano-ceria particles had a significant effect on *P. subcapitata* toxicity compared against commercial nano-ceria particles, due to the particle size. The shape of commercial nano-ceria particles are predicted to contribute to the changes in measured physicochemical characteristics of NPs. The shape of synthesized nano-ceria particles may therefore also have a contributing effect on *P. subcapitata* toxicity due to changes in physicochemical characterisations being measured.

What effect do nano-ceria particles have on human health?

Toxic effects of nano-ceria particles associated with aquatic species may result in food-chain accumulation and the future uses of nano-ceria in e.g. diesel fuels and cosmetics, may increase inhalation and dermal exposures of these particles. Investigating inhalation, dermal exposure and ingestion effects of synthesized nano-ceria particles as a function of size and dose using human test conditions is a further area of study essential for the continued technological progression of nano-ceria particles.

How much nano-ceria is used per annum and what is the rate of release associated with nano-ceria products?

Increasing our knowledge and understanding regarding the annual release of ceria NPs during manufacture, through run-off, combustion of materials and that emitted from e.g. exhaust following NP uses as catalysts in fuels and from waste disposal is

essential. No systematic description of natural and anthropogenic ceria NPs and their occurrence, fate or effects on the environment is yet available. Until this is fully understood, it is difficult to calculate the true risk using models of e.g. PEC/PNEC ratios.

How are nano-ceria particles transported and how do they behave in environmental systems?

Environmental transport and behaviour of nano-ceria particles is essential to determine potential sinks and bioavailability of nano-ceria particles in environmentally relevant conditions. Transportation of nano-ceria in e.g. groundwater, marine systems, estuarines and percolation through limestone, sandstone or peat, along with the interactions of nano-ceria particles with known organic compounds such as leachate would aid in future risk assessments of these particles.

Do particle coatings have an effect on physicochemical characterisations?

The use of ligands (PVP, citrates), proteins and humic materials during nano-ceria synthesis may have an effect on particle toxicity and bioavailability over time. Particle coatings may be used as food source by other organisms, rapidly releasing the particle core to the environment. Also, different particle coatings may degrade over time, releasing particles after several decades with variable effects for the future.

8.2.2 Long term studies

What effect do nano-ceria particles have over time?

Chronic exposures of nano-ceria particles as a function of size, shape and dose, to a range of species will help identify species sensitivity to these particles under simulated environmental conditions.

How do real environmental conditions compare with laboratory tests?

True environmental conditions including water temperature fluctuations and biological (bacterial and algal) interactions may change particle characteristics over time. These conditions can not be fully explored in the confinements of a laboratory so a move towards environmentally relevant conditions conducted outside the laboratory would benefit future understanding of NP behaviour.

How can nano-ceria particle characterisations be predicted under different environmental conditions?

Theoretical models of colloids e.g. DLVO theory cannot meet a true representation of particles at the nano-scale, due to their variable properties. A model of risk for all MNPs would therefore benefit future NP research and equally the public's perception of NPs.

VI. References

Adams, L. K., Lyon, D. Y., and Alvarez, P. J. J., (2006). Comparative eco-toxicity of nanoscale TiO2, SiO2, and ZnO water suspensions. Water Research 40:3527-3532.

Aitken, R. J., Chaudhry, M. Q., Boxall, A. B. A., and Hull, M., (2006). Manufacture and use of nanomaterials: current status in the UK and global trends. Occupational Medicine (London) 56:300-306.

Ajie, H.; Alvarez, M. M.; Anz, S. J.; Beck, R. D.; Diederich, F.; Fostiropoulos, K.; Huffman, D. R.; Krätschmer, W.; Rubin, Y.; Schriver, K. E.; Sensharma, D.; Whetten, R. L. (1990). Characterization of the Soluble All-Carbon Molecules C_{60} and C_{70} . Journal of Physical Chemistry. *94:(* 8630-8633).

Alargova, R. G., Deguchi, S., Tsujii, K., (2001). Stable colloidal dispersions of fullerenes in polar organic solvents. Journal of the American Chemistry Society. 123:10460-10467.

Alvarez, P. J., (2006). Nanotechnology in the Environment-The Good, the Bad and the Ugly. Journal of Environmental Engineering. 132:(10) 1233.

Amin, K. A, Hassan, M. S., Awad, E-S. T., Hashem, K. S., (2011). The protective effects of cerium oxide nanoparticles against hepatic oxidative damage induced by monocrotaline. International Journal of Nanomedicine. 6:(143-149).

Amro, N. A., Kotra, L. P., Wadu-Mesthrige, K., Bulychev, A., Mobashery, S., Liu, G-y., (2000). High-resolution atomic force microscopy studies of the *Escherichia coli* outer membrane: structural basis for permeability. Langmuir. 16:2789-2796.

Andrievsky, G. V., Klochkov, V.K., Karyakina, E.L., Mchedlov-Petrossyan, N. O., (1999). Studies of aqueous colloidal solutions of fullerene C_{60} by electron microscopy. Chemical Physics Letters. 300: 329-396.

Aruoja, V., Dubourguier, H-C., Kasemets, K., Kahru, A., (2009). Toxicity of nanoparticles of CuO, ZnO and TiO2 to microalgae Pseudokirchneriella subcapitata. Science of the Total Environment. 407:(1461-1468).

AshaRani, P. V., Mun, G. L. K., Hande, M. P., Valiyaveettil, S., (2009). Cytotoxicity and Genotoxicity of Silver: Nanoparticles in Human Cells. ASC Nano. 3;(2):(279–290).

ASTM (American Society for Testing and Materials) (2007): Nanomaterial Toxicity Testing Standards. Viewed online at http://www.astm.org

Auffan, M., Rose, J., Bottero, J-Y., Lowry, G. V., Jolivet, J-P., Wiesner, M. R., (2009). Review Article: Towards a definition of inorganic nanoparticles from an environmental, health and safety perspective. Nature Nanotechnology. 4:(634-641).

Baalousha, M., Ju-Nam, Y., Cole, P. A., Tyler, C., Jones, I., Stone, V., Fernandes, T., Jepson, M., Lead, J. R., Hriljac, J., (2011). Characterization of cerium oxide nanoparticles Part II: Non-size measurements. Environmental Toxicology and Chemistry. (in Press).

Baalousha M, Le Coustumer P, Jones I, and Lead J.R., (2010). Characterization of structural and surface speciation of representative commercially available cerium oxide nanoparticles. Environmental Chemistry. 7 377-385.

Baalousha, M., Manciulea, A., Cumberland, S., Kendall, K., Lead, J. R., (2008). Aggregation and surface properties of iron oxide nanoparticles: influence of pH and natural organic matter. Environmental Toxicology and Chemistry. 27(9):(1875-1882).

Baalousha, M., and Lead, J. R., (2007). Size fractionation and characterization of natural aquatic colloids and nanoparticles. Science of the Total Environment. 386:(93-102).

Baker, A and Inverarity, R., (2004). Protein-like fluorescence intensity as a possible tool for determining river water quality. Hydrological Processes. 18:(2927-2945).

Baker, A., and Spencer, R. G. M., (2004). Characterization of dissolved organic matter from source to sea using fluorescence and absorbance spectroscopy. Science of the Total Environment. 333:(217-232).

Bali, R., Razak, N., Lumb, A., Harris, A. T., (2006). The synthesis of metallic nanoparticles inside live plants. Abstract for presentation at Chemeca 2007 Viewed 12.12.07 from http://ieeexplore.ieee.org/iel5/4143299/4140639/04143372.pdf

Balnois, E., Papastavrou, G. and Wilkinson, K. J., (2007). Force Microscopy and Force Measurements of Environmental Colloids, in Environmental Colloids and Particles: Behaviour, Separation and Characterization, Volume 10 (eds K. J. Wilkinson and J. R. Lead), John Wiley & Sons, Ltd, Chichester, UK. doi: 10.1002/9780470024539.ch9

Bankinter., (2006). Fundación de la Innovación. Viewed 19th July 2010 http://www.fundacionbankinter.org/system/documents/6591/original/5_nanotechnology_EN.pdf

Bar-Ilan, O., Albrcht, R. M., Fako, V. E., Furgeson, D. Y., (2009). Toxicity Assessments of Multi sized Gold and Silver Nanoparticles in Zebrafish Embryos. Small. 5;(16):(1897-1910).

Barnes, J. H. I. V., Hieftje, G. M., Denton, M. B., Sperline, R., Koppernaai, D. W., Varinaga, G., (2003). MS detector array that provides truly simultaneous detection. American Laboratory (Shelton, CT, US). 35;(15-16).

Batchelli, S., Muller, F. L. L., Baalousha, M., Lead, J. R., (2009). Size fractionation and optical properties of colloids in an organic-rich estuary (Thurso, UK). Marine Chemistry. 113:(227-237).

Benhra A, Radetski CM, Fe´rard JF., (1997). Cryalgotox: Use of cryopreserved alga in a semistatic microplate test. Environmental Toxicology and Chemistry. 16:(505–508).

Bhatt, I., and Tripathi, B. N., (2010). Review - Interaction of engineered nanoparticles with various components of the environment and possible strategies for their risk assessment. Chemosphere.

Bhattacharjee, S., Chen, J. Y., Elimelech, M., (2000). DLVO interaction energy between spheroidal particles flat surface. Colloids and Surfaces A: Physicochemical and Engineering Aspects. 165:(143-156).

Binig, G., Quate, C. F., Gerber, C., (1986). Atomic Force Microscopy. Physical Review Letters. 56:(9):(930-933).

Birnwar, Y. A., Bare, K. R., Mahajan, V. R., Sapte, M. K., Baviskar, D. T., (2011). Erythrocyte Drug Delivery System. International Journal of Pharmaceutical Sciences Review and Research. 8;(1):(124-128).

Biswas, P; Wu, C. Y., (2005). Nanoparticle and the environment, Critical review paper. Journal of air waste management Association. 55:(708-746).

Bolea, E., Gorriz, M. P., Bouby, M., Laborda, F., Castillo, J. R., Geckeis, H., (2006). Multielement characterization of metal-humic substances complexation by size exclusion chromatography, asymmetrical flow filed-flow fractionation, ultrafiltration and inductively coupled plasma-mass spectrometry detection: A comparative approach. Journal of Chromatography A. 1129:(236-245).

Bölling, C., and Fiehn, O., (2005). Metabolite Profiling *of Chlamydomonas reinhardtii* under Nutrient Deprivation. Plant Physiology. 139:(1995-2005).

Borm, P. J. A., Robbins, D., Haubold, S., Kuhlbusch, T., Fissan, H., Donaldson, K., Schins, R., Stone, v., Kreyling, W., Lademann, J., Krutmann, J., Warheit D., and Oberdorster, E., (2006). The potential risks of nanomaterials: a review carried out for ECETOC. Particle and Fibre Toxicology. 3:(11-46).

Bouldin, J. L., Ingle, M. T., Sengupta, A., Alexander, R., Hannigan, R. E., Buchanan, R. A., (2008). Aqueous toxicity and food chain transfer of quantum dots™ in freshwater algae and *ceriodaphnia dubia*. Environmental Toxicology and Chemistry. 27(9):(1958-1963).

Boyle, N. R., and Morgan, J. A., (2009). Flux balance analysis of primary metabolism in *Chlamydomonas reinhardtii*. BMC Systems Biology. 3;(4). doi:10.1186/1752-0509-3-4

Brant, J., Lecoanet, H., Wiesner, M. R., (2005). Aggregation and deposition characteristics of fullerene nanoparticles in aqueous systems. Journal of Nanoparticle Research. 7:(545-553).

Britton G, Liaaen-Jensen S, Pfander H., (2004). Carotenoids handbook. Birkhäuser, Basel. ISBN: 3-7643-6180-8.

Brunauer, S., Emmett, P. H., and Teller, E., (1938). Adsorption of Gases in Multimolecular Layers. Journal of the American Chemical Society. 60(2):(309-319).

Brunner, T. J., Wick, P., Manser, P., Spohn, P., Grass, R. N., Limbach, L. K., Bruinink, A., Stark, W. J., (2006). In Vitro Cytotoxicity of Oxide Nanoparticles: Comparison to Asbestos, Silica and the Effect of Particle Solubility. Environmental Science and Technology. 40;(14):(4374-4381).

BSI (The British Standards Institution)., (2007). Guidance on the labeling of manufactured nanoparticles and products containing manufactured nanoparticles. ISBN 978 0 580 61315 9, viewed online http://www.bsigroup.com/

Buffle, J., (2006). The key role of Environmental Colloids/Nanoparticles for the Sustainability of Life. Journal of Environmental Chemistry. 3:(155-158).

Buffle J., Wilkinson, K. J., Stoll, S., Filella, M., Zhang, J., (1998). A generalized description of colloid interactions: The three-colloidal component approach. Environmental Science and Technology. 32:(2887–2899).

Bullard, J. W., and Cima, M. J., (2006) Orientation Dependence of the Isoelectric Point of TiO_2 (Rutile) Surfaces. *Langmuir*. *22* (24), pp 10264–10271

Calabrese, E. J., (2008). Hormesis: Why it is Important to Toxicology and Toxicologists. Environmental Toxicology and Chemistry. 27;(7):(1451-1474).

Casiraghi, M. P., Luporini, S., Silva, E. M., (2005). Uptake of cadmium by *Pseudokirchneriella supcapitata*. Brazilian Archives of Biology and Technology. 48;(6):(1027-1034).

Cedergreen, N., (2008). Is the growth stimulation by low doses of glyphosate sustained over time? Environmental Pollution. 156;(3):(1099-1104).

Chapman, P. M., (2006). *Editorial*; Emerging Substances-Emerging Problems? Environmental Toxicological Chemistry 25(6):(1445-1447).

Chen, H-I., and Chang, H-Y., (2005). Synthesis of nanocrystalline cerium oxide particles by the precipitation method. Ceramics International. 31:(795–802).

Chen, J., Patil, S., Seal, S., McGinnis, J. F., (2006). Rare earth nanoparticles prevent retinal degeneration induced by intracellular peroxides *Nature Nanotechnology* **1**: (142 – 150)

Chen, K., L., and Elimelech, M., (2006). Aggregation and Deposition Kinetics of Fullerene (C_{60}) Nanoparticles. Langmuir. 22:(10994-11001).

Chen, K., L., and Elimelech, M., (2007). Influence of humic acid on the aggregation kinetics of fullerene (C_{60}) nanoparticles in monovalent and divalent electrolyte solutions. Journal of Colloidal and Interface Science. 309:(126-134).

Chen, L., Mccrate, J. M., Lee, J. C-M., Li, H., (2011). The role of surface charge on the uptake and biocompatibility of hydroxyapatite nanoparticles with osteoblast cells

Chen, L., X., Lui, T., Thurnauer, M. C., Csenesits, R., Rajh, T., (2002). Fe_2O_3 Nanoparticle structures investigated by X-ray Absorption Near-Edge Structure, Surface Modifications, and Model Calculations. Journal of Physical Chemistry B. 106;34:(8539-8546).

Cerion., (2011). Cerion Enterprizes: Nanopartilce-eneabled Drug Delivery. Viewed online http://www.cerionenterprises.com

Chodos, A., (2009). Discovery of Graphene, *APS News* 18(9):2, viewed *www.aps.org/publications/apsnews/200910/physicshistory.cfm*

Chow, J. C., Watson, J. G., Savage, N., Solomon, C. J., McMurry, P. H., Corey, L. M., Bruce, G. M., Pleus, R. C., Biswass, P., Wu, C-Y., (2005). Introduction to the A&WMA 2005 Critical Review. Nanoparticle and the Environment. Journal of the Air and Waste Management Association. 55:(1411-1417).

Clinton, J., (2008). Colloidal Cerium Oxide Nanoparticles: Synthesis and Characterization Techniques. Online thesis viewed June 2010. http://scholar.lib.vt.edu/theses/available/etd-01292008-104526/unrestricted/jamie_clinton_thesis_rev2.pdf

Coble, P. G., (1996). Characterisation of marine and terrestrial DOM in seawater using excitation-emission matrix spectroscopy. Marine Chemistry. 51:(325-346).

Coello, F and Khan, M. A. Q., (1996). Protection against heavy metal toxicity by mucus and scales in fish. Archives of Environmental Contamination and Toxicology. 30, 319-326.

Colomban, P., (2009). The Use of Metal Nanoparticles to Produce Yellow, Red and Iridescent Colour, from Bronze Age to Present Times in Lustre Pottery and Glass: Solid State Chemistry, Spectroscopy and Nanostructure. Journal of Nanoparticle Research *8:(109-132).*

Colvin, V. L., (2003). The potential environmental impact of engineered nanomaterials. National Biotechnology. 21(10):(1166-1170).

Conesa, J. C., (1995). Computer modeling of surfaces and defects on cerium dioxide. Surface Science. 339;(3):(337-352).

Connor, E.E., Mwamuka, J., Gole, A, Murphy, C. J., Wyatt, M. D., (2005). Gold Nanoparticles Are Taken Up by Human Cells but Do Not Cause Acute Cytotoxicity. Small 2005, 1, No. 3, 325 –327

Cook D, Fowler S, Fiehn O, Thomashow, M. F., (2004). A prominent role for the *CBF* cold response pathway in configuring the low-temperature metabolome of *Arabidopsis*. Proceedings of the National Academy of Sciences, USA. 101:(15243–15248).

Cotton, S., (1991). Lanthanides and Actinides. Chapter 2. The Lanthanides. MacMillan Physical Science Series. MacMillan Education Ltd.

Cumberland, S. A., and Lead, J. R., (2009). Particle size distributions of silver nanoparticles at environmentally relevant conditions. Journal of Chromatography A. 1216;(52):(9099-9105).

Cumberland, S. A., and Baker, A., (2007). The freshwater dissolved organic matter fluorescence–total organic carbon relationship. Hydrological Processes. 21:(2093-2099).

Daniel, M. C, and Astruc, D., (2004). Gold nanoparticles: assembly, supramolecular chemistry, quantum-size-related properties, and applications toward biology, catalysis, and nanotechnology. Chemical Reviews. 104:(293–346).

Darlington, T. K., Neigh, A. M., Spencer, M. T., Nguyen, O. T., Oldenburg, S. J., (2009). Nanoparticle Characteristics Affecting Environmental Fate and Transport Through Soil. Environmental Toxicology and Chemistry. 28;(**6**):(1191-1199).

Das, M., Patil, S., Bhargava, N., Kang. J. F., Riedel, l. M., Seal, S., Hickman, J. J., (2007). Auto-catalytic ceria nanoparticles offer neuroprotection to adult rat spinal cord neurons. Biomaterials, 28(10):1918-25.

DCS., (2011). Denehurst Chemical Safety Ltd CHEMICAL SAFETY
Risk Assessment of Chemicals. Viewed at http://www.denehurst.co.uk/id28.html

Derjaguin and Landau., (1941). Thery of the stability of strongly charged lyophobic sols and of the adhesion of strongly charged particles in solution of electrolytes. Acta Physicochim. USSR 14:(633-62).

Deshpande, S., Patil, S., Kuchibhatla, S. V. N. T., Seal, S., (2005). Size dependency variation in lattice parameter and valency states in nanocrystalline cerium oxide. Applied Physics Letters. 87:(133113-1).

Diallo, M. S., Glinka, C. J., Goddard, W. A., Johnson Jr, J. H., (2005). Characterization of nanoparticles and colloids in aquatic systems 1. Small angle neutron scattering investigations of Suwannee River fulvic acid aggregates in aqueous solutions. Journal of Nanoparticle Research. 7:(435-448).

Domingos, R. F., Peyrot, C., Wilkinson, K. J., (2010). Aggregation of titanium dioxide nanoparticles: role of calcium and phosphate. Environmental Chemistry 7(1) 61–66.

Domingos, R. F., Baalousha, M. A., Ju-Nam, Y., Reid, M., Tufenkji, N., Lead, J. R., Leppard, G., and Wilkinson, K. J., (2009a). Characterizing Manufactured Nanoparticles in the Environment: Multi-method Determination of Particle Sizes. Environmental Science and Technology. 43:(7277-7284).

Domingos, R.F., Tufenkji., N. Wilkinson, K. J., (2009b). Aggregation of titanium dioxide nanoparticles: role of natural organic matter. *Environ. Sci. Technol.* 43: 1282-1286

Donaldson. K., Beswick, P. H., Gilmour, P. S., (1996). Free radical activity associated with the surface of particles: a unifying factor in determining biological activity? Toxicology Letters. 88:(293–298).

Doty, R. C., Tshikhudo, T. R., Brust, M., Fernig, D. G., (2005). Extremely Stable Water-Soluble Ag Nanoparticles. Chemistry of Materials. 17:(4630:4635).

Dreher, K. L., (2004). Toxicological Highlight: Health and Environmental Impact of Nanotechnology: Toxicological Assessment of Manufactured Nanoparticles. Toxicological Sciences. 77:(3–5).

Duval, J. F. L., (2007). Electrophoresis of soft colloids. (*In Wilkinson, K. J., and Lead, J. R. Environmental Colloids and Particles: Behaviour, Separation and Characterisation).* Wiley. ISBN: 978-0-470-02432-4.

Duval J.F.L., and Ohshima H., (2006) - Electrophoresis of diffuse soft particles, Langmuir, 22, 3533-3546.

Dwivedi, P., Puzon, G., Tam, M., Langlais, D., Jackson, S., Kaplan, K., Siems, W. F., Schultz, A. J., Zun, L., Woods, A., Hill, H. H., (2010). Metabolomic profiling of *Escherichia coli* by ion mobility-mass spectrometry with MALDI ion source.

Eggleston, C. M. and Jordan, G., (1998). A new approach to pH of point of zero charge measurement: Crystal-face specificity by scanning force microscopy (SFM). Geochemica et Cosmochimica Acta. 62;(11):(1919-1923).

Egerton, R., (2005). Physical principles of electron microscopy. Springer. ISBN 0387258000

Elechiguerra, J. L., Burt, J. L., Morones, J. R., Camacho-Bragado, A., Goa, X., Lara, H. H., Yacaman, M. J., (2005). Interaction of silver nanoparticles with HIV-I. Journal of Nanobiotechnology. 3;(6). doi:10.1186/1477-3155-3-6

ENV., (2007). Chemical Substances Control Law for cerium and its compounds. Viewed at http://www.env.go.jp/en/chemi/chemicals/profile_erac/profile8/pf1-07.pdf

Elidrissi B., M. Addou, M. Regragui, C. Monty, A. Bougrine & A. Kachouane,, (2000). Structural and optical properties of CeO_2 thin films prepared by spray pyrolysis. Thin Solid Films 379, 23.

Elimelech, M., Gregory, J., Jia, X., Williams, R. (1995) Particle Deposition & Aggregation. Measurement, Modelling and Simulation, Butterworth-Heinemann, Oxford, England.

Eom, H-J., and Choi, J., (2009). Oxidative stress of CeO_2 nanoparticles via p38-Nrf-2 signalling pathway in human bronchial epithelia cell, Beas-2B. Toxicology Letters. 187:(77-83).

Fadeel, B., Kagan, V., Krug, H., Shvedova, A., Svartengren, M., Tran, L., Wiklund, L., (2007). Review; There's plenty of room at the forum: Potential risks and safety assessment of engineered nanomaterials. Nanotoxicology. 1;(2):(73-84).

Federici, G., Shaw, B. J., Handy, R. D., (2007). Toxicity of titanium dioxide nanoparticles to rainbow trout (*Oncorhynchus mykiss*): Gill injury, oxidative stress, and other physiological effects. Aquatic Toxicology. 84:(415-430).

Fiehn, O., (2002). Metabolomics - the link between genotypes and phenotypes. Plant Molecular Biology. 48:(155–171).

Fisker, R., Carstensen, J. M., Hansen, M. F., BØdker, F., MØrup, S., (2000). Estimation of nanoparticle size distribution by image analysis. Journal of Nanoparticle Research. 2:(267-277).

Gaiser, B. K., Fernandes, T. F., Jepson, M. A. Lead, J. R., Tyler, C. R., Baalousha, M., Biswas, A., Britton, G., Cole, P. A., Johnston, B. D., Ju-Nam, Y., Rosenkranz, P., Scown, T. M., Stone, V., (2011). Interspecies comparisons on the uptake and toxicity of silver and cerium dioxide nanoparticles. Environmental Toxicology and Chemistry. (In press).

Gaiser, B. K., Fernandes, T. F., Jepson, M., Lead, J. R., Tyler, C. R., Stone, V., (2009). Assessing exposure, uptake and toxicity of silver and cerium dioxide nanoparticles from contaminated environments. Environmental Health. 8:(S2).

Garnett, M. C., and Kallinteri, P., (2006). Nanomedicines and nanotoxicology: some physiological principals. Occupational Medicine. 56:(307-311).

Gasaymeh, S. S., Radiman, S., Heng, L. Y., (2010). Synthesis and characterization of Silver/Polyvinilpirrolidone (Ag/PVPV) Nanoparticles Using Gamma Irradiation Techniques. African Physical Review. 4;(0006):(31-41).

Getzlaff, M., (2008). Fundamentals of magnetism (pp 203). Springer. ISBN:978-540-31150-8

Gibson, C. T., Turner, I. J., Roberts, C. J., Lead J. R., (2007). Quantifying the Dimensions of Nanoscale Organic Surface Layers in Natural Waters. Environmental Science and Technology. 41:(1339-1344).

Gilbert, B., Lu, G., Kim, C. S., (2007). Stable cluster formation in aqueous suspensions of iron oxyhydroxide nanoparticles. Journal of Colloid and Interface Science. 313:(157-159).

Gilbert, B., Huang, F., Zhang, H., Waychunas, G. A., Banfield, J. F., (2004). Nanoparticles: Strained and Stiff. Science. 305:(651-654).

Gimbert, L. J., Hamon, R. E., Casey, P. S., Worsfold, P. J., (2007). Partitioning and stability of engineered ZnO nanoparticles in soil suspensions using flow field-flow fractionation. Environmental chemistry. 4;(1):(8-10).

Goodwin, J., (2004). Colloids and interfaces with surfactants and polymers; an introduction. John Wiley and Sons Ltd. ISBN: 0470841435

Gonçalves, C., and Gama, F. M., (2008). Characterization of the self-assembly process of hydrophobically modified dextrin. European Polymer Journal. 44:(3529-3534).

Goslan, E. H., Voros, S., Banks, J., Wilson, D., Hillis, P., Campbell, A. T., Parsons, S. A., (2004). A model for predicting dissolved organic carbon distribution in a reservoir water using fluorescence spectroscopy. Water Research. 38:(783-791).

Griffitt, R. J., Luo, J., Goa, J., Bonzongo, J-C., Barber, D. S., (2008). Nanomaterials in the Environment: Effects of particle composition and species on toxicity of metallic nanomaterials in aquatic organisms. Environmental Toxicology and Chemistry. 27(9):(1972-1978).

Guo, L., Hunt, B. J., Santschi, P. H., Ray, S. M., (2001). Effect of Dissolved Organic Matter on the Uptake of Trace Metals by American Oysters. Environmental Science and Technology. 35:(885-893).

Guy, C., Kaplan, F., Kopka, J., Selbig, J., Hincha, D. K., (2008). Metabolomics of temperature stress. Physiologia Plantarum. 132;(2):(220-235).

Guzmán, K. A., D., Taylor, M. R., Banfield, J. F., (2006). Environmental Risks of Nanotechnology: National Nanotechnology Initiative Funding, 2000-2004. Environmental Science and Technology. 40;(5):(1401 -1407).

Haasch, M. L., McClellan-Green, P., Oberdörster, E., (2005). Consideration of the toxicity of manufactured nanoparticles. American Institute of Physics Conference Proceedings. 786:(586-590).

Haken, H., and Wolf, H. C., (2004). The Physics of Atoms and Quanta. Introduction to Experiments and Theory. Sixth Ed. Springer. ISBN: 3-540-67274-5

Hampel, C. A., (1968). The encyclopaedia of chemical elements. Reinhold Book Corporation 62-299938.

Handy, R., (2007). Planet Earth-Summer edition; Natural Environment Research Council. Is small a big problem for fish? 20-21.

Handy, R. D., (1989). The Ionic composition of Rainbow Trout Body Mucus. Comparative Biochemistry and Physiology. 93A:(3);(571-575).

Handy, R. D., and Eddy, F., B., (1989). Surface absorption of aluminum by gill tissue and body mucus of rainbow trout, *Salmo gairdneri*, at the onset of episodic exposure. Journal of Fish Biology. 34:(865-874).

Handy, R. D., von der Kammer, F., Lead, J. R., Hassellöv, M., Owen, R., Crane, M., (2008a). The ecotoxicology and chemistry of manufactured nanoparticles. Ecotoxicology. 17:(4):(287-314).

Handy, R. D., Henry, T. B., Scown, T. M., Johnston, B. D., Tyler, C. R. (2008b). Manufactured nanoparticles: their uptake and effects on fish—a mechanistic analysis. Ecotoxicology. 17:396–409.

Hansen, T., Clermont, G., Alves, A., Eloy, R., Brochhausen, C., Boutrand, J. P., Gatti, A. M., and Kirkpatrick, C. J., (2006). Biological tolerance of different materials in bulk and nanoparticulate form in a rat model: sarcoma development by nanoparticles. Interface 3:(11):767–775.

Hao, L., Wang, Z., Xing, B., (2009). Effect of sub-acute exposure to TiO_2 nanoparticles on oxidative stress and histopathological changes in Juvenile Carp (*Cyprinus carpio*). Journal of Environmental Sciences 21:(1459–1466).

Hassellöv, M and von der Kammer, F., (2008) Iron Oxides as Geochemical Nanovectors for Metal Transport in Soil-River Systems *Elements*; December 2008; v. 4;(6):(401-406).

Hassellöv, M., Readman, J. W., Ranville, J. F., Tiede, K., (2008). Nanoparticle analysis and characterization methodologies in environmental risk assessment of engineered nanoparticles. Ecotoxicology. 17:(344-361).

Hassellöv, M and Kaegi, R., (2009). Analysis and Characterization of Manufactured NPs in Aquatic Environments (*in Lead and Smith, Environmental and Human Health Impacts of Nanotechnology).* Wiley-Blackwell. ISBN: 978-1-4051-7634-7.

Hartman, N. B., Von der Kammer F, Hofmann T, Baalousha M, Ottofuelling S, Baun A., (2010). Algal testing of titanium dioxide nanoparticles--testing considerations, inhibitory effects and modification of cadmium bioavailability Toxicology. 269;(2-3):(190-7).

He, X., Zhang, H., Ma, Y., Bai, W.,m, Zhang, Z., Lu, K., Ding, Y., Zhao, Y., Chai, Z., (2010). Lung deposition and extrapulmonary translocation of nano-ceria after intratracheal instillation. Nanotechnology 21;(28):(5103).

HEI (Health Effects Institute)., (2001). Evaluation of Human Health Risk from Cerium Added to Diesel Fuel. Communication 9.

Hendee, W. R., and Ritenour, E. R., (2002). Medical Imagering Physics. 4th Edition. Wiley-Liss.

Henderson, R. K., Baker, A., Murphym, K. R., Hambly, A., Stuetz, R. M., Khan, S. J., (2009). Fluorescence as a potential monitoring tool for recycled water systems: A review. Water Research. 43:(4);(863-881).

Herman, G. S., (1999). Characterization of surfdace defects on epitaxial CeO2 (001) films. Surface Science. 437;(1-2):(207-214).

Herrera M, Carrion P, Baca P, Liebana J, Castillo A., (2001). *In vitro* antibacterial activity of glass-ionomer cements. *Microbios* 4:(141-148).

Herschend, B., Baudin, M., Hermansson, K., (2005). Electronic structure of the CeO_2(110) surface oxygen vacancy. Surface Science. 599:(173-186.

Hoecke, K. V., Quik, J. T. K., Mankiewicz-Boczek, J., De Schamphelaere, K. A. C., Elsaesser, A., Van Der Meeren, P., Barnes, C., McKerr, G., Howard, C. V., Van De Meent, D., Rydzynski, K., Dawson, K. A., Salvati, A., Lesniak, A., Lynch, I., Silversmit, G., De Samber, B., Vincze, L., Janssen, C. R., (2009). Fate and Effects of CeO_2 Nanoparticles in Aquatic Ecotoxicity Tests. Environmental Science and Technology. 43;(12):(4537-4546).

Hoek, C., van den., Mann, D. G, Jahns, H. M., (1995). Algae: An introduction to phycology. University of Cambridge Press. ISBN: 0 521 31687 1.

Hoet, P. H. M., Brüske-Hohlfeld, I., Salata, O. V., (2004). Nanoparticles – known and unknown health risks. Journal of Nanobiotechnology. 2;(1):(doi:10.1186/1477-3155-2-12).

Hoo, C. H., Starostin, N., West, P., Mecartney, M. L., (2008). A comparison of atomic force microscopy (AFM) and dynamic light scattering (DLS) methods to characterise nanoparticle size distributions. Journal of Nanoparticle Research. Published on line ISSN: 1572-896X 20th June 2008.

Hsiao, I-L., and Huang, Y-J., (2011). Effects of various physicochemical characteristics on the toxicities of ZnO and TiO2 nanoparticles toward human lung epithelial cells. Science of the Total Environment. 409;(7):(1219-1228).

Hubbard, A., (1995). The Handbook of surface imaging and visualization. CRC Press. ISBN: 0849389119

Hyung, H., Fortner, J. D., Hughes, J. B., Kim, J-H., (2007). Natural Organic Matter Stabilizes carbon Nanotubes in the Aqueous Phase. Environmental Science and Technology. 41;(1):(179-184).

ISO (International Standard)., (1996). Particle size analysis spectroscopy-Photon Correlation. 13321 First Edition. Analyse granulométrique – Spectroscopie par corrélation de photons. Ref: ISO 13321:1996(E).

Ise, N. and Sogami, I. S., (2005). Structure Formation in Solution: Ionic Polymers and Colloidal Particles. Springer, Heidelberg. ISBN: 10 3-540-25271-1

Ispas, C., Andreescu, D., Patel, A., Foia, D. V., Silvana, A., Wallace, K. N., (2009). Toxicity and developmental defects of different sizes and shape nickel nanoparticles in zebrafish. Environmental Science and Technology. 43;(16):(6349-6356).

Israelachvili, J. N., (1985). Intermolecular and surface forces. With application to colloidal and biological systems. London: Academic Press Harcourt Brace Jovanovich 450.

Ivanov, V. K., Fedotov, G. N., Nikulina, M. V., Polezhaeva, O. S., Omel'yanyuk, G. G., Romanenko, S. N., Korol, S. G., Tret'yakov, Y. D., (2008). Biological Activity of Nanocrystalline Cerium Dioxide. Chemistry. 420;(2):(141-143).

Jamers, A., Blust, R., Coen, W. D., (2009). *Omics* in algae: Paving the way for a systems biological understanding of algal stress phenomena? Aquatic Toxicology. 92:(114-121).

Jeon, H. J., Yi, S. C., Oh, S. G., (2003). Preparation and antibacterial effects of Ag–SiO_2 thin films by sol–gel method. Biomaterials. 24:(4921–4928).

Jia, G., Wang, H. F., Yan, L., Wang, X., Pei, R. J., Yan, T., Zhao, Y. L, Guo, Z. B., (2005). Cyto-toxicity of carbon nanomaterials: single-wall nanotubes, multi-wall nanotubes, and fullerene. Environmental Science and Technology. 39:(1378-1383).

Jia , Z., Saha, S., Zhu, H., Li, Y., Misra, H. P. (2010). Spectrofluorometric Measurement of Reduced Glutathione Levels in Human Neuronal Cells. Methods in Redox Signaling. (235-237). ISBN: 1-934854-06-9

Jiang, J., Oberdörster, G., Biswas, P., (2009). Characterization of size, surface charge, and agglomeration state of nanoparticles dispersions for toxicological studies. Journal of Nanoparticle Research. 11:(77-89).

Jiye A,, Trygg, J., Gullberg, J., Johansson, a. I., Jonsson, P., Antti, H., Marklund, S. L., Moritz, T., (2005). Extraction and GC/MS Analysis of the Human Blood Plasma Metabolome. Analytical Chemistry. 77:(8086-8094).

Johnson G. T., and Kyker, G. C., (1961). Fission-Product and Cerium Uptake by Bacteria, Yeasts, and Molds. Journal of Bacteriology. 81;(5):(733–740).

Joner, E. J., Hartnik, T., Amundsen, C. E., (2008). Environmental fate and ecotoxicity of engineered nanoparticles. Stans forurensningstilsyn Norwegian Pollution Control Authority. ISBN: 978-82-7655-540-0.

Jones, G., J., (2001). Tutorial Chemistry Texts. *d*- and *f*- block Chemistry. RSC Publishing. ISBN: 0-85404-637-2

Ju-Nam, Y., Baalousha, M., Cole, P. A., Gaiser, B., Fernandes, T., Hriljac, J., Jepson, M., Stone, V., Tyler, C., Lead, J. R., (2011). Characterization of cerium oxide nanoparticles Part 1: Size measurements. Environmental Toxicology and Chemistry. (In Press).

Ju-Nam, Y., and Lead, J. R., (2008). Manufactured nanoparticles: An overview of their chemistry, interactions and potential environmental implications. Science of the Total Environment. 400:(396-414).

Jullien, R and Botet, R., (1987). Aggregation and fractal aggregates. World scientific Publishing. ISBN: 9971-50-248-8.

Kakkar, R., Mantha, S. V., Radhi, J., Prasad, K., Kalra, J. (1998). Increased oxidative stress in rat liver and pancreas during progression of streptozotocin-induced diabetes. Clinical Science. 94:(623-632).

Kallay, N. and Žalac, S., (2002). Stability of Nanodispersions: A Model for Kinetics of Aggregation of Nanoparticles. Journal of Colloid and Interface Science. 253:(70-76).

Kammer, F., Baborowski, M., Friese, K., (2005). Field-flow fractionation coupled to multi-angle laser light scattering detectors: Application and analytical benefits for the analysis of environmental colloids. Annalytica Chimic Acta. 552:(166-174).

Karakoti, A.S., Monteiro-Riviere, N. A., Aggarwal, R., Davis, J. P., Narayan, r. J., Self, T., McGinnis, J., Seal, S., (2008). Nanoceria as Antioxidant: Synthesis and Biomedical Applications Jounral of Medicine. 1;(60):(3): 33–37.

Karlsson, H. L., Gustafsson, J., Cronholm, P., Möller, L., (2009). Size-dependent toxicity of metal oxide particles–A comparison between nano- and micrometer size. Toxicology Letters. 188:(112-118).

Kashiwada, S., (2006). Distribution of Nanoparticles in the See-through Medaka (*Oryzias Iatipes*). Environmental Health Perspectives. 114;(11):(1697-1702).

Kaszuba, M., McKnight, D., Connah, M. T., McNeil-Watson, F. K., Nobbmann, U., (2008). Measuring sub nanometre sizes using dynamic light scattering. Journal of Nanoparticle Research. 10:(823-829).

Khawaja, E. E., Durrani, S. M. A., Al-Kuhaili, M. F., (2003). Determination of average refractive index of thin CeO_2 films with large inhomogeneities. Journal of Physics D: Applied Physics. 36:(545-551).

Khoo, S. H. G., and Al-Rubeai, M., (2007). Chapter 8: Metabolomics: an emerging tool for understanding metabolic systems. *In Al-Rubeai, M., and Fussenegger, M., (eds) Systems Biology*. (237-273).

Klaine, S., J., Alvarez, P. J. J., Batley, G. E., Fernandes, T. F., Handy, R. D., Lyon, D. Y., Mahendra, S., McLaughlin, M. J., Lead, J. R., (2008). Critical review: Nanomaterials in the environment: Behaviour, fate, bioavailability and effects. Environmental Toxicology and Chemistry. 27; 9:(1825-1851).

Klaine, S. J., (2009), Considerations for research on the environmental fate and effects of nanoparticles. Environmental Toxicology and Chemistry, 28: 1787–1788. doi: 10.1897/09-203.1

Kluender, C., Sans-Pichè, F., Riedl, J., Altenburger, R., Härtig, C., Laue, G., Schmitt-Jansen, M., (2008). A metabolomics approach to assessing phototoxic effects on the green alga *Scenedesmus vacuolatus*. Metabolomics. 5:(1):(59-71).

Korsvik, C., Patil, S., Seal, S., Self, W. T., (2007). Superoxide dismustase mimetic properties exhibited by vacancy engineered ceria nanoparticles. Chemical Communication. 10:(1056-1058).

Koukal B, Rossé P, Reinhardt A, Ferrari B, Wilkinson KJ, Loizeau JL, Dominik J., (2007). Effect of *Pseudokirchneriella subcapitata* (Chlorophyceae) exudates on metal toxicity and colloid aggregation. Water Research. 40;(1):(63-70).

Kroto, H. W., Heath, J. R., O'Brien, S. C., Curl, R. F., Smalley, R. E., (1985). C_{60}: Buckminsterfullerene. Nature. 318:(162-163).

Kuzma, J., (2007). Moving forward responsibility: Oversight for the nanotechnology-biology interface. Journal of Nanoparticle Research. 9:(165-182).

Kydd, R., Scott, J., Teoh, W. Y., Chiang, K., Amal, R., (2010). Understanding photocatalytic metallization of pre-adsorbed ionic gold on titania, ceria and zirconia. Langmuir. 26;(3):(2099-2166).

Lakowicz, J. R., (1983). Principles of Fluorescence Spectroscopy. Plenum Press, New York ISBN: 0-306-41285-3

Lakowicz, J. R., (1999). *Principles of Fluorescence Spectroscopy*, Klumer Academic/Plenum Publishers, 2nd Edition, 0-306-46093-9, New York, USA.

Lanone, S., Rogerieux, F., Geys, J., Dupont, A., Maillot-Marechal, E., Boczkowski, J., Lacroix, G., Hoet, P., (2009). Comparative toxicity of 24 manufactured nanoparticles in human alveolar epithelial and macrophage cell lines. Particle and Fibre Toxicology. 6:14.

Lauwerys, R., (1998). Chapter 27: Biological Monitoring. (Ed. Stellman, J. M. Encyclopaedia of occupational health and safety. International Labour Office, Geneva, Fourth Edition). 1;(5):(27.2-).

Lead, J. R., and Wilkinson, K. J., (2006). Aquatic colloids and nanoparticles: current knowledge and future trends. Environmental Chemistry. 3(3) 159-171.

Lecoanet, H. F., Bottero, J-Y., Wiesner, M. R., (2004). Laboratory Assessment of the Mobility of Nanomaterials in Porous Media. Environmental Science and Technology. 38;(19):(5164-5169).

Lee, D. Y., and Fiehn, O., (2008). High quality metabolomic data for Chlamydomonas reinhardtii. Plant Methods. 4:7.

Lee. W-M., An, Y-J., Yoon, H., Kweon, H-S. (2008). Toxicity and bioavailability of copper nanoparticles to the terrestrial plants mung bean (*Phaseolus radiatus*) and wheat (*Triticum aestivum*): Plant agar test for water-insoluble nanoparticle. Environmental Toxicology and Chemistry. 9:(27):(1915-1921).

Leppard, .G. G., (1995). Evaluation of electron microscope techniques for the description of aquatic colloids. In: J. Buffle and H.P. van Leeuwen, Editors, *Environmental Particles: I*, Lewis, Chelsea, Mich. (1992), pp. 231–289.

Limbach. L. K., Li. Y., Grass, R. N., Brunner, T. J., Hintermann, M. A., Muller, M., Gunther, D., Stark, W. J., (2005). Oxide Nanoparticle Uptake in Human Lung Fibroblasts: Effects of Particle Size, Agglomeration, and Diffusion at Low Concentrations. Journal of Environment, Science and Technology. 39:(9370-9376).

Lin, Y, L., Chiou, C. S., Kumar, S, K., Lin, J-J., Sheng, Y-J., Tsao, H-K., (2011). Self-Assembled Superstructures of Polymer-Grafted Nanoparticles: Effects of Particle Shape and Matrix Polymer. Journal of Physical Chemistry C. 115;(13):(5566-5577).

Lin, W., Huang, Y-W., Zhou, X-D., Ma, Y., (2006). Toxicity of cerium oxide nanoparticles in human lung cancer cells. International journal of toxicology, 25;(6):(451-457).

Linkov, I., Satterstrom, F. K., Steevens, J., Ferguson, E., Pleus, R. C., (2007). Multi-criteria decision analysis and environmental risk assessment for nanomaterials. Journal of Nanoscience Research. 9;(4):(543-554).

Liu, R., Lead, J. R., Baker, A., (2007). Fluorescence characterisation of cross flow ultrafiltration derived freshwater colloidal and dissolved organic matter. Chemosphere 68: (7)1304-1311.

Liu, X., Yin, S., Sato, T., (2009). Synthesis and UV-Shielding Characterization of Plate-Like Titanate/Calcia-Doped Ceria Composite. IOP Conf. Series: Materials Science and Engineering 1:(012013).

Lodhia, J., Mandarano, G., Ferris, N. J., Eu, P., Cowell, S. F. (2010) Development and use of iron oxide nanoparticles (Part 1):Synthesis of iron oxide nanoparticles for MRI. Biomedical Imaging and Intervention Journal. *6(2):e12*

Loutfy, R. O., Lowe, T. P., Moravsky, A. P., Katagiri, S., (2002). Commercial production of fullerenes and carbon nanotubes. In Perspectives of fullerene nanotechnology. Springer, Netherlands, pp. 35-46.

Lovern, S. B., and Klaper, R., (2006). *Daphnia magna* Mortality When Exposed to Titanium Dioxide and Fullerene (C_{60}) Nanoparticles. Environmental Toxicology and Chemistry. 25;(4):(1132-1137).

Lovern, S. B., Strickler, J. R., Klaper, R., (2007). Behavioural and Physiological Changes in *Daphnia magna* when Exposed to Nanoparticle Suspensions (Titanium Dioxide, Nano-C_{60} and $C_{60}H_xC_{70}H_x$). Environmental Science and Technology. 41:(4465-4470).

Lubick, N., (2007). Spoonful of Caution with Nano Hype. Interview. Environmental Science and Technology. 41;(8):(2661-2665).

Luther, G. W., and Rickard, D. T., (2003). Metal Sulfide Cluster Complexes and Their biogeochemical Improtance in the Environment. Journal of Nanoparticle Research. 7;(4-5):(389-407).

Lyon, D. Y., Adams, L. K., Falkner, J. C., Alvarez, P. J. J., (2006). Antibacterial Activity of Fullerene Water Suspensions: Effects of Preparation Method and Particle Size. Environmental Science and Technology. 40;(14):(4360-4366).

Ma, J., Wang, P., Chen, J., Sun, Y., Che, J., (2007). Differential Response of Green Algal Species *Pseudokirchneriella subcapitata*, *Scenedesmus quadricauda*, *Scenedesmus obliquus*, *Chlorella vulgaris* and *Chlorella pyrenoidosa* to Six Pesticides. Polish Journal of Environmental Studies. 16;(6):(847-851).

Madden, A. S., and Hochella, M. F., (2005). A test of geochemical reactivity as a function of mineral size: manganese oxidation promoted by hematite nanoparticles. Geochim. Cosmochim. Acta 69, 389e398.

Makino, K., Fukai, F, Hirata, S., Hiroyuki, O., (1996). Electro-osmotic studies of endothelial cell surface. Colloids and Surfaces B: Biointerfaces. 7:(235-238).

Malvern., (1997). Malvern Instruments Ltd. Sample dispersion and refractive index guide. MAN 0079 Version 3.1.

Mann, J., (1987). Secondary Metabolism: 2nd Edition. Oxford Science Publications.

Masciangioli, T., and Zhang, W.-T., (2003). Environmental Technologies at the Nanoscale. Environmental Science and Technology. 37(5):102A-108A.

Masui, T., Hirai, H., Hamada, R., Imanaka, N., Adachi, G-y., Sakatac, T., Moric, H., (2003). Synthesis and characterization of cerium oxide nanoparticles coated with turbostratic boron nitride. Journal of materials science 13:(622–627).

Masui, T., Hirai, H, Imanaka, N., Adachi, G., Sakata, T., Mori, H., (2002). Synthesis of cerium oxide nanoparticles by hydrothermal crystallisation with citric acid. Journal of Materials Science Letters. 21:(489-491).

Mavrocordatos, D., Perret, D., Leppard, G. G., (2007).Strategies and Advances in the Characterization of Environmental Colloids by Electron Microscopy. *In* Wilkinson, K. J., and Lead, J. R. Environmental Colloids and Particles. IUPAC.

Mayer, P., Frickmann, J., Christican, E. R., Nyholm, N., (1998). Influence of Grwoth Conditions on the results obtained in algal toxicity tests. Environmental Toxicology and Chemistry. 17;(6):(1091-1098).

Maynard, A. D. (2009). Ten things everyone should know about nanotechnology safety. 2020 Science. Viewed at http://2020science.org/2009/08/29/10things/

Maynard, A. D. (2006). Nanotechnology: A research strategy for addressing risk, PEN 03 Washington DC,, Woodrow Wilson International Center for Scholars. Project on Emerging Nanotechnologies. Viewed 19 July 2010. http://www.tinhoahoc.com/Nanotechnology/RiskRelatedResearch_Maynard_7-06-Final.pdf

McKelvie, J. R., Yuk, J., Xu, Y., Simpson, A. J., Simpson, M. J., (2009). H NMR and GC/MS metabolomics of earthworm responses to sub-lethal DDT and endosulfan exposure. Metabolomics. 5:84–94

Mermet, J. M. (1987). Induc*tively Coupled Plasma Emission Spectroscopy-Part 2*; (Boumans, P. W. J. M., Ed.) Wiley-Interscience: New York. 90:(353– 386).

Molot, L. A., Li, G., Findlay, D. L., Watson, S. B., (2010). Iron-mediated suppression of bloom-forming cyanobacteria by oxine in a eutrophic lake. Freshwater Biology. 55:(1102-1117).

Morimoto, T., Tomonaga, H., Mitani, A., (1999). Ultraviolet ray absorbing coatings on glass fo automobiles. Thin Solid Films. 351;(61-65).
Morones, J. R., Elechiguerra, J. L., Camacho, A., Holt, K., Kouri, J. B., Ramírez, J. T., and Yacaman, M. J., (2005). The bactericidal effects of silver nanoparticles. Nanotechnology. 16:(2346-2353).

Mowrey, R. C., Brenner, D. W., Dunlap, B., Mintmire, J. W., White, C. T., (1991). Simulation of Cbo Collisions with a Hydrogen-Terminated Diamond {111) Surface. The Journal of Physical Chemistry. 95;(19):(7138-7142).

Müller, N., (2007). Nanoparticles in the Environment; Risk Assessment based on Exposure-Modelling: What concentrations of nano titanium dioxide, carbon nanotubes and nano silver are we exposed to? Diploma thesis, accessed online at: http://e-collection.ethbib.ethz.ch/eserv/eth:30071/eth-30071-01.pdf January 2011.

Mueller, N., and Nowack, B., (2008). Exposure modelling of engineered nanoparticles in the environment. Environmental Science and Technology. 42:(4447-4453).

Mulholland, G. W., and Bauer, B. J., (2000). Nanometer calibration particles: what is available and what is needed? Journal of Nanoparticle Research. 2:(5-15).

Munkegaard, M., Abbaspoor, M., Cedergreen, N., (2008). Organophosphorous insecticides as herbicide synergists on the green algae *Pseudokirchneriella subcapitata* and the aquatic plant *Lemna minor*. Ecotoxicology. 17:(29-35).

Murray, C. B., Kagan, C. R., Bawendi, M. G., (2000). Synthesis and Characterisation of Monodisperse Nanocrystals and Close-Packed Nanocrystal Assemblies. Annual Review Material Science. 30:(545-610).

Nam, J. M., Thaxton, C. S., Mirkin, C. A., (2003). Nanoparticle-based bio-bar codes for the ultrasensitive detection of proteins. Science 301:(1884–1886).

Navarro, E., Baun, A., Behra, R., Hartmann, N. B., Filser, J., Miao, A-J., Quigg, A., Santschi, P. H., Sigg, L., (2008). Environmental behaviour and ecotoxicity of engineered nanoparticles to algae, plants and fungi. Ecotoxicology. 17:(372-386).

Nel, A. Xia, T. Madler, L. Li, N., (2006). Toxic potential of materials at the nanolevel. Science. 311:(622-627).

Nemmar, A., Vanbilloen, H., Hoylaerts, M. F., Hoet, P. H. M., Verbruggen, A., Nemery, B., (2001) Passage of Intratracheally Instilled Ultrafine Particles from the Lung into the Systemic Circulation in Hamster American Journal of Respiratory and Critical Care Medicine. 164;(9):(1665-1668).

NNI (National Nanoparticle Initiate)., (2011). Viewed online http://www.nano.gov/

Nobel Prize., (2010). View at http://nobelprize.org/nobel_prizes/physics/laureates/2010/

Novoselov, K. S., Geim, A. K., Morozov, S. V., Jiang, D., Zhang, Y., Dubonos, S.V., Grigorieva, I. V. and Firsov, A. A., (2004). Electric Field Effect in Atomically Thin Carbon Films, Science 306(5696): 666–669.

Nowack, B., and Bucheli, T. D., (2007). Occurrence, behaviour and effects of nanoparticles in the environment. Environmental Pollution. 15:(5-22).

Oberdörster, E., Zhu, S., Blickley, M. T., McClellan-Green, P., Haasch, M. L., (2006). Ecotoxicology of carbon-based engineered nanoparticles: Effects of fullerene (C_{60}) on aquatic organisms. Carbon. 44:(1112-1120).

Oberdörster, G., Oberdörster, E., and Oberdörster, J., (2005). Nanotoxicology: An Emerging Discipline Evolving from Studies of Ultrafine Particles. Environmental Health Perspectives. 113;(7):(823-839).

Oberdörster, G., Sharp, Z., Atudorei, V., Elder, A., Gelein, R., Kreyling, W., Cox, C., (2004). Translocation of inhaled ultrafine particles to the brain. Inhalation toxicology. 16(6-7):437-45.

Oberdörster, G., Ferin, J., Gelein, R., Soderholm, S. C., Finkelstein, J., (1992). Role of the Alveolar Macrophage in Lung Injury: Studies with Ultrafine Particles. Environmental Health Perspectives. 97:(193-199).

OECD (Organisation of Economic Cooperation and Development)., (1984). Algal growth inhibition test. OECD guideline for testing of chemicals 201. Paris: Organisation of Economic Cooperation and Development.

OECD., (2002). Guidelines for testing of chemicals section 4: Other test guidelines. OECD publishing.

OECD., (2008). Environment Directorate Joint Meeting of the Chemicals committee and The Working Party on Chemicals, Pesticides and biotechnology Series on The Safety of Manufactured Nanomaterials. Number 6; List of Endpoints for Phase one of the OECD Testing Programme. Viewed http://www.oecd.org/officialdocuments/displaydocumentpdf/

Ofir, E., Oren, Y., Adin, A., (2007). Electrohflocculation: the effect of zeta-potential on particle size. Desalination. 204:(33-38).

Ohshima, H., (1995). Electrophoretic mobility of soft particles. Colloids and Surfaces A: Physicochemical and Engineering Aspects. 103:(249-255).

Ohshima, H., (2002). Electrophoretic mobility of a charged spherical colloidal particle covered with an uncharged polymer layer. Electrophoresis. 23:(1993-2000).

O'Melia, C. R., (1980). Aquasols: The behaviour of small particles in aquatic systems. Environmental Science and Technology. 14;(9):(1052-1060).

O'Melia C. R., (1995). From Algae to Aquifers: Solid-Liquid Separation in Aquatic Systems. Aquatic Chemistry; Advances in Chemistry. (244:(314-337). ISBN13: 9780841229211

Oxonica., (2005). Catalysis: Catalytic Function of Cerium Oxide. [Online] www.oxonica.com/_get_file.php?file=15_1 catalysis.pdf&cat=promo_lit [accessed 19 November 2007]

Oxonica., (2003). Cerulean's Nanocatalyst Technology, Envirox www.oxonica.com/products/envirox.htm

Palmer, S., (2007). The Nano Diet. Focus. April Edition. 175:(39-42).

Pan, J. R., Huang, C., Chuang, Y-C., Wu, C-C., (1998). Dewatering characteristics of algae-containing alum sludge. Colloids and surfaces A. Physicochemical and Engineering Aspects. 150:(185-190).

Park, B., (2007). 'Current and Future Applications of Nanotechnology', in Hester, R. E., and Harrison, R. M. (ed.) *Nanotechnology: consequences for Human Health and the Environment. Issues in Environmental Science and Technology.* RCS Publishing.

Park, E.J., Choi, J., Park, Y. K., Park, K., (2008). Oxidative stress induced by cerium oxide nanoparticles in cultured BEAS-2B cells. Journal of Toxicology 12;245(1-2):90-100.

Park, B., Martin, P., Harris, C., Guest, R., Whittingham, A., Jenkinson, P., Handley, J., (2007). Initial in vitro screening approach to investigate the potential health and environmental hazards of Envirox^{TM} - a nanoparticulate cerium oxide diesel fuel additive. Particle and Fibre Toxicology. 4;(1):(12).

Pecora, R., (2000). Dynamic light scattering measurement of nanometer particles in liquids. Journal of Nanoparticle Research. 2:(123-131).

Pelley, A. J., and Tufenkji, N., (2008). Effect of particle size and natural organic matter on the migration of nano- and microscale latex particles in saturated porous media. Journal of Colloid and Interface Science. 321:(74-83).

Pereira, M. J, Resende, P., Azeiteiro, U. M, Oliveira, J., Figueiredo, D. R., (2005) Differences in the effects of metals on growth of two freshwater green algae. Bull Envrion Contam Toxicol 75:(515–522).

Perez, J.M., Asati, A., Nath, S., Kaittanis, C., (2008). Synthesis of biocompatible dextran-coated nanoceria with pH-dependent antioxidant properties. Small. 2008 May;4(5):552-6.

Peters, R., (2000). Fiber optic Device for Detecting the Scattered Light or Fluorescent Light from a Suspension. United States Patent 6,016,195.

Phenrat, T., Saleh, N., Sirk, K., Tilton, R. D., and Lowry, G. V., (2007). Aggregation and Sedimentation of Aqueous Nanoscale Zerovalent Iron Dispersions. Environmental Science and Technology. 41:(284-290).

Pierscionek, B. K., Li, Y., Yasseen, A. A., Colhoun, L. M., Schachar, R. A., Chen, W., (2011). Nanoceria have no genotoxic effect on human lens epithelial cells. Nanotechnology 21.

Pike, J., Chan, S-W., Zhang, F., Wang, X., Hanson, J., (2006). Formation of stable Cu_2O from reductions of CuO nanoparticles. Applied Catalysis A: General. 3030:(273-277).

Porter, A. E., Gass, M., Muller, K., Skepper, J. N., Midgley, P., Welland, M., (2007). Visualising the Uptake of C_{60} to the Cytoplasm and Nucleus of Human Monocyte-Derived Macrophage Cells Using Energy-Filtered Transmission Electron Microscopy and Electron Tomography. Environmental Science and Technology. 41;(8):(3012-2017).

Powers, K. W., Brown, S. C, Krishna, V. B., Wasdo, S.C., Moudgil, B. M., Roberts, S. M., (2006). FORUM SERIES: Research Strategies for Safety Evaluation of Nanomaterials. Part VI. Characterization of Nanoscale Particles for Toxicological Evaluation. Toxicological Sciences. 90;(2):(296-303).

Prospect., (2010). Toxiological Review of Nano Cerium Oxide. Viewed at http://www.nanotechia-prospect.org/managed_assets/files/prospect_nano-ceo2_literature_review.pdf

Purves, D., Augustine, G. J., Fitzpatrick, D., Katz, L. C., LaMantia, A-S., McNamara, J. O., Wiliams, S. M. (2001). Neuroscience (2nd ed.) Chapter 4: Channels and Transporters. Sinauer Associates Publishers. ISBN-10: 0-87893-742-0.

Qu, F., Oliveira, R. H., Morais, P. C., (2004). Effects of nanocrystal shape on the surface charge density of ionic colloidal nanoparticles. Journal of Magnetism and Magnetic Material. 272-276:(1668-1669).

Quintanilla-Carvajal, M.X., Camacho-Dı´az, b. H., Meraz-Torres, L. S., Chanona-Pe´rez, J. J., Alamilla-Beltra´n, L., Jimene´z-Aparicio, A., Gutie´rrez-Lo´pez, G. F., (2010) Nanoencapsulation: A New Trend in Food Engineering Processing. Food Engineering Reviews. 2:(39–50).

Rao, A. V., and Rao, L. G., (2007) Carotenoids and human health. Pharmacology Research. 55:(207–216).

Rappoport, J. Z., Preece, J., Chipman, K. (2011). How do Manufactured Nanoparticles Enter Cells? Description for a problem studied at the UK Mathematics-in-Medicine Study Group Reading 2011. Viewed online: October 2011. < http://www.maths-in-medicine.org/uk/2011/nanoparticles/

Raven (2001). Algal Metabolism. ENCYCLOPEDIA OF LIFE SCIENCES, John Wiley & Sons, Ltd. www.els.net DOI: 10.1038/npg.els.0000321

RCEP (Royal commission on environmental pollution)., (2008). Twenty-seventh Report: Novel Materials in the Environment: The case of nanotechnology. Viewed online at http://www.official-documents.gov.uk/document/cm74/7468/7468.pdf.

Reimann, C., Siewers, U., Skarphagen, H., Banks, D., (1999). Do bottle type and acid washing influence trace element analyses by ICP-MS on water samples ? - A test covering 62 elements and four bottle types (high density polyethene (HDPE), polypropene (PP), fluorinated ethene propene copolymer (FEP) and perfluoralkoxy polymer (PFA)). The Science of the Total Environment. 239:(111-130).

Reeves, J. F., Davies, S. J., Dodd, N. J. F., Jha, A. N., (2008). Hydroxyl radicals (.OH) are associated with titanium dioxide (TiO2) nanoparticle-induced cytotoxicity and oxidative DNA changes in fish cells. Mutation Research/Fundamental and Molecular Mechanisms of Mutagenesis. 640;(1-2):(113-122).

Requicha, A. A. G., Arbuckle, D. J., Mokaberi, B., Yun, J., (2009). Algorithms and Software for Nanomanipulation with Atomic Force Microscopes. The International Journal of Robotics Research. 2;(4):(512-522).

Roa, G. R., and Sahu, H. R., (2001). XRD and UV-Vis diffuse reflectance anlaysis of CeO_2-ZrO_2 solid solutions synthesized by combustion method. Journal of Chemcial Sciences. 113;(5-6):(651-658).

Robichaud, C. O., Tanzil, D., Weilenmann, U., Wiesner, M. R., (2005). Relative Risk Analysis of Several Manufactured Nanomaterials: An Insurance Industry Context. Environmental Science and Technology. 39:(8985-8994).

Rodea-Palomares I, Boltes K, Fernández-Piñas F, Leganés F, García-Calvo E, Santiago J, Rosal R., (2011). Physicochemical characterization and ecotoxicological assessment of CeO2 nanoparticles using two aquatic microorganisms. Toxicological Science. 119(1):(135-45).

Roessner, U and Bowne, J., (2009). What is metabolomics all about? BioTechniques Special Issue. (46);(5):(363–365).

Rogers, N. J., Franklin, N. M., Apte, S. C., Batley, G. E., Lead, J. R., Baalousha, M**.,** (2010). Physico-chemical behaviour and toxicity to algae of nanoparticulate CeO_2 in freshwater. Environ.Chem. 7:(50-60).

Roh, J. Y., Park, Y. K., Choi, J., (2010). Ecotoxicological investigation of CeO_2 and TiO_2 nanoparticles the soil nematode *Caenorhabditis elegans* using gene expression, growth, fertility, and survival as endpoints. Environmental Toxicololology and Pharmacololgy.*29:*(*167-172).*

RSRAEN (The Royal Society and Royal Academy of Engineering Nanotechnology)., (2004). Nanoscience and nanotechnologies: opportunities and uncertainties. http://www.nanotec.org.uk/ viewed 4 December 2007.

Rzigalinski, B. A., Meehan, K., Davis, R. M., Xu, Y., Miles, w. C., Cohen, C. A., (2006). Radical nanomedicine. Nanomedicin*e* 4:(399–412).

Savage, N., and Diallo, M. S., (2005). Nanomaterials and water purification: Opportunities and challenges. Journal of Nanoparticle Research. 7:(331-342).

Sayes, C. M., Fortner, J. D., Guo, W., Lyon, D., Boyd, A. M., Ausman, K. D., Tao, Y. J., Sitharaman, B., Wilson, L. J., Hughes, J. B., West, J. L., Colvin, V. L., (2004). The differential cytotoxicity of water-soluble fullerenes. Nano Letters. 4;(10):(1881–1887).

Schamphelaere, K. A. C., Vasconcelos, F. M., Heijerick, D. G., Tack, F. M. G., Delbeke, K., Allen, H. E., Janssen, C. R., (2003). Development and field validation of a predictive copper toxicity model for the green alga *Pseudokirchneriella subcapitata.* Environmental Toxcioligy and Chemsitry. 22;(10):(2454-2465).

Scheffer, A., Engelhard, C., Sperling, M., Buscher, W., (2007). ICP-MS as a new tool for the determination of gold nanoparticles in bioanalytical applications. Analytical and Bioanalytical Chemistry. 390;(1):(249-252).

Schubert, D., Dargusch, R., Raitano, J., Chan, S-W., (2006). Cerium and yttrium oxide nanoparticles are neuroprotective. Biochemical and Biophysical Research Communications. 343:(86-91).

Schulte, P. A., and Salamanca-Buentello, F., (2007). Ethical and Scientific Issues of Nanotechnology in the Workplace. Environmental Health Perspectives. 115;(1):(5–12).

SCENIHR (Scientific Committee on Emerging and Newly Identified Health Risks)., (2009). Risk Assessment of Products of Nanotechnologies. European Commission. Viewed online http://ec.europa.eu/health/ph_risk/committees/

Scintag, Inc., (1999). Chapter 7: Basics of X-ray Diffraction. [online] http://epswww.unm.edu/xrd/xrdbasics.pdf. [accessed June 2008].

Scown, T. M., van Aerle, R., Tyler, C. R., (2010). Review: Do engineered nanoparticles pose a significant threat to the aquatic environment? Critical Reviews in Toxicology 40:7, 653-670

Sharma, R., Chandra, B. P., Bisen, D. P., (2010). Effect of Molar concentration on Optical Absorption Spectra of ZnS:Mn Nanoparticles. E-Journal of chemistry. 7(S1), S23-S26.

Shaw, D. J., (1980*).* Introduction to Colloid and Surface Chemistry. 3rd edtiion. Butterworths,

Shieh, J-N., Chao, M-R., Chen, C-Y., (2001). Statistical comparisons of the no-observed-effect concntration and the effective concntratino at 10% inhibition (EC10) in algal toxicity tests. Water Science and Technology. 43;(2):(141-146).

Sierra, M. M. D., Giovanela, M., Parlanti, E., Soriano-Sierra, E. J., (2005). Fluorescence fingerprint of fulvic and humic acids form varied origins as viewed by single-scan and excitation/emission matrix techniques. Chemosphere. 58:(715-733).

Slistan-Grijalva, A., Herrera-Urbina, R., Rivas-Silva, J. F., Ávalos-Borja, M., Castillón-Barraza, F. F., Posada-Amarillas, A., (2005). Classical theoretical characterization of the surface plasmon absorption band for silver spherical nanoparticles suspended in water and ethylene glycol. Physica E. 27:(104-112).

Silva, G. A., (2006). Seeing the benefits of ceria. Nature Nanotechnology. 1:(92-94).

Silver, S., (2003). Bacterial silver resistance: molecular biology and uses and misuses of silver compounds. FEMS Microbial Reviews 27:(341-353).

Simakov, S. A., and Tsur, Y., (2007). Surface stabilisation of nano-sized titanium dioxide: improving the colloidal stability and sintering morphology. Journal of Nanoparticle Research 9:(403-417).

Singleton, H. J., (1989). Ambient Water Quality Criteria for Chlorine. Water Management Branch, BC Ministry of Environment. Victoria, BC.

Skorodumova, N. V., Ahuja, R., Simak, S. I., Abrikosov, I. A., Johansson, B., Lundqvist, B. I., (2001). Electronic, bonding, and optical properties of CeO_2 and Ce_2O_3 from first principals. Physical Review B. 64:(115108-1).

Sobek, J. M., and Talburt, D. E., (1968). Effects of the Rare Earth Cerium on *Escherichia coli.* Journal of Bacteriology. 95;(1):(47-51).

South, G. R., and Whittick, A., (1987). Introduction to Phycology. Blackwell Scientific Publications. ISBN: 0-632-01769-4

Spencer, R. G. M., Bolton, L., Baker, A., (2007). Freeze/thaw and pH effects on freshwater dissolved organic matter fluorescence and absorbance properties from a number of UK locations. Water Research. 41:(2941-2950).

Stauber, J. L., Franklin, N. M., Adams, M. S., (2005). 'Microalgal toxicity tests using flow cytometry'. In: *Small-scale Freshwater Environment Toxicity Test Methods* Blaise, C. and Ferard, J. F. (eds). Kluwer Academic Publishers. 978-1-4020-3119-9

Stoimenov, P. K., Klinger, R. L., Marchin, G. L., Klabunde, K. J., (2002). Metal Oxide Nanoparticles as Bactericidal Agents. Langmuir. 18:(6679-6686).

Stumm, W., and Morgan, J. J., (1996). Aquatic Chemistry. Chemical equilibria and rates in natural waters (Third edition), John Wiley & Sons, Inc (pp. 284).

Sun, X-C., Toledo, J. A., Cui, Z. L., Zhang, Z. K., (2001). Synthesis and structure of magnetic core-shell Ni-Ce nanocomposite particles. Journal of nanoparticle research 3:325-328.

Suttiponparnit, K., Jiang, J., Sahu, M., Suvachittanont, S., Charinpanitkul, T., Biswas, P., (2011). Role of Surface Area, Primary Particle Size, and Crystal Phase on Titanium Dioxide Nanoparticle Dispersion Properties. Nanoscale Research Letters. **6**:27

Suzuki, T., Kosacki, I., Anderson, H. U., (2002). Microstructure-electrical conductivity relationships in nanocrystalline ceria thin films. Solid State Ionics. 151;(1-4):(111-121).
Swinehart, D. F. (1962). The Beer-Lambert Law. Journal of chemical Education. 39;(7):(333-335).

Sydlik, U., Gallitz, I., Albrecht, C., Abel, J., Krutmann, J., Unfried, K., (2009). The Compatible Solute Ectoine Protects against Nanoparticle-induced Neutrophilic Lung Inflammation. American Journal of Respiratory Critical Care. 180;(1):(29-35).

Sze, A., Erickson, D., Ren, L., Li, D., (2003). Zeta-potential measurement using the Smoluchowski equation and the slope of the current-time relationship in electroosmotic flow. Journal of Colloidal and Interface Science. 261:(402-410).

Tago, T., Tashiro, S., Hashimoto, Y., Wakabayashi, K., Kishida, M., (2003). Synthesis and optical properties of SiO_2-coated CeO_2 nanoparticles. Journal of Nanoparticle research. 5:(55-60).

Tang, Y. J. J., Ashcroft, J. M., Chen, D., Min, G. W., Kim, C. H., Murkhejee, B., Larabell, C., Keasling, J. D,. Chen, F. Q. F., (2007). Charge-associated effects of fullerene derivatives on microbial structural integrity and central metabolism. Nano Letters. 7:(754–60).

Tarantola, M., Pietuch, A., Schnider, D., Rother, J., Sunnick, E., Rosman, C., Pierrat, S., Sonnichsen, C., Wegener, J., Janshoff, A.. (2010). Toxicity of gold-nanoparticles: Synergistic effects of shape and surface functionalization on micromotility of epithelial cells. 5;(2):(254-268).

Tarnuzzer, R. W., Colon, J., Patil, S., Seal, S., (2005). Vacancy Engineered Ceria Nanostructures for Protection from Radiation-Induced Cellular Damage *Nano Letters. 5:* (12):(2573–2577).

Thill, A., Zeyons, O., Spalla, O., Chauvat, F., Rose, J., Auffan, M., Flank, A. M., (2006). Cytotoxicity of CeO_2 Nanoparticles for Escherichia coli. Physico-Chemical insight of the Cytotoxicity Mechanism. Environmental Science and Technology. 40: (6151-6156).

Thomas, M. J. K., (1996). Analytical Chemistry by Open Learning – Ultraviolet and Visible Spectroscopy. Second Edition. University of Greenwich UK, John Wiley and Sons, Ltd., England.

Tiede, K., Hassellöv, M., Breitbarth, E., Chaudhry, Q., Boxall, A. B. A., (2009). Considerations for environmental fate and ecotoxicity testing to support environmental risk assessments for engineered nanoparticles. Journal of chromatography A. 1216:(503-509).

Tillmann, P., (2004). Stability of Silver Nanoparticles in Aqueous and Organic Media. NNIN REU Research Accomplishments. (140-141).

Tinkle, A., S., (2008). Nanotechnology: Collaborative opportunities for ecotoxicology and environmental health, Editorial. Environmental Toxicology and Chemistry. 27;(9):(1823-1824).

Tkachenko, A. G., Xie, H., Coleman, D., Glomm, W., Ryan, J., Anderson, M. F., Franzen, S., Feldheim, D. L., (2003). Multifunctional gold nanoparticle-peptide complexes for nuclear targeting. Journal of the American Chemical Society. 125;(16):(4700-1).

Tong, Z., Bischoff, M., Nies, L., Applegate, B., Turco, R. F., (2007). Impact of Fullerene (C_{60}) on a Soil Microbial Community. Environmental Science and Technology. 41:(2985-2991).

UNECE (United Nations Economic Commission for Europe)., (2004). Globally Harmonized System of classification and labeling of chemicals (GHS). Annex 8, Guidance on hazards to the aquatic environment. Viewed; http://live.unece.org/trans/danger/publi/ghs/ghs_rev00/00files_e.html

Usenko, C. Y., Harper, S. L., Tanguay, R. L., (2008). Fullerene C_{60} exposure elicits an oxidative stress response in embryonic zebrafish. Toxicology and Applied Pharmacology.

USEPA (United States Environmental Protection Agency)., (2007). Final Nanotechnology White Paper. Viewed online at http://www.epa.gov/osa/pdfs/nanotech/epa-nanotechnology-whitepaper-0207.pdf

Vanderborough, N. E., and Buyers, A. G., (1974). Phosphate Removal by Algal Systems. Journal - Water Pollution Control Federation. 46;(4):(726 -734).

Verwey, E. J. W., (1947). Theory of the Stability of Lyophobic Colloids. The Journal of Physical and Colloid Chemistry. 51;(3):(631-636).

Viant, M. R., Bearden, D. W., Bundy, J. G., Burton, I. W., Collette, T. W., Ekman, D. R., Ezernieks, V., Karakach, T. K., Lin, C. Y., Rochfort, S., De Ropp, J. S., Teng, Q., Tjeerdema, R. S., Walter, J. A., Wu, H. (2009). International NMR-Based Environmental Metabolomics Intercomparison Exercise. Environmental Science and Technology. 43:(219-225).

Viant, M. R., Pincetich, C. A., Hinton, D. E., Tjeerdema, R. S. (2006a) Toxic actions of dinoseb in medaka *(Oryzias latipes)* embryos as determined by *in vivo* 31P NMR, HPLCUV and 1H NMR metabolomics. Aquatic Toxicology 76: 329–342

Viant, M. R., Pincetich, C. A., Tjeerdema, R. S., (2006b). Metabolic effects of dinoseb, diazinon and esfenvalerate in eyed eggs and alevins of chinook salmon *(Oncorhynchus tshawytscha)* determined by 1H NMR metabolomics. Aquatic Toxicology. 77:(359–371).

Viant, M. R. Rosenblum, E. S., Tjeerdema, R. S., (2003). NMR-based metabolomics: A powerful approach for characterizing the effects of environmental stressors on organism health. Environmental Science and Technology. 37:(4982-4989).

Villas-Bôas, S. G., Nielsen, J., Smedsgaard, J., Hansen, M. A. E., Roessner-Tunali, U., (2007). Metabolome Analysis: An Introduction. John Wiley & Sons, Inc. Hoboken

Vonderheide, A. P., Zoriy, M. V., Izmer, A. V., Muller, C., Pickhardt, C., Caruso, J. A., Ostapczuk, P., Becker, J. S., (2004). Investigation of Inductively Coupled Plasma Mass Spectrometry for the Determination of Ultratrace Radioactive Strontium in Urine Samples. Journal of Atomic Analytical Spectrometry. 19:(675-680).

Wamkam, C. T., Opoku, M. K., Hong, H., Smith, P., (2011). Effects of pH on heat transfer nanofluids containing ZrO2 and TiO2 nanoparticles. Journal of applied physics [0021-8979vol:109 iss:2 pg:024305

Wang, Q., Yin, B., Wang, Z., Shen, G., Chen, Y., (2010). Preparation and characterisations of monodisperse ceria microspheres. Engineering Materials. 434-435:(850-852).

Wang, C-Y., BÖttcher, C., Bahnemann, D. W., Dohrmann, J. K., (2004). In situ electron microscopy investigation of Fe(III)-doped TiO_2 nanoparticles in an aqueous environment. Journal of Nanoparticle Research. 6:(119-122).

Ward, T., Kowalski, P., Boeri, R., (1995). Acute toxicity of N2803-2 to the freshwater alga, *Pseudokirchneriella subcapitata*. Submitted to Office of Pollution Prevention and Toxics, US Environmental Protection Agency, Washington, DC (OPPT Administrative Record AR226-1030a).

Warren, B. E., (1969). X-Ray Diffraction (Ch. 1) X-Ray Scattering by Atoms. (Ch.2) Crystal Axes and the Reciprocal Lattice. (Ch. 13) Diffraction by imperfect Crystals. Addison-Wesley Publishing Company.

Weckwerth, W., Loureiro, M. E., Wenzel, K., Fiehn, O., (2004). Differential metabolic networks unravel th effects of silent plant pheontypes. PNAS. 101;(10):(7809-7814).

Wiesner, M. R., Lowry, G. V., Alvarez, P., Dionysiou, D., (2006). Assessing the Risks of Manufactured Nanomaterials. Environmental Science and Technology. 40;(14):(4336-4345).

Wigginton, N. S., Haus, K. L., Hochella, M. F. Jr., (2007). Aquatic environmental nanoparticles. Journal of Environmental Monitoring 9;(12):(1285-1432).

Wilkinson, K. J., Balnois, E., Leppard, G. G., Buffle, J., (1999). Characteristic features of the major components of freshwater colloidal organic matter revealed by transmission electron and atomic force microcopy. Colloids and Surfaces A: Physicochemical and Engineering Aspects. 155:(287-310).

Xia, T., Kovochick, M., Liong, M., Madler, L., Gilbert, B., Shi, H., Yeh, J. I., Zink, J. I., Nel, A. E., (2008). Comparison of the Mechanism of Toxicity of Zinc Oxide and Cerium Oxide Nanoparticles Based on Dissolution and Oxidative Stress Properties. ACSNano. 2;(10):(2121-2134).

Yamashito, Y., and Tonoue. E., (2003). Chemical characterization of protein-like fluorophores in DOM in relation to aromatic amino acids. Marine Chemistry. 82;(3-4):(255-271).

Yang, A., Woo, T. K., Baudinm M., Hermansson, K., (2004). Atomic and electronic structure of unreduced and reduced CeO_2 surfaces: A first-principles study. Journal of Chemical Physics. 120:(7741-7750).

Yeh, H. J., and Chen, C. Y., (2006). Toxicity assessment of pesticides to *Pseudokirchneriella subcapitata* under air-tight test environment. Journal of Hazardous Materials A. 131:(6-12).

Yoshida, H., Mori, Y., Masuda, H., Yamamoto, T., (2009). Particle size measurement of standard reference particle candidates and theoretical estimation of uncertainty region. Advanced Powder Technology. 20:(145-149).

Yuan, X., Schnell, M., Muth, S., Schartl, W., (2008). Cluster Formation and Rheology of Photoreactive Nanoparticle Dispersions. Langmuir. 24;(10):(5299–5305).

Zattoni, A., Reschiglian, P., Montalti, M., Zaccheroni, N., Prodi, L., Picca, R. A., Malitesta, C., (2007). Characterization of titanium dioxide nanoparticles imprinted for tyrosine by flow field-flow fractionation and spectrofluorimetric analysis. Inorganica Chimica Acta. 360:(1063-1071).

Zhang, F., Wang, P., Koberstein, J., Khalid, S., Chan, S-W., (2004). Cerium oxidation state in ceria nanoparticles studied with X-ray photoelectron spectroscopy and absorption near edge spectroscopy. Surface Science. 563:(74-82).

Zhang, F., Chan, S-W., Spanier, J. E., Apak, E., Jin, Q., Robinson, R. D., Herman, I. P., (2002). Cerium oxide nanoparticles: Size-selective formation and structure analysis. Applied Physics Letters. 80;(1):(127-129).

Zhang, H., Gilbert, B., Huang, F., Banfield, J. F., (2003). Water-driven structure transformation of nanoparticles at room temperature. Nature. 424:(1025-1029).

Zhang, J., Wu, J. Y., Rong, L. X., Dong, B. Z., (2005). Temperature Dependence of the Growth of Cerium Oxide Nanoparticles investigated by SAXS and XANES Physica Scripta. T115:(661–663).

Zhou, F., Zhoa, X., Xu, H., Cuant, C., (2007). CeO_2 spherical crystallites synthesis, formation mechanism, size control and electrochemical property study. Journal of Physcial Chemistry C. (4):(1651-1657)

Zhu, S., Oberdörster, E., Haasch, M. L., (2006). Toxicity of an engineered nanoparticle (fullerene, C_{60}) in two aquatic species, *Daphnia* and Fathead minnow. Marine Environmental Research. 62:(S5-S9).

Zhu, X., Zhu, L., Chen, Y., Tian, S., (2009). Acute toxicities of six manufactured nanomaterial suspensions to *Daphnia magna*. Journal of Nanoparticle Research. 11:(67-75).

Zhu, X., Zhu, L., Lang, Y., Chen, Y., (2008). Oxidative Stress and Growth Inhibition in the Freshwater Fish *Carassius auratus* Induced by Chronic Exposure to Sublethal fullerene Aggregates. Environmental Toxicology and Chemistry. 27;(9):(1979-1985).

APPENDIX A
Additional results

CD Rom

APPENDIX B
Published work

Published contributions

Ju-Nam, Y., Baalousha, M., Cole, P. A., Gaiser, B., Fernandes, T., Hriljac, J., Jepson, M., Stone, V., Tyler, C., Lead, J. R. (2011). Characterization of cerium oxide nanoparticles Part 1: Size measurements. Environmental Toxicology and Chemistry. (*In Press*).

Baalousha, M., Ju-Nam, Y., Cole, P. A., Tyler, C., Jones, I., Stone, V., Fernandes, T., Jepson, M., Lead, J. R., Hriljac, J. Characterization of cerium oxide nanoparticles Part II: Non-size measurements. Environmental Toxicology and Chemistry. (*In Press*).

Gaiser, B.K., Fernandes, T.F., Jepson, M.A. Lead, J.R., Tyler, C.R., Baalousha, M., Biswas, A., Britton, G., Cole, P. A., Johnston, B.D., Ju-Nam, Y., Rosenkranz, P., Scown, T.M. & Stone, V. (2011). Interspecies comparisons on the uptake and toxicity of silver and cerium dioxide nanoparticles. Environmental Toxicology and Chemistry. (*In press*).

Goodhead, M., Johnston, B. D., Cole, P. A., Baalousha, M., Iguchi, T., Lead, J. R., Tyler, C. R. (2011). Natural organic matter affects bioavailability in fish of cerium oxide nanomaterials exposed via the water. (*Under construction*).

Merrifield, R., Cole, P. A., Lead, J. R. (2011). Characterisations of synthesized nano-ceria particles in environmentally relevant toxicity test media. (*Under construction*).

Cole, P. A., Merrifield, R., Viant, M., Pettitt, M., Sommer, U., Lead, J. R., (2011). Size dependent toxicity of *Pseudokirchneriella subcapitata* to discrete synthesized nano-ceria particles using a metabolic approach. (*Under construction*).

Published presented abstracts

Baalousha, M., Ju-Nam, Y., Cole, P. A., Lead, J. R. (2010). Characterization of nanoparticle, size, shape, morphology, oxidation state and crystalinity: A multi-method approach. Geochimica Et Cosmo Chimica ACTA. 74;(12):(A37) ISSN: 0016-7037

Merrifield, R, C., Cole, P., Lead, J. R. (2010). The size related toxicity of cerium oxide nanoparticles. Geochimica Et Cosmo Chimica ACTA. 74;(12):(A700)

Cole, P. A. (2008). Nanoparticles in Natural Aquatic Environments: A physical, chemical and ecotoxicological study of cerium dioxide and silver-an extended abstract. U21 Postgraduate conference proceedings I; Water - how need drives research and research underpins solutions to world-wide problems. 20th-25th July 2008, University of Birmingham, Birmingham UK. ISSN 2075-2881.

APPENDIX C
Additional metablomic data

Venn diagram produced courteous of Dr. Ulf Sommer. Representation of the overlapping metabolomic signals obtained during analysis of *Pseudokirchneriella subcapitata* to nano-ceria particle sizes 5 nm and 35 nm diameters.

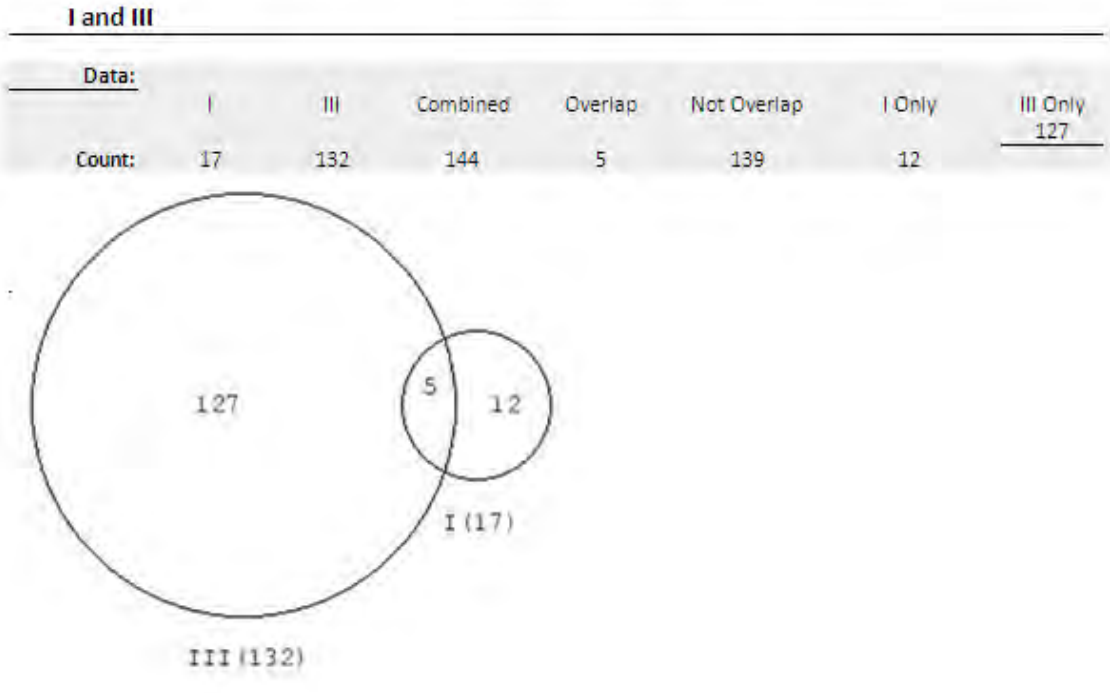

Figure C1. Venn diagram showing overlap of metabolomic signals from Hypothesis 3.

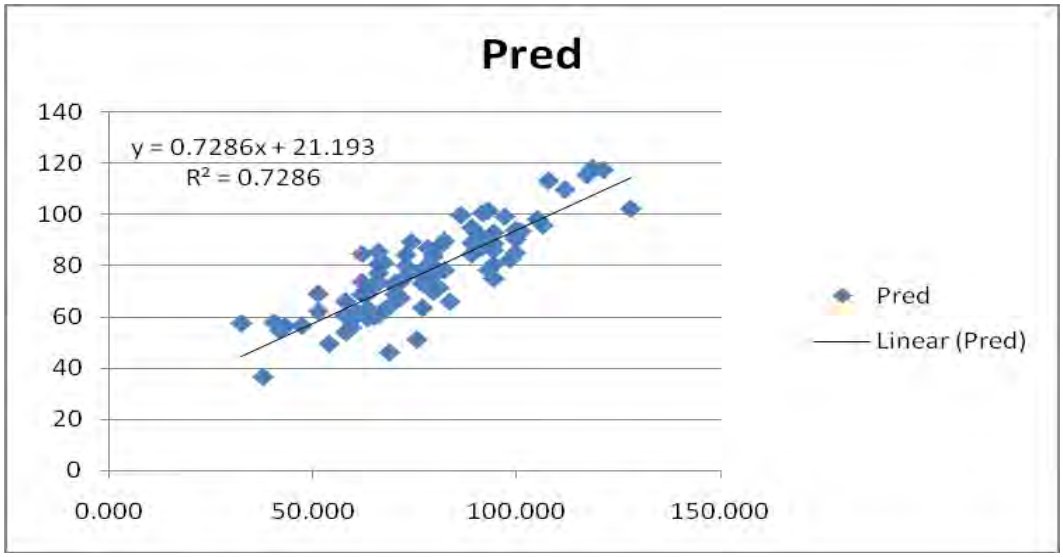

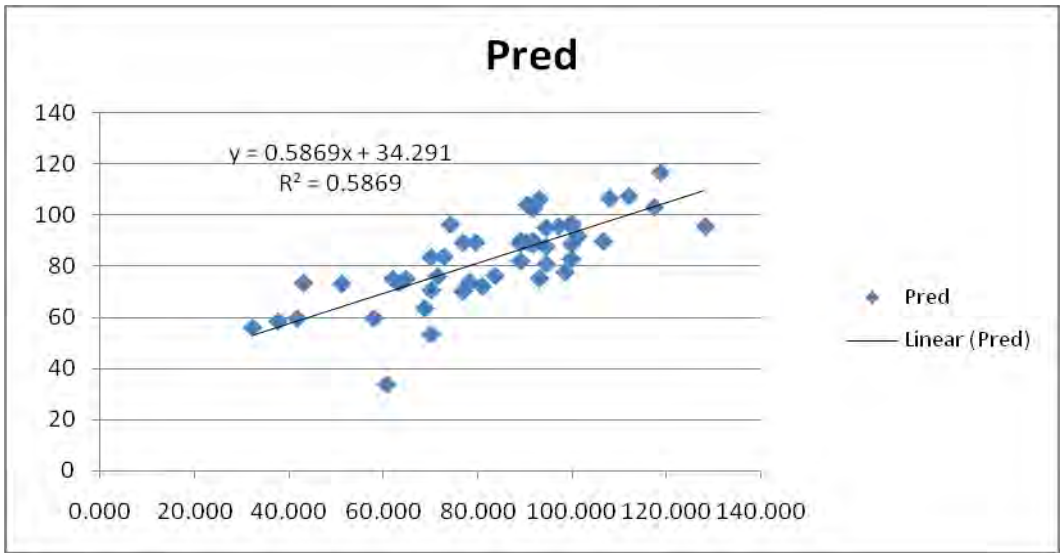

Figure C2. Plots of 72 h grwoth counts obtraiend during hypothesis 3 tests and proecidted counts from PLS regression model by Dr ulf Sommer.

A) A plot of the actual cell counts (x-axis) at 72 h against the predicted cell counts derived from the PLS regression models.
B A plot of the actual control cell counts and all 5 nm partilces counts (x-axis) at 72 h against the pedicted cell counts from the PLS regression model.

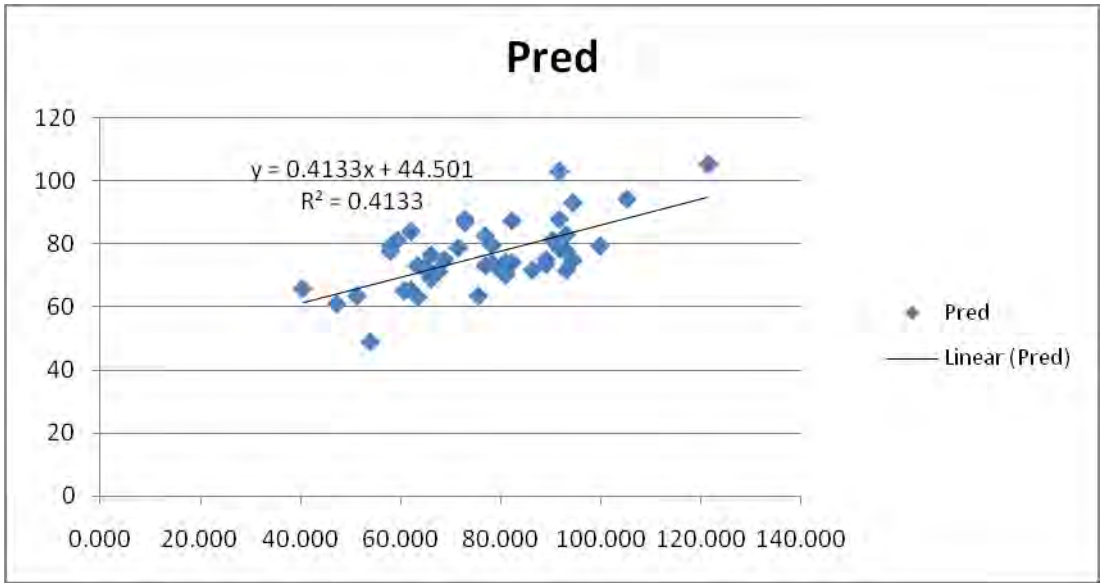

Figure C3. A plot of the actual control cell counts and all 35 nm partilces counts (x-axis) at 72 h against the predicted cell counts from the PLS regression model.

Counts at 72 h: 4 LVs, initial p-value = 0.492, where 105 metabolomic peaks offer the best separation from the data. After forward selection, p-value = 0.000.
Counts at 72 h: 2 LVs, initial p-value = 0.664, where 102 metabolomic peaks offer the best separation from the data. After forward selection, p-value = 0.007.